EFFECT OF SPECIMEN GEOMETRY ON CRACK TIP PLASTIC FLOW AND FRACTURE OF STEELS AND A STUDY ON THE STABILITY OF VOID SHAPE

By

NIRBHAY SINGH

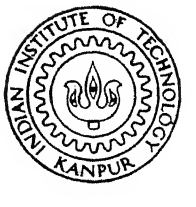

DEPARTMENT OF METALLURGICAL ENGINEERING

INDIAN INSTITUTE OF TECHNOLOGY KANPUR

DECEMBER, 1979

EFFECT OF SPECIMEN GEOMETRY ON CRACK TIP PLASTIC FLOW AND FRACTURE OF STEELS AND A STUDY ON THE STABILITY OF VOID SHAPE

A Thesis Submitted
In Partial Fulfilment of the Requirements
for the Degree of

DOCTOR OF PHILOSOPHY

By

NIRBHAY SINGH

to the

DEPARTMENT OF METALLURGICAL ENGINEERING

INDIAN INSTITUTE OF TECHNOLOGY KANPUR

DECEMBER, 1979

To

MY PARENTS

CERTIFICATE

This is to certify that the present work "EFFECT OF SPECIMEN GEOMETRY ON CRACK-TIP PLASTIC FLOW AND FRACTURE OF STEELS AND A STUDY ON THE STABILITY OF VOID SHAPE" has been carried out by Mr. Nirbhay Singh under our supervision and it has not been submitted elsewhere for a degree.

G. S. Murty

Dr. G. S. Murty
Professor
Dept. of Metallurgical Engineering
Indian Institute of Technology
Kanpur

S N Bandyopadhyay

Dr. S. N. Bandyopadhyay
Assistant Professor
Dept. of Mechanical Engineering
Indian Institute of Technology
Kanpur

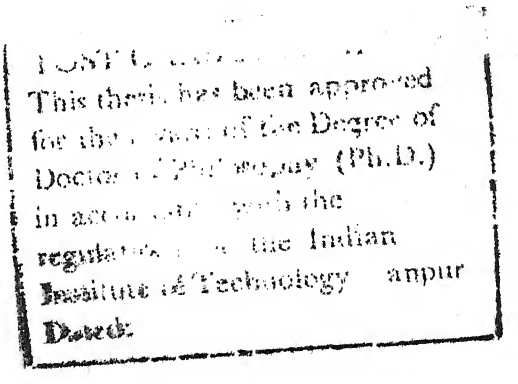

ACKNOWLEDGEMENTS

Author wishes to express his sincere gratitude to Dr. S.N. Bandyopadhyay, Department of Mechanical Engineering and Professor G.S. Murty, Department of Metallurgical Engineering for their valuable guidance and constant supervision of this work. Author is indebted to Dr. Bandyopadhyay and Dr. Murty not only for suggesting the problems, but also for their helpful discussions in interpreting the results.

Thanks are due to Professor P. Dayaratnam, Civil Engineering Department, for providing the facilities to use the Servo-hydraulic pulsator. Thanks are also due to Messers B.P. Kashyap, Yogesh Chandra, M.M.S. Sodhi, P.B. Kadam, Kultar Singh, V.P. Malhotra and others who helped him in innumerable ways in completing this investigation.

The author is very grateful to Mr. N.B. Ballal who consistently encouraged him and took pains in helping him from time to time.

Author is grateful to Messers M.H. Rahman and D.K. Sarkar of Mechanical Engineering Department for their kind help during the experimental work. Messers S.P. Rai, K.P. Mukherjee, K.K. Malhotra and V. Kumar of Metallurgical Engineering Department, and Messers S.C. Goel and H. Singh of Civil Engineering Department, were immensely helpful during the experiments conducted.

Thanks are also due to Mr. R.N. Srivastava for typing the manuscript and Mr. V.P. Gupta for tracing of figures.

The author wishes to record a deep sense of appreciation to his brother Ajeya for his encouragement. Finally, the author wishes to thank his wife Madhulika for proof reading the manuscript.

Kanpur
December 1979

Nirbhay Singh

TABLE OF CONTENTS

LIST OF TABLES

LIST OF FIGURES

SYNOPSIS

EFFECT OF SPECIMEN GEOMETRY ON CRACK-TIP PLASTIC FLOW AND FRACTURE OF STEELS AND A STUDY ON THE STABILITY OF VOID SHAPE

A thesis submitted
In partial fulfilment of the Requirements
For the Degree of
DOCTOR OF PHILOSOPHY
by

NIRBHAY SINGH
Department of Metallurgical Engineering
Indian Institute of Technology, Kanpur
December 1979

The purpose of this investigation was primarily to study the crack-tip plasticity and fracture behaviour of materials in the post-yield regime of fracture mechanics in order to assess the limitations for a valid plane strain fracture toughness (K_{Ic}) test, to consider the loss in resistance for crack-tip plastic flow and to compare the toughness obtained by different methods. 0.6% C steel and mild steel were chosen for this purpose. Specimens of varying crack lengths starting from 1 mm to a maximum of 12.5 mm were produced by fatigue pre-cracking of specimens of varying thicknesses in the range of 3 mm to 25 mm in both the materials. The load versus crack opening displacement (COD) data of all these specimens were carefully recorded in three point bend tests. Direct observations on crack-tip and the growth of the plastic zone by photoelastic coating

technique were made at various loads during the fracture test. The values of apparent fracture toughness were calculated by various methods, wherever possible.

In 0.6% C steel, all the investigated specimens showed fast fracture. The load versus clip gauge displacement (CGD) plots were linear upto the point of fracture for long cracks and thicker specimens, with very little crack-tip plastic flow. On the other hand, some crack-tip plastic flow and increase in compliance in load-CGD records were seen to occur in 3 mm thick specimens with short cracks. The K_{Ic} of this material was found to be of the order of 150 Kg $mm^{-3/2}$. A significant observation is that the apparent toughness decreased below this level for very short crack lengths. Further, it is confirmed that the ASTM recommendations for the required crack size and thickness of specimens for a valid K_{Ic} test were found to be too conservative.

In the case of mild steel specimens, there was no catastrophic failure in any of the samples tested and extensive non-linear behaviour in the load-CGD plots was dominant in all cases. Large plastic zones and considerable crack-tip blunting were observed in the non-linear region. There was an abrupt increase in the size of the plastic zone at the crack-tip as soon as the load increased above the maximum linear load indicating the loss in the plastic constraint at the crack-tip. The nominal stress corresponding to the maximum linear load was even higher than the yield

strength of uncracked beams indicating the notch strengthening effect. Due to this, the load carrying capacity of the beam increased by about 50% of the yield load when calculated on the basis of the net ligament section. The stress intensity factor at which crack-tip yielding suddenly became appreciable was observed to be around 103 Kg $mm^{-3/2}$ for all thicknesses and this is seen to occur near about 5% secant shift load. The nature of variation of this stress intensity factor, which is a measure of the resistance to crack-tip plastic flow, is analogous to the variation of apparent crack toughness against crack size and specimen thickness for 0.6% C steel. Beyond 5% secant shift load the toughness was calculated based on Irwin-McClintock's corrected crack length, crack opening displacement and energy methods.

A study has also been made on the stability of a single isolated hole inside a medium due to the importance of void growth and coalescence in ductile fracture of metals. The shape dependent instability of a single spheroidal hole has been studied theoretically under uniaxial tension and shear. If an initially spherical hole grows in the shape of a prolate spheroid inside an incompressible medium, there will be a shearing instability around 1.39 prolateness ratio, and a similar instability at some prolateness takes place in uniaxial tension as well. This analytical study agrees favourably with the experimental results of others.

In the present work, a lead-tin alloy having initially an isolated spherical hole has been loaded in tension and the shape change of this hole has been observed at different nominal strains. An abrupt growth of the void was noticed beyond a certain nominal strain, which further confirms the analytical prediction.

CHAPTER - I

INTRODUCTION

Since strength has been the major guiding design parameter in engineering practice so far, it is considered to be the most important mechanical property of a structural material. But, with the development of high strength alloys and their increasing applications, particularly in defence and aerospace, this older design concept is found to be inadequate, because of the awareness of the possibility for a catastrophic failure based on such a design criterion. Hence, there is a need for design against fracture, especially, in high strength materials. This has stimulated research into the fracture of materials and has resulted in the development of a number of design criteria based on the fracture process of metals. None of these criteria proved to be fully satisfactory for elastic-plastic materials. Nevertheless, the property of the material required for the purpose of design against fracture has been identified, and is known as the fracture toughness.

1.1: Fracture Toughness:

The fracture toughness can be regarded as a critical value of the strain energy release rate for a material, which is also a measure of the resistance against crack extension. The purpose of measuring the fracture

toughness of a material is to determine a single parameter, which is capable of characterising the material's resistance to fast fracture. Following ASTM recommendations[1], the valid plane strain crack toughness gives a measure of the load carrying capacity of a structural member containing a known flaw size. This procedure involves, firstly, proper selection of specimen geometries like crack size, specimen thickness, ligament depth etc., secondly, fatigue pre-cracking in a controlled manner, and finally, the specimens are loaded until they break. The load at which crack extends, is measured in relation to the load versus crack opening displacement record and the fracture toughness can be estimated. The toughness measured by this procedure can be regarded as a basic property of the material, provided the plastic deformation near the crack-tip is highly localised in a very small zone compared to the crack size. Toughness measurement normally assumes a high degree of constraint to plastic flow of the material at the crack tip. When the crack is sufficiently long in a large heavy-section structure, all these conditions can be fulfilled for a low strength material. However, this condition can also be easily fulfilled with relatively shorter cracks and thinner sections in a high strength material. In practice, it is not always possible to follow the above requirements and the ASTM recommendations, and thus, the toughness measured will be a function of the degree of constraint together with specimen and crack size dimensions.

Thus, there is a need for a careful study for the effects of crack length and specimen thickness on the toughness. The non-valid toughness data measured in this way, firstly, may help to assess the valid toughness of a material, and secondly, to find a lower limit of the parameters related to the specimen geometry for a valid test. Thus, if one understands the effect of these geometrical variables on the toughness property, then only it might be possible to carry out fracture test more satisfactorily and economically.

1.2: Fracture Behaviour of Metals:

Fracture of engineering materials can broadly be identified as (a) brittle fracture and (b) ductile fracture. Brittle fracture is characterised by a fast catastrophic failure, whereas a ductile fracture is easily recognised from the extensive slow stable plastic flow before rupture.

These broad categories of brittle and ductile fracture can further be classified into the following four divisions based on the load versus crack opening displacement (COD) diagram and fracture surface observations (Figure 1.1).

(i) Truely brittle solid giving a perfect linear elastic fracture, as observed in glass. This is seen to occur in high strength materials or in a heavy section beam with relatively longer cracks in medium strength materials,

(ii) Small scale yielding material, having fast fracture and a rapid propagation of crack, medium strength materials with relatively longer cracks or in high strength materials with short cracks and thin sections may behave in this manner,

(iii) Low strength (or moderately medium strength) materials, with a sizeable amount of plastically deformed zone near the root of a crack, and appreciable tip blunting associated with a slow stable crack growth. During fracture of mild steel plate at room temperature with moderate thickness such type of behaviour is noticed near the root of a crack, and

(iv) Ductile metals with a capability of accommodating large plastic strain, producing voids and fibrous growth before discontinuous fracture. The final fracture is due to plastic instability and ductile tearing. Metals at elevated temperature and some pure metals at room temperature usually fracture in this manner.

Some amount of overlapping is bound to be there as there is no clear cut boundary for such types of behaviour. In the first category, the plastic zone is completely neglected and a linear elastic concept is valid, whereas, in the second category, the plastic zone size can be included in the analysis without much alteration in the basic approach for linear elastic model. For example Irwin-McClintock's

plasticity correction[2] and ASTM recommended 5% secant shift load method[1] may be sufficient for such situations. Analysis based on the extrapolation of linear elastic model or even a non-linear elastic solution may suffise for the purpose. On the contrary, for the class of materials in Category (iii), such oversimplified approach neither describes the fracture process nor can predict the fracture strength. Therefore, new criteria need to be evolved for such a large strain dominant situation, and possibly, a careful study should be made to understand the local fracture process in the background of the mechanism proposed for the fracture of ductile materials.

1.3: Brittle Fracture:

A brittle fracture is normally recognised by a catastrophic fast propagation of crack and having a very little, or practically no plastic deformation at the crack tip. However, a ductile fracture is easily characterised by a slow stable crack growth with large tip blunting associated with fairly large amount of plastic deformation ahead of the crack tip. At the atomistic level, a brittle fracture can be described as a result of breaking atomic bonds at the tip of a crack. Griffith[3,4] first made a systematic study on the problem of brittle fracture for an ideal elastic solid in the presence of a crack. Griffith considered the first law of thermodynamics at the onset of crack instability leading to catastrophic failure. So, the Griffith's equation is based

on an energy balance criterion. Figure 1.2 was considered by Griffith, showing centrally through cracked plate having crack length 2a, which was loaded by a remotely applied stress, σ. According to Griffith, this crack will propagate under a constant applied stress, if an incremental increase in crack length produces no change in the total energy of the system. This means, the incremental surface energy is compensated by a decrease in elastic strain energy at the onset of crack instability. Thus, a crack will propagate when the decrease in elastic strain energy is at least equal to the energy required to create the new surface. For the geometry shown in Figure 1.2, Griffiths condition at the onset of fracture gives,

$$\sigma_f = \sqrt{\frac{2E\gamma_s}{\pi a}} \quad \text{for plane stress}$$

$$\text{and} \quad \sigma_f = \sqrt{\frac{2E\gamma_s}{\pi a(1-\nu^2)}} \quad \text{for plane strain} \qquad (1.1)$$

where γ_s is the surface energy per unit area, E and ν are Young's modulus and Poisson's ratio of the material respectively.

If a plane strain situation prevails in a centrally cracked plate (Figure 1.2) the crack toughness can be expressed as

$$K_{Ic} = \sigma_f \sqrt{\pi}\sqrt{a} = \sqrt{\pi} \times \text{fracture stress} \times (\text{semi-crack length})^{1/2}$$

$$= \sqrt{\frac{2E\gamma_s}{1-\nu^2}} \quad \text{which is a material property} \qquad (1.2)$$

where, K_{Ic} is defined as the plane strain crack toughness property of the material, which is obtained from the critical value of the stress intensity factor for a central crack, defined as, $K_I = \sigma \sqrt{\pi} \sqrt{a}$ (Roman I stands for mode one, i.e., tensile or opening mode). The subscript c on K_I stands for the critical value of K_I. The fracture stress is calculated from the load at which a crack extends. Hence, at the onset of fracture, $\sigma = \sigma_F$ and $K_I = K_{Ic}$ for a plane strain situation.

It is important to determine the energy release rate at the onset of fracture in terms of the critical stress intensity factor. The change of energy released due to the extension of a crack from "a to a + Δ a" is given by

$$G_I = \frac{1}{\Delta a} \int_0^a \sigma_{11} u_{11} \, dr \qquad (1.3)$$

where, σ_{11} and u_{11} are explained in Figure 1.3. So, there exists a relationship between K_{Ic} and the critical value of G_I as

$$G_{Ic} = \frac{K_{Ic}^2}{E} \quad \text{for plane stress}$$

$$= \frac{K_{Ic}^2}{E} (1 - \nu^2) \quad \text{for plane strain} \qquad (1.4)$$

G_{Ic} is known as the critical strain energy release rate or the Crack Extension Force in a material.

As our major objective is to find a reliable design criterion for predicting the stress level at which rapidly

propagating fracture occurs, the quantity of interest essentially will be, "the crack extension force", G_{Ic}. In brittle or high strength materials with ideal plane strain condition, from Griffith's equation of energy balance, this may give the stored elastic energy released from a cracking specimen as a result of the extension of a rapidly advancing crack. It also represents the fraction of the total work expended on the system to create new fracture surfaces.

1.4: Elastic-Plastic Fracture of Metals:

Griffith's concept of Fracture, strictly speaking, is applicable to truely brittle elastic solids only. However, metals invariably show some plastic deformation at the tip of a crack[5,6]. In metals, during static fracture, before crack becomes unstable, the tip root blunting and crack surfaces opening with some spread of plasticity are commonly seen. The presence of plastic zone tends to increase the resistance to fast fracture. This means, the applied forces not only have to do work to supply the surface energy, but also the energy required for the formation of plastic zone. Orowan[5] and Irwin[6] suggested that Griffith's Eqn. (1.1), could be made more compatible with brittle fracture in metals, by adding a plastic work term with the energy required to create a new surface. Thus, for metals, in plane strain

$$\sigma_f = \left[\frac{2E(\gamma_s + \gamma_p)}{\pi a(1 - \nu^2)}\right]^{1/2} \simeq \left[\frac{2E\,\gamma_p}{\pi a(1 - \nu^2)}\right]^{1/2} \qquad (1.5)$$

The surface energy term, γ_s, is normally very small compared to the plastic work term, γ_p, in metals. So, γ_s may be completely neglected for all practical purposes. Therefore, when the plastically yielded zone formation is highly localised near the tip region compared to the crack size and other specimen dimensions, Irwin's concept of crack extension force along with it's relation to the local strain energy release rate should be valid. On the contrary, if the plastic flow is excessive before any catastrophic failure, then Griffith's energy balance criterion will be insufficient. Thus, in an yielding situation, there is a need for a careful study to measure the Irwin's crack extension force at the onset of slow stable crack growth. The mechanisms which govern the resistance to crack advancement, and the unstable stage of slow crack growth should also be examined for medium and low strength materials, especially, when the plastically yielded zone is not all that small. As brittle fracture of mild steel has frequently been observed under a plane strain condition, it is highly important that one must judge the situation, considering the degree of plastic constraint below the crack tip as well. Theoretical study has confirmed that in a metal a high order of triaxiality could exist under a plane strain situation[7]. Thus, it is apparent that the degree of plastic constraint in triaxiality not only determines the value of the crack extension force, but also is a function of the specimen dimensions like crack-size, thickness and

ligament depth. Hence, the validity of a crack toughness test in a metal needs to be investigated from the lower limit of these specimen dimensions.

1.5: Ductile Fracture of Metals:

In a ductile metal, fracture usually occurs due to the growth and coalescence of holes[8]. The formation of voids (around inclusions or second phase particles), and their subsequent growth and coalescence in an unstable manner should be understood. Small ellipsoidal cavities are usually observed inside the plastic zone[9]. These voids are easily formed around a second phase particle in the presence of a high hydrostatic tension and pure shear. Orowan[10] first pointed out that, during a tensile test, at the centre of a round specimen, i.e., in the middle portion of the necked region, there would be a large quadrilateral (or prolate spheroidal) void. This can be understood as a uniaxial tension is resolved into a hydrostatic tension plus two 45° shears. Hydrostatic tension at the center helps to create the void and the rotationally symmetric 45° shear deforms it into a prolate spheroid. The unstable growth of the void produces a quadrilateral shape. Thus, the shape dependent stability of a single growing void and the fracture instability of the ligament for a pair of adjacent holes describe the ductile discontinuous fracture of plastically yielded material. Experimental observations on fractured surface

reveals that the characteristic feature of ductile fracture is a series of concave depressions as dimples and surface tearing. Obviously, a high local strain was necessary to cause such ruptures due to large plastic flow. At high temperature, the nucleation of voids inside a metal involves various other complex mechanisms such as diffusion or micro-voids initiations on grain boundaries and second phase particles.

As elastic stress field in an incompressible solid gives a prior history of plastic stress field at the incipience of yielding, it might be worthwhile to consider the stability of a single prolate spheroidal hole inside a rubber like material. To understand this three dimensional hole growth problem, Bandyopadhyay and Singh[11] made a theoretical study on the shape dependent stability of a single prolate spheroidal hole inside an incompressible medium under shear and uniaxial tension.

In a simple shear field, the shear bursting strength of a single prolate hole is given by the shear modulus times a shape factor. A single prolate hole, in the presence of a source of disturbance in the nearly region, can also become unstable under uniaxial tension field, especially when the major axis is aligned to the direction of applied tension. Recent analytical investigation by Deysarkar and Bandyopadhyay[12] has revealed that the ligament between a pair of adjacent holes can become unstable due to the shear-localization which

follows a large increase in the local normal strain on the void surface. Thus, a ductile fracture mechanism in the presence of spheroidal hole involves the condition for shear strain localization (or localised flow), followed by a critical local normal strain attained on the void surfaces causing coalescence in an unstable manner. Such a large shear strain localization in a narrow band is favourable for local plastic necking instability associated with velocity discontinuity, which will possibly be tantamount to fracture at a critical strain level.

1.6: Limitations of ASTM Fracture Toughness Testing Method in the Presence of Crack Tip Yielding:

The fracture strength of a structural member may be well below it's yield strength for sufficiently long cracks in heavy sections. Under these conditions only, the effects of plasticity spread are negligible, and the fracture strength obeying Griffith's criterion, will then be inversely proportional to the square root of the crack length. However, recent experimental observations[13,14] have shown that, for short cracks, the fracture strength could be in the order of the yield strength of the material, and the effects of plasticity spread and the tip root blunting cannot be ignored. In the presence of a large yielding near the crack tip, one would possibly measure an apparent toughness, instead of the basic K_{Ic} property. For such non-valid situations, the

transverse high plastic constraint may not be possible to be maintained, and will suddenly be relieved at a particular load through a local plastic flow ahead of the crack tip. This results in increased resistance to crack propagation, leading to a slow stable crack extension. Such effects are reflected in the measurements of plasticity spread, micro observations on crack-tip deformation, and in the load-COD records as increased deviation from the linearity before reaching a maximum load. The increase in global specimen compliance in the presence of a sizeable plastic zone, leads to a loss of stress triaxiality ahead of the crack, so that the material could become apparently tougher[15].

Plastic zone size on the plane of the crack extension is found to be proportional to $(K_{Ic}/\sigma_y)^2$, where σ_y is the yield strength of the material[16]. Based on this, to be on the safer side, ASTM recommends[1]

$$a \geq 2.5\left(\frac{K_{Ic}}{\sigma_y}\right)^2 \quad \text{and} \quad B \geq 2.5\left(\frac{K_{Ic}}{\sigma_y}\right)^2$$

and similarly for the ligament (1.6)

where a is the crack length for edge cracked beam measured in inches, B being the thickness of the specimen in inches. σ_y and K_{Ic} are in Ksi and Ksi $\sqrt{\text{inch}}$ units respectively.

Many investigators[13, 14, 17, 18] questioned the basis of selecting the factor 2.5, which is being multiplied in Eqn. (1.6). Thus, there is a need for a careful experimental investigation on the effects of crack size and

specimen thickness on the apparent toughness and the load at which a crack extends in elastic-plastic materials. Hence, ASTM recommended procedure, for fracture toughness tests based on the load-COD record, demands a proper selection of specimen dimensions and crack-size, to get an accurate K_{Ic} value, which can be taken as the valid plane strain crack toughness property for a given temperature, strain-rate and environmental conditions. Hence, the specimen dimensions are assigned as a function of the two principal pre-conditions:

(a) plane strain situation must be ensured at the tip region of the crack, and

(b) the size of the plastically deformed zone should be small compared to the characteristic dimensions of the specimen, like thickness, crack size and ligament depth. This permits us to measure the valid K_{Ic} of the material, which is obtained from a mathematical relation of the critical stress intensity factor derived from linear elastic fracture mechanics concepts.

1.7: Objective of the Present Work:

The major objective of undertaking this work is to study the plastic deformation at the root of a crack and its relation to the crack extension force, in the post-yield regime of fracture mechanics. Firstly, the load versus crack opening displacements are recorded carefully, in relation to the plastic zone size in two different steels.

Secondly, the effects of crack size and specimen thickness on crack-toughness and crack-tip plastic flow are investigated experimentally for these materials. The increase in plastic zone size is measured experimentally to explain the loss in the resistance to crack extension. Thirdly, the apparent toughness is also determined by other methods, like COD and J-integrals, for the purpose of comparing toughnesses obtained by different methods. Finally, the shape dependent stability of a changing prolateness for a spheroidal void is studied under uniaxial tension and shear in an incompressible solid. These analytical results are verified by experiments on a lead alloy.

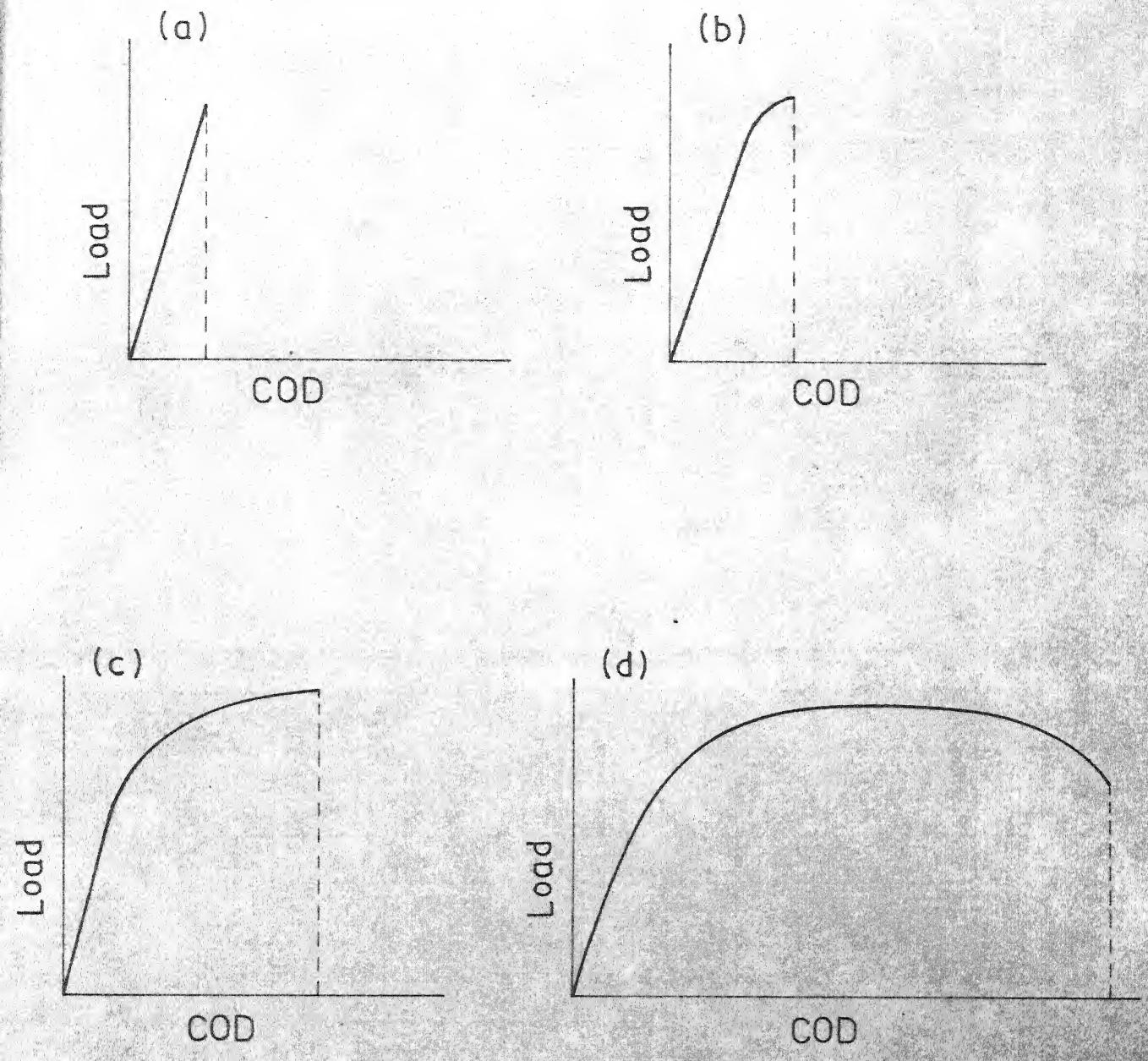

Fig. 1.1 Schematic Load - COD plot for different materials : (a) ideal linear fast fracture (b) small scale yielding fast fracture (c) moderately yielding fracture (d) fully ductile fracture.

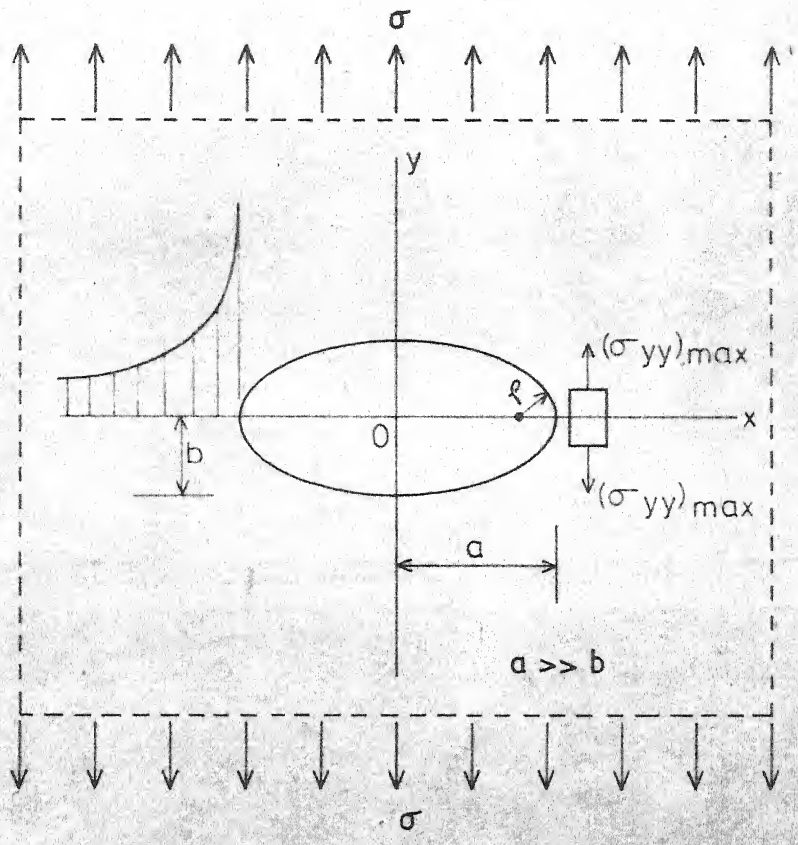

Fig. 1.2 Elliptic hole under uniaxial tension.

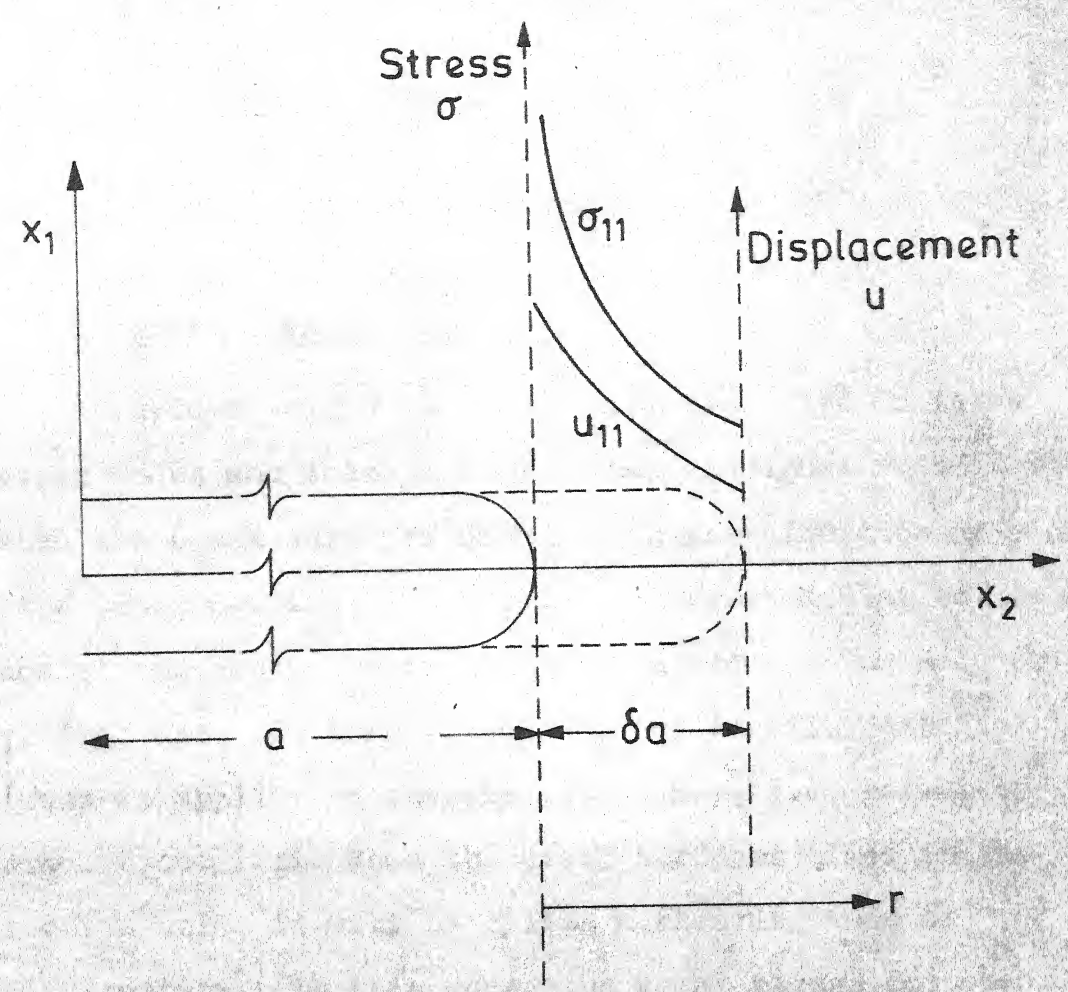

Fig. 1.3 Calculation of G from work done by crack tip stress field.

CHAPTER - II

LITERATURE REVIEW

2.1: Different Modes of Fracture:

Fracture toughness is normally evaluated in three different modes and these are described in Figure 2.1: (i) When the crack surfaces separate in the direction of y only i.e. the crack opening displacement is perpendicular to the surface of the crack, it is normally called opening mode or Mode I fracture. In this situation, the tensile component of stress is applied in the direction of y, i.e. normal to the crack face. (ii) When the crack surfaces slide in the x-direction only, it will be called a shearing mode or Mode II fracture. In this mode, the shear stress component acts normal to the leading edge of the crack, which is also parallel to the crack surfaces. (iii) If the crack surfaces slide in the z-direction only, it will be called an antiplane strain shearing mode or Mode III. In this case, the shear component of stress is applied parallel to the crack surface, which is also parallel to the leading edge of the crack.

The present work is primarily confined to Mode I fracture in three point bend test.

2.2: Elastic Stresses and Displacements Around a Crack-Tip:

If one assumes that the tip of a crack is very sharp in a brittle material, then an inverse square root singularity of stresses is seen very close to the crack-tip. Westergaard[19], Williams[20], Muskhelliville[21], Sih[22], and Liebowitz[23] gave the following expressions for the stresses and displacements near the root of a crack (Figure 2.2):

$$\sigma_{xx} = \frac{K_I}{\sqrt{2\pi r}} \left[1 - \sin\theta/2 \sin\frac{3\theta}{2}\right] \cos\frac{\theta}{2} + \ldots\ldots$$

$$\sigma_{yy} = \frac{K_I}{\sqrt{2\pi r}} \left[1 + \sin\theta/2 \sin\frac{3\theta}{2}\right] \cos\frac{\theta}{2} + \ldots\ldots$$

$$\tau_{xy} = \frac{K_I}{\sqrt{2\pi r}} \left[\sin\frac{\theta}{2} \cos\frac{\theta}{2} \cos\frac{3\theta}{2}\right] + \ldots\ldots$$

$$u_x = K_I \frac{\sqrt{2\pi r}}{8G} \left[(2\chi - 1) \cos\frac{\theta}{2} - \cos\frac{3\theta}{2}\right] + \ldots\ldots$$

$$u_y = K_I \frac{\sqrt{2\pi r}}{8G} \left[(2\chi + 1) \sin\frac{\theta}{2} - \sin\frac{3\theta}{2}\right] + \ldots\ldots \qquad (2.1)$$

where, K_I is a constant very close to the tip, and known as the stress intensity factor for a crack in mode one. G is the shear modulus and $\chi = 3 - 4\nu$ for plane strain and $(3 - \nu)/(1 + \nu)$ for generalised plane stress, and ν being the Poisson's ratio of the material. Thus, there is a need for a careful definition of the term "stress intensity factor for a crack".

2.3: Griffith's Criterion and Brittle Fracture of Solids:

Inglis[24] analysed the stress distribution around an elliptical hole in a flat plate under uniaxial tension. The maximum stress at the tip of a hole is $(\sigma_{yy})_{max.} = \sigma_o(1 + \frac{2a}{b})$. Thus, when b/a ratio is small, there is a very large stress build up at the root of a narrow elliptic notch. For very small values of b/a ratio, Griffith[3,4] calculated the decrease in strain energy due to the cut-out in a tension plate, using Inglis's[24] result. As the elliptic cut-out becomes a crack, the decrease in strain energy of the plate per unit thickness tends to be

$$U_E = -\frac{\pi p_o^2 a^2}{E}(1 - \nu^2) \qquad (2.2)$$

for a plane strain situation. Figure 2.3 shows the nature of U_E against the semi-crack length, a.

Furthermore, Griffith considered the energy required to create a new surface per unit area. In a brittle elastic solid, this is obtained as area under the force-displacement relation between the pairs of atoms representing the cohesion of a solid. Thus, if the energy required to create a new surface per unit area in a material is termed as γ_S, then the surface energy required per unit thickness in creating a crack of length "2a" is given by

$$U_S = 4a\,\gamma_S \qquad (2.3)$$

The nature of variation for U_E, U_S and U_{total} are shown in Figure 2.3.

Griffith[3,4] then applied the first law of thermodynamics at the onset of fracture, considering the energy balance criterion. Thus, the crack will be in a stable equilibrium so long as $\Delta U_{total} \geq 0$, and a crack will start propagating when the decrease in elastic strain energy is at least equal to the energy required to create the new surface. Hence, at the onset of crack extension $\Delta U_{total} = 0$, and the fracture stress is given by Eqn. (1.1). Thus, an unstable catastrophic fracture would take place when an incremental release of stored elastic strain energy in a cracked body becomes more than (or at least equal to), the energy required to create the new surface.

It is also interesting to note that in Griffith's equation $\sigma_F \sqrt{a}$ = constant for a material, and this constant is termed as the toughness of the material, which gives a measure of the energy release rate in the crack-tip region at the onset of fracture.

Barenblatt[25] studied the nature of the crack-tip shape and the finiteness of stresses at the root of an equilibrium crack. According to this hypothesis, the opposite faces of a crack close smoothly at the crack contour-end where cohesive forces are present in a small zone. The distance between the two crack faces at the tip

is in the order of an interatomic spacing at the onset of a brittle fracture, giving a stress level as high as the cohesive strength of the material.

Thus, based on Griffith's criterion for brittle fracture and also Barenblatt's description of crack tip, it may be possible to define the stress intensity factor for a crack. For mode one opening of a crack, under tension loading, in a centrally slit crack of length 2a,

$$K_I = \sigma_o \sqrt{\pi} . \sqrt{a} \qquad (2.4)$$

where, σ_o is the applied stress normal to the crack face. Hence, at the onset of fracture, σ_o becomes fracture stress σ_f, and K_I reaches a critical value of K_{Ic}, which is given as

$$K_{Ic} = \sigma_f \sqrt{\pi} . \sqrt{a} \qquad (2.5)$$

for an elastic brittle fracture under a plane strain situation.

2.4: Irwin-Orowan Modification and the Concept of Fracture Toughness of a Metal:

Experimental evidence shows that in all engineering metals and alloys, a small plastic zone would always be present ahead of the crack tip before the onset of fracture. Orowan[5] and Irwin[6] suggested a modification in Griffith's equation. According to them, the energy released at the crack tip is a function of the plastic energy dissipation plus the energy required to create a new surface. Hence, γ_s

is modified as $\gamma_s + \gamma_p$ to account for the plastic deformation at the tip region. In metals, the magnitude of γ_s is very small compared to the plastic energy dissipation rate. Thus, at the onset of fracture, the critical value of the stress intensity factor becomes entirely due to the plastic energy dissipation rate. Thus, the crack toughness can be regarded as the critical value of the strain energy release rate for that material at the onset of fracture. As the purpose of measuring the fracture toughness is to find a single parameter characterising the material's resistance to fast fracture, the toughness will also be a measure of the resistance to crack extension.

2.5: Linear Elastic Fracture Mechanics (LEFM) Approach in High Strength Materials as Recommended by ASTM:

The stress intensity factor for calculating the fracture load of a cracked beam is well founded in an elastic medium. The load is always proportional to the crack opening displacement for such materials. Experiments on high strength materials show a linear load-COD record upto the point of fracture, especially under plane-strain situation. Thus, in the presence of a high degree of plastic constraint in a very localized region, a perfect linear elastic brittle fracture can take place for such materials. If a precracked beam fractures in a plane strain condition, at a stress level which is well below the yield

strength of the material, then ASTM recommends[1] that the measurement of K_{Ic} should give a valid crack toughness property of the material.

In some cases, before the onset of fracture, some non-linearity in load-COD diagram is noticed due to the crack-tip deformation. So long as this deviated region is small compared to the linear region then it may be possible still to use the basic LEFM approach. In such cases, as the maximum linear load and fracture load are not coinciding exactly with each other. ASTM[1] suggests that a 5% secant offset load which will fall very close to the crack extension load should be adequate, and would approximately give a measure of crack toughness property in such materials. The materials which show some amount of sub-critical crack growth and considerable amount of plastic deformation are described later.

Brown and Srawley[1] recommended the ideal linear elastic type fracture for a valid K_{Ic} test. Thus, in a perfectly plane strain fast fracture with either very little or practically no subcritical crack growth can only give an accurate measurement of valid K_{Ic}. Methods for measuring plane strain crack toughness, K_{Ic}, of a material, through simple experimental tests on standard specimen geometry and dimensions are given by ASTM[1,2].

If a pre-cracked specimen is slowly loaded either in bending or tension, the load at which an abrupt crack

extension takes place is observed carefully in relation to the load-COD record. The applied nominal fracture stress can be calculated based on the critical linear elastic fracture mechanics stress intensity factor

$$K_{Ic} = \sigma_F Y \cdot \sqrt{a} \qquad (2.6)$$

where, σ is the gross nominal bending stress and is equal to $3/2 \cdot \frac{PS}{BW^2}$. At the onset of fracture $P = P_F$, $\sigma = \sigma_F$, and calibration factor Y can be obtained either from Figure 2.4 or using the following equation given by ASTM[1]

$$Y = A_o + A_1 \left(\frac{a}{w}\right) + A_2 \left(\frac{a}{w}\right)^2 + \ldots\ldots \qquad (2.7)$$

where A_o, A_1 etc. are tabulated in Table 2.1.

2.6: ASTM Recommendations and Size Requirements for a Valid 'K_{Ic}' Test:

On one hand, a brittle fracture of low strength materials, like mild steel, is noticed near the middle portion of a beam at low fracture stress in a heavy section. Whereas, on the other hand, a ductile type of fracture with substantial amount of plastic flow is common in a very short cracked and/or thin beams for a medium or high strength material. In general, if a short crack emanating from a flat surface of a beam is stressed either in tension or bending upto the fracture stress of the beam , the plastic zone size could be as large as the crack length, especially when the fracture stress is in the order of yield strength

of the material. In such situations, a considerable deviation from the plane strain condition could occur. The major sources of inaccuracy in measuring crack toughness arise due to the increase in specimen compliance as a result of crack-tip blunting and excessive plastic flow near the tip region. In order to avoid this difficulty of measuring the valid K_{Ic} instead of measuring an apparent toughness due to the loss in triaxiality, Brown and Srawley[1] (through ASTM) recommended that the size of plastic zone should be the guide line for selecting proper specimen dimensions. As it is known that the plastic zone sizes are in the order of $\frac{1}{6\pi}\left(\frac{K_{Ic}}{\sigma_y}\right)^2$ for plane strain and three times of that in the case of plane stress, Brown and Srawley[1] in ASTM, recommend for a valid crack toughness test that the crack size, thickness and ligament depth should be as follows:

$$a \geq 2.5 \left(\frac{K_{Ic}}{\sigma_y}\right)^2$$

$$B \geq 2.5 \left(\frac{K_{Ic}}{\sigma_y}\right)^2$$

$$\text{and} \qquad a \leq 0.5\, W \tag{2.8}$$

Here the units of K_{Ic} are in Ksi $\sqrt{\text{in}}$, σ_y is Ksi and a, B and W are in inches. These recommendations are based on experiments on high strength materials.

2.7: Yielding Fracture Mechanics and Fracture Toughness Determination by COD Method:

When fracture occurs in the presence of a significant amount of yielding, it is important to find a relationship between the applied stress, crack-size and material toughness. The major objective of yielding fracture mechanics is to describe the fracture behaviour for a material of some limited plastic yielding at the root of a notch or crack. A completely ductile fracture situation with a very large plastic flow involving void growth and coalescence inside the material is outside the regime of yielding fracture mechanics. Thus, the yielding fracture mechanics mainly relies upon the extrapolation of basic linear elastic fracture mechanics concepts, but with some modifications, so as to incorporate the effects of plastic zone and stress-strain distributions inside the deformed region on the calculations of the fracture strength of that material. This subject mainly studies the nature of plastic deformation at the root of a crack which is being deformed to a notch with some plasticity spread ahead of the root, producing some localized slip and a new elastic-plastic stress field near the root region. The plastic zone and the deviation from an ideal plane strain deformation play important roles in affecting the final fracture process. Thus, in an yielding situation, the conditions for fracture of metals demand additional information on crack-tip deformation and plastic strain field

together with elastic-plastic stress distributions ahead of a notch. A subcritical crack growth may occur before the final collapse of the notched body.

Orowan[5] and Irwin[6] first emphasized the importance of evaluating a single material toughness parameter where it would be possible to use the basic LEFM approach. Irwin-McClintock's correction[2] and 5% secant shift load recommended by ASTM[1] are a few such examples to calculate toughness in small scale yielding situations.

Fracture criterion based on the SIF approach is found to be inadequate to describe the fracture for an yielded crack-tip situation. Additional information on strain level at the crack-tip region is also needed to describe such a fracture. For a plane stress yielding situation, fracture criterion entirely based on crack opening displacement has proved to be useful. Based on Green and Hundy's[26] experimental observations, Dugdale[27], Bilby, Cottrell and Swinden[28], Hult and McClintock[16] and Goodier and Field[29] presented a mathematical relationship between the crack length, plastic-zone, yield strength and the crack-tip opening displacement for an elastic-plastic material. Thus, so long as, σ/σ_y at the onset of fracture is less than 0.7 or so, the plastic zone, R, and the COD, δ, can be obtained as

$$\frac{a}{R + a} = \cos \frac{\pi\sigma}{2\sigma_y} \tag{2.9}$$

and

$$\delta = \frac{8\sigma_y . a}{\pi E} \ln \sec . \frac{\pi\sigma}{2\sigma_y} \tag{2.10}$$

where, σ_y is the yield strength of the material, E is Young's modulus and 2a being the central slit crack size. For plastic yielding situation in plane stress, Bilby-Cottrell-Swinden model proposes that Irwin's toughness is entirely given by the crack tip opening displacement, δ, as

$$G_{Ic(\text{plane stress})} = \sigma_y \delta_c \qquad (2.11)$$

Nichols[30], Tetelman and Robinson[31], Banerjee and Pandey[32] found the above relation to be very useful for predicting fracture stress at large plastic strain induced situations. Wells[33], Turner[34], Green and Knott[35], Rice[36], Burdekin[37], and Paris and Liebowitz[38] made attempts to use a similar expression for an yielded crack-tip plane strain situation based on COD criterion. Either in a plane strain condition or when a deviation from plane strain occurs (mixed mode of plane strain and plane stress), the toughness may be calculated as

$$G_{Ic(\text{plane strain})} = \alpha \sigma_y \cdot \delta_c \qquad (2.12)$$

where, α is the correction for accommodating the plastic constraint factor ahead of the notch. The value of α is somewhat unknown and mostly relied on experimental data. Turner[34] and Green and Knott[35] recommended a value of α = 2.1 for an ideal plane strain metal fracture. Thus, this method of calculating the toughness considers the effects of crack-tip strain δ and the plastic stress elevation. For an yielding crack-tip, it is necessary to modify the LEFM stress

field near the root of a crack. In a recent work Deysarkar and Bandyopadhyay[39] examined the combined effects of crack-opening and tip-blunting on elastic as well as elastic-plastic stress field near the root of a crack like notch. For short cracks in thicker section beams, normally the plastic yielding near the tip could be significant. Irwin[40] and Cottrell[41] suggested that the load, at which the crack was just at the onset of extending, should be measured carefully. The critical COD and the crack extension load would give an idea of resistance to crack extension for that material. As correctly pointed out by Sumpter and Turner[42] that during an yielding fracture it is as much important to record gradually increasing plastic zone as its crack extension load and critical COD.

Another alternative method of calculating the toughness of a material under yielded situation is by J-integral approach, developed by Rice[36]. Other methods of measuring fracture toughness for different materials are described in subsequent sections.

From the above discussion it is clear that, to a first approximation, the fracture stress during a fast fracture, can still be used to calculate the fracture toughness of a yielding material. But, the amount of plastic deformation preceding the fracture also gives a measure of the energy dissipated near the tip for such materials. Thus, an understanding of a metal's toughness also depends on the size and shape of the plastically deformed zone.

A mere attainment of plane strain does not always guarantee a fast fracture in such yielding materials, because the plastic zone preceeding fracture must be small also with respect to crack length and ligament depth. So, it is not only the elastic-plastic stress ahead of the tip but also the distribution of plastic strains associated with fracture are of major importance. All such complexities are predominant near the root region of a short edge crack or a thin section cracked beam. COD criteria for fracture conveniently evaluate the toughness in plane stress for large strain induced slow crack growth situation, whereas the critical stress intensity factor approach determines the toughness in fast fracture under plane strain situation in high strength materials.

To understand the fracture behaviour of a cracked body which is neither fully plane strain nor completely plane stress near the tip region, it is necessary to measure the plastic zone size to calculate the fracture toughness in such elastic-plastic situations. In a recent paper Rice and Sorensen[43] concluded that there is a good correlation between the toughness, J-integral value and the measured COD for an elastic-plastic material. Thus, it seems that, other than K_I concept, either COD or J-integral method offers a reasonable one-term description of the conditions at the tip of an elastic-plastic crack. Several researchers[44,45] made a systematic comparison of these methods of calculating toughness in elastic-plastic materials.

2.8: Measurement of Fracture Toughness by J-integral Method:

Recently considerable attention has been focussed on strain energy methods applied to crack and notch problems. The principle is primarily based on the calculation of potential energy and the analysis of virtual work in a stressed body. Rice[36] extended this concept to elastic-plastic materials. Strictly speaking, the analysis is valid for elastic solids. The foundations of the theory on pseudo-potential energy in an elastic-plastic material are not very well established. Thus, theoretically it is difficult to justify such energy concepts of fracture in yielding materials. Nevertheless, attempts are being made in the literature to define a single parameter characterising the fracture behaviour of materials on the basis of this concept.

If one defines the change in potential energy of a cracked body by a line-integral J along any cracked path Γ surrounding the notch tip(starting from the lower surface, and ending on the upper surface of the notch) such that

$$J = \int_{\Gamma} \bar{W}(\varepsilon_{mn})\, dx_1 - T \frac{\partial u}{\partial x_2}\, ds \qquad (2.13)$$

where Figure 2.5(a) shows that the curve is traversed in the anticlockwise direction, s is the arc length, T is the traction-vector ($T = \sigma_{ij}\, n_j$) defined on Γ according to outward normal to the path Γ. $W(\varepsilon_{mn})$ is the strain energy density given by

$$\bar{W}\ (\varepsilon_{mn}) = \int_{0}^{\varepsilon_{mn}} \sigma_{ij}\ d\ \varepsilon_{ij} \qquad (2.14)$$

For a linear elastic body subjected to a single unidirectional stress, σ, with a strain ε, the expression for $\bar{W}$ becomes $\frac{1}{2}\ \sigma\varepsilon$. As the free surface of the notch cannot withstand a stress normal to its boundary, the traction vector becomes zero. The path independent nature of J makes it a valuable analytical tool. Rice has further shown that the J-integral may be interpreted as the potential energy difference between two identically loaded bodies having crack sizes "a" and "a + Δa"

$$J = -\frac{1}{B} \underset{\Delta a \to 0}{\text{Lt.}} \frac{\Delta U}{\Delta a} \qquad (2.15)$$

where ΔU is the potential energy change of the body due to an incremental increase in crack length by Δa. For a linear elastic solid, the strain energy release rate, G, and J defined as the change in potential energy per unit crack extension per unit thickness of the plate, are primarily the same quantity. Figure 2.5(b) shows schematic linear and non-linear loading curves corresponding to specimens with crack lengths "a" and "a + Δa" under displacement control. The area is given by JB Δa, which gives a direct experimental measurement of J.

Begley and Landes[46] have shown experimentally that the critical value of J may be used as a fracture

characterizing parameter. They have observed that J at fracture is independent of the specimen geometry and loading system. According to them, J_{Ic} is thus a material property. However, at present there is certain controversy regarding J_{Ic} concept as a fracture criterion in elastic-plastic solids[47], but many people found[48] J as a single parameter characterising the fracture as reasonably accurate. Rice and Sorensen[43] have found an excellent agreement between J-integral value and critical COD toughness calculated in several elastic-plastic materials (Figure 2.6).

Recently, considerable attention has been focussed on how to apply J-integral fracture concept for studying the effects of specimen thickness and crack size. Vitek and Chell[49] studied the validity of J-integral calculations in the post-yield fracture mechanics regime. J appears to be more appropriate to fast fracture situations than the one based on COD. However, while studying the thickness effect on apparent toughness Taira and Tanaka[50] found a satisfactory experimental interrelationship between notch tip opening displacement and J-integral calculated. As the thickness effect on elastic-plastic crack-tip stress field is basically a three-dimensional problem, it is important to understand experimentally how the effect of plane stress can alter the plastic constraint in plane strain. J-integral approach has also been used to study such non-valid data so as to find out a valid toughness in such post-yield regime[18].

The equivalent energy concept was introduced by Witt and Mager[51] based on the analysis of J-integral[36,46]. It is primarily an extension of critical J_I concept (J_{Ic}) proposed by Rice[36], Begley and Landes[46]. As there are practical difficulties in measuring the differential area under the load versus load-point displacement recorded curves of the similar cracked bodies, it would perhaps be convenient, if one measures the area under the entire diagram. The principle is based on the idea that for two geometrically similar bodies $J/\bar{A}$ will be constant, where $\bar{A}$ = area under the graph at any point per unit thickness of the specimen.

In this procedure, firstly, a normalised P/B^2 versus δ/B diagram is drawn and then the area under the normalised load-deflection curve upto the fracture is termed as the volumetric energy of the body. For an elastic-plastic situation using this concept an effective way of measuring toughness was due to Chell-Milne and Kirby[18], who found the following modified method. The crack toughness by this equivalent energy procedure is equal to:

Apparent crack toughness for the maximum linear load

$$X \left(\frac{\text{Total normalised area under load - COD diagram}}{\text{Area under the linear portion of load - COD diagram}}\right)^{1/2}$$

2.9: R-Curve Method of Determining Toughness:

An important feature of fracture under fully plane stress condition is the stable crack growth prior to fracture.

It is also frequently referred to as slow crack growth situation for an yielded crack-tip. Large plastic yielding ahead of the crack-tip and substantial tip blunting are common in plane stress deformation. However, for a plane strain elastic-plastic fracture, the thickness of a cracked beam is sufficiently large to maintain a high plastic constraint with practically no slow stable crack growth producing a square fracture surface. Whereas, a slow stable crack growth preceding a slant fracture surface is easily seen for plane-stress. When a plane strain fully constrained situation changes to an unconstrained plane stress yielding, R-curve method is found to be very useful in these situations. Krafft, Sullivan and Boyle[52] suggested that a crack extension resistance parameter can be proposed based on the plastic work expended due to slant and square fractures. Thus, from the onset of crack extension, it would be possible to calculate Irwin's $G_{I_{critical}}$ for plane stress and similarly, for a slow stable crack growth situation, the fracture instability load can be obtained from G_R, where G_R is calculated from an experimentally determined R-curve. As there is always a continuous balance between the released energy due to the creation of new surface and the consumed plastic energy, a Considére type plastic instability condition can be derived. Thus, if one plots the value of G_R against the percentage of crack extension and draws a tangent line on R-curve passing through the point $a = -a_o$, the instability

point on the R-curve corresponding to G_{IR} can be obtained (a is the crack length and a_o is the initial crack length). In this way, G_{IR} critical (plane stress) can be calculated for any elastic-plastic material under stable crack growth situation. To study the effect of thickness on fracture toughness, R-curve method has been found to be very useful[53,54].

2.10: Effects of Crack Length and Specimen Thickness on Crack Toughness Measurements:

For sufficiently long cracks, the strength of a fracture test specimen may be well below the yield strength of the material and the size of the plastically yielded zone may not be all that large. However, either for a short crack or for a thin section cracked beam neither the size of the plastic zone is small nor the fracture stress is well below the yield strength. For a valid K_{Ic} test, ASTM made certain recommendations of size requirements, which should be strictly followed. Thus, it has become necessary to understand how specimen thickness and crack size alter the crack toughnesses property of a material. As ASTM only accepts the valid toughness data, most of the tests conducted for such thin section beams or short cracked beams will be considered as invalid by ASTM criteria, inspite of the fact that the failures still could have occurred by unstable crack propagation. ASTM recommends 5% secant offset criterion equivalent to 2% crack extension. Clearly

it will reject tests where slow crack extension has occurred beyond 2%, and/or where plasticity spread has been sufficient to cause deviations beyond 5% secant shift limits. To find a lower limit of the crack size and specimen thickness in different materials for a valid toughness test Cottrell and Longstone[13], Jones and Brown[14], Bandyopadhyay and Griffith[17] and Chell, Milne and Kirby[18] investigated the validity of these ASTM recommendations. Figures 2.7 to 2.11 show these results which clearly demonstrate that ASTM recommendations are mostly an overestimate for testing different materials. Thus, the specimen thickness and crack size are the two most important geometrical parameters which can substantially alter the plane strain valid crack toughness property of a material. The need for a careful study of these effects on toughness property of a material has been emphasized by others as well[55,56].

In all these non-valid tests, as plastic flow is significant, some amount of crack-tip blunting is inevitable. The effect of notch-tip root radius on fracture toughness measurements was first due to Wilshaw, Rau and Teteleman[57]. The combined effects of root radius and crack size on toughness were considered by Heald, Spink and Werthington[58]. For a blunted notch with radius ρ and semi-crack length, c, the apparent fracture toughness is given by

$$K_A = \frac{\sqrt{\pi c}\,\sigma_u}{1 + (\rho/c)^{1/2}} \cdot \left\{ \frac{2}{\pi} \cos^{-1} e^{-\frac{\pi K_{Ic}^2}{8\sigma_o^2 c}} + \rho/c \right\} \qquad (2.16)$$

where σ_u is the ultimate strength and K_{Ic} is the true valid plane strain crack toughness of the material.

In the presence of crack-tip yielding for short cracks or thin beams, some amount of non-linearity in the load-COD record during the fracture test is invariably noticed. Increase in specimen compliance can be due to a slow stable crack growth as well as large crack-tip plastic flow because of deviation from plane strain condition. For short cracks, Sumpter and Turner[42], Mubeen and Bandyopadhyay[59] observed that the plastic zone size and shape ahead of the crack-tip mainly describe the nature of fracture. For a very short crack the yielded boundary may even touch the free machined specimen surface. So far, no single satisfactory method of crack toughness measurement is available to evaluate the crack-toughness property in such a complex non-valid testing regime. Unless a careful analytical and experimental study is made on such mixed mode plane stress-plane strain deformation situations, it would be difficult to obtain the toughness value in this regime accurately. Dixon[60], Boyd[61] and Ritter[62] studied the effect of elastic-plastic deformation stress field and fracture surface considering the effect of triaxiality. Miller and Kfouri[63] obtained an elastic-plastic stress field and plastic zone size of crack-tip under uniaxial and biaxial loading conditions. Their analysis shows that the local stress ahead of an yielded tip can be several times the yield strength of

the material. This further confirms the study on charpy notch by Knott and Cottrell[64], Griffiths and Cottrell[65], Griffiths and Owen[66]. In all these above investigations a predominant effect of notch strengthening is noticed. Loss of triaxiality, due to the side and through thickness plastic flow near the tip region, can increase the crack toughness of a material. As the thickness is decreased, the effect of plane stress becomes increasingly dominant over the ideal plane strain deformation. The effect of thickness has been studied systematically by Wessel[67], Irwin, Kies and Smith[68], Krafft, Sullivan and Boyle[52], Brown and Srawley[1], Tetelman and McEvily[69], May[70] and Pellini[71]. Chell, Milne and Kirby[18], and Chell and Worthington[72] used equivalent energy method to calculate apparent crack-toughness in the non-valid regime and compared their results with the calculated toughness based on COD, ASTM and observed crack extension load. Bluhm[73], Taira and Tanaka[50] also examined the effect of specimen thickness on notched mild steel specimen and emphasized that there is a need for careful examination of plastic zone at the tip.

In the present work, a careful observation of the plastically yielded zone has been made in relation to the load-COD diagram together with the crack-tip deformations for short cracked and thin beams of two different steels mostly in the non-valid regime.

2.11: Experimental Observations on Plastic Deformation Near a Crack-tip:

There are few reliable experimental data on the development of plastic zones around cracks, because of difficulties associated in measuring the deformed zone inside the material under plane strain, particularly with small scale yielding situation. It is generally recognized that small plastic zone (compared to crack size, specimen thickness, ligament etc.) forms in conditions close to plane strain, while the large ones are commonly seen under plane stress situations.

Dugdale[27] evaluated the size of the plastic zone ahead of a crack in a thin mild steel plate. Green and Hundy[26], Vitvitskii et al[74] carried out more detailed experimental study of plastic deformation near a crack in low carbon steel plate.

Hahn and Rosenfield[75] made a careful study on the plastic flow and slip at the root of a crack under plane stress situation by etching process.

Localization of plastic strains in thin slip band layers and plastic deformation near the root of notches are also observed by Knott and Cottrell[64], Griffiths and Cottrell[65] and Ewing and Richards[76]. Dixon[60], Pratt[77], Gerberich[78], Sedlow[79], Mubeen and Bandyopadhyay[59] described an alternative procedure of measuring plastic zone at the root of a crack, mainly by photoelastic coating method. A

metallic specimen cemented with photoelastic coating is loaded to get the fringe patterns showing iso-shear stress lines. Assuming Von-Mises or Tresca yielding condition, a particular fringe order boundary normally gives the yielded boundary. By this technique, one can get a consistent measurement of plastic zone, contours of which very well resemble those of the theoretical calculations of Irwin[80], Williams[20], Westergaard[19], and Wells and Post[81]. Using a replica technique and electron microscopy similar observations were also made by others[82]. In recent years several investigators used Moire fringe patterns[83], Caustics[84] and recrystallization methods[85] to find the plastically deformed zones near the tip region. In the present work, photoelastic coating method has been used to observe the plastic zones at the tip of the crack.

2.12: A Study on the Stability of Void Shape Under Uniaxial Tension and Shear:

In ductile metals fracture occurs due to the growth and coalescence of voids. During the tensile test of a ductile metal, small cavities are commonly seen to occur in the necked region before the final fracture of the specimen. Orowan[10] first observed that at the centre of a round tensile specimen, spheroidal type void would be produced in the middle portion of the necked region. The hydrostatic tension at the centre helps to create a void around inclusion

(or a second phase particle), the 45° shear stress deforms the void into a spheroid first, and then at the onset of instability it becomes a quadrilateral shape. Recently, considerable attention has been focussed on the development of a theory of ductile fracture due to spheroidal hole growth inside a plastically yielded medium. McClintock[8] first made a systematic study on the cylindrical hole growth problem inside a plastically yielded material. According to this analysis, ductile fracture involves (a) shear localization between the spheroidal holes and (b) a critical normal strain level needs to be achieved on the void surface before unstable fracture. The plane strain deformation of a cylindrical hole in copper was studied by Perra and Finnie[86] which further confirmed the unstable shear growth of a void. The problems of localized shear strain build-up and its role in plastic flow-localization were considered by Price and Kelly[87], Cottrell and Stokes[88], Buvers and Honeycombe[89] and Rudnicki and Rice[90]. The necking mode of plastic instability due to void-coalescence was studied by Argon[91], Backofen[92], Thomason[93], ~~Berg, McClintock,~~ Nagpal et al[94], El-Sudani and Knott[95], and further by Tait and Taplin[96], and Raj and Ashby[97].

Bilby, Eshelby et al[98] pointed out that a single prolate hole could have a shape dependent instability inside a liquid matrix. Thus, it may be necessary to understand the shape dependent instability of a void and it's

relation to ductile fracture. Duysarkar and Bandyopadhyay[99] recently calculated the interaction of strain field between two prolate spheroidal holes inside an incompressible solid, which showed distinct conditions for shear localization in the ligament and abrupt increase in normal strain on the void surface causing instability. In the present work, the shape dependent instability of an initially spherical hole is studied under uniaxial tension as well as simple shear.

TABLE 2.1

Coefficients for calculating Y-factor[1] for four-point and three-point bend specimen

	A_o	A_1	A_2	A_3	A_4
Four-point	1.99	-2.47	12.97	-23.17	24.80
Three-point					
S/W = 8	1.96	-2.75	13.66	-23.98	25.22
S/W = 4	1.93	-3.07	14.53	-25.11	25.80

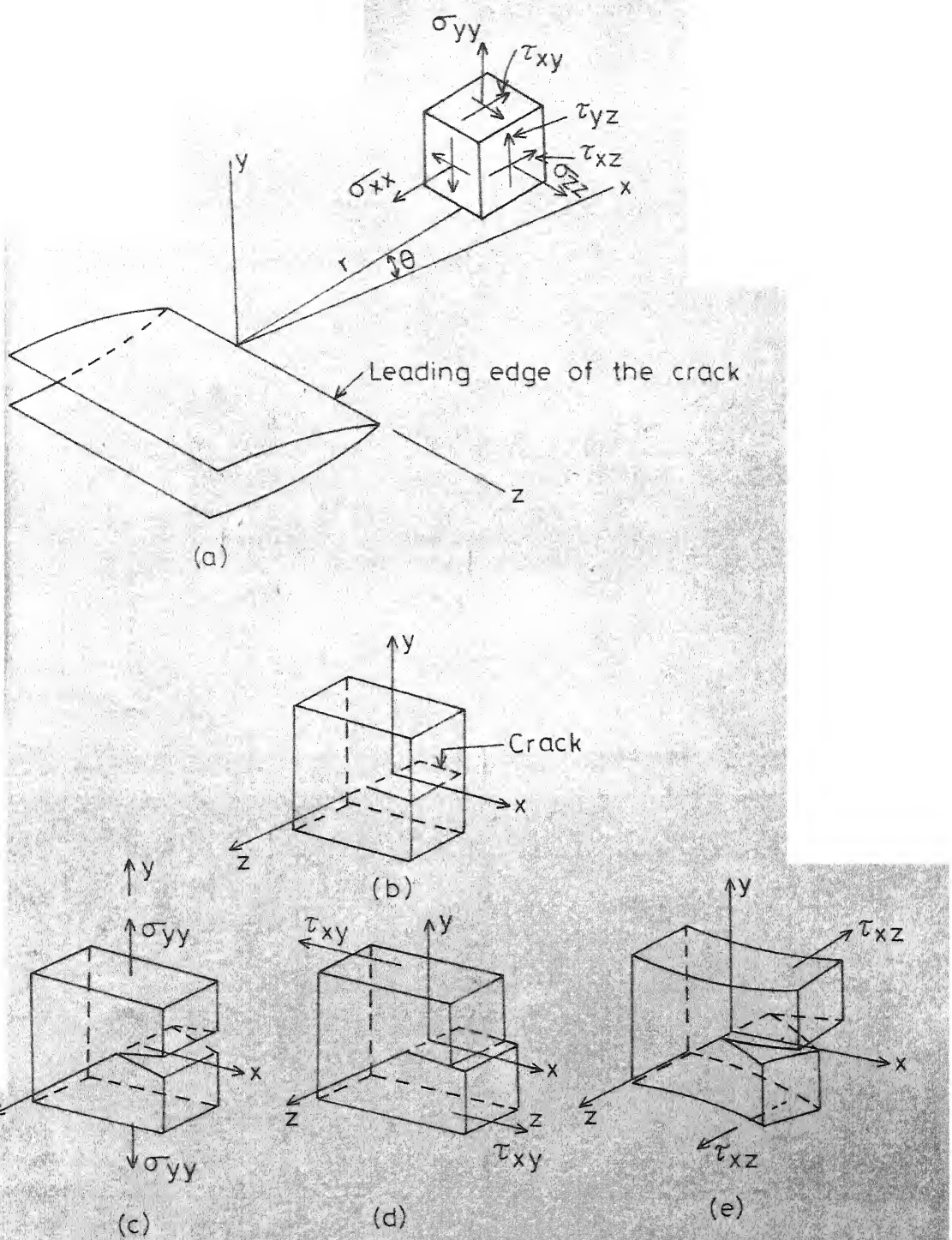

a = Crack length.

(a) Stress components at the crack tip
(b) Crack and frame of reference
(c) Mode 1 or opening mode.
(d) Mode 2 or shearing mode.
(e) Mode 3 or antiplane shearing mode.

Fig. 2.1 Modes of fracture and crack surface displacements.

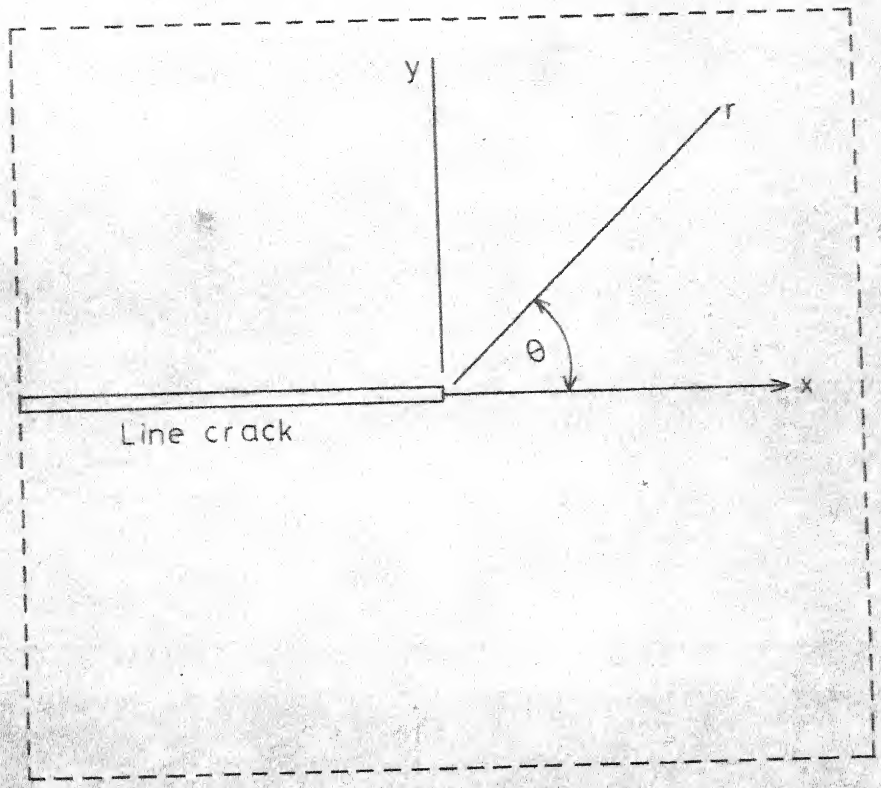

Fig. 2.2 A crack in an infinite medium.

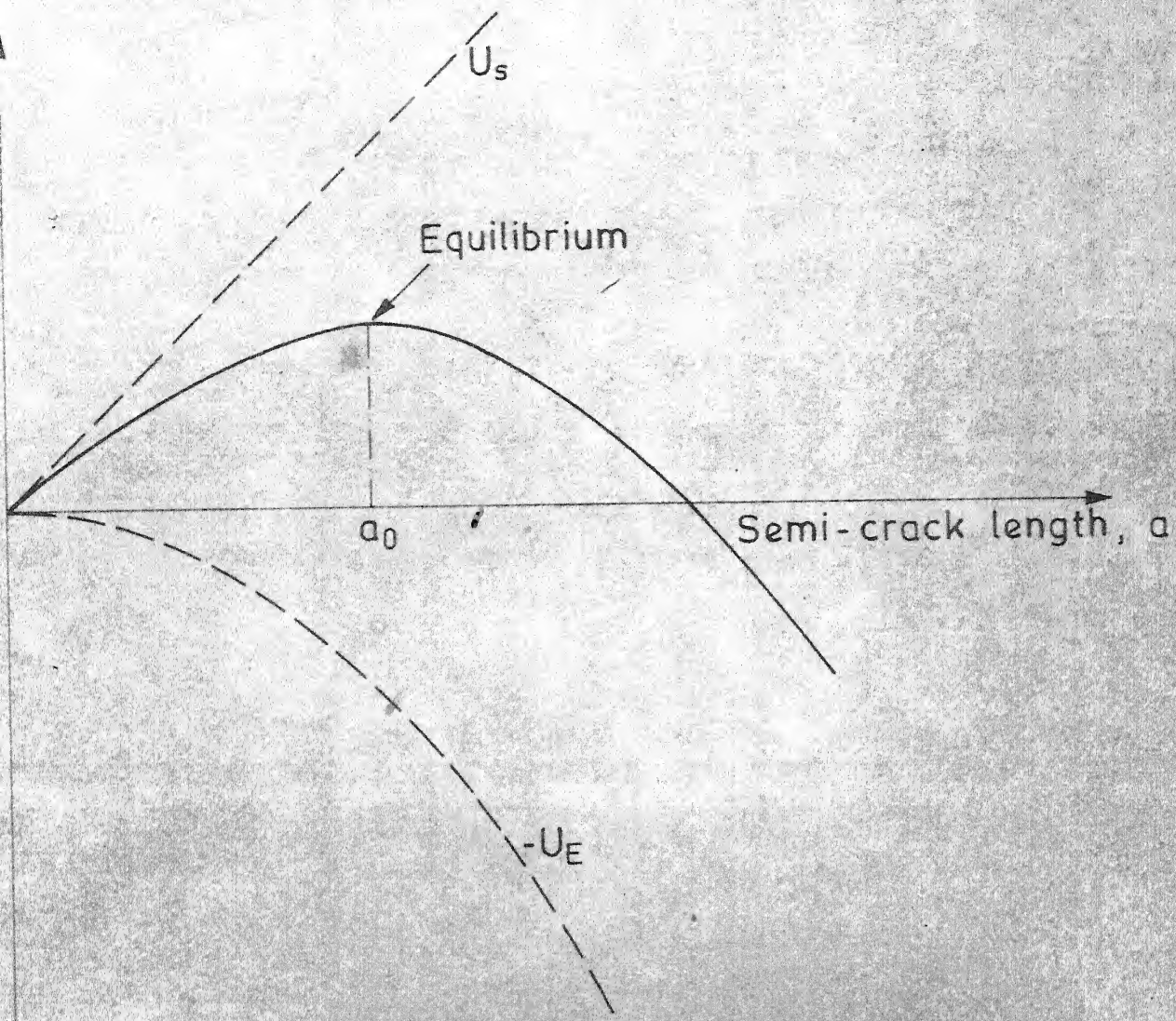

2.3 Variation of total potential energy, U, with crack length at a given stress, σ.

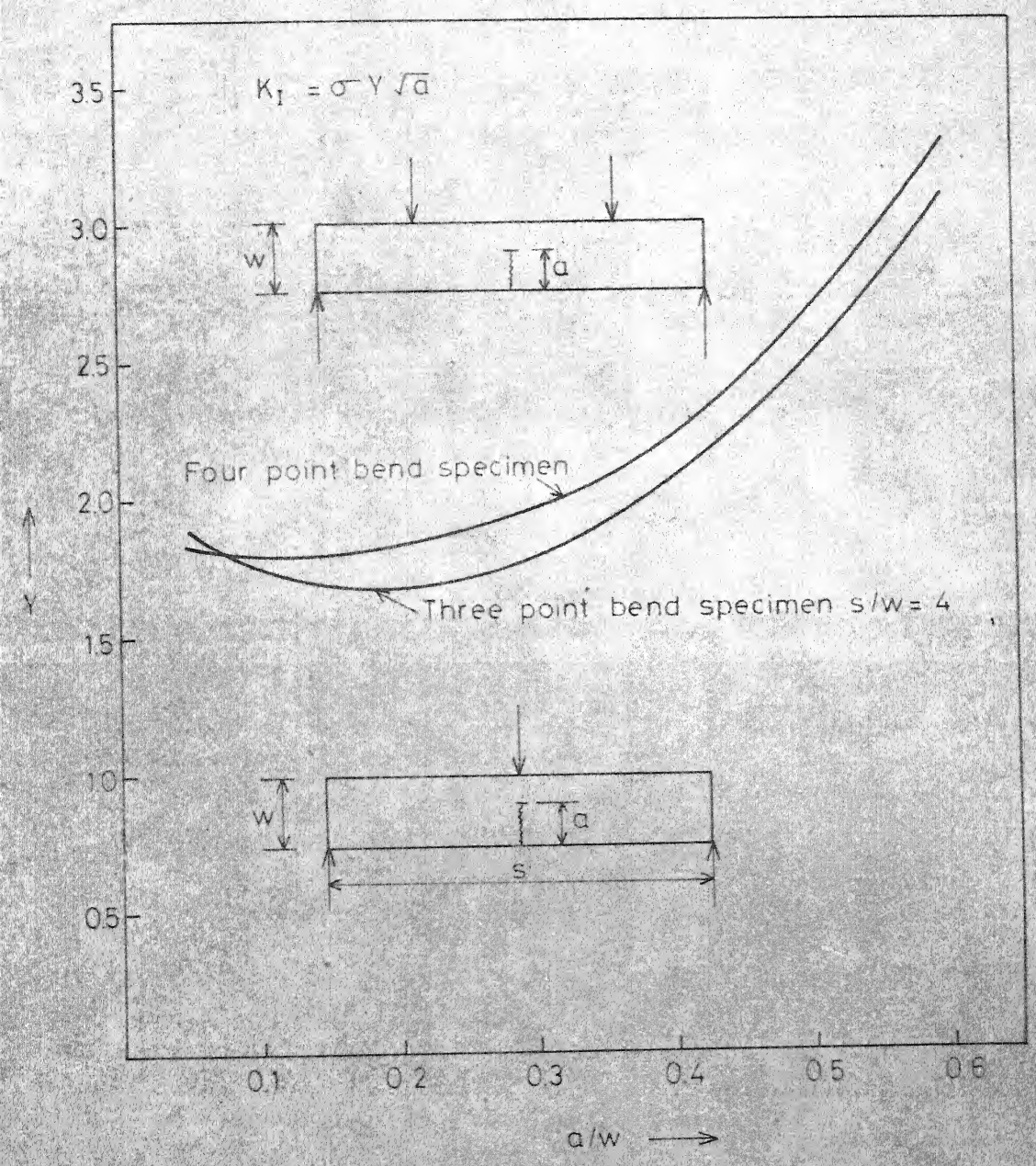

Fig. 2.4 Y Factor for three-point and four-point bend specimens [1]

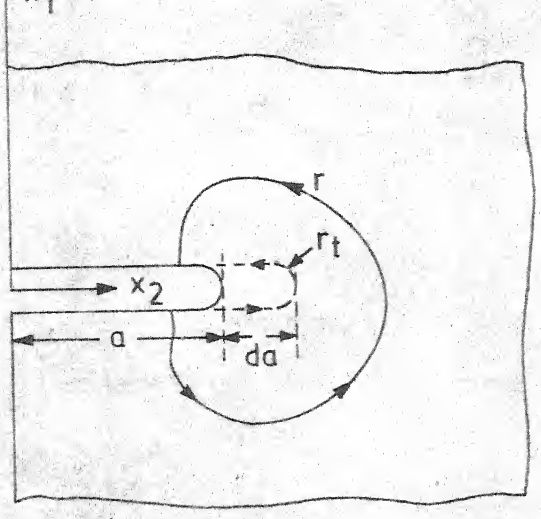

g. 2.5a- Relationship between change in potential energy and line integral.

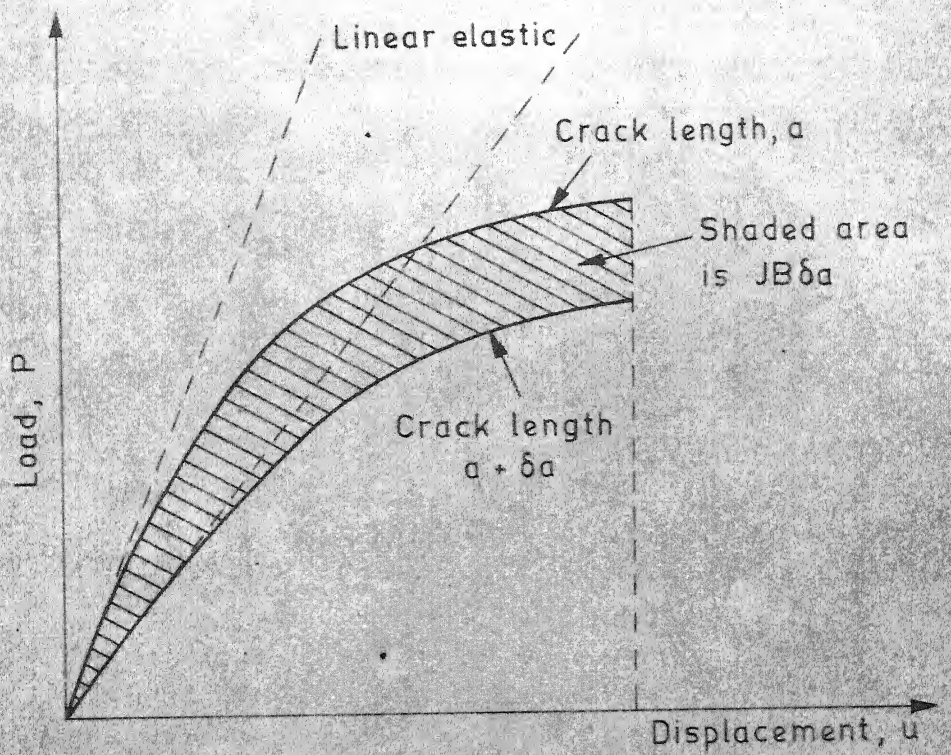

Fig. 2.5b- The J-integral (displacement control)

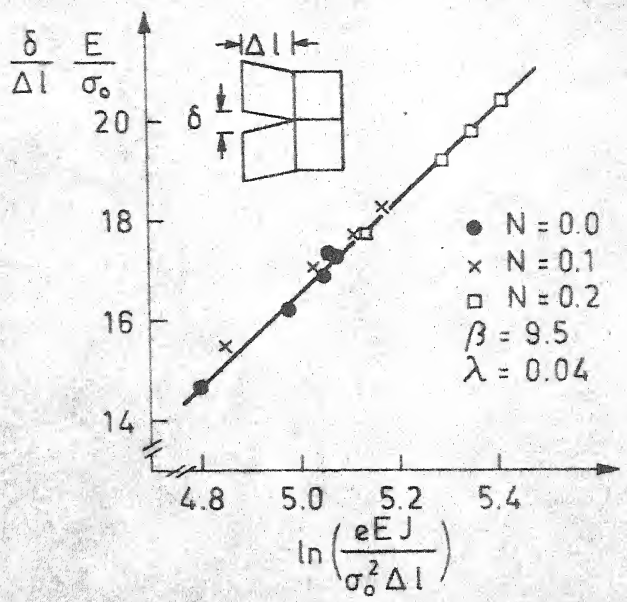

Fig. 2.6a Correlation of crack opening displacement with crack advance at 1st node behind the crack tip in Sorensen's analysis. [43]

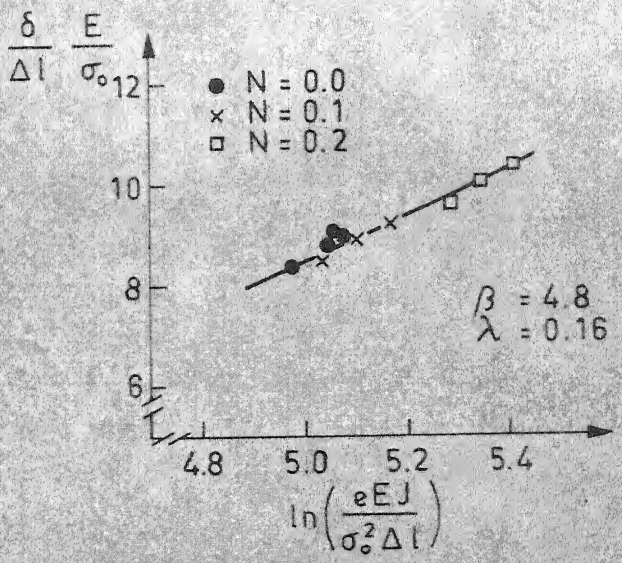

Fig. 2.6b Correlation of crack opening displacement with crack advance at 2nd node behind the crack tip in Sorensen's analysis. Here, the δ represents the additional opening in crack growth by one element spacing. [43]

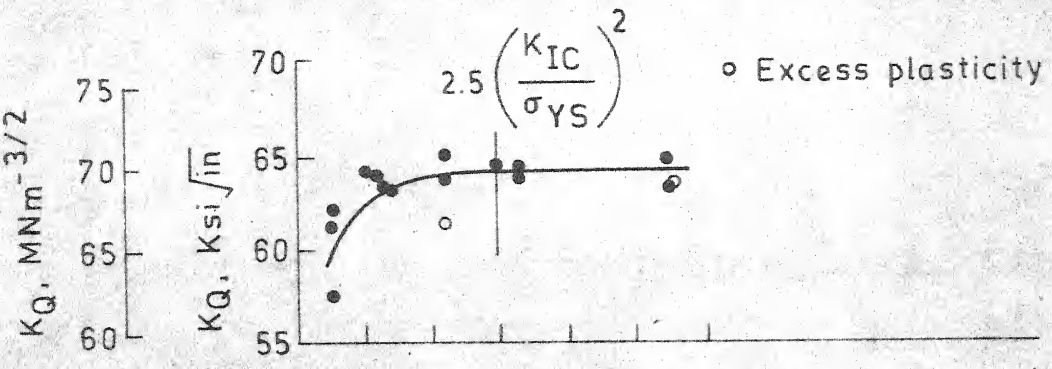

(a) Bend specimen crack length, 0.27 inch (6.9 mm), width, 0.55 inch (13.9 mm).

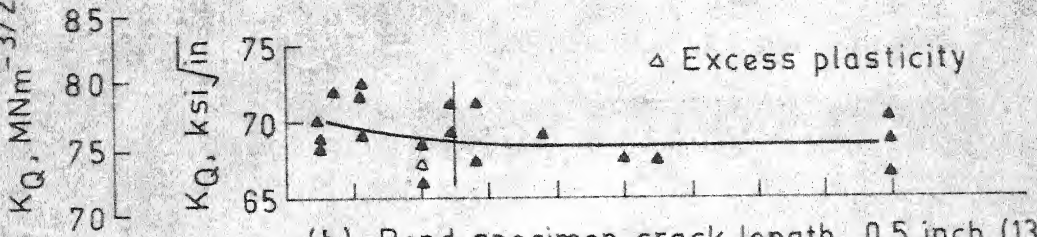

(b) Bend specimen crack length, 0.5 inch (13 mm), width 1.0 inch (25 mm).

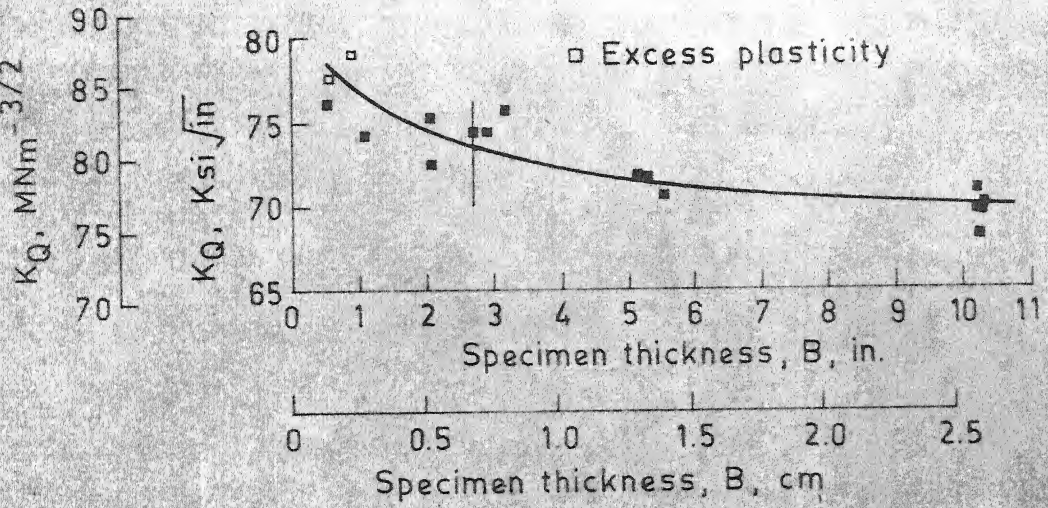

(c) Bend specimen crack length 1.1 inch (27.9 mm), width, 2.2 inches (55.8 mm).

Fig. 2.7 K_Q values as function of specimen thickness for 4340 steel tempered at 750° F (672 K) for 1 hour. Conventional yield strength 213 ksi (1467 MN/m^2). Jones and Brown [14]

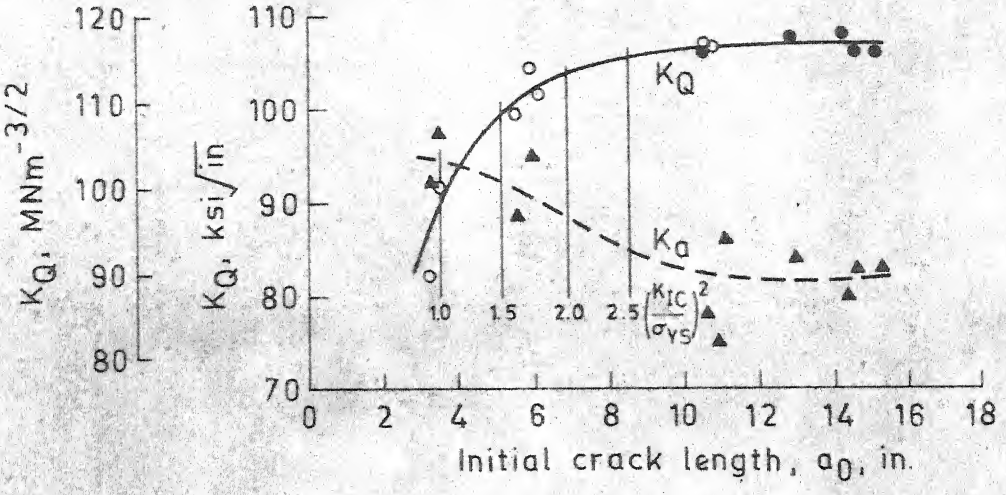

(a) Bend specimen thickness, 1.0 inch (25 mm), width, 2.0 inches (51 mm).

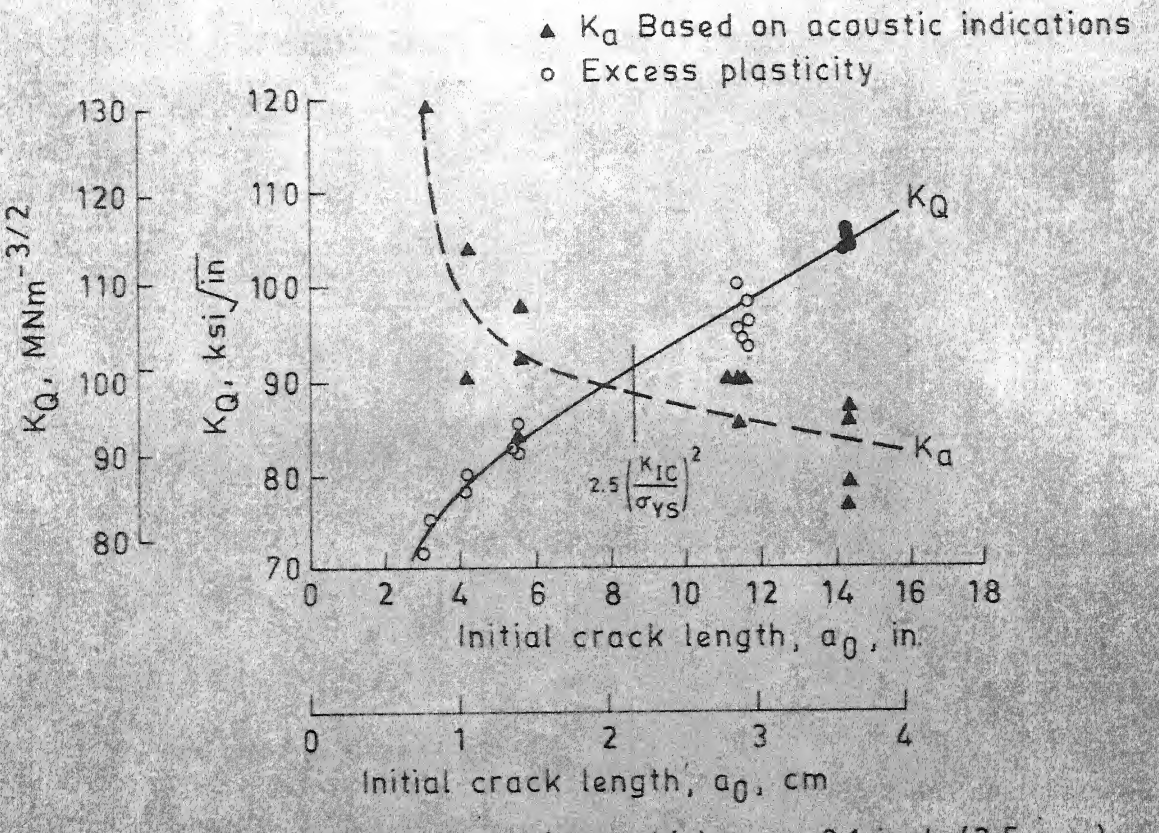

(b) Bend specimen thickness, 0.1 inch (2.5 mm), width, 2.0 inches (51 mm).

Fig. 2.8 K_Q and K_a values as function of crack length for 4340 steel tempered at 925° F (769 K) for 1 hour. Conventional yield strength, 182 ksi (1253 MN/m^2). [14]

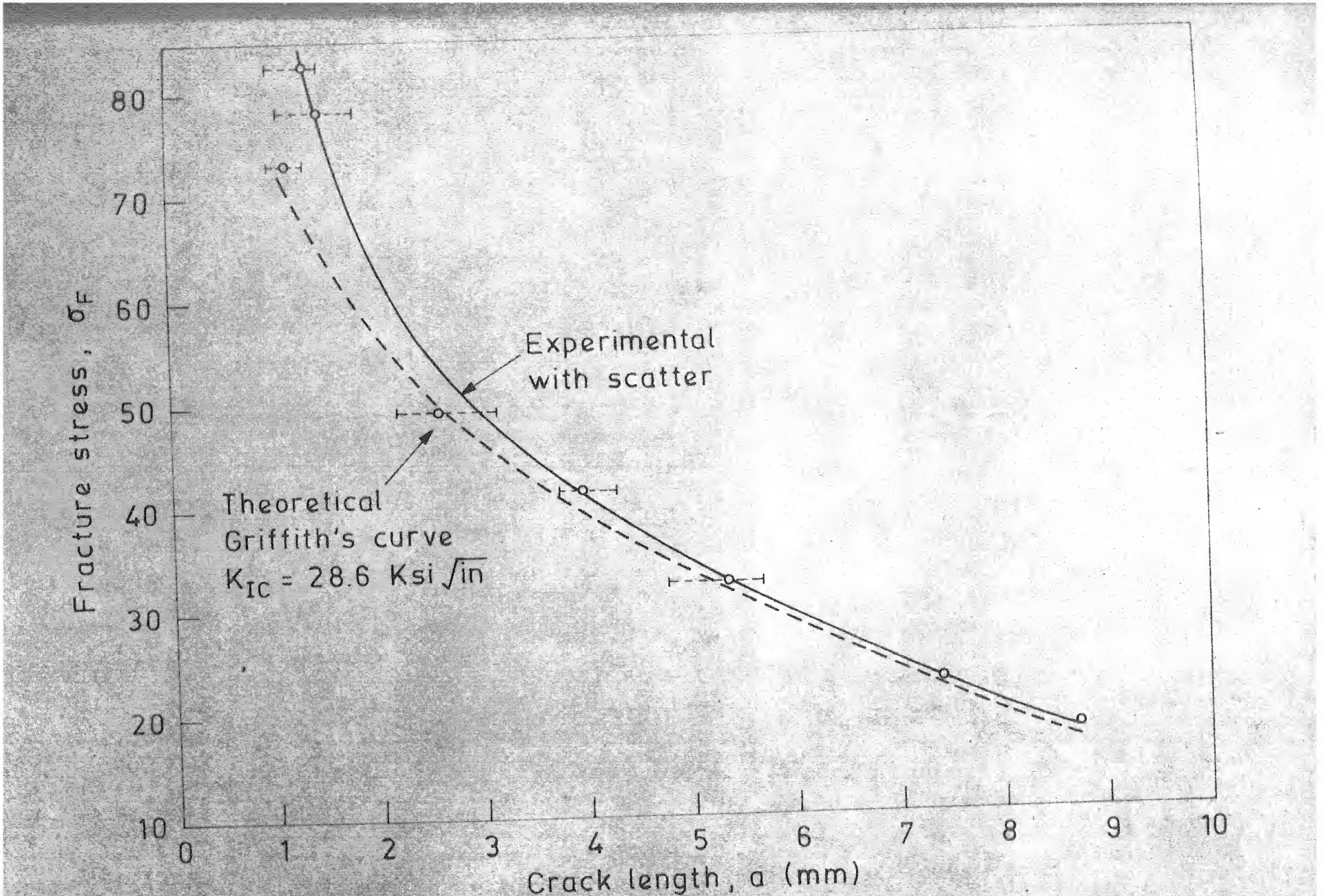

Fig 2.9 Variation of fracture stress against crack length for EN 31 steel gauge plate [17]

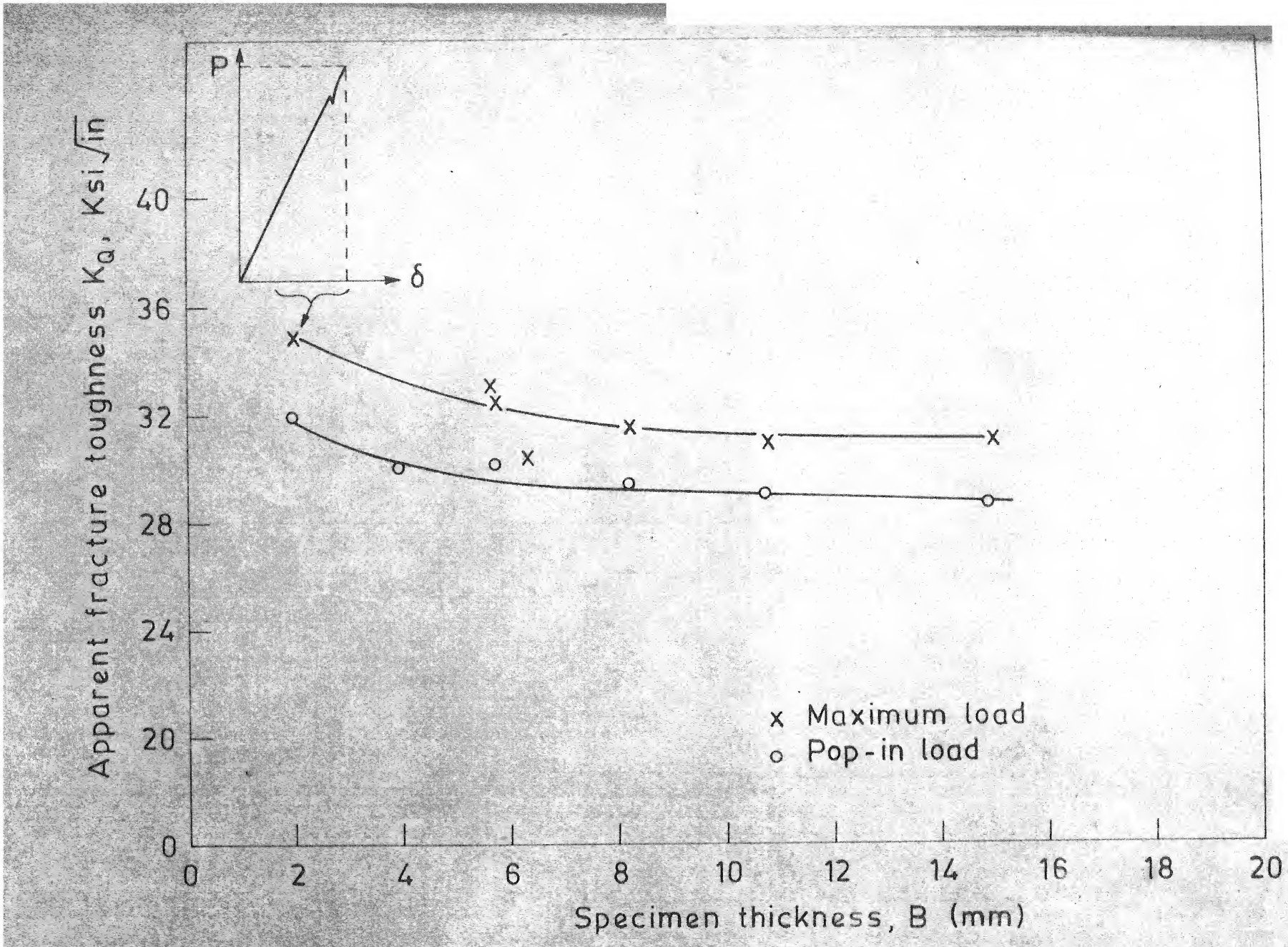

Fig. 2.10 Variation of apparent fracture toughness against specimen thickness for EN 31 steel gauge plate [17]

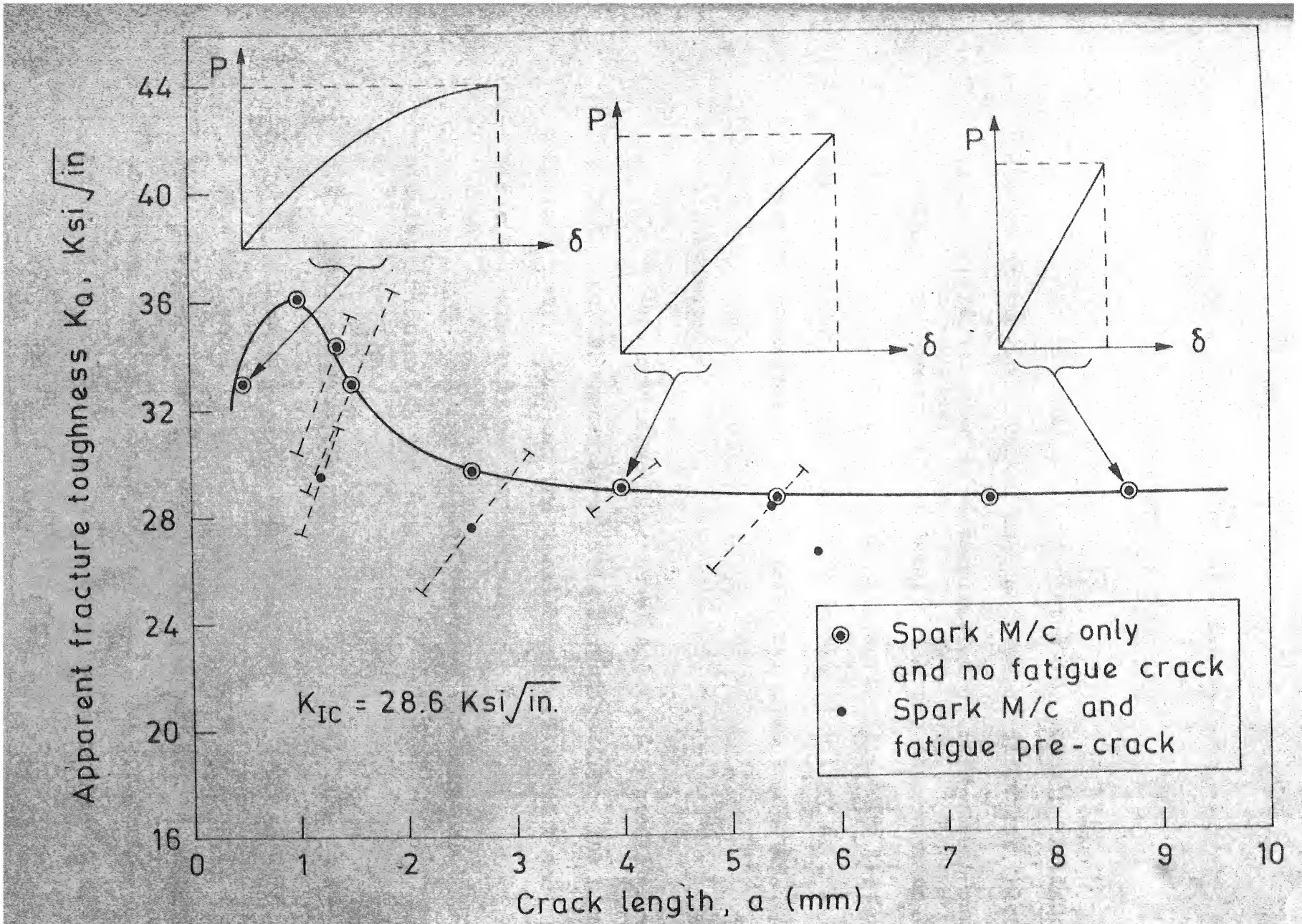

Fig. 2.11 Variation of apparent fracture toughness against crack length for EN 31 steel gauge plate [17]

CHAPTER - III

EXPERIMENTAL PROCEDURE

Experimental work consisted of producing fatigue cracks of varying lengths in specimens of different thicknesses in two different steels, determination of load versus crack opening displacement (COD) data, crack tip observations and determination of plastic zone size during fracture tests of pre-cracked specimens. A study on the stability of a single spherical hole in a Lead-Tin alloy was also conducted.

3.1: Materials:

Two materials (mild steel and 0.6% C steel) were selected for the purpose of this investigation. The composition, grain size and the tensile properties of these materials are reported in Table 3.1.

Lead-Tin (30%) alloy was used for hole growth studies in uniaxial tension.

3.2: Fatigue Pre-cracking:

Beam type specimens of mild steel (242 mm x 50.8 mm x 25.4 mm) and 0.6% carbon steel (242 mm x 29 mm x 25.4 mm) were prepared from the bulk of the two steels. Both mild steel and 0.6% carbon steel specimens, thus prepared, were annealed at 600°C for a period of 4 hours duration. After

the annealing treatment, 45° charpy V-notches were made in the specimens. The details of notch geometry for the two materials are shown in Figures 3.1 and 3.2. In order to remove any residual stresses from milling, all the specimens were further annealed at 250°C for 4 hours. The two side faces of the specimens were finished first by grinding with an abrasive wheel and then using emery papers. Mirror like surfaces were thus obtained. Preparation of the surface, in this manner, was essential in order to make crack-tip observations and plastic zone measurements. Each specimen was fatigued in three point bend test by using a Servo-hydraulic pulsator in order to grow a crack ahead of the V-notch. The maximum and minimum loads of the load-cycles are controlled during fatiguing. During fatiguing, the maximum capacity of the hydraulic jack used was 7273 Kg, whereas the minimum load that could be applied was 800 Kg. Thus, during fatiguing, this minimum load of 800 Kg was maintained constant and only the maximum load was adjusted.

At the beginning, the maximum load to be applied on the specimen was estimated from the measured fracture load in monotonic loading. The maximum load applied on the specimen during fatiguing never exceeded 70% of the yield load. Stress Intensity Factors (SIF) for the maximum and minimum loads were calculated using the following well known expressions

$$K_{max} = 1.5 \cdot \frac{P_{max} \cdot S}{B \cdot W^2} Y \cdot \sqrt{a} \qquad (3.1)$$

and $$K_{min} = 1.5 \cdot \frac{P_{min} \cdot S}{B \cdot W^2} Y \cdot \sqrt{a} \qquad (3.2)$$

where K_{max} = Maximum stress intensity factor

K_{min} = Minimum stress intensity factor

P_{max} = Maximum load

P_{min} = Minimum load

S = Length of support-span

B = Thickness of the specimen

W = Width of the specimen

Y = A calibration factor[1]

a = Length of crack.

Initially by taking the depth of V-notch as the value of a, the SIF was calculated based on Eqn. (3.1) and (3.2). Once a small crack appeared on the tip of the V-notch, the effective crack length would be given by the length of the V-notch plus length of crack appeared.

Based on the values of K_{max} and K_{min}, a chart for P_{max} loads that correspond to constant ΔK was prepared for 0.5 mm interval crack lengths. Accordingly P_{max} was adjusted to maintain the range of stress intensity factor (ΔK) constant, as the crack length increased progressively. Thus, while growing cracks in the specimens, ΔK was kept constant and small as for as possible. In this way, the size of the

plastic zone near the tip of a growing crack was controlled to the minimum possible level. The following ΔK values were found to be suitable during fatigue cracking of the specimens:

(i) For mild steel specimens

$$\Delta K = K_{max} - K_{min} = 103.34 - 22.73 = 80.61 \text{ Kg mm}^{-3/2}$$

(ii) for 0.6% Carbon steel specimens

$$\Delta K = K_{max} - K_{min} = 129.72 - 54.88 = 74.84 \text{ Kg mm}^{-3/2}$$

Several specimens with varying crack lengths over 0.8 mm were thus prepared for this investigation.

The rate of crack growth was 9 to 10 mm per million cycles in both the materials.

3.3: Specimen Preparation for Fracture Tests:

After removing the V-notch, the samples were further fatigued to obtain the final samples for fracture tests(Figure 3.3). Four sets of specimens were prepared for each material. In each set, keeping the thickness B constant, the crack lengths were varied from 0.80 mm to 12.9 mm. Thereby, in each material, for a constant thickness, at least five crack sizes could be tested. The range of thickness was selected from 3 mm to 25 mm. For convenience 3 mm, 6 mm, 10 mm and 25 mm thicknesses were tested in these materials. Crack lengths were measured with sufficient accuracy with a travelling microscope before and after fracture. Figure 3.4 shows the

diagram of the specimens for varying thickness. All the specimen surfaces were carefully polished over a zone near the crack-tip region for crack-tip observations as well as plastic zone size measurements..

3.4: Plastic Zone Measurement by Photoelastic Coating Technique:

The plastic zone size measurement by photoelastic coating technique consists of three stages: (1) preparation of photoelastic specimen for plastic zone measurement, (2) collecting data of fringe size measurement and (3) plotting of the plastic zone sizes from the observed data.

A detailed description of the photoelastic analyser polariser, used for this experiment, and the procedure for the measurement of plastic zone sizes are also presented.

3.4.1: Preparation of Photoelastic Specimens:

After repolishing of the two sides of the specimens with emery papers, a thin sheet of photoelastic sensitive material PS-3B was cemented on one of the side faces of the specimen. This plastic sheet material PS-3B manufactured by Photoelastic Inc. was found to be suitable for post-yielding and crack propagation studies. This is fairly soft compared to other photoelastic plastic materials. It was thus easy to make a fine razor blade cut in this sheet material exactly coinciding with the crack line. Some of the

properties of PS-3B plastic have been listed in the Table 2.1. For cementing this plastic coating on the specimen surface, Araldite was used. Some load was kept over the plastic after cementing it on the specimen surface and curing of 24 hours was adopted in order to have maximum strength between the metallic surface and the coated plastic. To remove any residual stresses in the photoelastic coated material, specimens containing these coatings were annealed in an oven at a temperature of 60°C for 8 hours duration. Specimens were cooled in the oven itself so as to avoid the introduction of thermal stresses in the photoelastic coating material. The coated sheet was then examined for any undesirable residual stress fringes. The plastic coating was then given a fine cut with the help of a razor blade just to coincide with the fatigue crack in the metal specimens. After that, fine lines were marked on the coating surface at different inclinations of 0°, 30°, 45°, 60°, 70° and 90° with respect to the plane of the crack on either side.

3.4.2: Description of Photoelastic Analyzer:

The analyzer, for photoelastic studies, consists of polarizer and analyzer assemblies mounted on a common tripod stand. The analyzer has two colour coated scales for measuring the direction and magnitude of the difference in principal strains using Tardy compensator. A high intensity white light source with built-in internal reflector is fixed

on to the polarizer assembly. A uniform field digital compensator model 232 is fitted to the analyzer assembly. This compensator works on the null-balance principle and is useful for accurate measurement of fractional fringe order in the areas of high strain gradients. Digital records can be converted into fringe orders from calibration graph given in Figure 3.6. Figure 3.7 shows the photographs of Reflection polariscope and Digital compensator.

A telemicroscope is fitted on to the tripod for examining details on the surface of the specimens. There is a provision for attaching a camera to the telemicroscope for taking photographs of isochromatics and isoclinics.

3.4.3: Description of the Procedure for the Measurement of Plastic Zone:

The first and most important thing for the measurement of plastic zone is the determination of the number of digital compensator for the fringe order corresponding to the yielding of the material. For materials obeying Tresca's yield criterion, the corresponding fringe order (N) can be calculated using the following equation

$$N = \frac{\sigma_y}{f \cdot E} \cdot (1 + \nu) \qquad (3.3)$$

where σ_y = Yield strength of the material

f = Fringe constant

E = Young's modulus

ν = Poisson's ratio.

The number on digital compensator for the yielding fringe order of mild steel and 0.6% Carbon steel are 59 and 68 respectively. The corresponding fringe orders for the yielding of the two materials are 0.22 and 0.41 respectively.

A graduated eye-piece was used to measure the length of plastic zone size along different lines marked on the photoelastic coating material. While making the observations, the center line of the graduated eye-piece was made to coincide with the line under observation. Now, the predetermined number corresponding to the fringe order for yielding of the material was set in the digital compensator. With the help of graduated eye-piece the length of plastic zone was measured along each line drawn at different angles. After making the measurement of the plastic zone at a certain load along each line, the load on the specimen was further increased and the observations were repeated. This way plastic zones were measured at different loads.

3.5: Fracture Test Procedure:

A suitable loading fixture (Figure 3.8) was used for three point loading of specimens. The ratio of support span (S) to the width of the specimen (W) was kept at a constant value of 8 for all fracture tests. Three point bend tests were performed in a 5-ton Instron machine under displacement controlled conditions (Figure 3.9). The cross-head speed of 0.02 cm/min was selected for all the fracture tests.

Before the application of load, a clip gauge was mounted on the specimen to measure the crack opening displacement.

A clip-gauge (Figure 3.10) was specially made for this purpose by mounting Rohit strain gauges on the four sides of a U-shaped spring steel sheet. The strain-gauges were cemented and dried for 24 hours under a small load. The clip-gauge was calibrated before each test with the help of a micrometer.

The specimen, with clip-gauge mounted on it, was placed on a loading fixture for the application of load. As the specimen is loaded, the record of load versus Time was obtained from the Instron machine using a chart speed of 2 cm/min. The crack opening displacement was simultaneously recorded by using another recorder to which the output of the clip gauge was fed through a strain indicator. Thus, from simultaneous recordings of load and clip-gauge displacement as a function of time, a load versus crack-opening displacement graph was plotted.

The crack-tip region, for all the specimens, was examined under an optical microscope at various loads by interrupting the loading. Photoelastic plastic zone measurements were also carried out intermittently. Crack-tip region was photographed at different loads in order to compare the behaviour of crack-tip at each load. These observations were repeated at various loads.

3.6: Spherical Hole Growth Experiments in Tension:

(a) Specimen Preparation:

The Lead-Tin alloy was melted and cast in a mould to give a slab of 10 mm thickness. These slabs were then rolled to a thickness of 5 mm. Finally, tensile specimens of required dimensions, as shown in Figure 3.11, were prepared from this rolled material. The specimens were annealed in an oven at a temperature of 100°C for 24 hours. A steel ball indentation of 1.5 mm diameter was used to make a hemispherical / of 0.75 mm radius in a tensile specimen. Two such 5 mm thick tensile specimens were glued together with Araldite to give one spherical hole of 1.5 mm diameter inside a 10 mm thick tensile specimen. Care was taken to see that the two hemispherical holes of the two specimens match well without any offset in the process of cementing them together.

(b) Measurement of Void Growth:

These specimens were loaded in tension in an Instron machine for different strains. 10%, 20%, 40% and 50% elongations were selected for this purpose. Although joining by Araldite of two specimens was not considered to be the best method of creating a void, no delamination of the joining faces was noticed in the range of nominal strain studied. The elongated shapes of the spherical holes were measured on the hemispherical surface by carefully opening

the Araldite joint. The change in the dimensions of the spheroidal hole is measured with sufficient accuracy by a travelling microscope.

TABLE 3.1

Chemical composition and mechanical properties of 0.6% carbon and mild steel

(a) Chemical composition

Material	Composition				
	C	Mn	Si	S	P
0.6% carbon steel	0.60	0.85	1.60	0.02	0.03
Mild steel	0.22	0.87	0.07	0.02	0.02

(b) Grain size and mechanical properties

Material	Grain size (in Microns)	Yield strength (σ_y) (Kg/mm^2)	Ultimate tensile strength (Kg/mm^2)	% elongation	Impact strength (ft-lb)
0.6% carbon steel	30	47.3	77.5	24	2
Mild steel	40	25.6	47.2	34	120

TABLE 3.2

Properties of PS-3B photoelastic coating

K Strain-optic coefficient	Maximum elongation	Modulus of elasticity	Thickness of sheet
0.02	30%	20 Kg/mm^2	2.0 mm

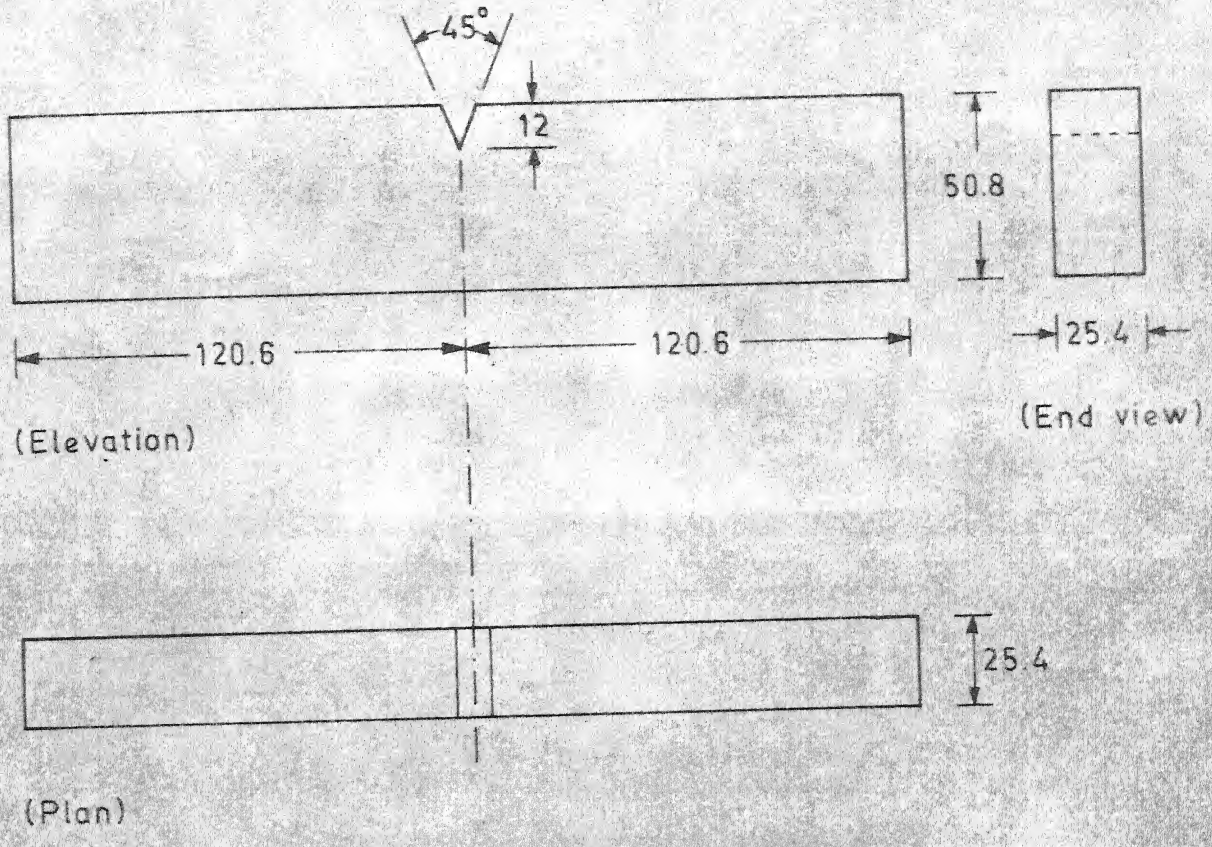

All dimensions in mm

Fig. 3.1 Diagram of mild steel specimen for producing fatigue cracks.

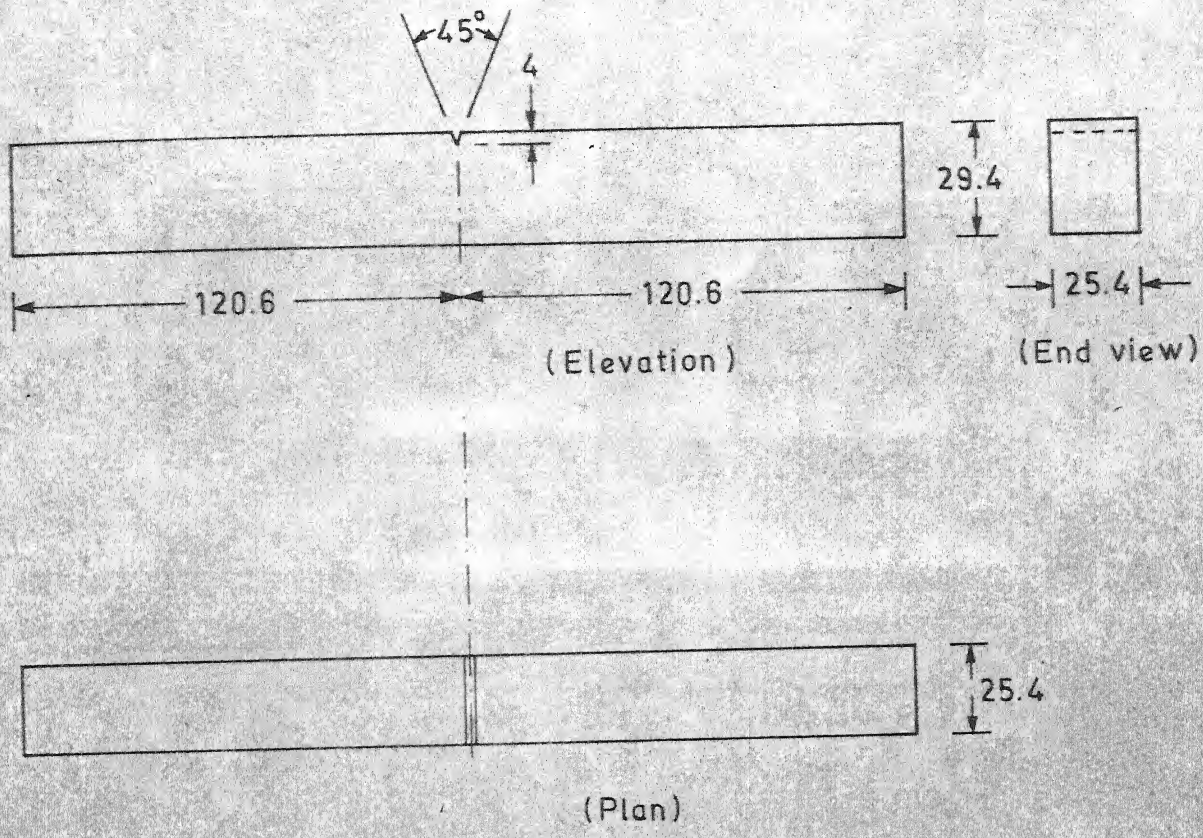

All dimensions in mm

Fig. 3.2 Diagram of 0.6 % carbon steel specimen for producing fatigue cracks.

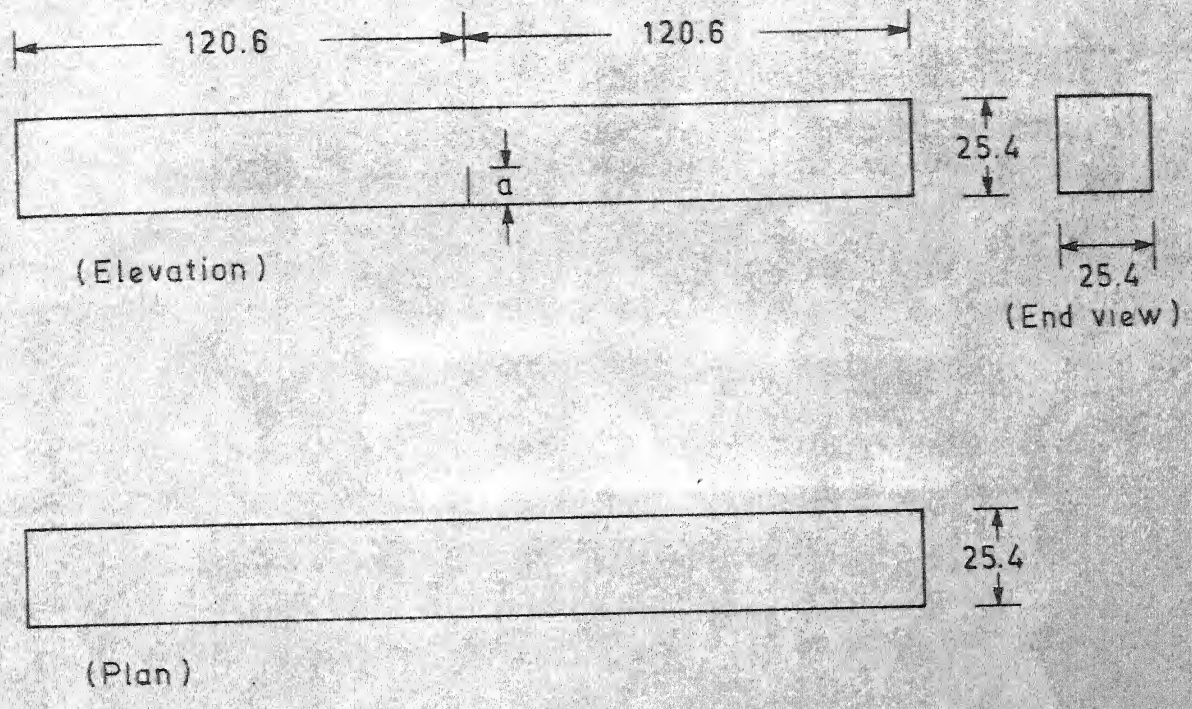

All dimensions in mm

Fig. 3.3 Diagram of fracture test specimen.

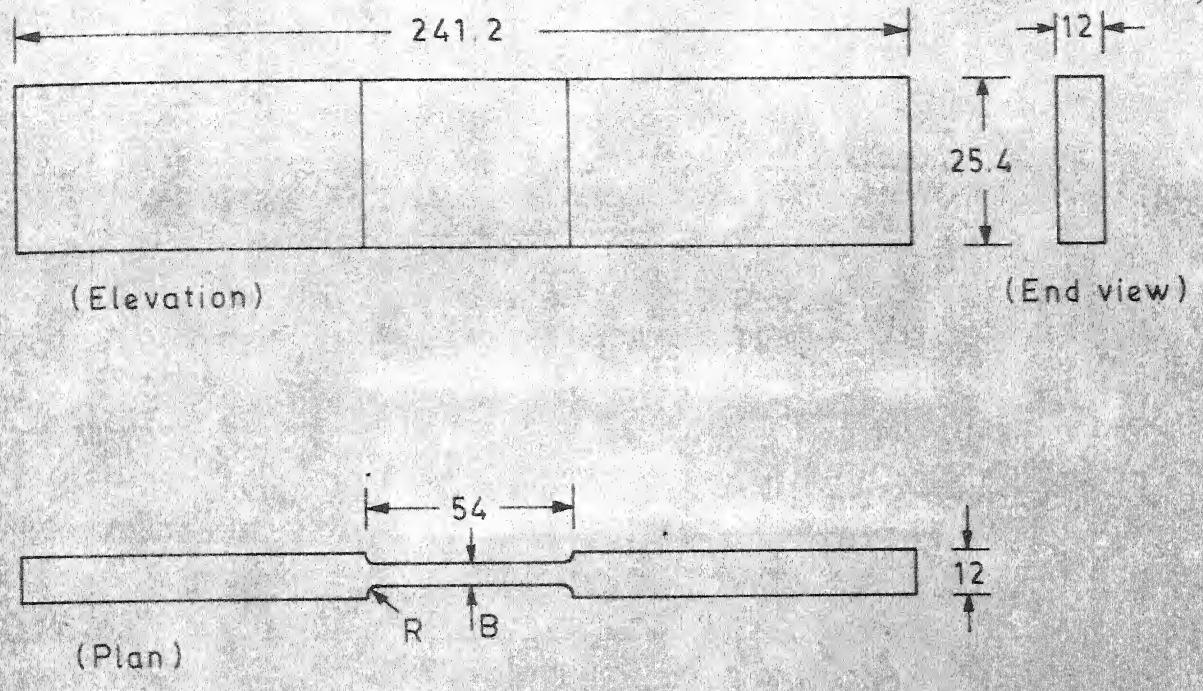

All dimensions in mm

Fig. 3.4 Diagram of specimen with varying thickness B.

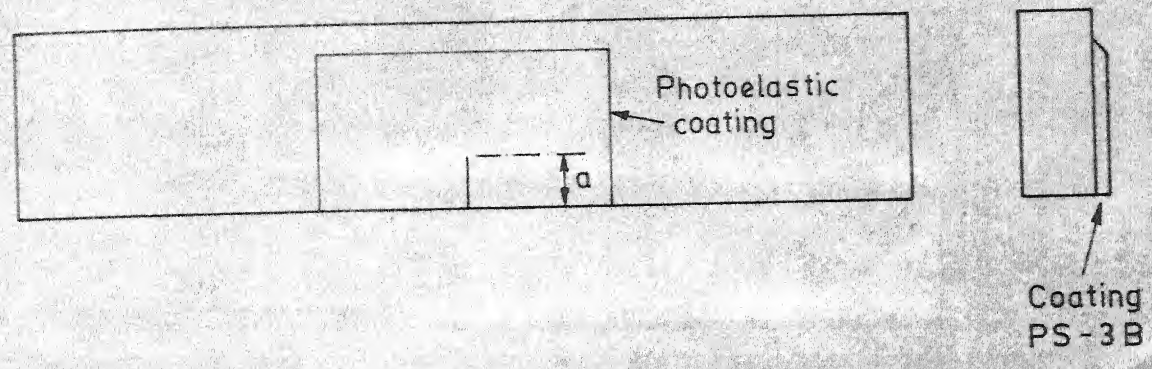

Fig. 3.5 Schematic diagram showing photoelastic coating on metal specimen.

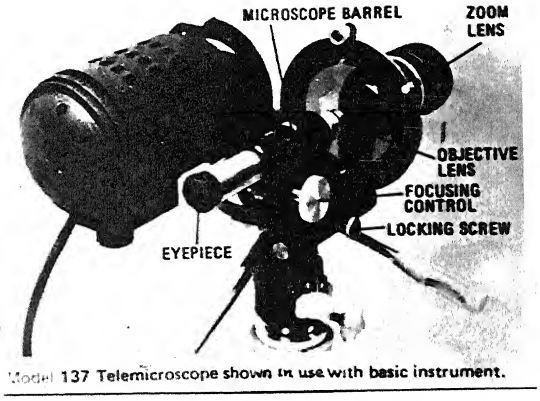

Fig. 3.6: Photograph showing the Reflection Polariscope with attachment.

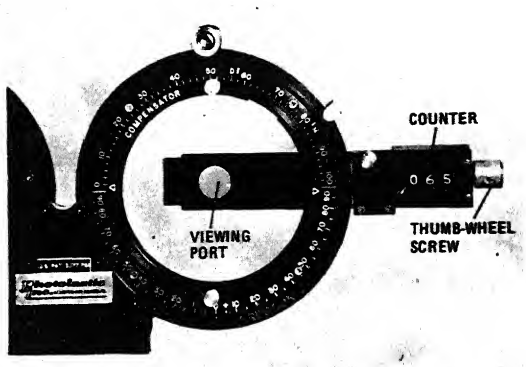

Model 232 Uniform Field Digital Compensator shown attached t
basic instrument.

Fig. 3.7: Photograph for uniform Field Digital Compensator.

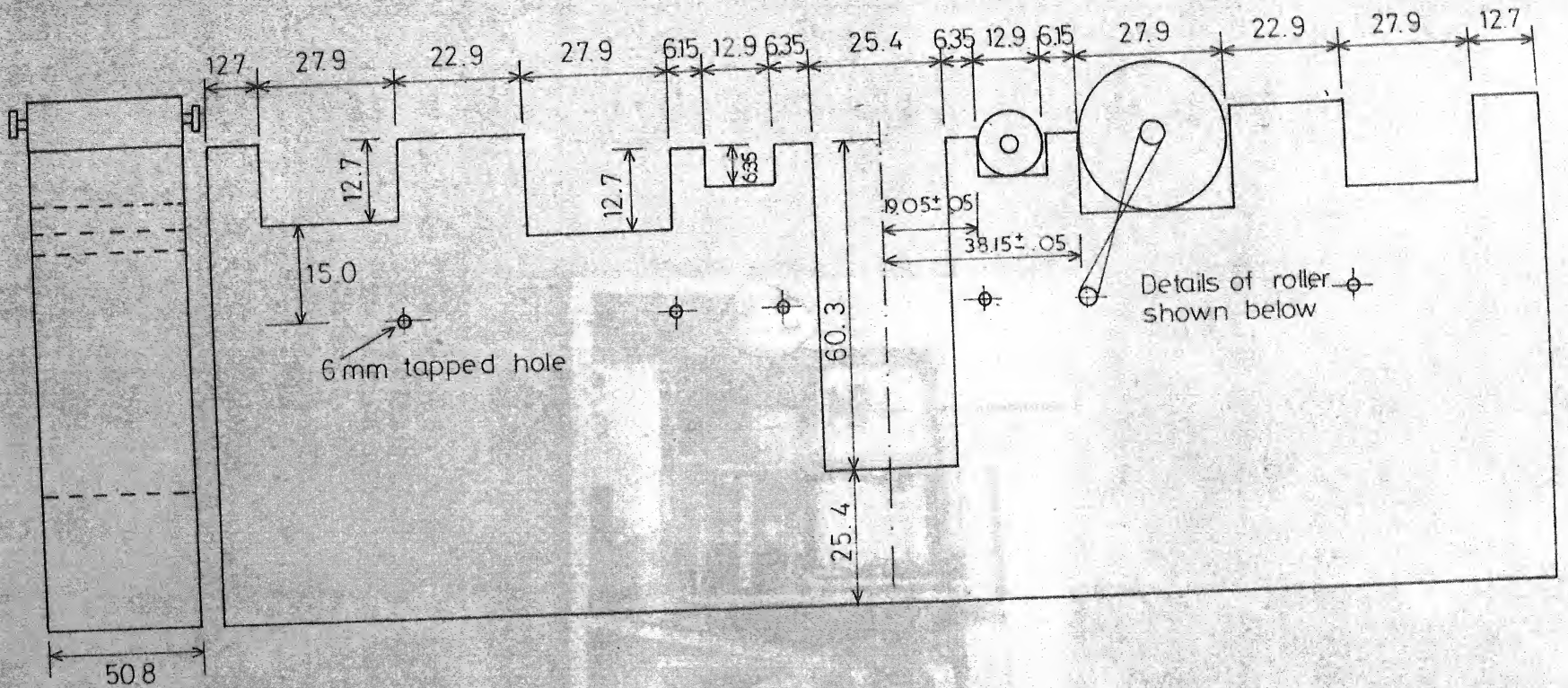

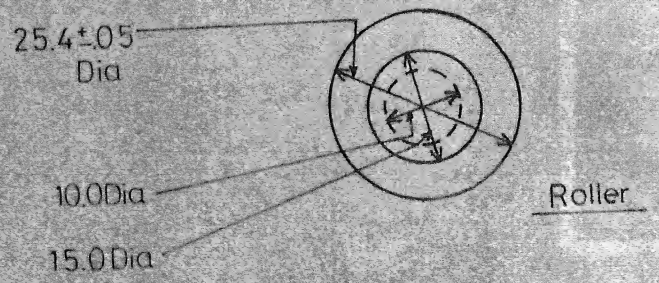

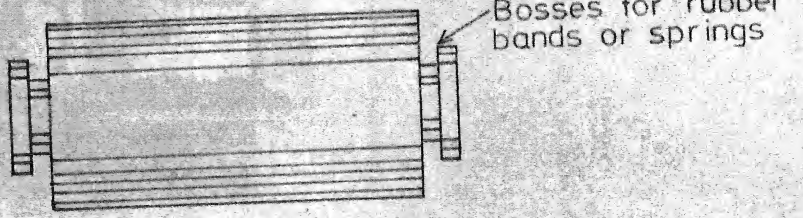

(Dimensions in mm)

Fig. 3.8 Loading fixture

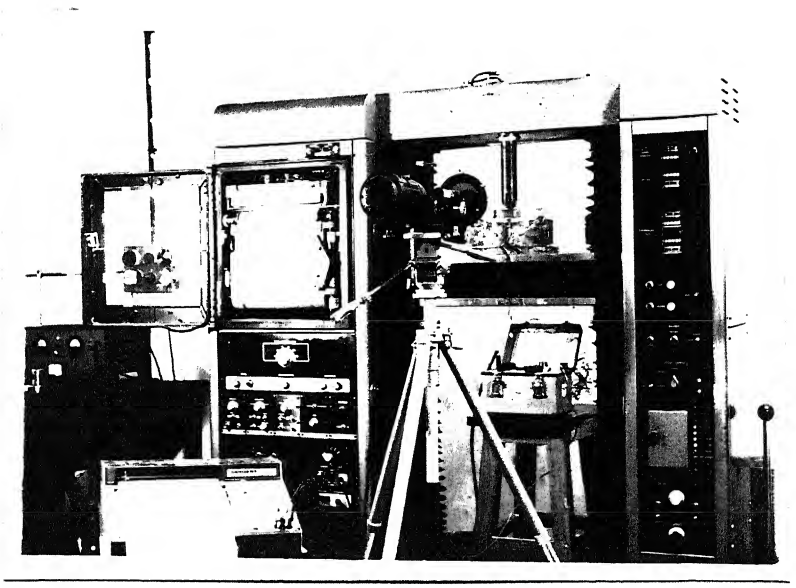

Fig. 3.9: Photograph showing experimental set-up with Reflection Polariscope. Mild steel specimen is loaded in three point bending in an Instron machine.

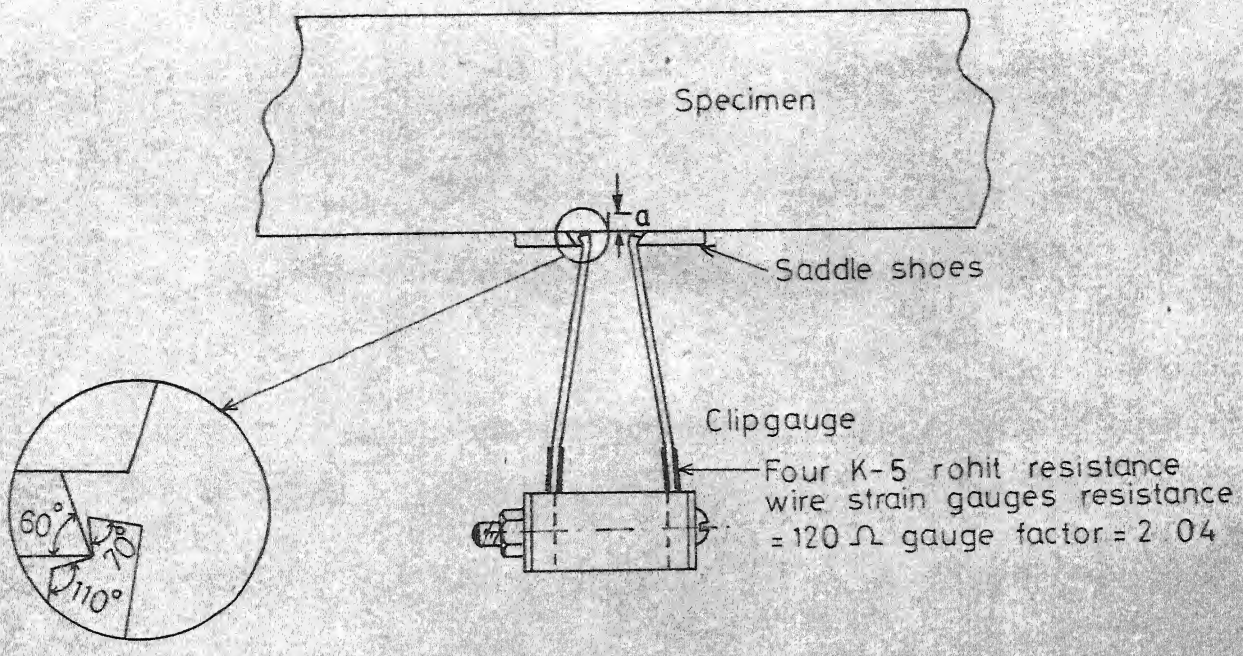

Fig. 3.10-Clip gauge to measure, C.O.D. mounted on three point bend specimen.

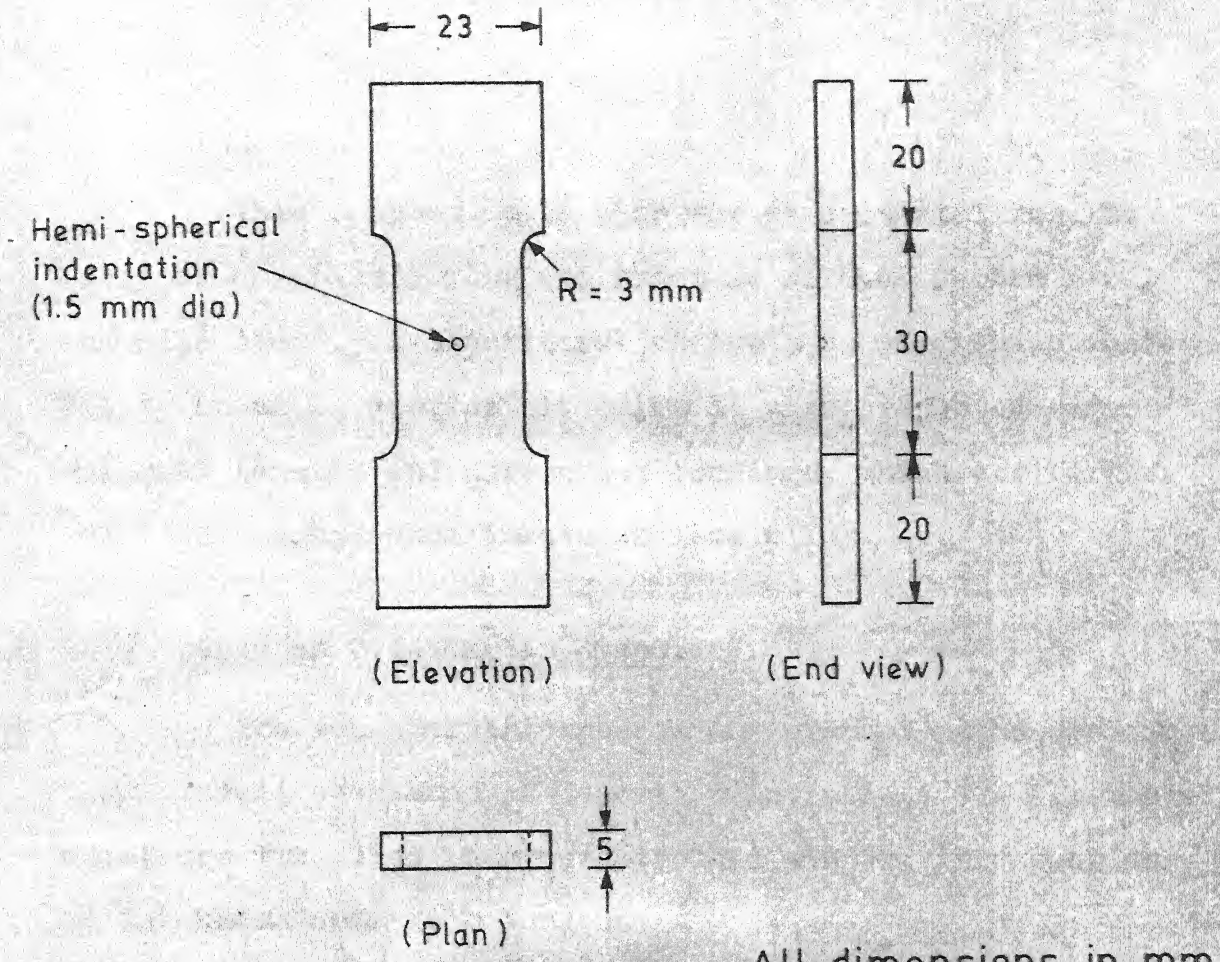

Two such specimens glued together for one ductile fracture test specimen.

Fig. 3.11 Diagram for 5 mm thick tensile specimen used for making ductile fracture test specimen.

CHAPTER - IV

RESULTS

This chapter deals with the experimental results obtained on plastic flow and fracture of 0.6% Carbon steel and mild steel. A theoretical analysis on void shape instability in an incompressible solid is also presented under uniaxial tension and pure shear loadings, which are further verified through experiments on lead alloy.

4.1: Tests on 0.6% Carbon Steel:

The range of thicknesses and crack lengths used in 0.6% C.steel specimens is described in Table 4.1. All tested specimens fractured in a catastrophic manner, irrespective of thickness and crack lengths.

4.1.1: Specimens of 25 mm Thickness:

In this thickness, a set of six specimens with different crack lengths were tested. Load versus clip gauge displacement (CGD) plots upto the point of fracture were observed to be linear for all crack lengths. A typical diagram of load versus CGD plot for specimen with 1.20 mm crack length is shown in Figure 4.1. The crack-opening and the plastic zone size, for specimens of 25 mm thickness, were found to be very small compared to the thinner samples.

4.1.2: Specimens of 10 mm Thickness:

Four specimens with crack lengths 0.80, 1.70, 2.65 and 4.70 mm were tested for this thickness. All the specimens, except that of 0.80 mm crack length, exhibited a linear variation of load versus CGD plot, whereas a non-linear behaviour was the typical characteristic of 0.80 mm crack length specimen. The load versus CGD plots for 1.70 and 0.80 mm crack length specimens are shown in Figures 4.2 and 4.3 respectively. Figures 4.4 and 4.5 show the photographs of the crack-tip region and the plastic zone at 650 Kg load of specimen with 1.70 mm crack length. From these figures it can be noted that crack opening and the size of the plastic zone are very small even at the fracture load.

4.1.3: Specimens of 6 mm Thickness:

It was observed that specimen with crack lengths 2.50 mm (Figure 4.6) and 4.30 mm show a linear behaviour in the load versus CGD record, whereas in the case of specimens with crack lengths of 1.53 mm (Figure 4.7) and 0.94 mm (Figure 4.8) the load versus CGD records are non-linear. For 2.5 mm crack length specimen, the size of the plastic zone was measured at various loads. It is observed that although the load versus CGD record is linear upto fracture for this specimen, there is an appreciable size of plastic zone formation well below the fracture load. Figure 4.9 shows the size of plastic zone plotted at different applied

loads for 2.5 mm crack length. The plastic zone sizes for other specimens of this thickness were measured. Plastic zone sizes at various loads for 1.53 mm crack length specimen are shown in Figure 4.10.

4.1.4: Specimens of 3 mm Thickness:

For this thickness, all specimens, except the largest crack length of 4.97 mm, showed a non-linear behaviour in load versus CGD record. Figure 4.11 shows such plots for crack lengths of 4.97 mm. Figure 4.12 shows the photographs of the crack-tip behaviour at 140 and 250 Kg loads for 4.97 mm crack length specimen. Such short cracked thin specimens show an appreciable amount of crack opening before catastrophic failure. The corresponding isochromatic fringes of plastic deformation at these loads are shown in Figure 4.13. Plastic zone sizes measured are presented in Figure 4.14.

Figure 4.15 shows the load-CGD record for 2.30 mm crack length specimen. The crack-tip deformation at loads of 140 Kg, 274 Kg and 307.5 Kg for this specimen is presented in Figure 4.16. Figure 4.17 shows the plotted plastic zone sizes at these loads. Photograph of the plastic zone fringe at 274 Kg load is shown in Figure 4.18. The degree of non-linearity in load versus CGD plot is observed to be maximum for 1.30 mm crack length specimen compared to other samples (Figure 4.19). The crack-tip deformation of this specimen at 335, 400 and 412.5 Kg loads is shown in Figure 4.20.

Thus, the fracture test results of 0.6% C steel specimens are summarized as follows:

All the specimens with 25 mm thickness show clearly linear behaviour in load versus CGD record upto the point of fracture, whereas specimens having thickness of 10 mm or less show a deviation from linearity, especially for short cracks. The degree of non-linear deformation before fracture is more for thin specimens with short cracks.

4.1.5: Plasticity Spread Along 0° and 45° Plane:

The spread of plastic zone along 0° and 45° plane with respect to the plane of the crack was plotted against the load for different specimens. Plastic zones along 0° plane versus σ/σ_y records for 6 mm thick specimens are shown in Figure 4.21 whereas Figure 4.22 shows the size of the plastic zone along 45° plane at various σ/σ_y values. The change in plastic zone size due to load increase is gradual for all the specimens of 6 mm thickness. Figure 4.23 shows the variation of the length of plastic zone along 0° plane against σ/σ_y, whereas Figure 4.24 shows the size of the plastic zone along 45° plane against σ/σ_y for 3 mm thick specimens. The change of the plastic zone size is more abrupt along 0° and 45° plane for 3 mm thick specimens.

4.1.6: Effect of Crack Length on Apparent Fracture Toughness and Fracture Stress:

Apparent crack toughness (K_Q) of a material has been calculated using the following expression

$$K = 1.5 \cdot \frac{P \cdot S}{B \cdot W^2} \cdot Y \cdot \sqrt{a} \qquad (4.1)$$

where P = the load at the onset of fracture

S = length of the support span

B = thickness of a specimen

W = width of a specimen

Y = a calibration factor[1]

a = fatigue crack length of specimen

Figure 4.25 shows the variation of apparent crack toughness of 0.6% C steel with crack length. Due to certain experimental difficulties, a perfect uniform crack length over the thickness was not possible to obtain in all the fatigue pre-cracked samples. The spread in the experimental points in Figure 4.25 represents the calculated values corresponding to average and maximum crack lengths. Apparent crack toughness (K_Q) approaches a constant value of 150 $(Kg/mm^2)\sqrt{mm}$ when the length of the crack is sufficiently long. This asymptotic value of K_Q is taken as the plane strain crack toughness (K_{Ic}) property of 0.6% carbon steel. The observed value of K_Q goes up by either decreasing the crack length or by reducing the thickness or a combination

of both. A decrease in K_Q value can be noticed if the crack length is too short.

In three point bend tests, the nominal fracture stresses were calculated using the following expression

$$\sigma_F = 1.5 \cdot \frac{P \cdot S}{B \cdot W^2} \qquad (4.2)$$

where P = the load measured at the onset of fracture

S = length of support span

B = thickness of specimen

W = width of specimen.

The fracture stress, which is equal to the nominal bending stress for uncracked beams, was plotted against crack lengths. Figure 4.26 shows the nature of variation for fracture stress of 25 mm and 10 mm thick specimens. Griffith's fracture stress, calculated on the basis of $K_{Ic} = 150 (Kg/mm^2)\sqrt{mm}$ is shown in Figure 4.26 by a dashed line. It was observed that for 25 mm and 10 mm thick specimens, the fracture stress versus crack length line coincided with the Griffith's fracture stress beyond a crack length of approximately 2.5 mm. The fracture stress was found to increase continuously by decreasing the crack length in the case of 10 mm thick specimens. For 25 mm thick specimens, the fracture stress was increasing with the reduction in crack length except for a very short crack. Similarly, plots of the fracture stress for 6 mm and 3 mm

thick specimens against the crack length are presented in Figures 4.27 and 4.28 respectively. From these plots, it is clear that the fracture stress keeps on increasing as the crack length is decreased. A further decrease in crack length causes the tendency for fracture stress to remain constant. For specimens which showed non-linear deformation before fracture, the stresses at the point of deviation from linearity (LEFM), 5% secant load and maximum loads as well as the corresponding K_Q values were calculated and shown in the respective plots. Whenever there is a non-uniformity of crack length over the thickness, the two extreme values consisting of average and maximum crack lengths of the specimen has been considered for fracture stress and K_Q calculations.

4.1.7: Comparison of Apparent Toughness Values Obtained by Different Methods:

K_Q values were calculated based on (a) Linear Elastic Fracture Mechanics (LEFM) SIF approach given by ASTM (b) Irwin-McClintock's plasticity correction on crack length (c) Equivalent energy method[51] and (d) Critical crack opening displacement criterion.

The K_Q value was calculated by taking loads corresponding to 5% secant, 10% secant and the maximum value from Equation (4.1).

If the plastic zone size is small on the plane of the crack, compared to the length of the crack, a modified

crack length of $a + \gamma_p$ was taken instead of 'a' only. So, according to this method, the apparent toughness will be

$$K_Q = \sigma \cdot Y \cdot \sqrt{a + \gamma_p} \qquad (4.3)$$

where γ_p is the size of the plastic zone along the plane of the crack.

Table 4.2 shows the values of K_Q calculated by the above methods.

The apparent toughness, K_Q, was also calculated based on the equivalent energy method introduced by DeWitt and further modified by Chell, Milne and Kirby. The total area under load-COD diagram and the area under the linear portion of load-COD diagram were measured by a planimeter. So, the equivalent K_Q from this procedure is given by apparent crack toughness for the maximum linear load

$$\times \left(\frac{\text{Total area under load-COD diagram}}{\text{Area under the linear portion of load-COD diagram}}\right)^{1/2}$$

Crack opening displacement (COD) values at the fracture load was obtained with the help of load-CGD plot. The COD(δ) was calculated from the load-CGD plot using the following equation

$$B_o + B_1 \, COD + B_2 \, COD^2 + B_3 \, COD^3 + B_4 \, COD^4 = 0 \qquad (4.4)$$

where

$$B_o = 0.04271 \, CGD$$

$B_1 = 0.09391\ CGD - \left(\frac{a + Z}{W - a}\right) - 0.04271$

$B_2 = -0.009313\ CGD - 0.09391$

$B_3 = 0.0003678\ CGD + 0.009313$

$B_4 = -0.0003678$

a = Crack length

Z = height of the knife edge above specimen surface

W = specimen width

The apparent toughness is calculated from the COD values using the formula

$$G_{I_Q} = \sigma_Y \delta_c \quad \text{-- for plane stress}$$

and

$$G_{I_Q} = \alpha \sigma_Y \delta_c \quad \text{-- for plane strain} \qquad (4.5)$$

where K_Q can be obtained from G_{I_Q} through Eqn. (1.4).

Table 4.2 shows these calculations on apparent toughness by COD and energy methods.

4.2: Mild Steel:

Mild steel specimens with four different thicknesses were investigated in this section. The range of thicknesses and crack lengths considered for this material is indicated in Table 4.3. No catastrophic fracture was noticed in any of the tests of this material.

4.2.1: Specimen of 25 mm Thickness:

In this thickness, seven specimens with different crack lengths were studied. Some typical plots of load versus CGD are presented.

Figure 4.29 shows the load versus CGD record for a specimen with crack length of 11.57mm. The deviation in linearity occurs around 650 Kg load. Figure 4.30 shows the deformed crack tip region at 300, 695 and 700 Kg loads. By increasing the load successively from 300 to 700 Kg, it is observed that the crack tip deformation is enormous and crack opening is significant. The isochromatic fringe pattern at the crack tip corresponding to 700 Kg load is shown in Figure 4.31. The plot of plastic zone size, shown in Figure 4.32 was measured at different loads for this specimen.

Figure 4.33 shows the load versus CGD plot for the specimen with crack length of 4.45 mm. This specimen shows linearity upto 1290 Kg load, while the specimen was loaded upto 1600 Kg load. The plastic zone size was measured mostly in the linear range. Figure 4.34 shows the plot of plastic zone sizes at different loads. It is observed that the plastic zone sizes are small in the linear range. Similarly, Figure 4.35 shows the load versus CGD plot for a specimen of 2.26 mm crack length. The plot of plastic zones measured at various loads is shown in Figure 4.36, while the fringe photograph at 1860 Kg load is presented in Figure 4.37. The plastic zone is quite large and there is an appearance of even second order fringe for this specimen.

4.2.2: Specimens of 10 mm Thickness:

Eight specimens in this thickness were investigated. The load versus CGD plots for specimens with longest and shortest crack lengths have been presented. Figure 4.38 shows the load versus CGD record for a crack length of 12.9 mm which is the longest crack length in this thickness range. This specimen was loaded upto 277 Kg. Plastic zone size was measured at different loads. The plot of plastic zone sizes is shown in Figure 4.39. The plot of load versus clip gauge crack opening displacement for the shortest crack length is presented in Figure 4.40. It may be noted from this plot that considerable increase in clip gauge displacement occurs without much increase in load beyond the point of deviation from linearity.

The crack-tip deformation and the plastic zone fringe photograph for this specimen are shown in Figures 4.41 and 4.42 respectively. Measured plastic zone sizes at the crack-tip for different loads are given in Figure 4.43.

4.2.3: Specimens of 6 mm Thickness:

In this thickness, three plots of load versus clip-gauge crack opening displacement record have been presented. Figure 4.44 shows the load versus clip gauge displacement for the longest crack length (12.5 mm) for this thickness. The specimen was loaded upto 180 Kg load, whereas deviation from linearity in load versus CGD plot

occurred at 132 Kg load. The size of the plastic zone is observed to be very small in the linear part of load versus CGD plot but in the non-linear range, it increased considerably. Figure 4.45 shows the plotted plastic zones at various loads.

The plot of load versus clip gauge displacement (CGD) for 6.65 mm crack length specimen is presented in Figure 4.46. Crack-tip deformations at various loads are shown in Figure 4.47. As the load on the specimen is increased, more and more blunting of crack-tip is noticed. The observed fringe photographs for this specimen at 310 and 332.5 Kg are given in Figure 4.48 whereas experimentally observed plastic zones at the crack-tip for different loads have been plotted in Figure 4.49. This specimen has shown 3rd order fringe at the maximum applied load of 332.5 Kg.

The load versus CGD plot for a specimen of 6 mm thickness and 3.78 mm crack length is given in Figure 4.50. Crack tip deformation at 330, 394 and 410 Kg loads is shown in Figure 4.51. At loads beyond the point of deviation from linearity in the load versus CGD plot, the crack tip deformation blunting and the resultant crack opening displacement are the dominant features. A typical photograph of the isochromatic fringe corresponding to a load of 410 Kg is shown in Figure 4.52, where even a third order fringe can be noticed. The plotted plastic zones at various loads for this specimen are given in Figure 4.53.

4.2.4: Specimens of 3 mm Thickness:

Five specimens of varying crack lengths in the range of 12.85, 5.20 and 2.20 mm were tested in the category of 3 mm thickness.

Figure 4.54 shows the plot of load versus clip gauge crack opening displacement for the specimen with the maximum crack length of 12.85 mm. Crack tip deformations at 70, 85 and 93 Kg loads and isochromatic fringes at 85 and 93 Kg are given in Figures 4.55 and 4.56 respectively. Plastic zones measured at various loads are plotted in Figure 4.57. Below the maximum linear load the measured plastic zone is small but the size of the plastic zone increases considerably at higher loads. The load versus clip gauge crack opening displacement record for the specimen with crack length of 5.2 mm is shown in Figure 4.58. The crack tip observations at different loads are shown in Figures 4.59. No crack tip deformation in observed upto the maximum linear load. However, at higher loads, the crack tip deformation is seen to increase progressively (Figure 4.59). It can be seen from Figure 4.60 that at smaller loads, well within linear range, the size of plastic zone is small and the plasticity spread is maximum along 45° plane. At higher applied loads of 130, 160 and 170 Kg, the size of plastic zone keeps on increasing and the maximum spread of plastic zones tries to shift from 45° plane to 30° plane of the crack. Further, an abrupt increase in the length of

plastic zone along the plane of the crack may also be noted when the load is increased from 130 Kg to 160 Kg.

Figure 4.61 shows the load versus CGD plot for the specimen of shortest crack length of 2.20 mm. Unlike other specimens, the plastic zone is found to be relatively large even at loads smaller than maximum linear load. It is observed that there is a sudden increase in the size of plastic zone along the plane of the crack (Figure 4.62) when load on the specimen is increased from 190 Kg to 220 Kg.

The results of mild steel specimens are summarized as follows:

(i) All the mild steel specimens show extensive non-linear behaviour in load versus clip-gauge displacement plots, without showing any catastrophic failure.

(ii) Specimens show a large plastic deformation at the crack-tip region along with heavy blunting at loads higher than the maximum linear load.

(iii) The size of the plastic zone increases continuously with the increase of load on the specimen. But at loads near the maximum linear load, the increase in size of the plastic zone is abrupt.

(iv) Thin specimens (of the order of 3 mm) exhibit a larger plastic zone size compared to thicker samples.

4.2.5: Plasticity Spread Along 0° and 45° Plane:

The plasticity spread along 0° and 45° planes with respect to the plane of the crack, for all the thicknesses of the specimens, were measured against different stress levels. Figure 4.63 shows some typical plots giving the variation of the plastic zone size on the plane of the crack against different loads for various crack sizes in 10 mm thick mild steel specimens. It may be seen from Figure 4.63 that the plasticity spread along the plane of the crack abruptly increases at some critical load for all crack lengths. Similar behaviour is noticed for specimens of 3 mm thickness (Figure 4.64).

The plasticity spread along 0° plane for 25 mm thick specimens is smaller than the spread along the 45° plane. Figures 4.65 and 4.66 show the plasticity spread on 45° plane against different loads for specimens of 25 mm thickness and 10 mm thickness respectively. An abrupt change in plastic zone size at some critical load may also be noted here.

Figure 4.67 shows the plasticity spread along 45° plane against different loads in the case of 3 mm thick specimens.

Figure 4.68 shows the variation of plasticity spread on 0° plane against specimen thickness at a constant stress level for a given crack size of 5.20 mm. It can be

noted that the plasticity spread along 0° plane increases with the decrease of the thickness of the specimen for a given crack length and stress. Similar plot is shown in Figure 4.69 for a crack length of 2.20 mm.

4.2.6: Effect of Crack Length and Specimen Thickness on Maximum Linear and Secant Shift Loads:

Based on ASTM approach of the stress intensity factor, K_I and $(\sigma_{nom.})_{bending}$ are calculated for this material at the maximum linear load, 5% and 10% secant shift loads.

The variation of the stress intensity factor, K_P, against crack length is shown in Figure 4.70 for different thicknesses. This shows an increase in the stress intensity factor with a decrease in crack length from a constant asymptotic value for thicker sections over 10 mm. For longer crack all the tested samples of varying thickness show a constant value of the stress intensity factor. Decrease in crack length causes a slight increase of the SIF values. On the contrary, with further decrease in crack length the stress intensity factor is seen to decrease for all the thicknesses.

The asymptotic value is found to be around 103 $(Kg/mm^2)\sqrt{mm}$ and this K_{Ipc} value has been taken as the equivalent to a "local K_{Ic}".

The nominal stress was calculated from Eqn. (4.2) based on maximum linear load, 5% and 10% secant loads. As there was no catastrophic failure or any fast crack growth

on the free surface upto 10% offset load, to understand the loss of the resistance to plastic flow at the crack tip, a Griffith's type of apparent fracture stress was calculated based on $\sigma_N = 103 \quad (Kg/mm^2)\sqrt{mm}/Y\sqrt{a}$.

Figure 4.71 shows the variation of nominal stress with crack length for 25 mm thick specimens. It can be seen that the nominal stress value increases if the crack length of the specimen is decreased. When the crack length is around 5 mm, the nominal stress reaches the yield stress of the material. A further decrease in crack length results an increase in the nominal stress beyond yield strength of the material. For very short cracks the nominal stress at which an abrupt increase in plastic zone occurs, is found to approach a constant value.

Figures 4.72, 4.73 and 4.74 show the variation of the nominal stress versus crack length for 10 mm, 6 mm and 3 mm thick specimens respectively. In all these three cases the observed nominal stress follows closely Griffith's type nominal stress.

Table 4.4 shows values of K_Q obtained by different methods based on ASTM, Irwin-McClintock's COD, J-integral and equivalent energy methods. Figure 4.75 shows the load versus load point displacement record for the purpose of calculating the equivalent K_Q by J-integral method.

4.3: Study on Stability of Void Shape in an Incompressible Solid Under Uniaxial Tension and Shear:

Spheroidal cavities are commonly seen during the void growth and in ductile metals, fracture normally occurs by the growth and coalescence of such holes. The change in shape of such cavities depends on the nature of external applied stress which causes the localized deformation of the void. The stability of a single deforming spheroidal hole is studied in this work, first theoretically, and then experimentally. The purpose of undertaking this study is to find how the strain in the equatorial plane of a prolate spheroid is accommodated when a remote pure shear field or a uniaxial tensile field is applied. The material surrounding the cavity is assumed to be an incompressible elastic (rubber like) solid, (with Poisson's ratio = 1/2). In simple shear, a shape dependent instability of the spheroidal hole is observed for the constant volume mode of void deformation. Under uniaxial tension field, a pure torque will be produced in the presence of asymmetry or local disturbance, which could give rise a pure shear unstable deformation of the void.

Firstly, the deformation of a prolate spheroid is analysed under pure shear, secondly, at what stage a single spheroid would become unstable in uniaxial tension, and finally, these results are verified experimentally on a lead-tin alloy. Using Eshelby's[102] strain transformation function, the maximum decrease in strain energy is found to

be at a particular prolateness, whereas applying Biot's analysis an orthotropic incremental deformation of the cavitated material, a condition for tensile instability is obtained. These theoretical calculations agree favourably with the observations of Orowan , Perra and Finnie and the present experimental study on lead-30% tin alloy.

4.3.1: Three-Dimensional Void Growth in Pure Shear Loading:

Figure 4.76 shows a three-dimensional prolate spheroidal hole in an incompressible elastic solid which is subjected to a remote pure shear loading. Due to the application of an external shear strain field e^A_{12} at a large distance from the void surface, the shear strain produced on equatorial plane of the surface of a prolate spheroid, for a small strain is given by

$$e^T_{12} = \frac{1}{1 - 2 S_{1212}} e^A_{12} = \gamma e^A_{12} \qquad (4.6)$$

where $\gamma = \frac{1}{1 - 2S_{1212}}$ = shear strain accommodating factor,

e_{12} is the shear strain on plane 1-2. Superscripts T and A on e stand for transformed and applied shear strain respectively. In an incompressible solid, the Poisson's ratio is 1/2. Therefore, for a prolate spheroid S_{1212} becomes

$$S_{1212} = (\tfrac{1}{4}) \frac{x^2+1}{x^2-1} \left[\frac{3x}{(x^2-1)^{3/2}} \{ x(x^2-1)^{1/2} - \cosh^{-1} x \} - 2\right] \qquad (4.7)$$

where $x = a/c$

a = semi-major axis; $b = c$ = semi-minor axis.

For this particular material, the value of γ lies between 5/3 and 2. Again, due to the creation of such spheroidal void, the decrease in strain-energy of the body per unit volume of the cavity is given by

$$-E = \frac{S^2}{2G}\gamma \tag{4.8}$$

where S = applied shear stress at a large distance from the void surface and G = shear modulus of the medium.

Therefore, we may regard γ as a measure of the extent to which the matrix is able to accommodate the shear strain transformation. In addition, it also describes the manner in which shearing strain energy is altered when the volume of a void remains constant during a pure shear deformation.

Figure 4.77 shows the nature of variation for γ as a function of a/c, where a and c are the semi-major and semi-minor axes of the ellipsoid. One can also plot the function γ for an oblate spheroid as well, in the region of $0 < a/c < 1$. It is interesting to note that, if the volume of the void remains unchanged during a pure shear deformation, then one could get a condition:

$$\begin{aligned} \Delta E &> 0 \quad \text{for} \quad a/c < 1.390 \\ \Delta E &< 0 \quad \text{for} \quad a/c > 1.390 \\ E &= 0 \quad \text{for} \quad a/c = 1.390 \end{aligned} \tag{4.9}$$

This gives a condition of instability for growing void in an incompressible elastic solid undergoing small pure shear deformation.

4.3.2: Three-dimensional Void Growth in Uniaxial Initial Tension with Slight Imperfection or Disturbance:

A pure shear loading on a prolate spheroidal void can cause instability, which can be considered as equivalent to tension and compression at 45°. Again, it is known that an uniaxial tension is equal to a hydrostatic tension plus two 45° shears. This is obtained from the following tensor relations:

$$\begin{pmatrix} 1 & 0 & 0 \\ 0 & 0 & 0 \\ 0 & 0 & 0 \end{pmatrix} = \begin{pmatrix} \frac{1}{3} & 0 & 0 \\ 0 & \frac{1}{3} & 0 \\ 0 & 0 & \frac{1}{3} \end{pmatrix} + \begin{pmatrix} \frac{1}{3} & 0 & 0 \\ 0 & -\frac{1}{3} & 0 \\ 0 & 0 & 0 \end{pmatrix} + \begin{pmatrix} \frac{1}{3} & 0 & 0 \\ 0 & 0 & 0 \\ 0 & 0 & -\frac{1}{3} \end{pmatrix} \tag{4.10}$$

Figure 4.78 shows a schematic diagram for the different stages of a void growth, which is typical in most materials. An oblate spheroidal void gradually changes its shape and becomes a spherical void at some stage of the growth. Any further applied nominal tensile strain normally causes the void to grow in the shape of a prolate spheroid, with its major axis parallel to the direction of applied tension. The stability of such a prolate spheroidal cavity in a linear incompressible elastic solid is investigated in this section.

When the applied tension is parallel to the major axis,

$$e^{T}_{11} = \varepsilon\, e^{A}_{11} \tag{4.11}$$

but if the applied tension is perpendicular to major axis

$$e^{T}_{22} = \xi e^{A}_{22} \tag{4.12}$$

and for applied shear stress in the plane 1-2

$$e^{T}_{12} = \gamma\, e^{A}_{12} \tag{4.13}$$

where ε and ξ are given in the Appendix A in terms of a/c, ε and ξ are continuous functions of a/c without any maxima, minima, saddle or inflexion point. It is also seen from Eqns. (4.11) to (4.13) that in the presence of a void the entire material is giving a directional orthotropic property. Depending on the value of a/c ratio, the strain amplification on void surface could be fairly large, especially for an incompressible solid. Thus, it would be more appropriate to treat the entire material in orthotropic medium. Figure 4.79 shows such an equivalent orthotropic continuum. The general theory for such a type of material has been developed by Biot. In finite elastic deformation, we will use Biot's notation N_1, N_2 and Q instead of ε, ξ and γ (which were introduced for small strains).

Let $2N_1$ = incremental elastic modulus of the entire matrix in the presence of a void, measured in the direction

of 1 (along major axis). $2N_2$ = incremental elastic modulus of the entire matrix in the presence of a void, measured in the direction of 2 (along minor axis), and 2Q = incremental shear modulus of the entire matrix in the presence of a void, when the tension is applied about axis 3 which will cause shear deformation in plane 1-2.

In the presence of an initial tensile stress, the stress-strain laws are

$$S_{11} - S = 2N_1 e_{xx} \tag{4.14}$$

$$S_{22} - S = 2N_2 e_{yy} \tag{4.15}$$

$$S_{12} = 2Q e_{xy} \tag{4.16}$$

for an homogeneous orthotropic elastic solid the equilibrium equations in three dimensions are:

$$\frac{\partial S_{11}}{\partial x} + \frac{\partial S_{12}}{\partial y} + \frac{\partial S_{13}}{\partial z} + T\left(\frac{\partial \omega z}{\partial y} - \frac{\partial \omega y}{\partial z}\right) = 0$$

$$\frac{\partial S_{21}}{\partial x} + \frac{\partial S_{22}}{\partial y} + \frac{\partial S_{23}}{\partial z} + T\frac{\partial \omega z}{\partial x} = 0$$

$$\frac{\partial S_{31}}{\partial x} + \frac{\partial S_{32}}{\partial y} + \frac{\partial S_{33}}{\partial z} - T\frac{\partial \omega y}{\partial x} = 0 \tag{4.17}$$

where, S_{ij} = incremental stresses and ω_K = rotational component, T = uniaxial initial tensile stress acting parallel to axis - 1 (i.e. along the major axis of the cavity).

If one assumes a plane strain deformation condition in X-Y (i.e. 1-2) plane, then the above equilibrium equations can be written as

$$\frac{\partial S_{11}}{\partial x} + \frac{\partial S_{12}}{\partial y} + \frac{\partial \omega_z}{\partial y} = 0$$

$$\frac{\partial S_{12}}{\partial x} + \frac{\partial S_{22}}{\partial y} + \frac{\partial \omega_z}{\partial x} = 0$$

The condition of incompressibility gives $e_{xx} + e_{yy} = 0$. Writing the displacements in terms of a single function ϕ:

$$u = -\frac{\partial \phi}{\partial y} \quad \text{and} \quad v = \frac{\partial \phi}{\partial x}$$

and then eliminating S from Eqn.(4.17) the differential equation becomes

$$(Q + \tfrac{T}{2}) \frac{\partial^4 \phi}{\partial x^4} + 2(N_1 + N_2 - Q) \frac{\partial^4 \phi}{\partial x^2 \cdot \partial y^2} + (Q - \tfrac{T}{2}) \frac{\partial^4 \phi}{\partial y^4} = 0$$

Biot has considered the characteristic roots of this equation for the existence of hyperbolic type solution which gives instability in internal buckling. The characteristic roots are:

$$\xi_1^2 = -m + \sqrt{m^2 - k^2}$$

and

$$\xi_2^2 = -m - \sqrt{m^2 - k^2}$$

where

$$m = (N_1 + N_2 - Q)/(Q - \tfrac{T}{2})$$

and

$$k^2 = (Q + T/2)/(Q - T/2)$$

In order to get a condition of instability, there must be at least a real root for ξ. So long as $2Q < T$ one gets four complex roots and there is no instability. As soon as $T > 2Q$ two roots become positive real and the other two roots are still complex. Such situation can be described as Biot's internal instability of the first kind (for case three). Thus, an internal instability can occur when the applied initial tension is at least equal to or more than the finite shear modulus of the material in the presence of a void. Biot's finite "slide modulus", $L = T - 2Q$, also becomes zero at this particular load (i.e. when $T = 2Q$). However, if one makes an assumption that in the presence of asymmetry and disturbance the "finite shear modulus of the material" is equal to the "shear modulus of the void" obtained by small strain theory, then in plane strain, the condition of instability for a prolate spheroidal void in simple shear would be:

$$T = G\gamma' \tag{4.18}$$

This means, in the presence of some disturbance or geometrical asymmetry of the void, when the applied uniaxial tensile stress exceeds $G\gamma'$ there will be a shearing instability of the void. Void will try to rotate at this load to increase its shear resistance, but it cannot due to the alignment of its major axis in the direction of applied tension. Therefore, the void becomes unstable in pure shear

deformation at this particular load. In this situation the principal axis of stresses and strains can only rotate.

This is analogous to Biot's problem on torsional rigidity of a bar under initial tensile stress. It can be seen that the resultant body forces calculated from surface integrals will vanish over the cross section in each direction leaving only a torque, provided the origin of the co-ordinate is located at the centre of gravity of the cross section. In this situation, in the absence of slide modulus, Saint-Venant type of torque vanishes and the torsional rigidity is entirely due to the initial stress. Thus, at the onset of instability, the uniaxial tension produces a pure shear deformation of void in plane 1-2. The metastable void shape is shown in Figure 4.80.

Thus, it is proved here, that (i) a prolate spheroidal hole inside an incompressible elastic solid can become unstable at $a/b = 1.39$ in pure shear field, and (ii) a prolate spheroidal hole would become unstable in uniaxial tension field at $a/b = 2.3$ for which the shearing resistance of the void is maximum.

Orowan and Ferra and Finnie observed similar shape dependent instability of voids inside plastically yielded materials.

4.3.3: Experimental Observations on Spheroidal Hole Growth in Tension:

The change in the shape of an isolated spherical hole inside a lead-tin alloy is experimentally measured at different nominal applied strains. The most convenient way was found to measure the eccentricity ratio and the mean radius ratio of the prolate hole at different stages of straining. Let the eccentricity m be defined as $(\frac{a - b}{a + b})$ where a and b are the semi-major and semi-minor axes, respectively, and the mean radius ratio be defined as $(\frac{a + b}{2 R_o})$ where R_o is the original radius of the spherical hole. Figure 4.81 shows the eccentricity of the hole against the nominal strain and Figure 4.82 gives the mean radius ratio against the nominal strain. Theoretical calculations based on McClintock's analysis and the experimental observations of Perra and Finnie on copper are also presented along with the results of the present investigation. Figure 4.83 shows the photographs illustrating the changes in void shape at different nominal strains in the lead-tin alloy.

TABLE 4.1

Crack lengths for 0.6% carbon steel three-point bend fracture test specimens (W = 25 mm)

Crack length, a, in mm			
Thickness : 25 mm	Thickness : 10 mm	Thickness : 6 mm	Thickness : 3 mm
1.20	0.80	0.94	1.30
1.67	1.70	1.53	1.63
1.92	2.65	2.50	2.30
2.83	4.70	4.30	4.97
3.40			
4.33			

TABLE 4.2

Apparent toughness (K_Q) calculated by different methods for 0.6% carbon steel (in Kg $mm^{-3/2}$)

Crack length a (mm)	Apparent toughness (K_Q) based on ASTM method corresponding to				Equivalent K_Q values calculated from Irwin-McClintock's corrected crack length method based on maximum linear load	Equivalent K_Q values obtained from plane stress $G_{Ic} = \sigma_y \delta_c$ by COD method with δ corresponding to the maximum load	Equivalent K_Q values by energy method
	Maximum linear load	5% secant shift load	10% secant shift load	Maximum load			
				Thickness : 25 mm			
1.20	104.7	-	-	104.7	-	-	-
1.67	152.9	-	-	152.9	-	-	-
1.92	150.5	-	-	150.5	-	-	-
2.83	148.1	-	-	148.1	-	-	-
3.40	146.6	-	-	146.6	-	-	-
4.33	149.5	-	-	149.5	-	-	-
				Thickness : 10 mm			
0.80	80.3	97.0	105.5	115.3	-	-	-
1.70	130.4	-	-	130.4	-	-	-
2.65	155.5	-	-	155.5	-	-	-
4.70	137.0	-	-	137.0	-	-	-
				Thickness : 6 mm			
0.94	116.9	129.9	135.7	142.9	-	128.8	203.4
1.53	103.1	121.8	132.2	144.3	-	127.8	-
2.50	105.3	-	-	105.3	-	-	-
4.30	139.4	-	-	139.4	151.7	-	-
				Thickness : 3 mm			
1.30	132.7	144.3	148.8	155.6	-	199.2	-
1.63	117.1	142.5	-	156.8	168.0	160.8	186.0
2.30	155.3	177.0	-	178.5	183.6	147.2	196.7
4.97	155.7	-	-	155.7	-	-	-

TABLE 4.3

Crack lengths for mild steel three-point bend fracture test specimens (W = 25 mm)

Crack length, a, in mm			
Thickness : 25 mm	Thickness : 10 mm	Thickness : 6 mm	Thickness : 3 mm
0.88	2.30	2.40	2.20
1.13	3.50	3.78	3.60
1.32	4.25	5.21	5.20
2.26	5.95	6.65	8.00
4.45	7.08	8.20	12.85
7.70	7.40	11.85	
11.57	11.00	12.50	
	12.90		

TABLE 4.4

Stress Intensity Factor, K_p, (in Kg $mm^{-3/2}$ units) which is a measure of the [illegible] resistance to crack-tip plastic flow in mild steel calculated by different methods

Specimen thickness (B) in mm	Crack length (a) in mm	K_p based on ASTM method corresponding to			Equivalent K_p calculated from Irwin-McClintock's corrected crack length method			Equivalent $K_p = \sqrt{E\sigma_y\delta}$ obtained from plane stress COD method, δ corresponding to the following loads			Equivalent K_p values by J-integral method			K_Q values by equivalent energy method
		Maximum linear load	5% secant shift load	10% secant shift load	Maximum linear load	5% secant shift load	10% secant shift load	5% secant shift load	10% secant shift load	Load at which the test was discontinued	Maximum linear load	5% secant shift load	10% secant shift load	
25	0.88	64.5	67.5	67.7	76.8	81.9	82.9	87.0	95.0	139.3	–	–	–	152.5
	1.13	62.4	69.7	72.1	70.1	82.2	136.3	84.4	96.0	158.7	–	–	–	174.9
	1.32	71.6	76.8	79.7	–	–	–	75.5	83.8	108.0	282.9	319.5	346.5	149.4
	2.26	85.7	93.0	97.0	–	–	–	82.6	92.6	129.1	88.3	93.1	155.7	236.9
	4.45	98.7	110.2	116.7	106.8	122.3	132.8	73.4	80.9	158.7	145.1	209.4	262.7	208.4
	7.70	117.3	131.3	140.6	–	–	–	93.7	129.7	202.4	168.4	–	–	–
	11.57	108.5	111.8	113.9	112.1	117.9	122.5	51.6	56.9	78.2	–	–	–	237.6
10	2.30	90.6	92.1	92.8	108.7	115.0	–	73.1	78.9	98.5	256.9	281.2	290.9	167.1
	3.50	100.2	103.6	105.3	109.5	119.3	–	72.9	80.9	114.4	–	–	–	236.5
	4.25	87.8	102.2	110.5	–	–	–	68.5	81.8	130.6	217.7	282.9	355.4	337.1
	5.95	89.2	122.0	132.9	108.6	113.9	117.3	57.5	–	83.5	215.8	238.4	256.5	214.3
	7.08	103.3	109.0	112.3	119.5	130.3	137.3	57.5	62.4	99.9	94.6	118.3	113.3	269.9
	7.40	102.6	123.4	135.6	–	–	–	86.9	117.1	258.3	–	–	–	–
	11.00	89.2	122.0	132.9	–	–	–	51.2	59.6	98.1	150.3	182.8	206.5	328.3
	12.90	91.9	99.3	103.2	95.8	108.6	114.9	46.7	53.5	89.6	–	–	–	312.5
6	2.40	84.1	98.7	108.6	–	–	–	73.3	85.6	150.2	–	–	–	220.2
	3.78	96.0	106.0	110.5	–	–	–	82.0	104.5	158.7	146.4	197.4	301.5	334.5
	5.21	93.5	110.4	114.0	99.4	139.2	157.1	72.9	85.0	154.4	–	–	–	394.5
	6.65	92.2	100.1	104.7	98.2	109.4	117.4	–	78.9	160.4	122.1	135.9	146.5	286.0
	8.20	91.2	103.3	110.3	–	–	–	56.0	66.4	124.3	135.9	167.0	239.8	–
	10.85	99.3	111.3	116.4	–	–	–	49.8	56.2	85.4	119.1	136.8	175.0	288.7
	12.50	93.1	100.5	106.2	99.2	109.1	117.3	45.5	53.3	150.2	–	–	–	326.5
3	2.20	76.8	85.3	88.8	96.5	–	–	97.1	107.3	144.6	118.7	156.8	159.6	182.4
	3.60	82.7	90.4	96.1	88.9	98.1	143.6	85.1	92.7	101.1	197.4	234.0	309.5	132.5
	5.20	84.5	98.7	104.9	91.9	156.8	–	84.3	93.6	114.7	80.4	97.8	–	184.4
	8.00	81.3	94.3	100.5	–	–	–	66.3	73.9	102.8	92.4	109.1	127.9	211.3
	12.85	84.4	97.7	103.8	90.4	106.6	115.5	49.1	56.3	89.7	–	–	–	293.7

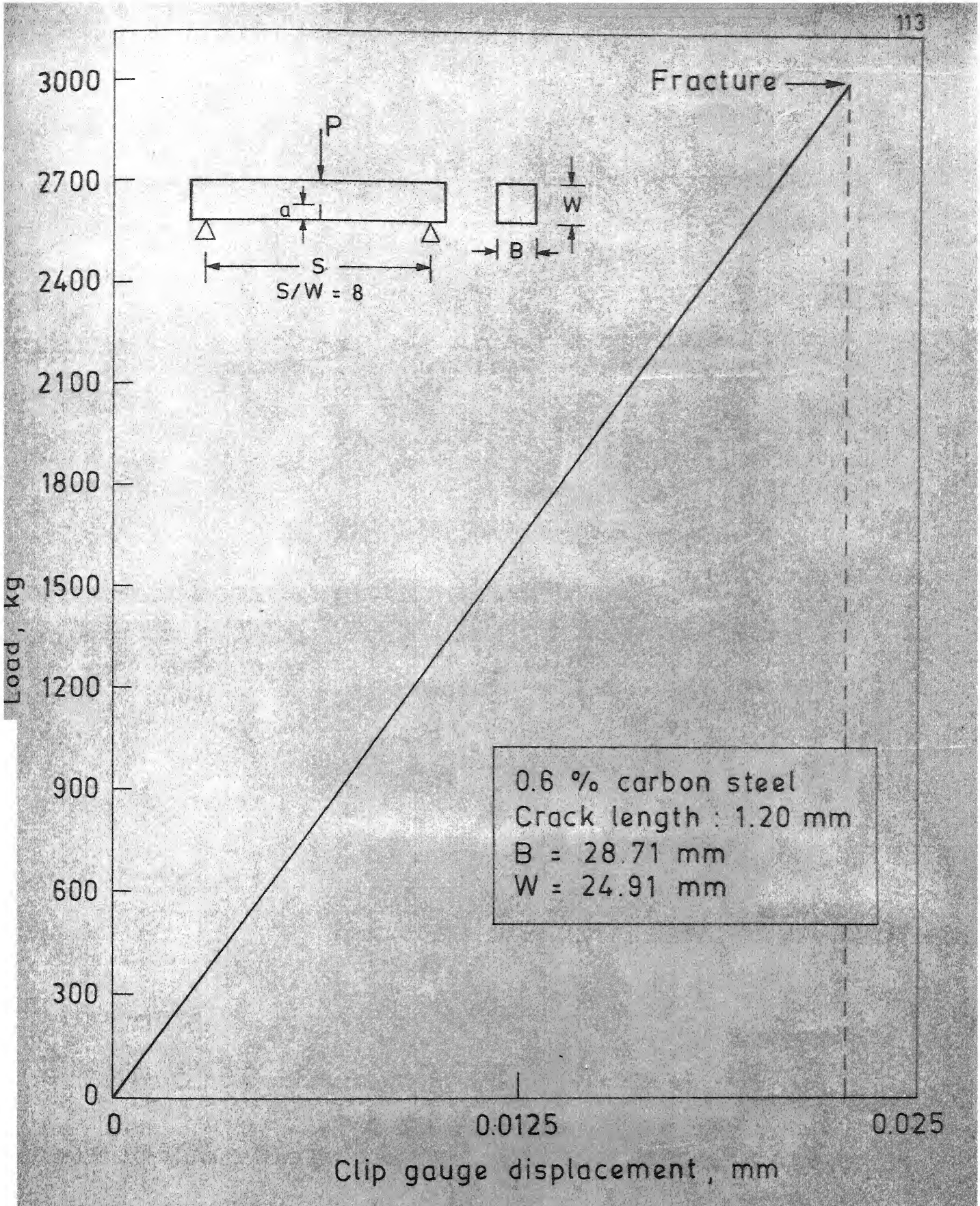

Fig. 4.1 Load versus clip gauge crack opening displacement for a crack length of 1.20 mm and thickness 28.71 mm in 0.6 % carbon steel specimen.

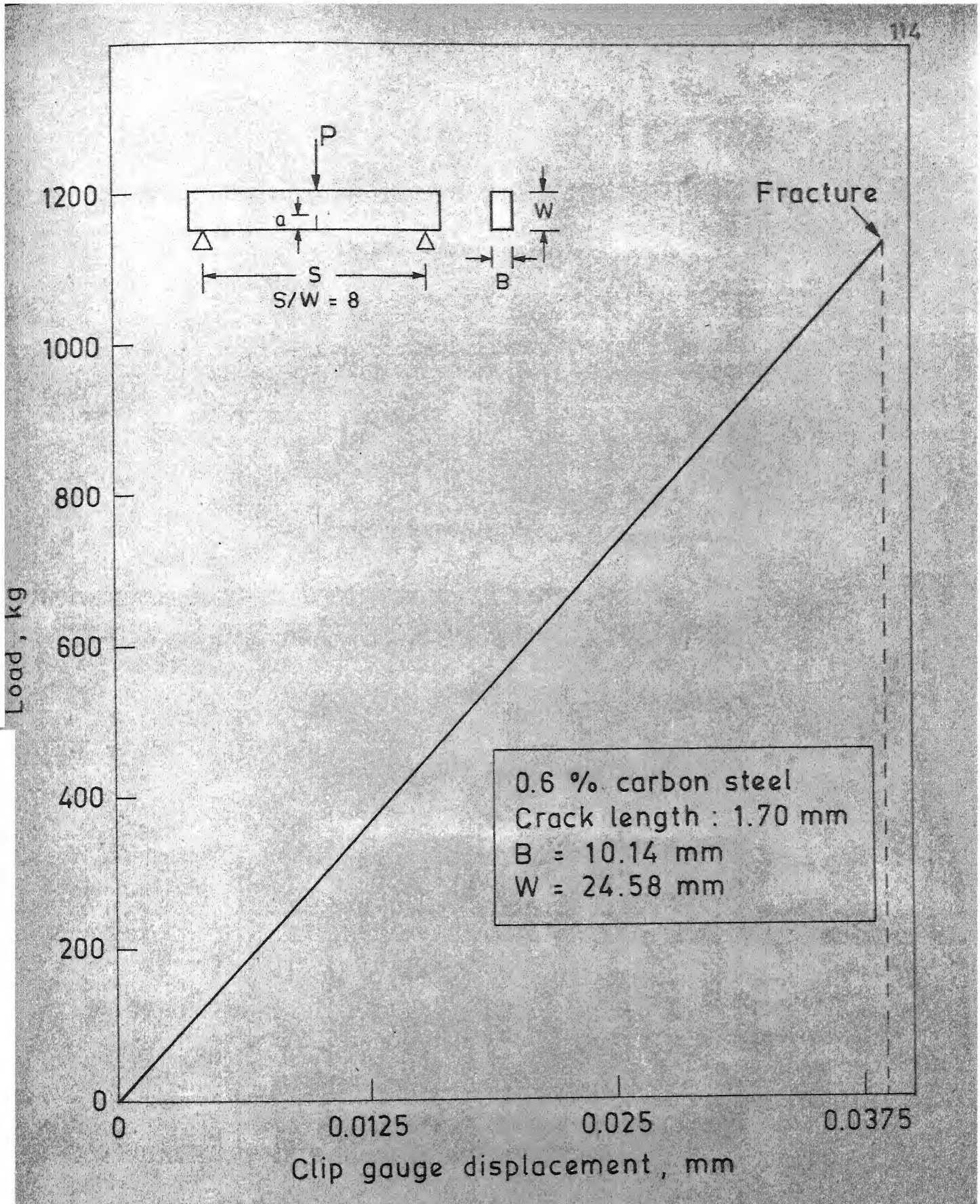

Fig. 4.2 Load versus clip gauge crack opening displacement for a crack length of 1.70 mm and thickness 10.14 mm in 0.6 % carbon steel specimen.

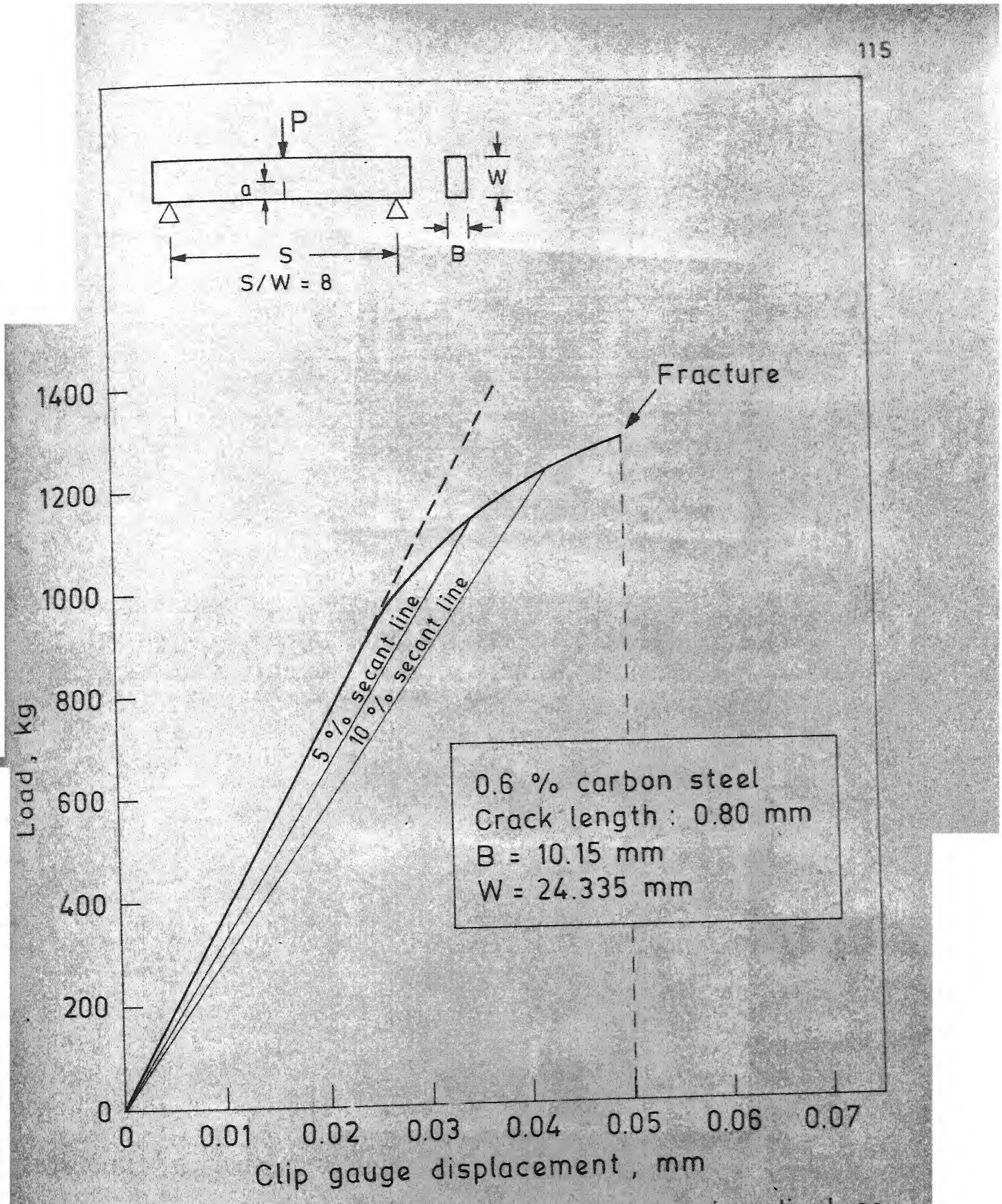

Fig. 4.3 Load versus clip gauge crack opening displacement for a crack length of 0.80 mm and thickness 10.15 mm in 0.6 % carbon steel specimen.

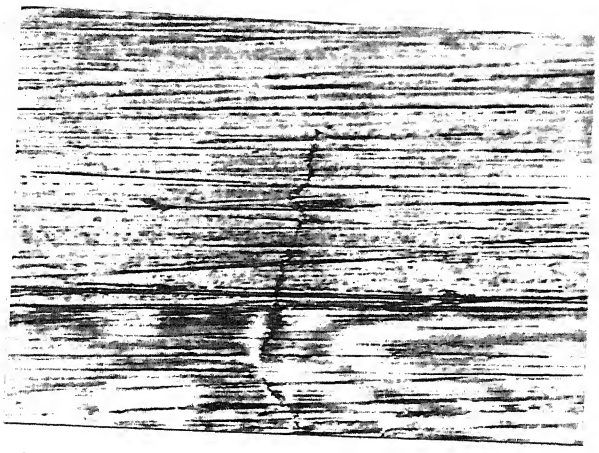

Fig. 4.4: Photograph showing the crack-tip deformation at 650 Kg (σ/σ_y = 0.68) for 0.6% carbon steel (Crack length = 1.70 mm, Thickness = 10.14 mm) (Magnification: 250X).

Fig. 4.5: Photographs showing isochromatic fringe pattern at crack-tip in 0.6% carbon steel at 650 Kg (σ/σ_y = 0.68) (crack length = 1.70 mm, Thickness = 10.14 mm).

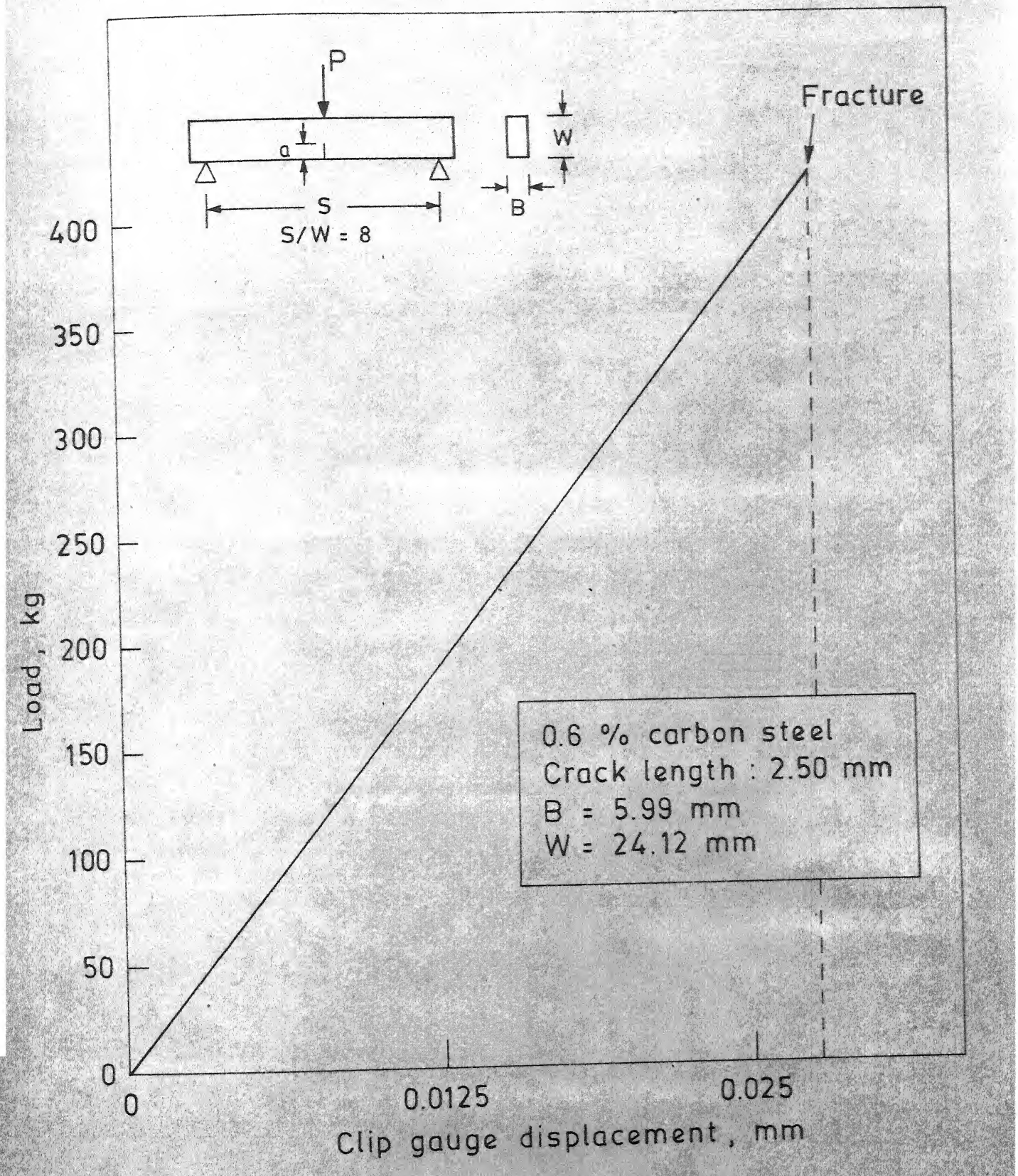

Fig. 4.6 Load versus clip gauge crack opening displacement for a crack length of 2.50 mm and thickness 5.99 mm in 0.6 % carbon steel specimen.

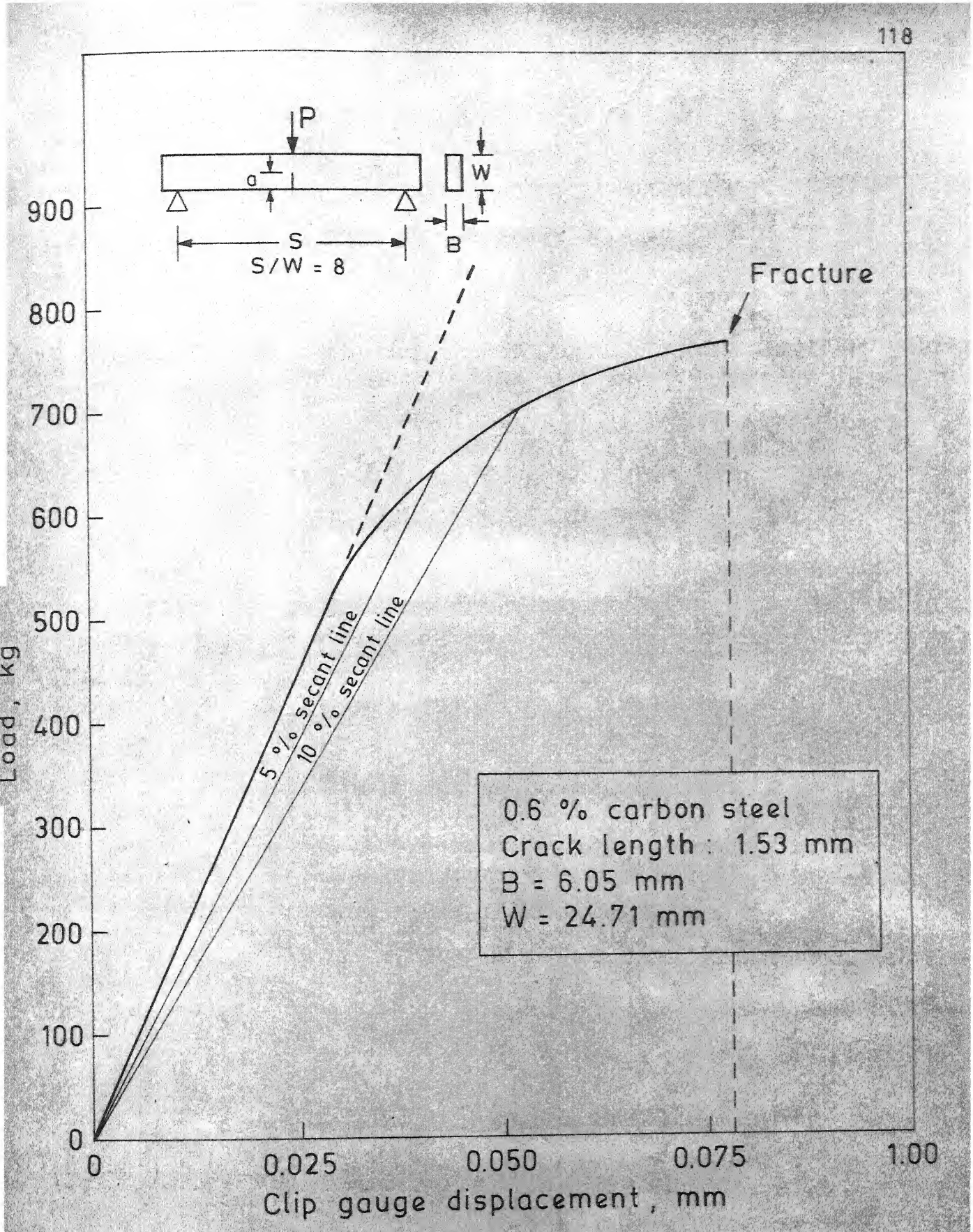

Fig. 4.7 Load versus clip gauge crack opening displacement for a crack length of 1.53 mm and thickness 6.05 mm in 0.6 % carbon steel specimen.

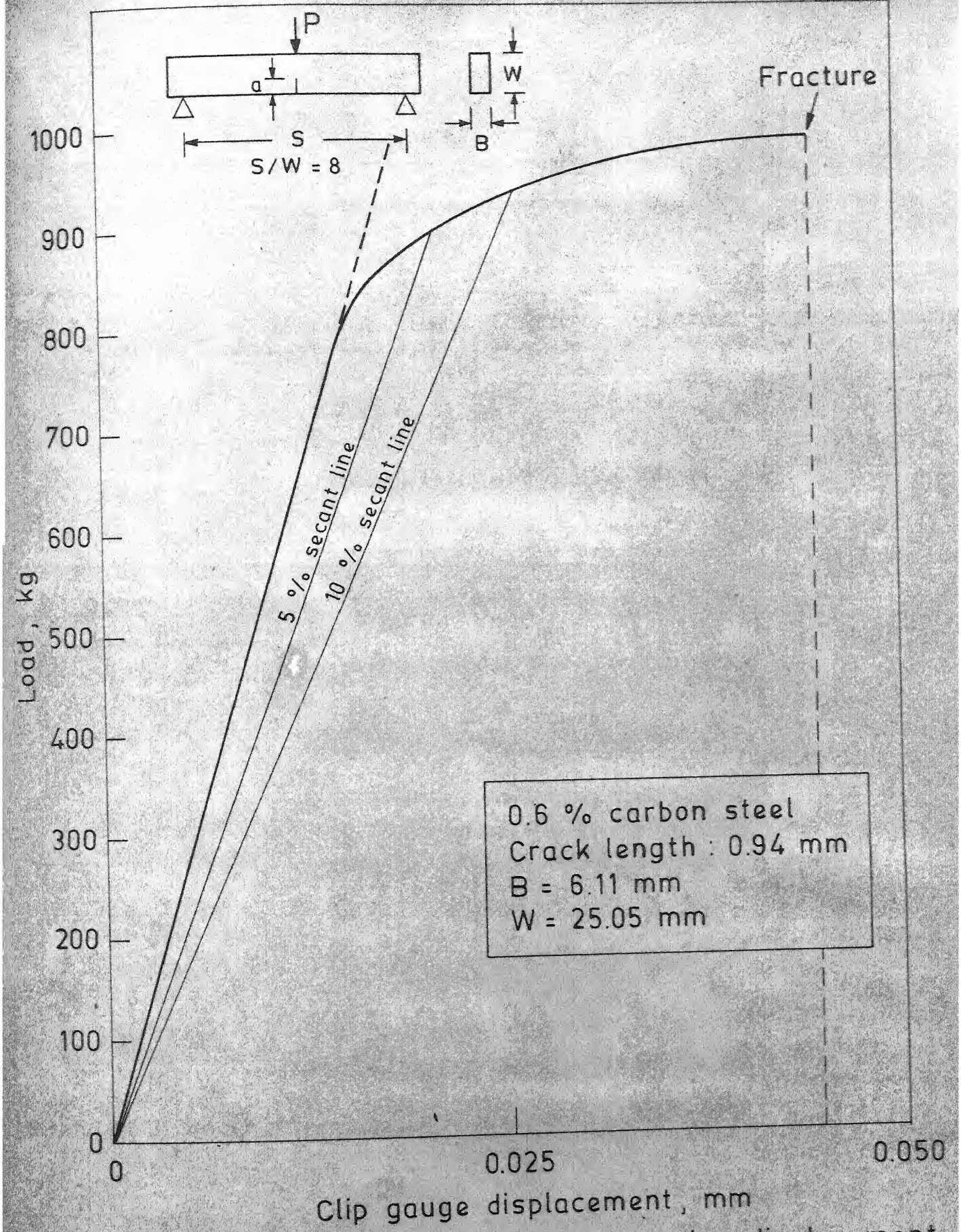

Fig. 4.8 Load versus clip gauge crack opening displacement for a crack length of 0.94 mm and thickness 6.11 mm in 0.6 % carbon steel specimen.

	P, kg	$\sigma/\sigma y$
d	470	0.83
c	400	0.71
b	300	0.53
a	250	0.44

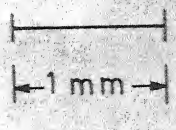

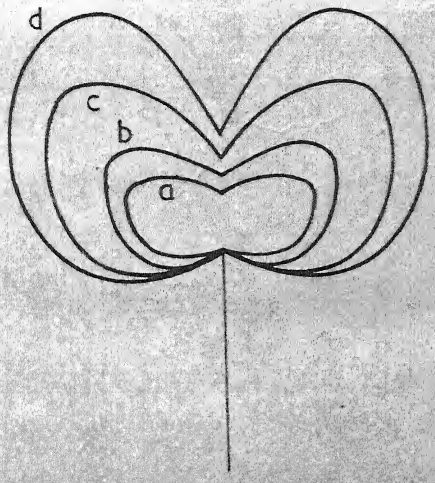

Fig. 4.9 Experimentally observed plastic zone sizes at the crack tip for different loads measured by photo-elastic coating technique in 0.6 % carbon steel specimen with crack length 1.53 mm and thickness 6.05 mm.

	P, kg	σ / σy
d	390	0.72
c	346	0.64
b	275	0.51
a	220	0.41

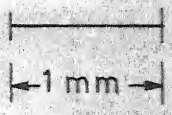

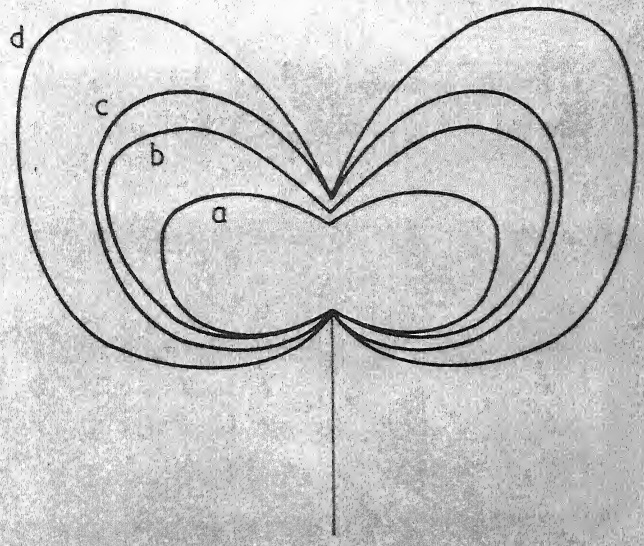

Fig. 4.10 Experimentally observed plastic zone sizes at the crack tip for different loads measured by photoelastic coating technique in 0.6 % carbon steel specimen with crack length 2.50 mm and thickness 5.99 mm.

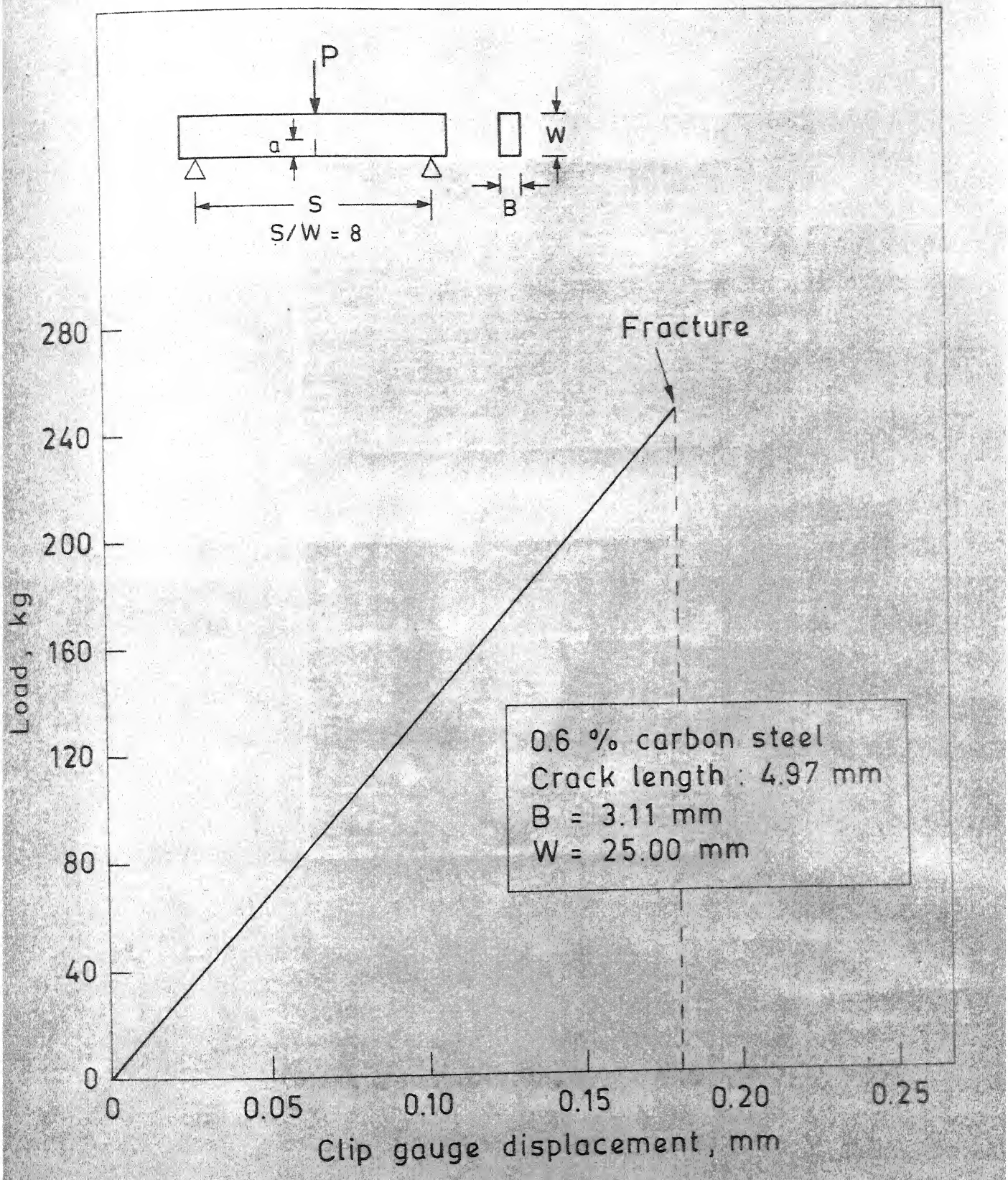

Fig. 4.11 Load versus clip gauge crack opening displacement for a crack length of 4.97 mm and thickness 3.11 mm in 0.6 % carbon steel specimen.

(a)

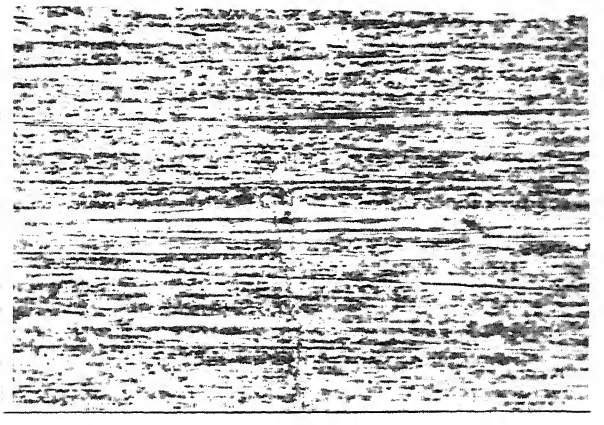

250X

(b)

120X

Fig. 4.12: Photographs showing crack-tip deformations in 0.6% carbon steel at
(a) 140 Kg (σ/σ_y = 0.46), Magnification: 250X
(b) 250 Kg (σ/σ_y = 0.83), Magnification: 120X
(crack length = 4.97 mm, Thickness = 3.13 mm).

(a)

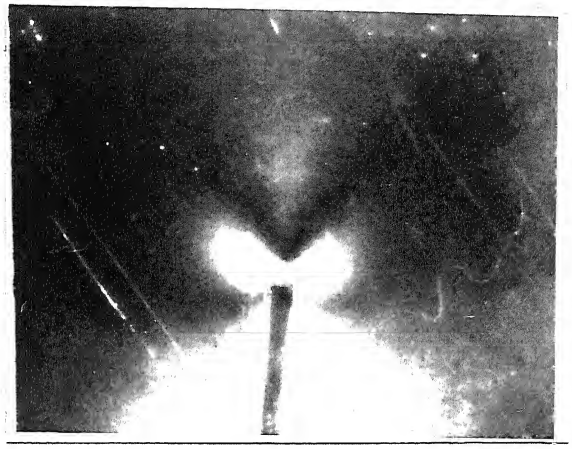

(b)

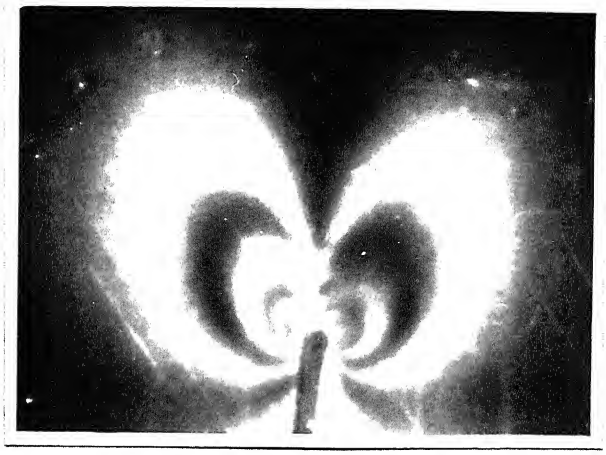

Fig. 4.13: Photographs showing isochromatic fringe patterns at crack-tip in 0.6% carbon steel at

(a) 140 Kg ($\sigma/\sigma_y = 0.46$)

(b) 250 Kg ($\sigma/\sigma_y = 0.83$)

(crack length = 4.97, Thickness = 3.13 mm).

	P, kg	σ / σy
f	250	0.83
e	160	0.53
d	140	0.46
c	90	0.30
b	70	0.23
a	50	0.16

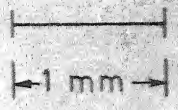

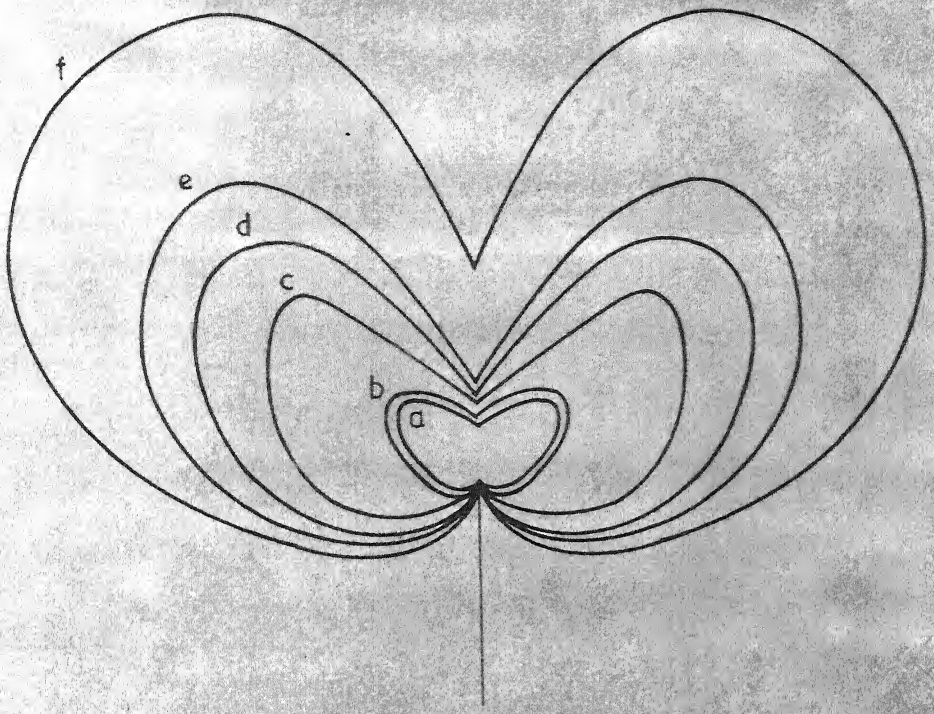

Fig. 4.14 Experimentally observed plastic zone sizes at the crack tip for different loads measured by photoelastic coating technique in 0.6 % carbon steel specimen with a crack length 4.97 mm and thickness 3.11 mm .

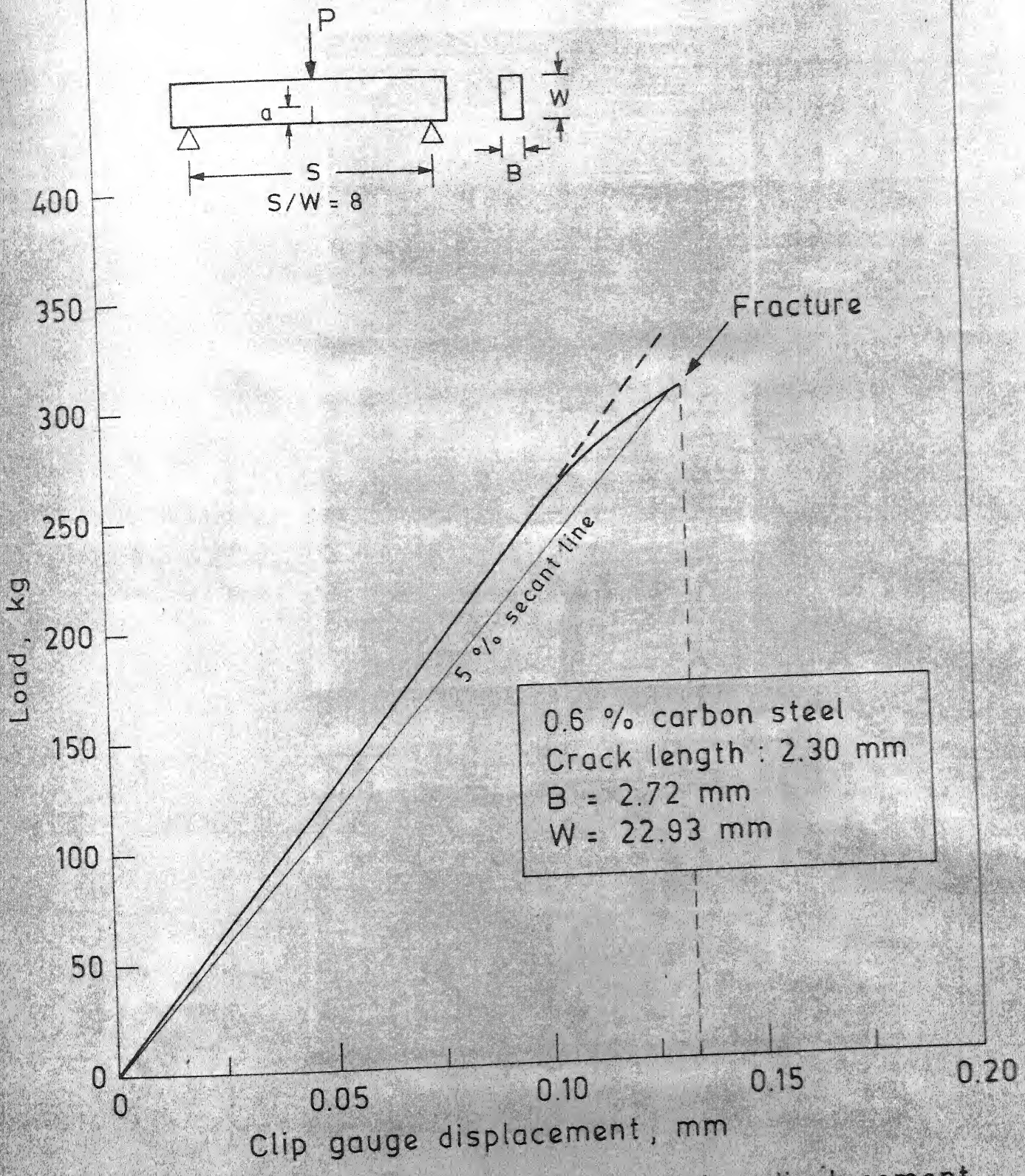

Fig. 4.15 Load versus clip gauge crack opening displacement for a crack length of 2.30 mm and thickness 2.72 mm in 0.6 % carbon steel specimen.

(a)

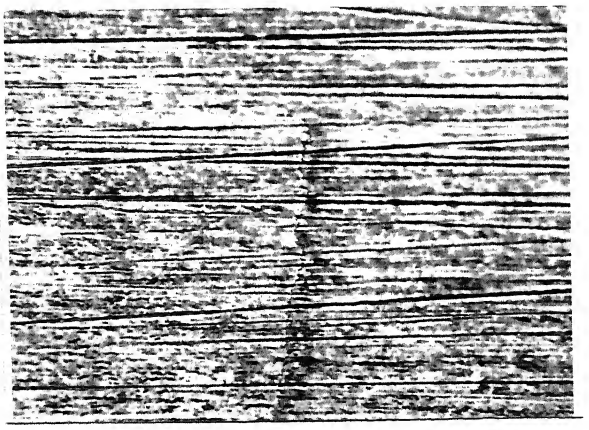

250X

(b)

250X

(c)

250X

Fig. 4.16: Photographs showing crack-tip deformations in 0.6% carbon steel at
(a) 140 Kg (σ/σ_y = 0.63), Magnification: 250X
(b) 274 Kg (σ/σ_y = 1.23), Magnification: 250X
(c) 307.5 Kg (σ/σ_y = 1.38), Magnification: 250X
(crack length = 2.30 mm, Thickness = 2.72 mm).

	P, kg	σ/σy
e	307	1.38
d	274	1.23
c	140	0.63
b	110	0.49
a	80	0.36

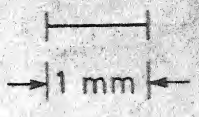

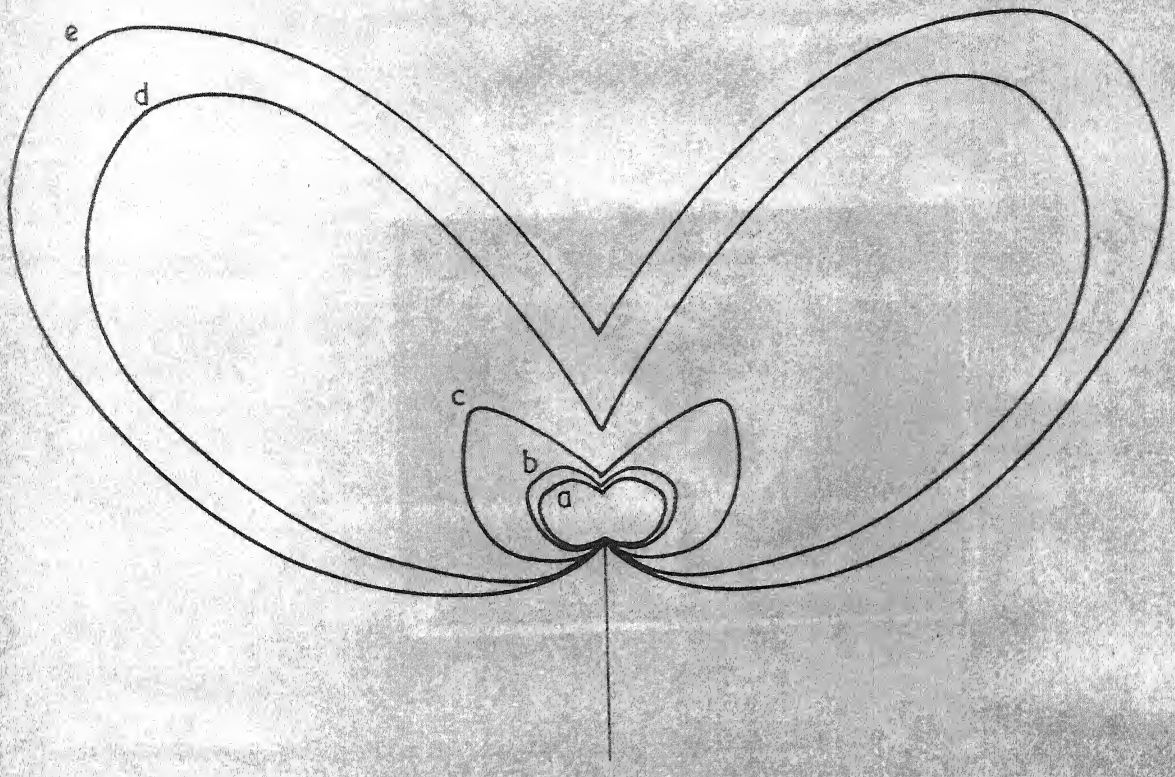

Fig. 4.17 Experimentally observed plastic zone sizes at the crack tip for different loads measured by photoelastic coating technique in 0.6 % carbon steel specimen with crack length 2.30 mm and thickness 2.72 mm .

Fig. 4.18: Photograph showing isochromatic fringe pattern at crack-tip in 0.6% carbon steel at 274 Kg (σ/σ_y = 1.23)
(crack length = 2.30 mm, Thickness = 2.72 mm).

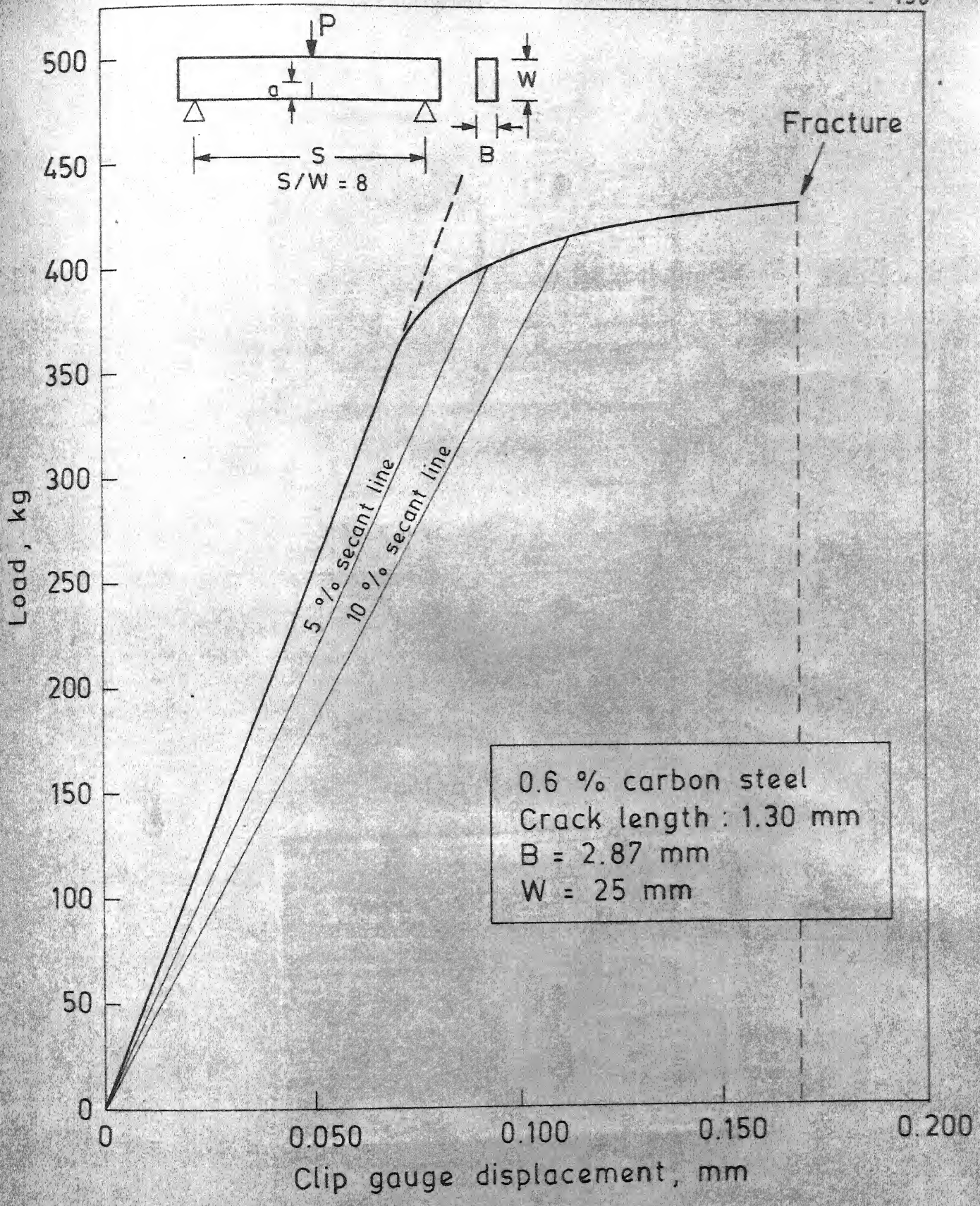

Fig. 4.19 Load versus clip gauge crack opening displacement for a crack length of 1.30 mm and thickness 2.87 mm in 0.6 % carbon steel specimen.

(a)

250X

(b)

250X

(c)

120X

Fig. 4.20: Photographs showing crack-tip deformations in 0.6% carbon steel at
(a) 335 Kg (σ/σ_y = 1.20), Magnification: 250X
(b) 400 Kg (σ/σ_y = 1.44), Magnification: 250X
(c) 412.5 Kg (σ/σ_y = 1.48), Magnification: 120X
(crack length = 1.30 mm, Thickness = 2.87 mm).

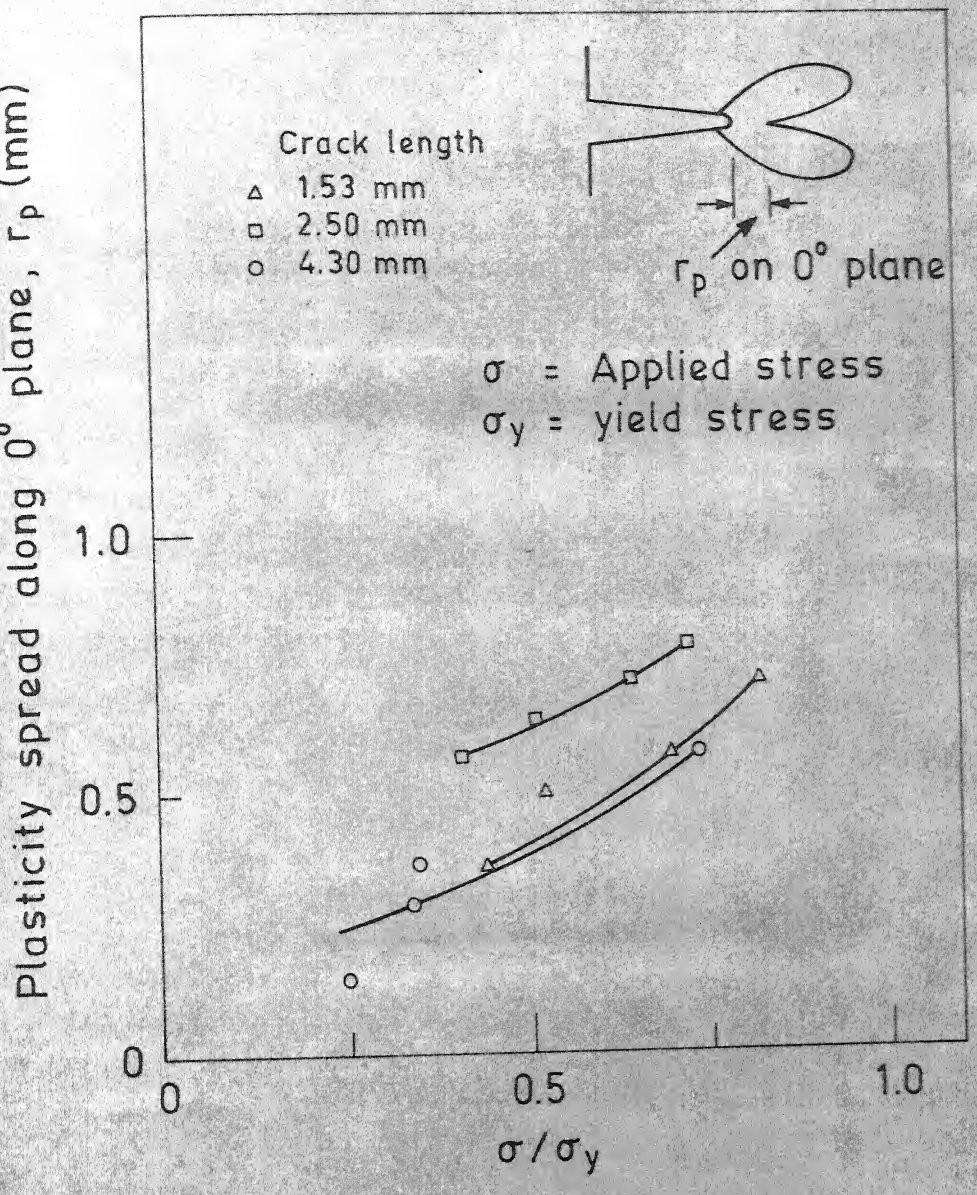

Fig. 4.21 Length of plastic zone (along 0° plane) versus σ/σ_y plot for 6 mm thick 0.6 % carbon steel specimens with varying crack length.

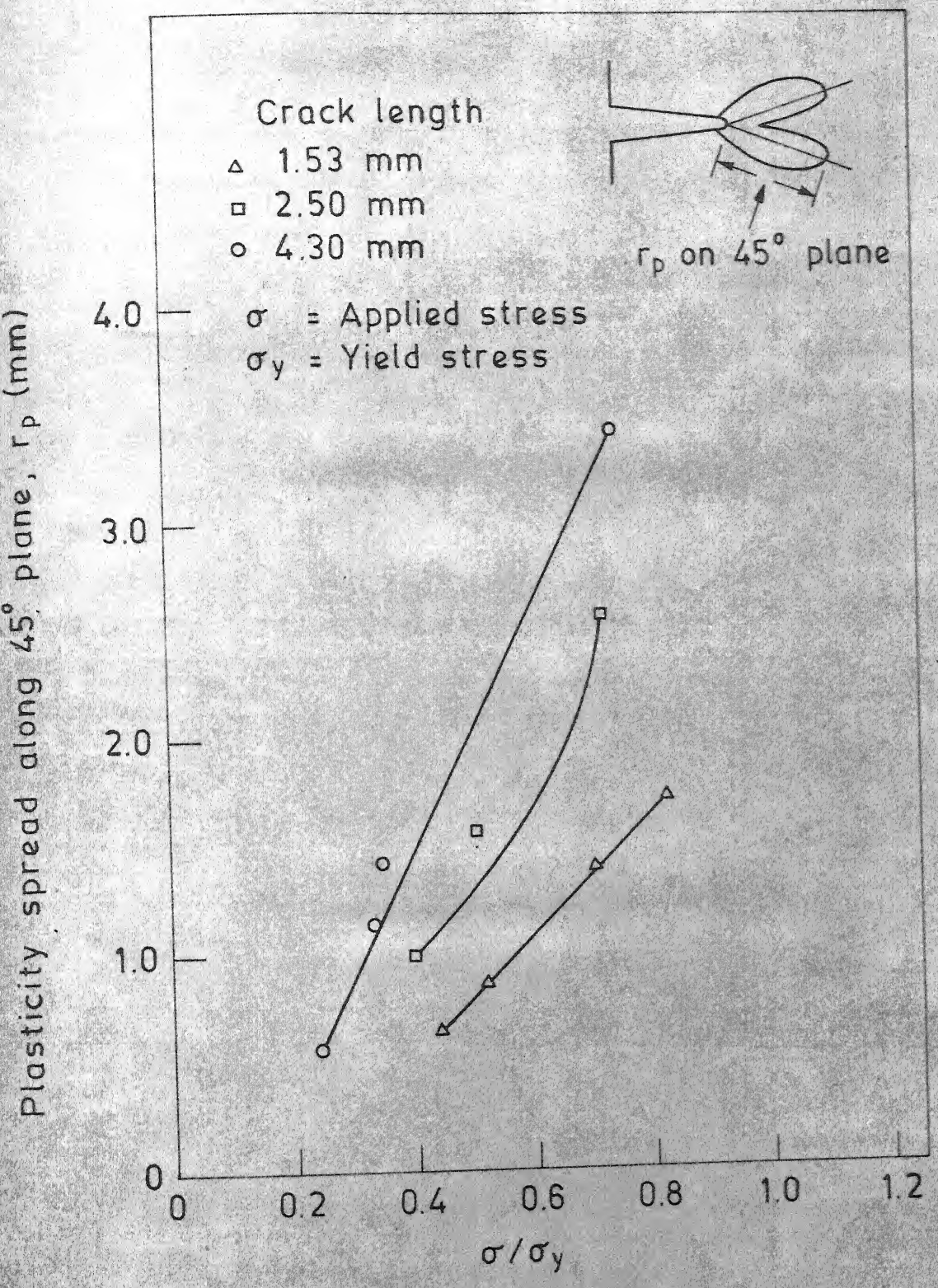

Fig. 4.22 Length of plastic zone (along 45° plane) versus σ/σ_y plot for 6 mm thick 0.6 % carbon steel specimens with varying crack length.

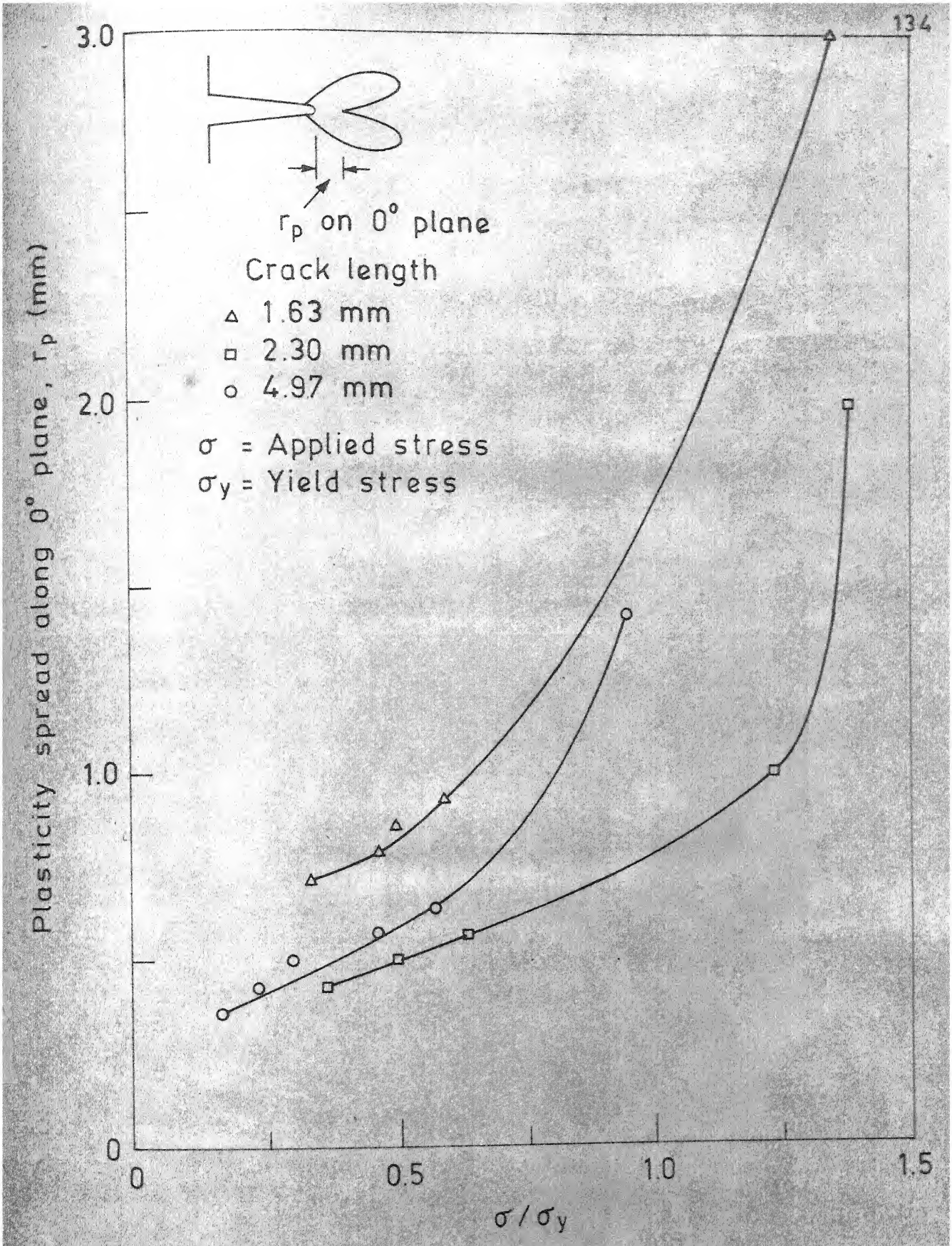

Fig. 4.23 Length of plastic zone (along 0° plane) versus σ/σ_y plot for 3 mm thick 0.6 % carbon steel specimens with varying crack length.

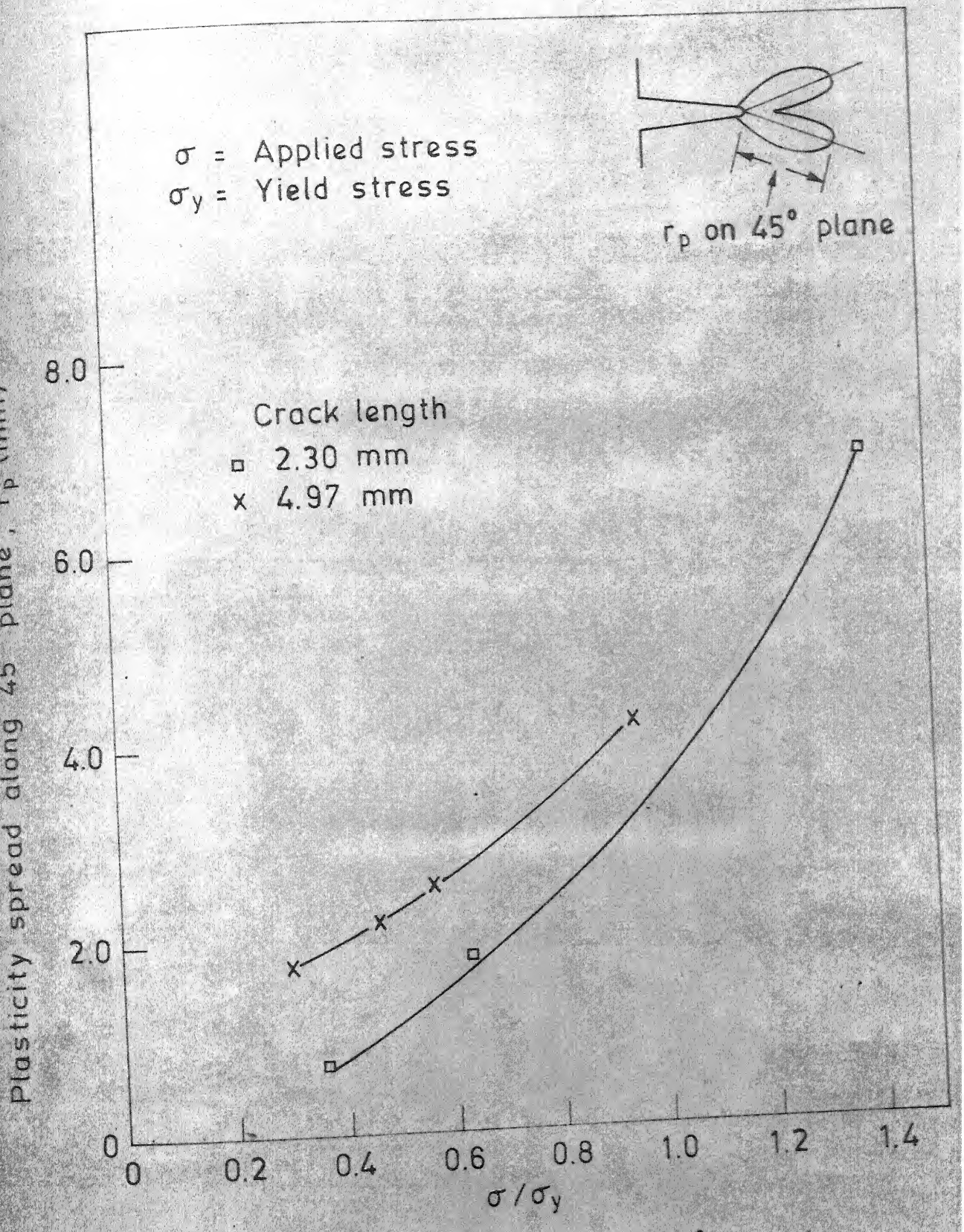

Fig. 4.24 Length of plastic zone (along 45° plane) versus σ/σ_y plot for 3 mm thick 0.6 % carbon steel specimens with varying crack length.

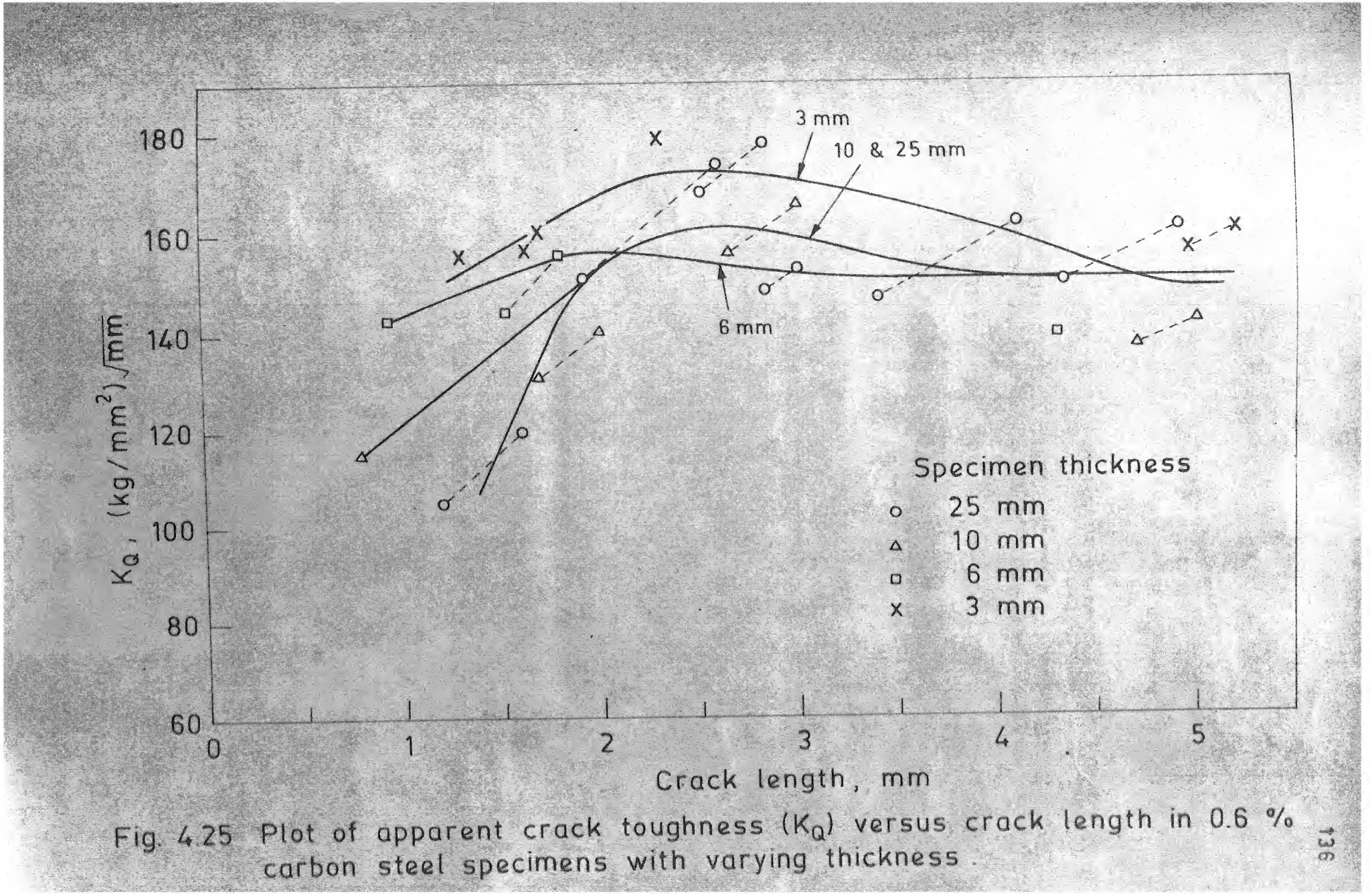

Fig. 4.25 Plot of apparent crack toughness (K_Q) versus crack length in 0.6 % carbon steel specimens with varying thickness.

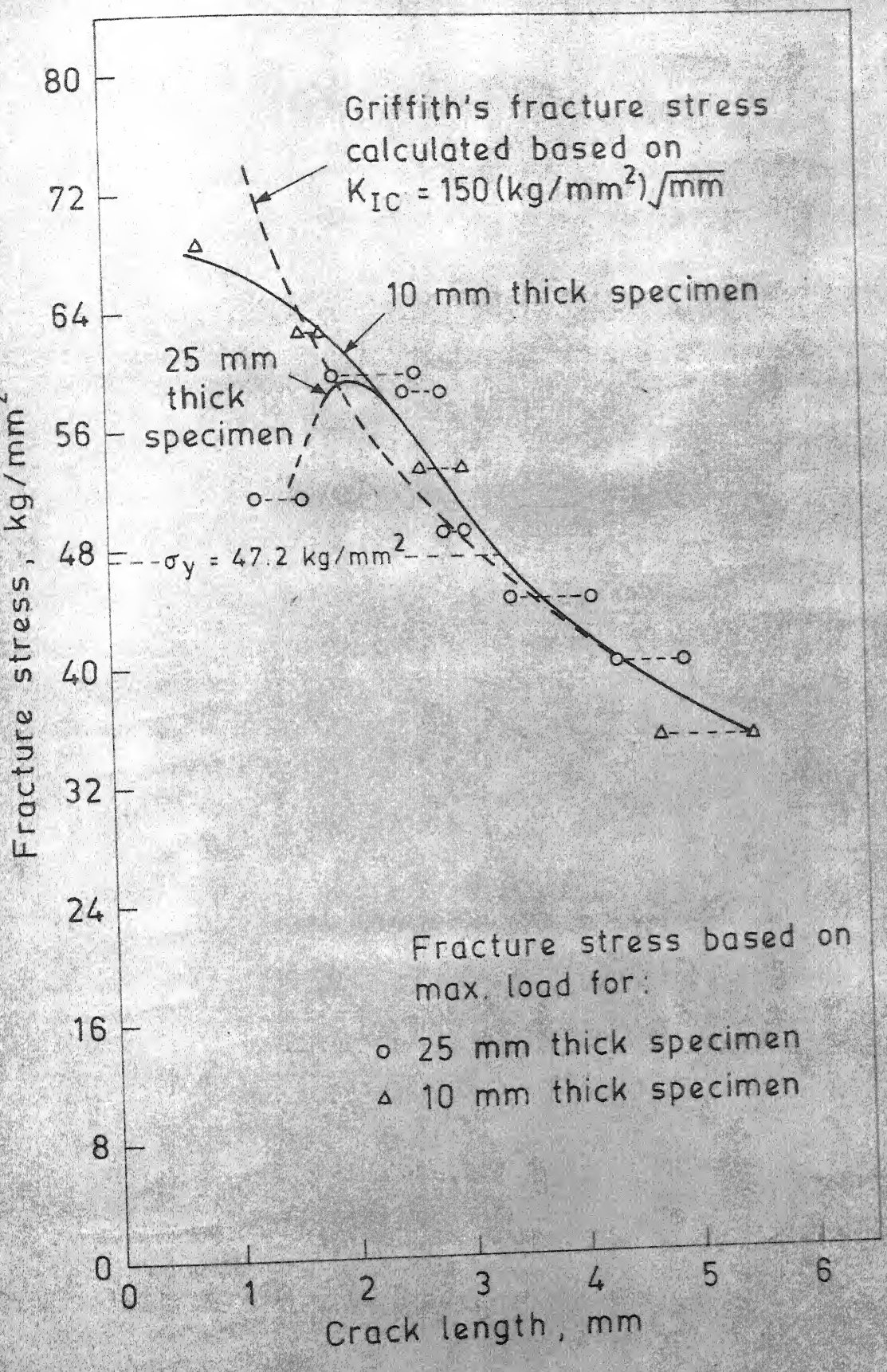

Fig. 4.26 Plot of fracture stress versus crack length in 10 mm and 25 mm thick 0.6 % carbon steel specimens.

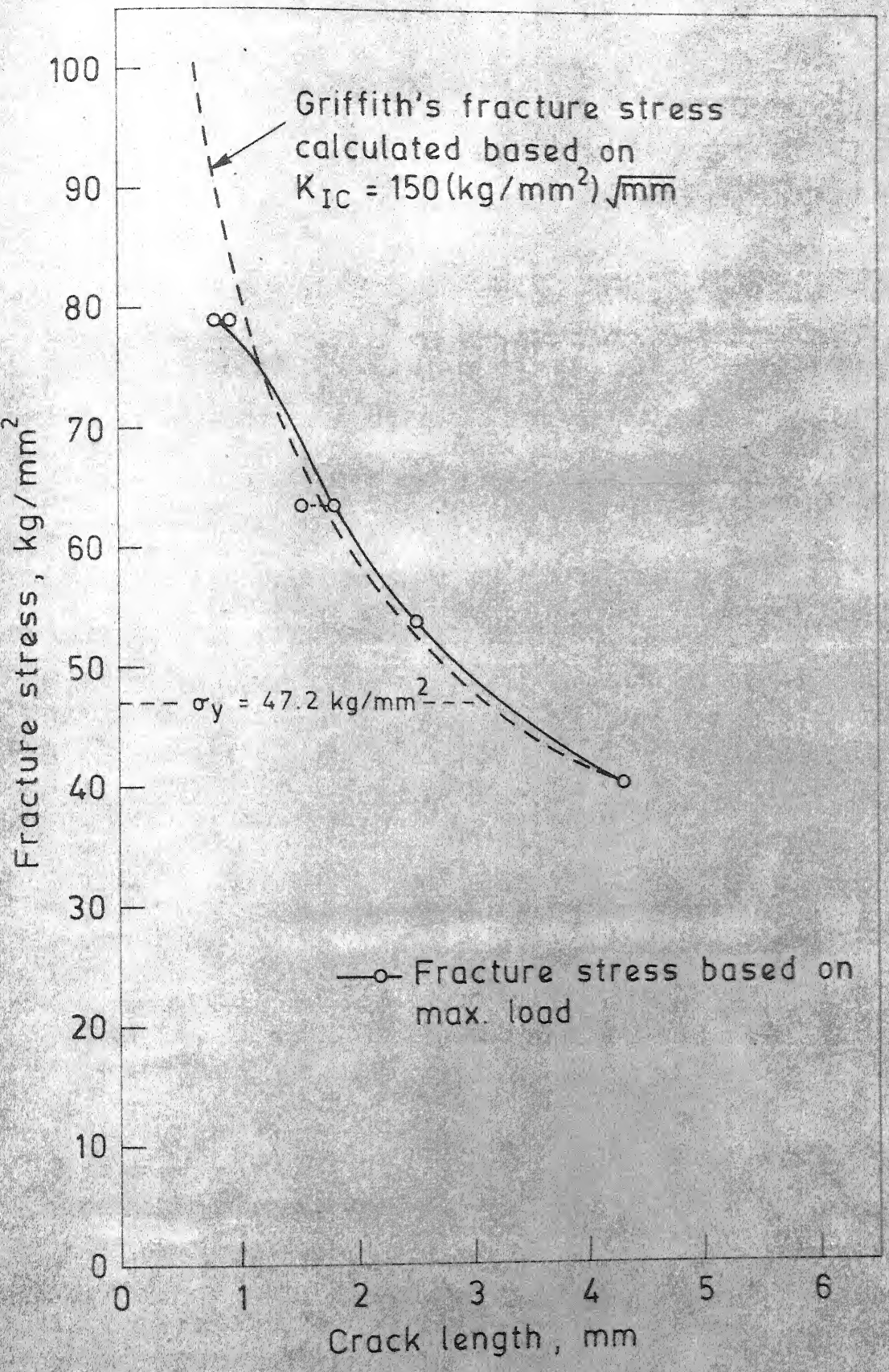

Fig. 4.27 Plot of fracture stress versus crack length in 6 mm thick 0.6 % carbon steel specimen.

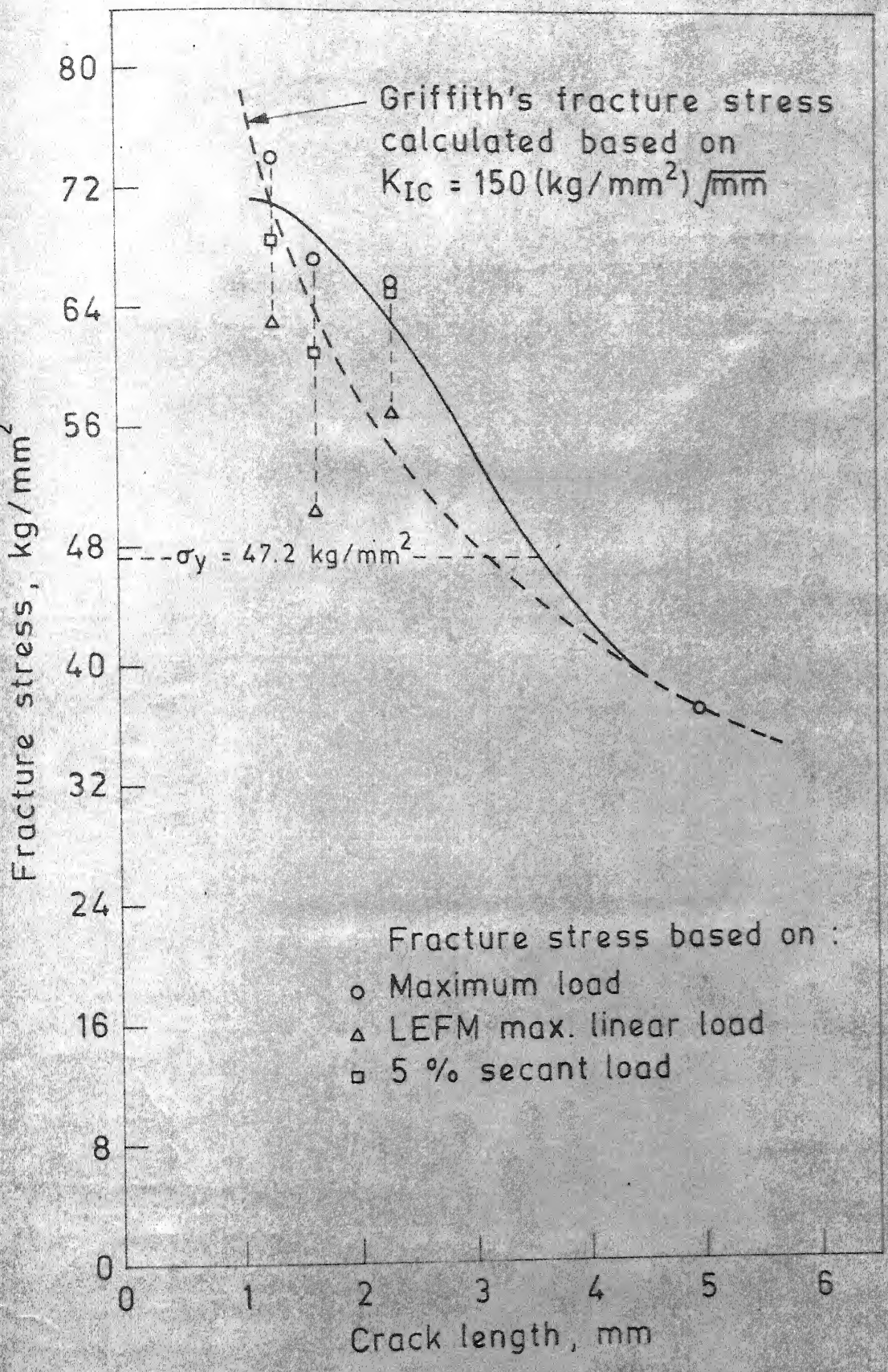

Fig. 4.28 Plot of fracture stress versus crack length in 3 mm thick 0.6 % carbon steel specimen.

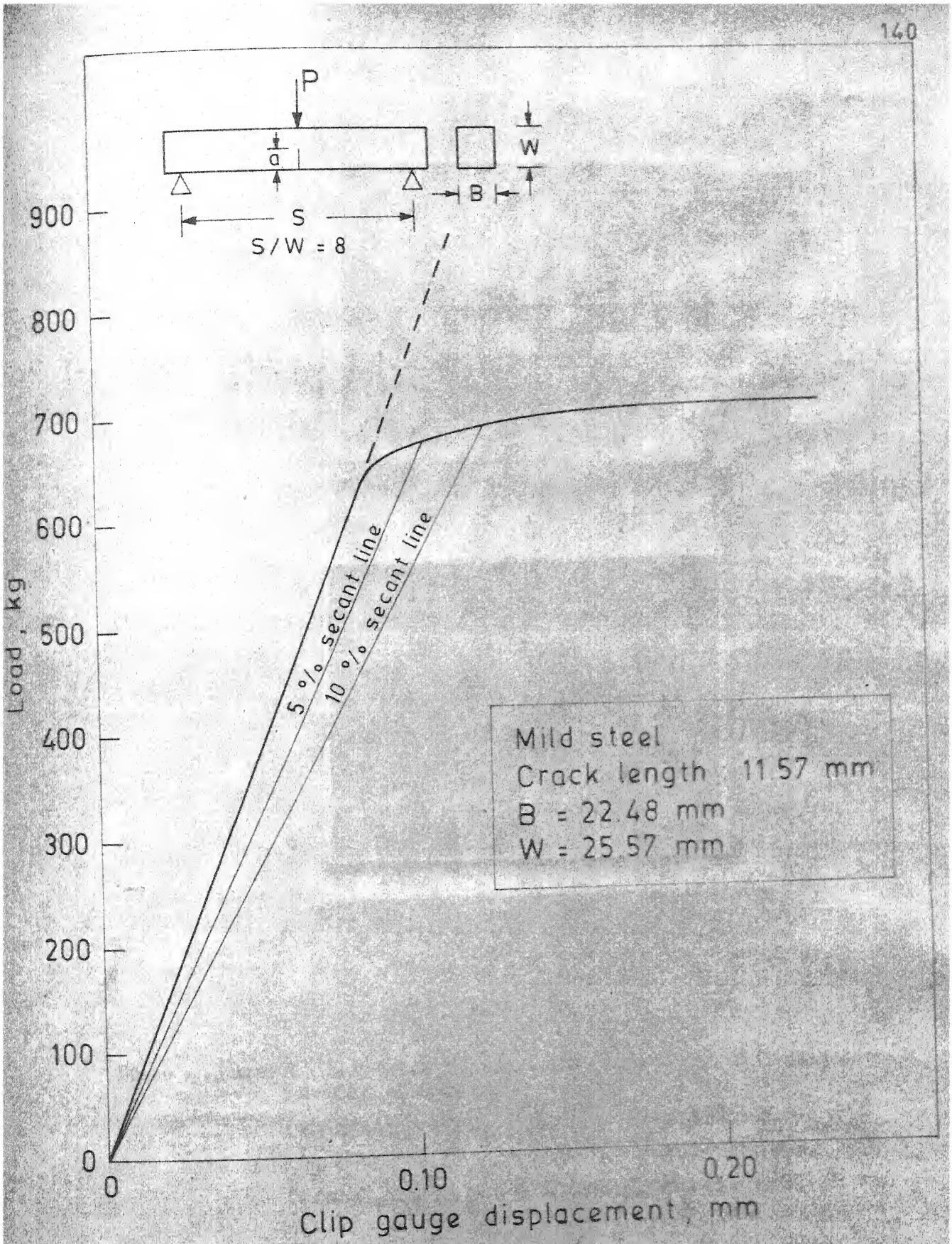

Fig. 4.29 Load versus clip gauge crack opening displacement for a crack length of 11.57 mm and thickness 22.48 mm in mild steel specimen.

(a)

250X

(b)

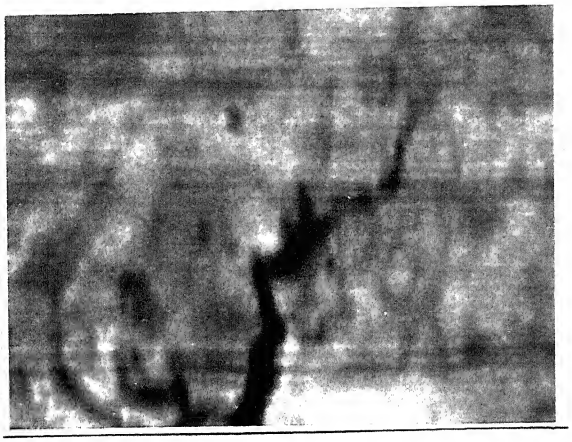

250X

Fig. 4.30: Photographs showing the crack-tip deformations in mild steel at:
(a) 300 Kg (σ/σ_y = 0.24), Magnification: 250X
(b) 670 Kg (σ/σ_y = 0.54), Magnification: 250X
(crack length = 11.57 mm, Thickness = 22.48 mm)

(continued on the next page)

(c)

250X

(d)

250X

(c) 695 Kg (σ/σ_y = 0.56), Magnification: 250X
(d) 700 Kg (σ/σ_y = 0.57), Magnification: 250X
(crack length = 11.57 mm, Thickness = 22.48 mm).

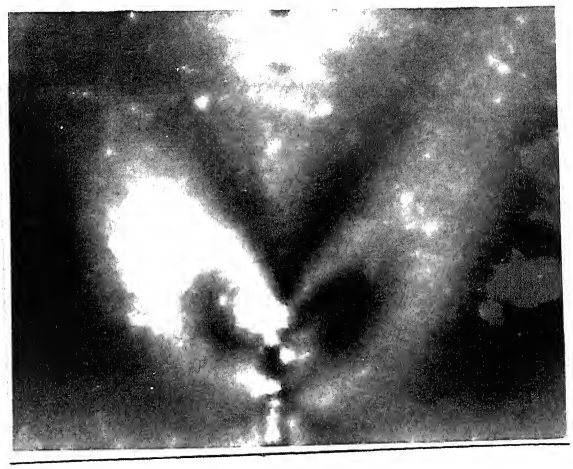

Fig. 4.31: Photograph showing isochromatic fringe pattern at crack-tip in mild steel at 700 Kg ($\sigma/\sigma_y = 0.57$) (crack length = 11.57 mm, Thickness = 22.48 mm).

	P, kg	σ / σy
d	700	0.57
c	695	0.56
b	670	0.54
a	650	0.53

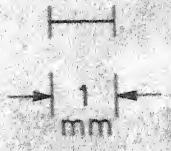

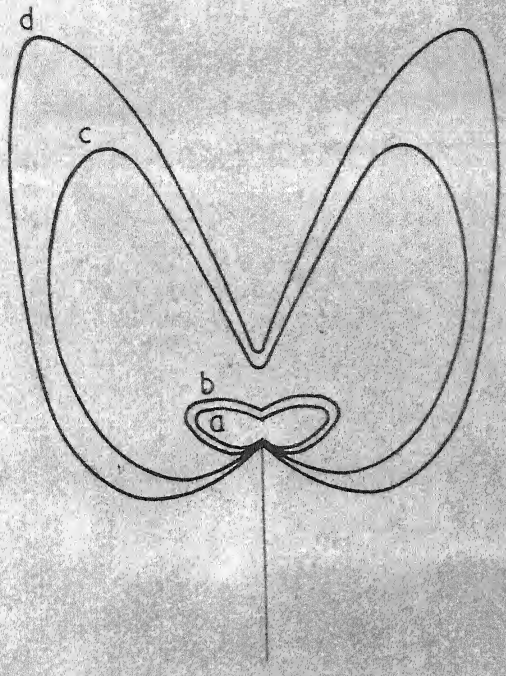

Fig. 4.32 Experimentally observed plastic zone sizes at the crack tip for different loads measured by photoelastic coating technique in mild steel specimen with crack length 11.57 mm and thickness 22.48 mm.

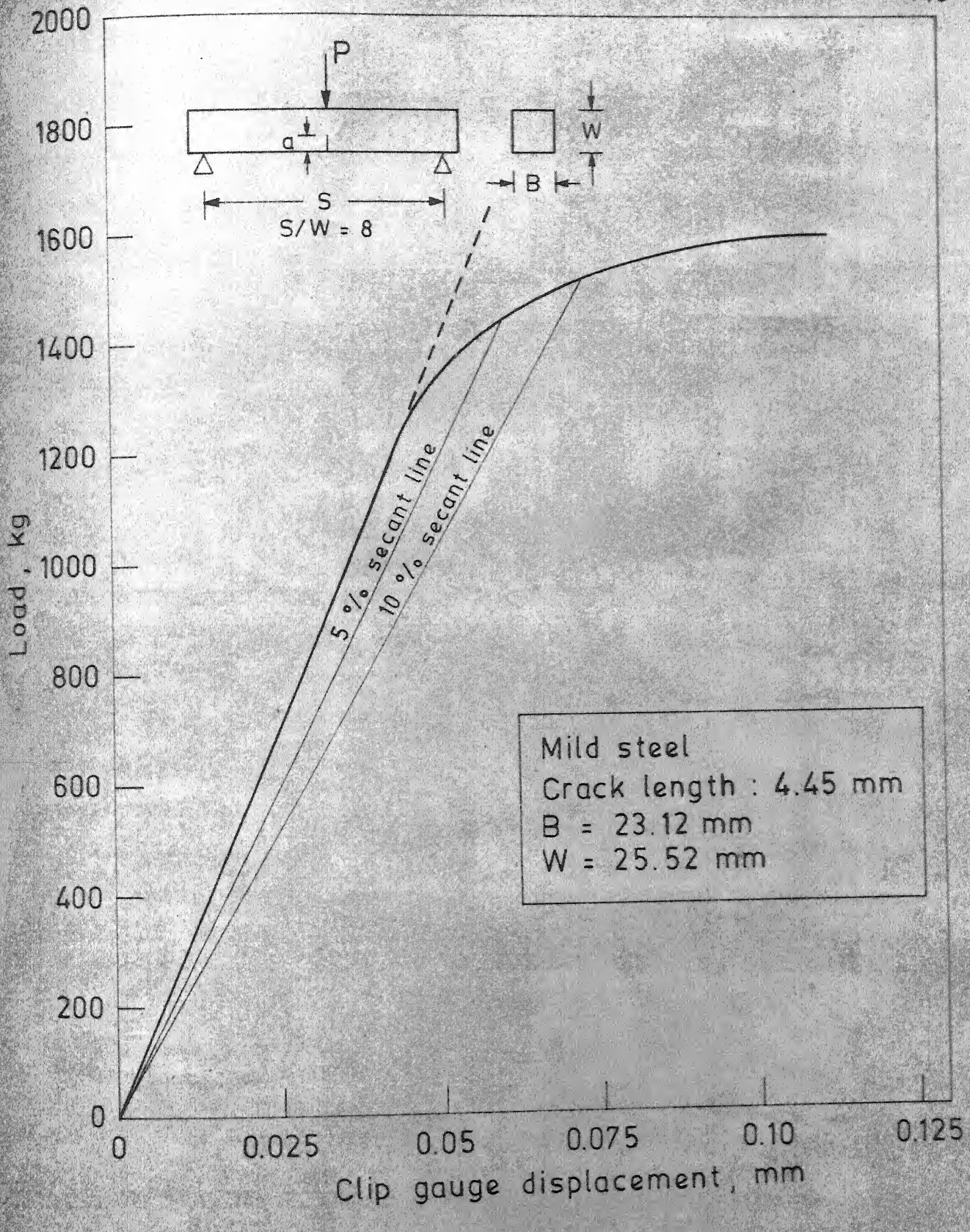

Fig. 4.33 Load versus clip gauge crack opening displacement for a crack length of 4.45 mm and thickness 23.12 mm in mild steel specimen.

	P, kg	σ / σ_y
f	1400	1.11
e	1300	1.03
d	1140	0.90
c	1100	0.87
b	1090	0.86
a	1080	0.85

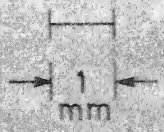

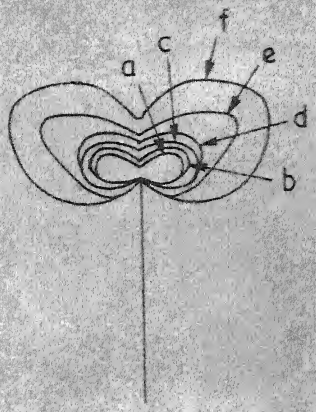

Fig. 4.34 Experimentally observed plastic zone sizes at the crack tip for different loads measured by photoelastic coating technique in mild steel specimen with crack length 4.45 mm and thickness 23.12 mm.

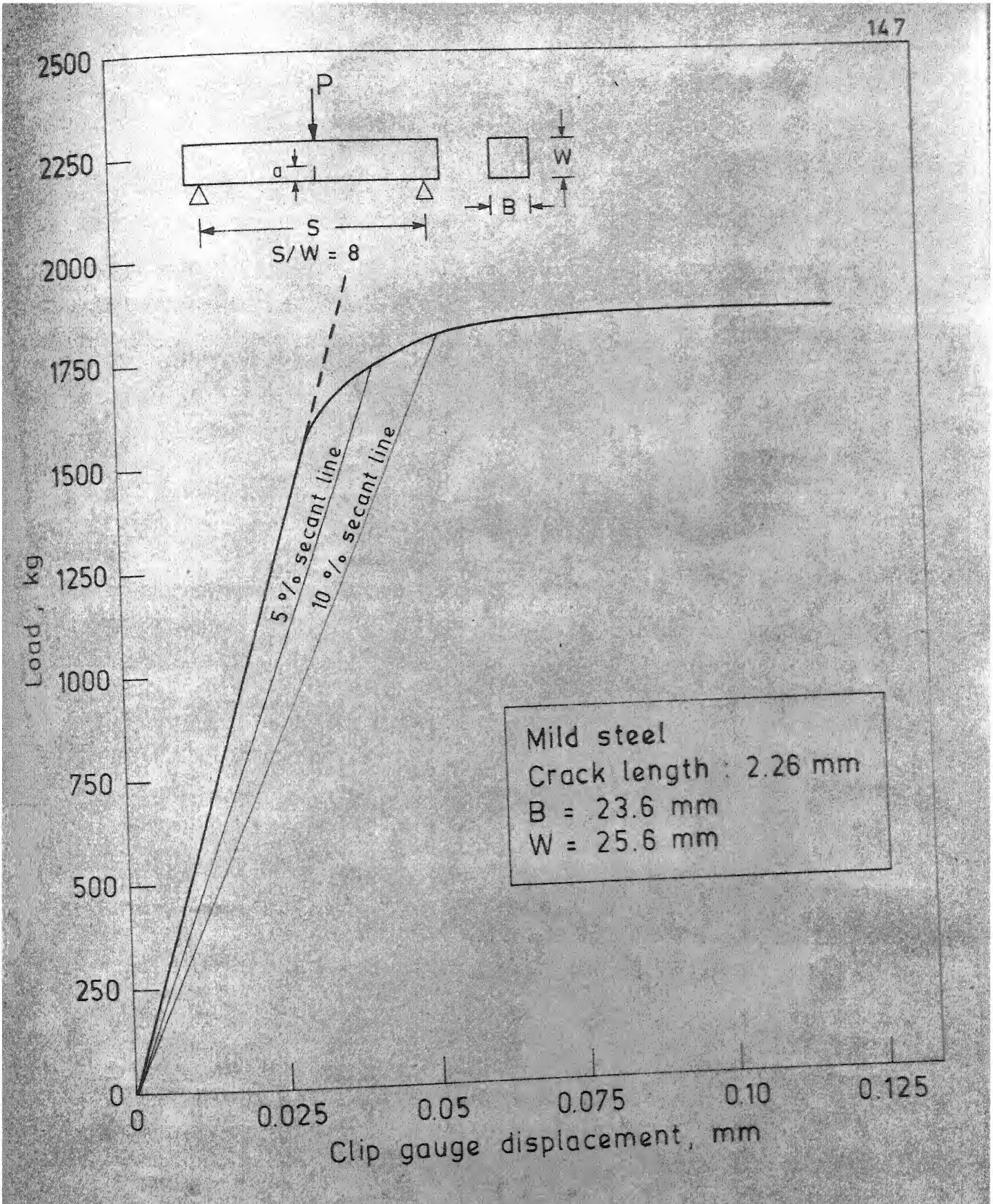

Fig. 4.35 Load versus clip gauge crack opening displacement for a crack length of 2.26 mm and thickness 23.6 mm in mild steel specimen.

	P, kg	σ / σy
e	1860	1.43
d	1760	1.35
c	1450	1.12
b	1300	1.00
a	1200	0.92

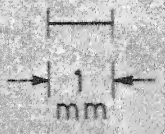

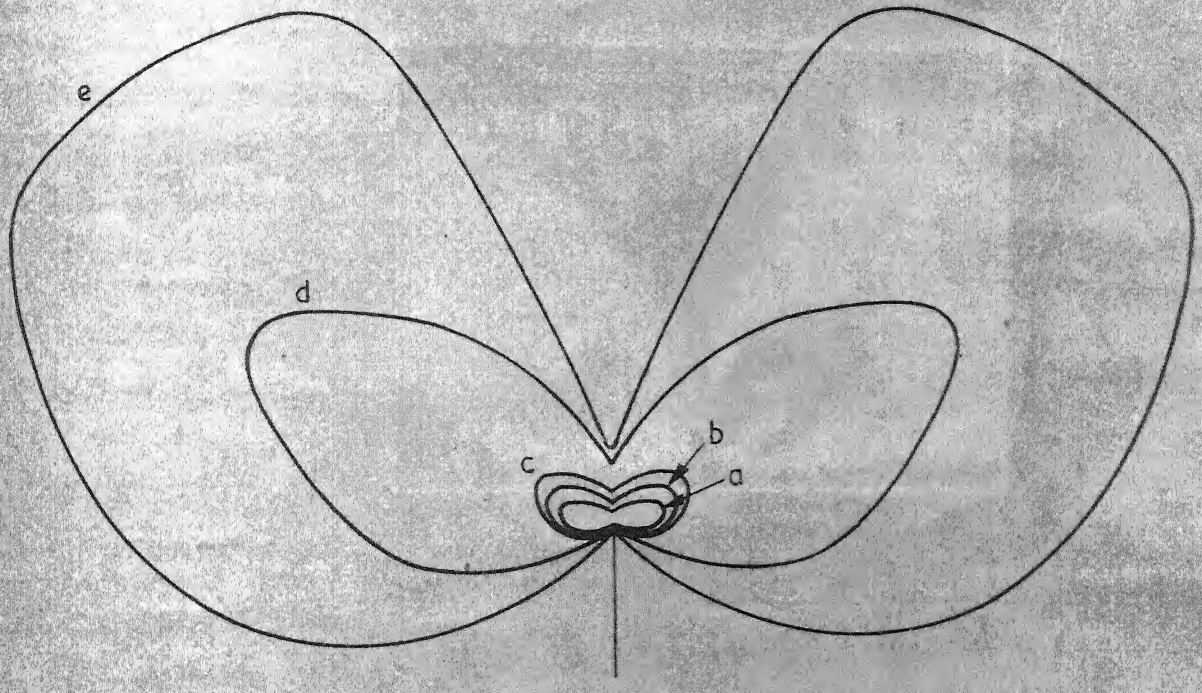

Fig. 4.36 Experimentally observed plastic zone sizes at the crack tip for different loads measured by photoelastic coating technique in mild steel specimen with crack length 2.26 mm and thickness 23.6 mm.

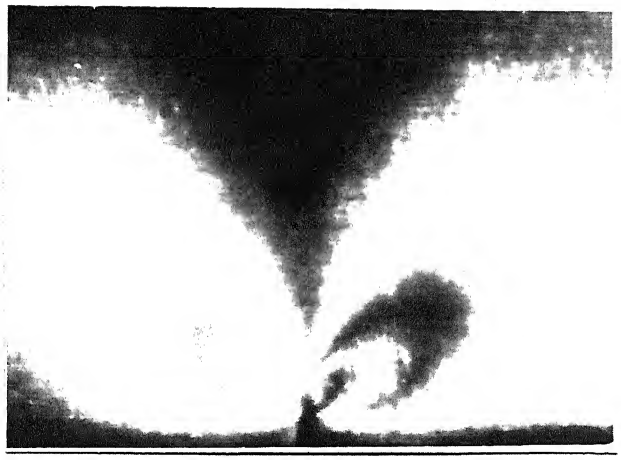

Fig. 4.37: Photograph showing isochromatic fringe pattern at crack-tip in mild steel at 1860 Kg (σ/σ_y = 1.43)
(crack length = 2.26 mm, Thickness = 23.6 mm).

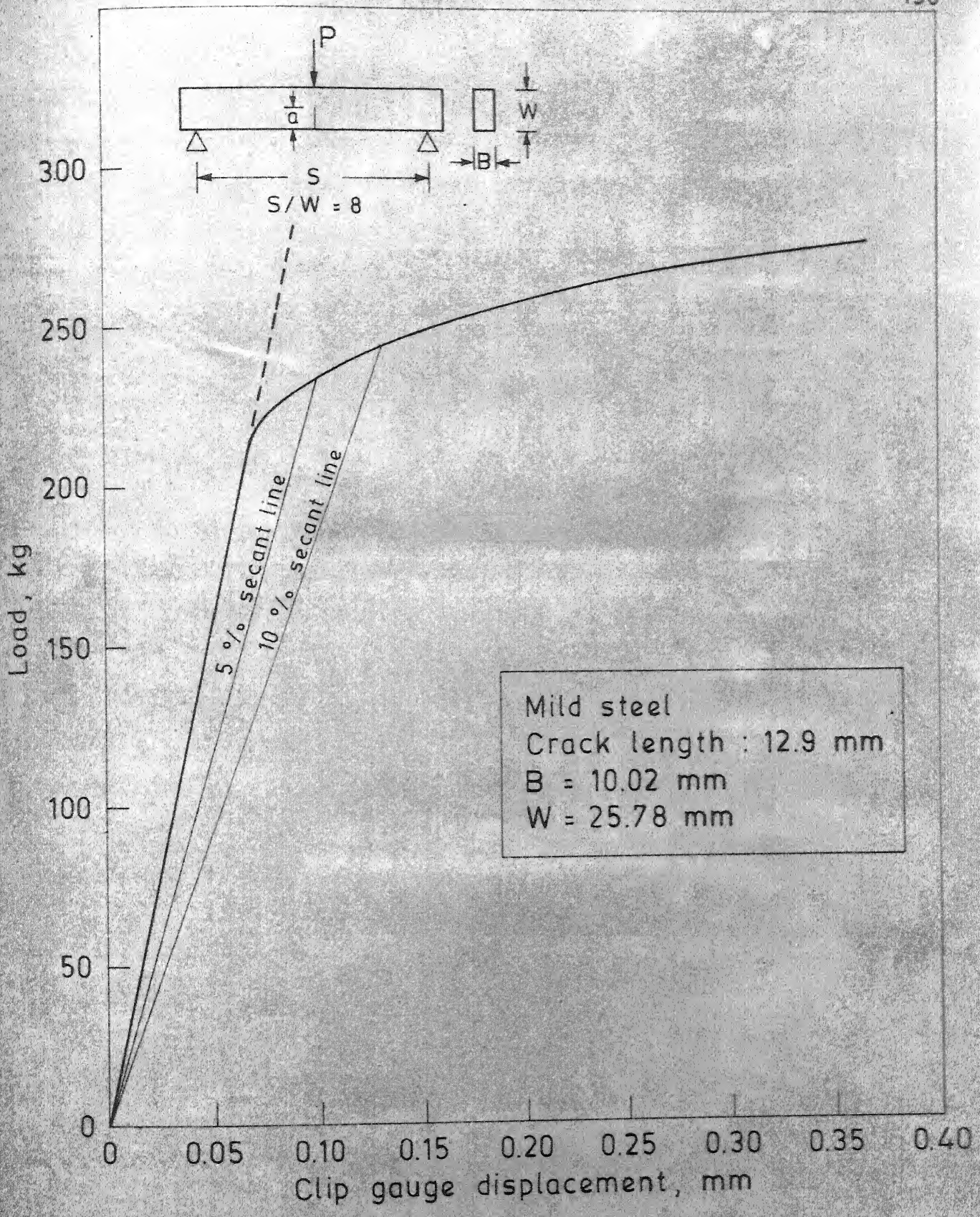

Fig. 4.38 Load versus clip gauge crack opening displacement for a crack length of 12.9 mm and thickness 10.02 mm in mild steel specimen.

	P, kg	σ / σy
e	257.5	0.46
d	235	0.42
c	190	0.34
b	150	0.27
a	120	0.21

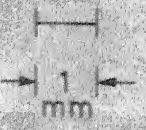

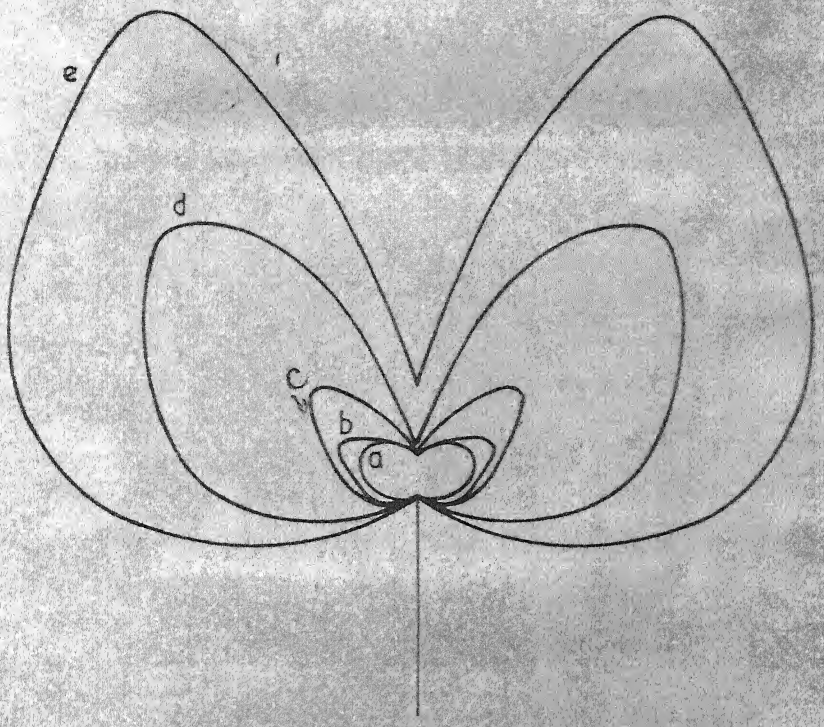

Fig. 4.39 Experimentally observed plastic zone sizes at the crack tip for different loads measured by photoelastic coating technique in mild steel specimen with crack length 12.9 mm and thickness 10.02 mm.

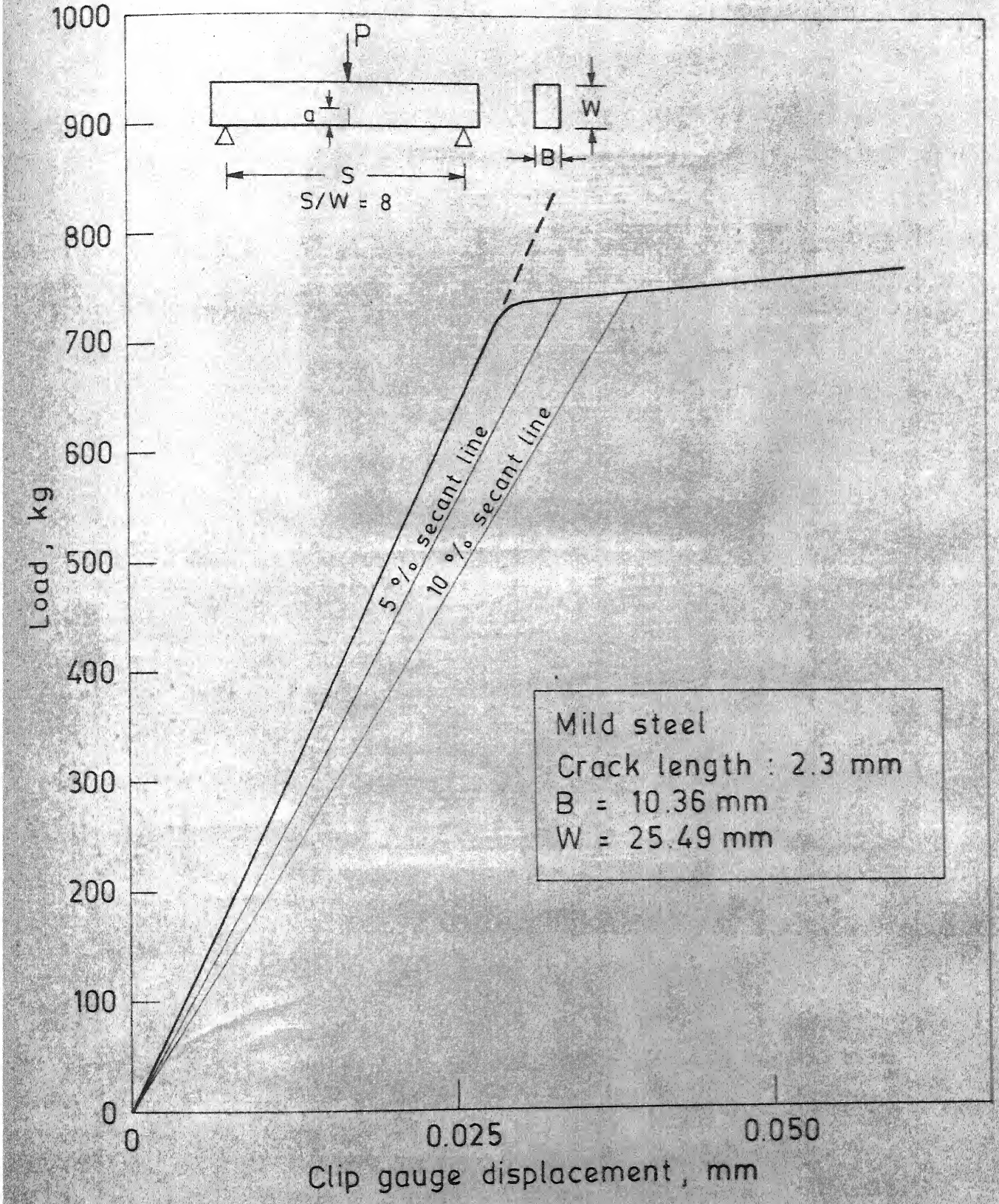

Fig. 4.40 Load versus clip gauge crack opening displacement for a crack length of 2.3 mm and thickness 10.36 mm in mild steel specimen.

(a)

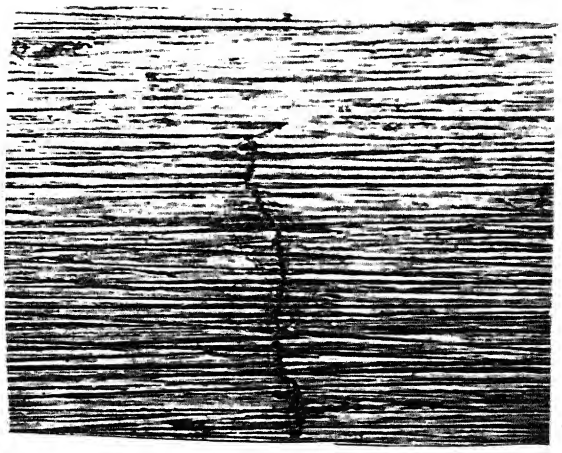

250X

(b)

250X

Fig. 4.41: Photographs showing the crack-tip deformation in mild steel at
(a) 698 Kg (σ/σ_y = 1.23), Magnification: 250X
(b) 770 Kg (σ/σ_y = 1.36), Magnification: 250X
(crack length = 2.3 mm, Thickness = 10.36 mm).

(a)

(b)

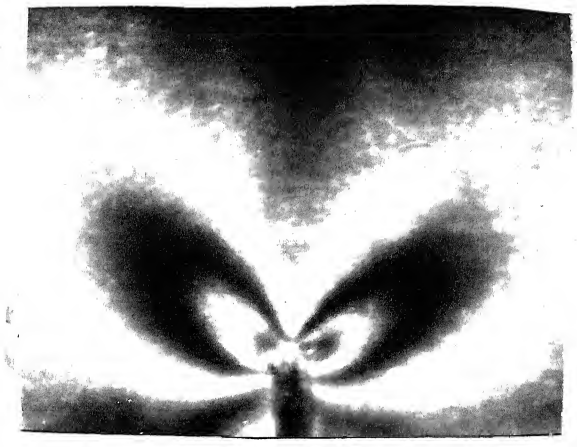

Fig. 4.42: Photographs showing isochromatic fringe patterns at crack-tip in mild steel at
(a) 698 Kg (σ/σ_y = 1.23),
(b) 770 Kg (σ/σ_y = 1.36),
(crack length = 2.3 mm, Thickness = 10.36 mm).

	P, kg	σ/σy
d	770	1.36
c	698	1.23
b	500	0.88
a	400	0.71

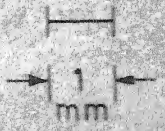

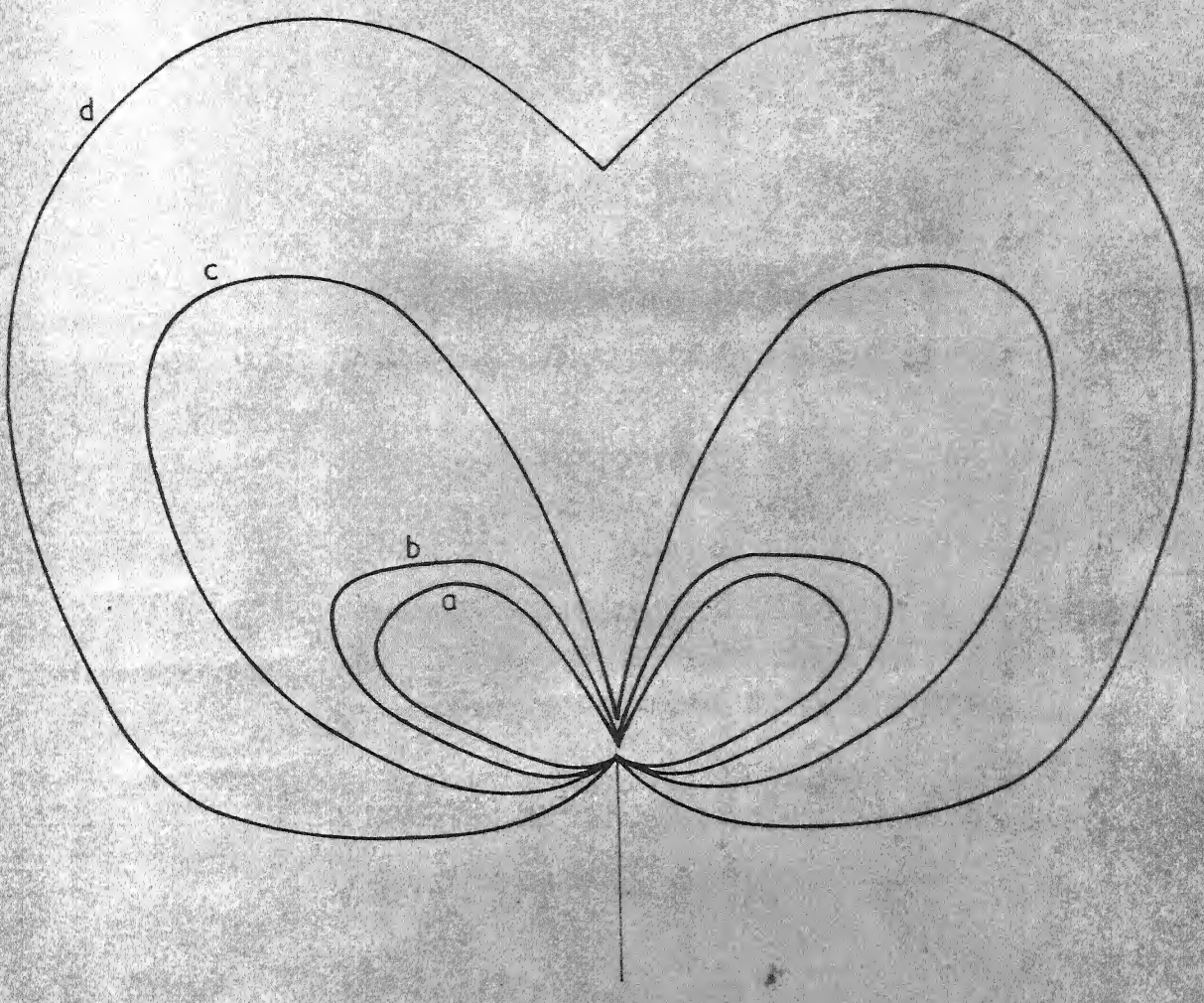

Fig. 4.43 Experimentally observed plastic zone sizes at the crack tip for different loads measured by photoelastic coating technique in mild steel specimen with crack length 2.3 mm and thickness 10.36 mm.

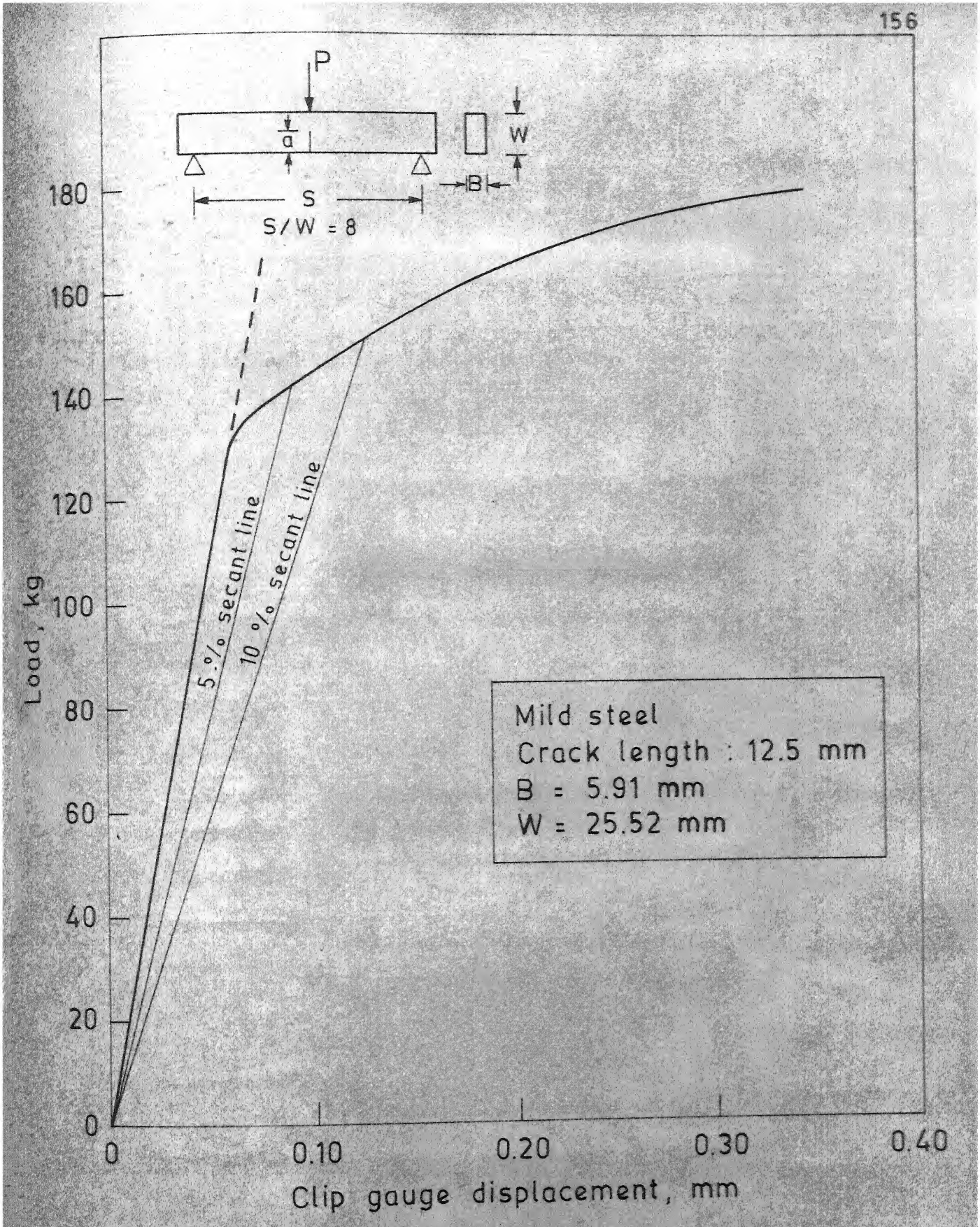

Fig. 4.44 Load versus clip gauge crack opening displacement for a crack length of 12.5 mm and thickness 5.91 mm in mild steel specimen.

	P, kg	σ / σy
e	180	0.56
d	168	0.52
c	138	0.43
b	90	0.28
a	70	0.22

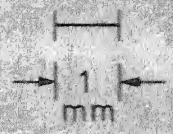

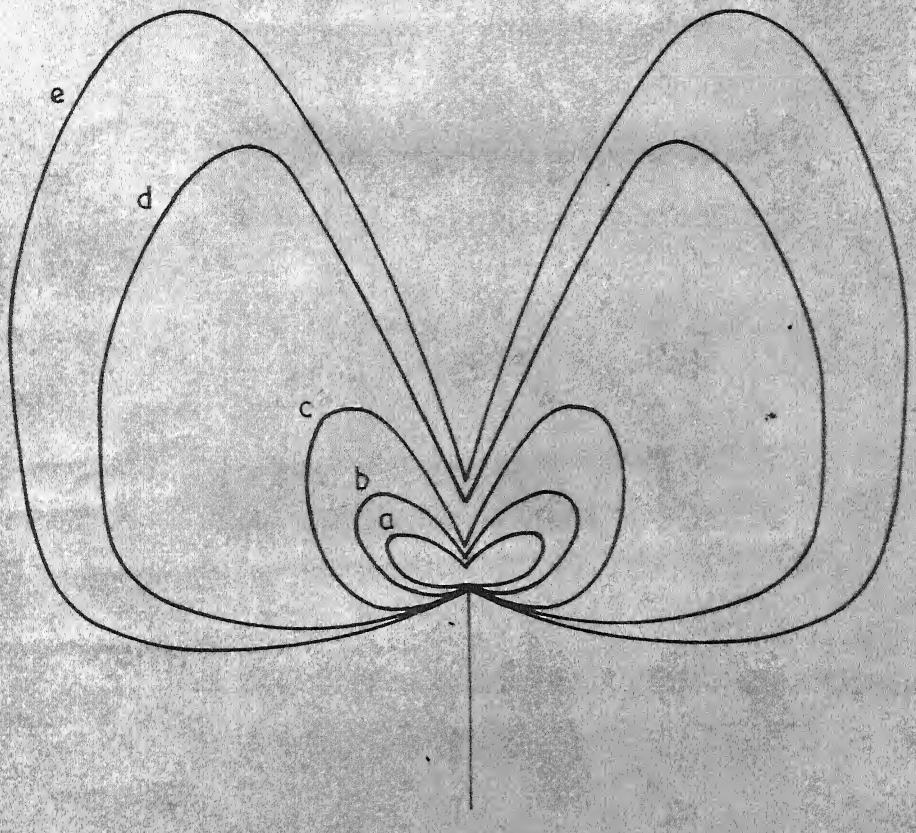

Fig. 4.45 Experimentally observed plastic zone sizes at the crack tip for different loads measured by photoelastic coating technique in mild steel specimen with crack length 12.5 mm and thickness 5.91 mm.

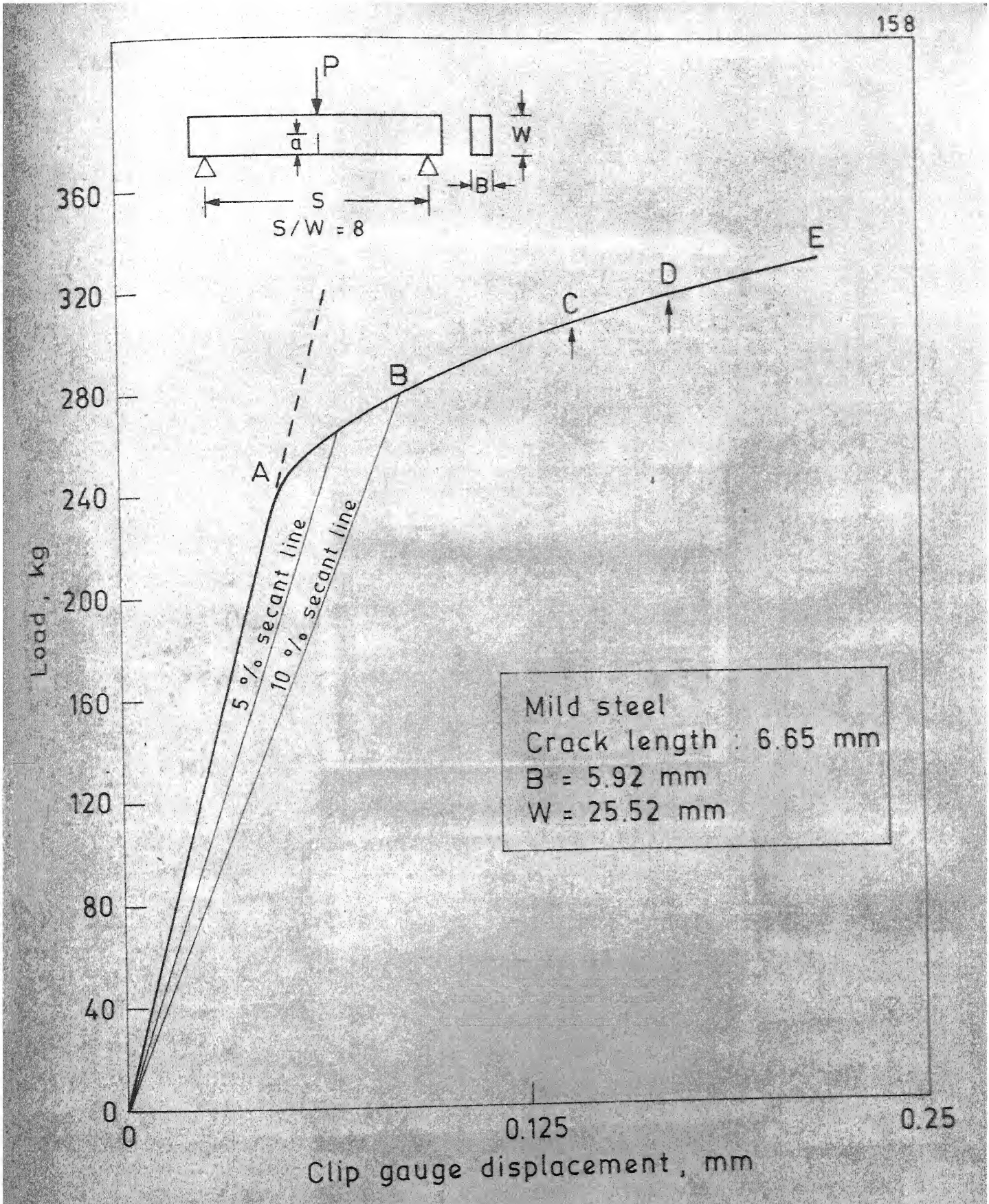

Fig. 4.46 Load versus clip gauge crack opening displacement for a crack length of 6.65 mm and thickness 5.92 mm in mild steel specimen.

(a) 250X

(b) 250X

(c) 120X

Fig. 4.47: Photographs showing the crack-tip deformations in mild steel at
(a) 240 Kg ($\sigma/\sigma_y = 0.74$), Magnification: 250X
(b) 310 Kg ($\sigma/\sigma_y = 0.96$), Magnification: 250X
(c) 332.5 Kg($\sigma/\sigma_y = 1.02$), Magnification: 120X
(crack length = 6.65 mm, Thickness = 5.92 mm).

(a)

(b)

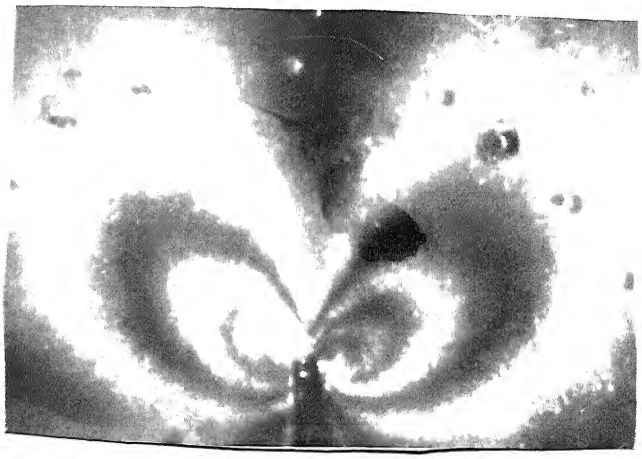

Fig. 4.48: Photographs showing isochromatic fringe patterns at crack-tip in mild steel at
(a) 310 Kg (σ/σ_y = 0.96)
(b) 332.5 Kg (σ/σ_y = 1.02)
(crack length = 6.65 mm. Thickness = 5.92 mm).

	P, kg	σ / σy
e	332.5	1.02
d	310	0.96
c	240	0.74
b	200	0.62
a	150	0.46

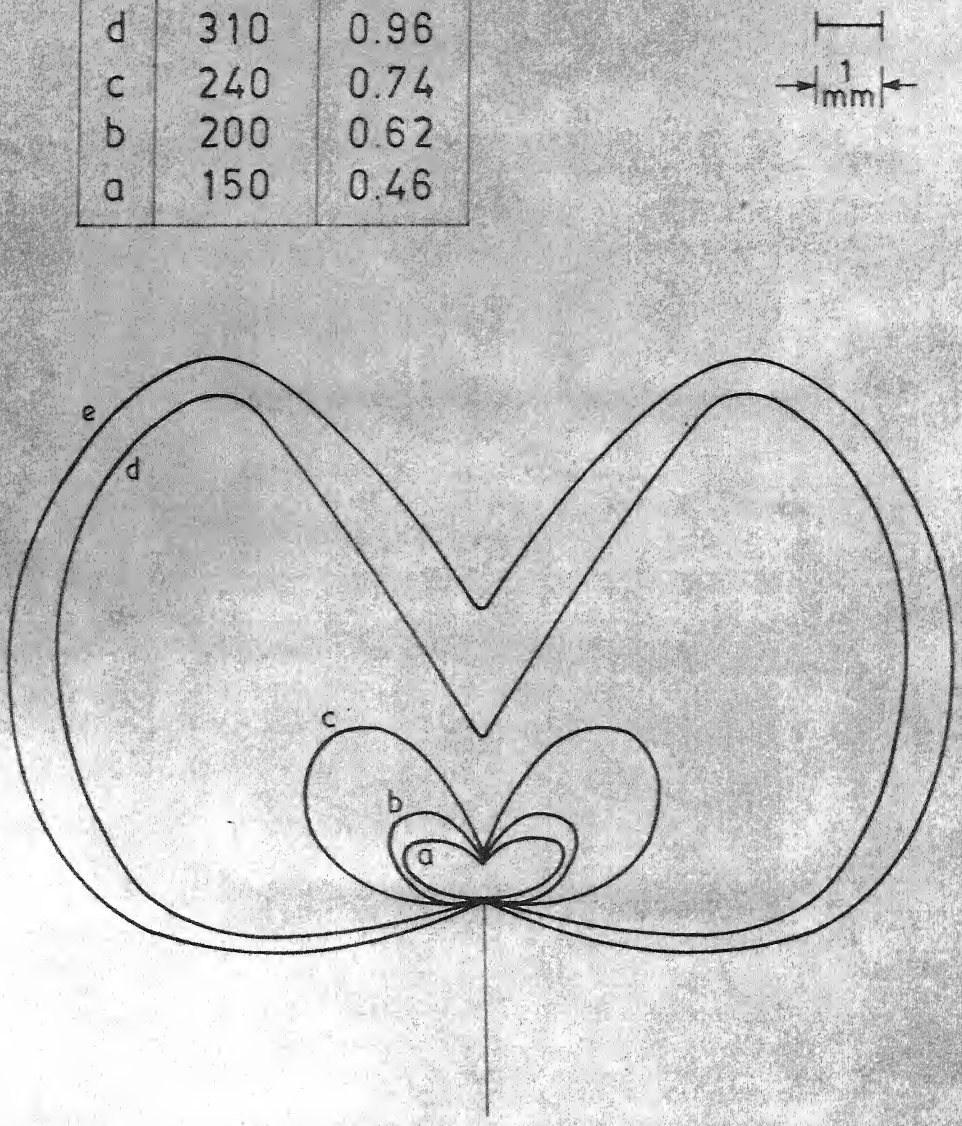

Fig. 4.49 Experimentally observed plastic zone sizes at the crack tip for different loads measured by photoelastic coating technique in mild steel specimen with crack length 6.65 mm and thickness 5.92 mm.

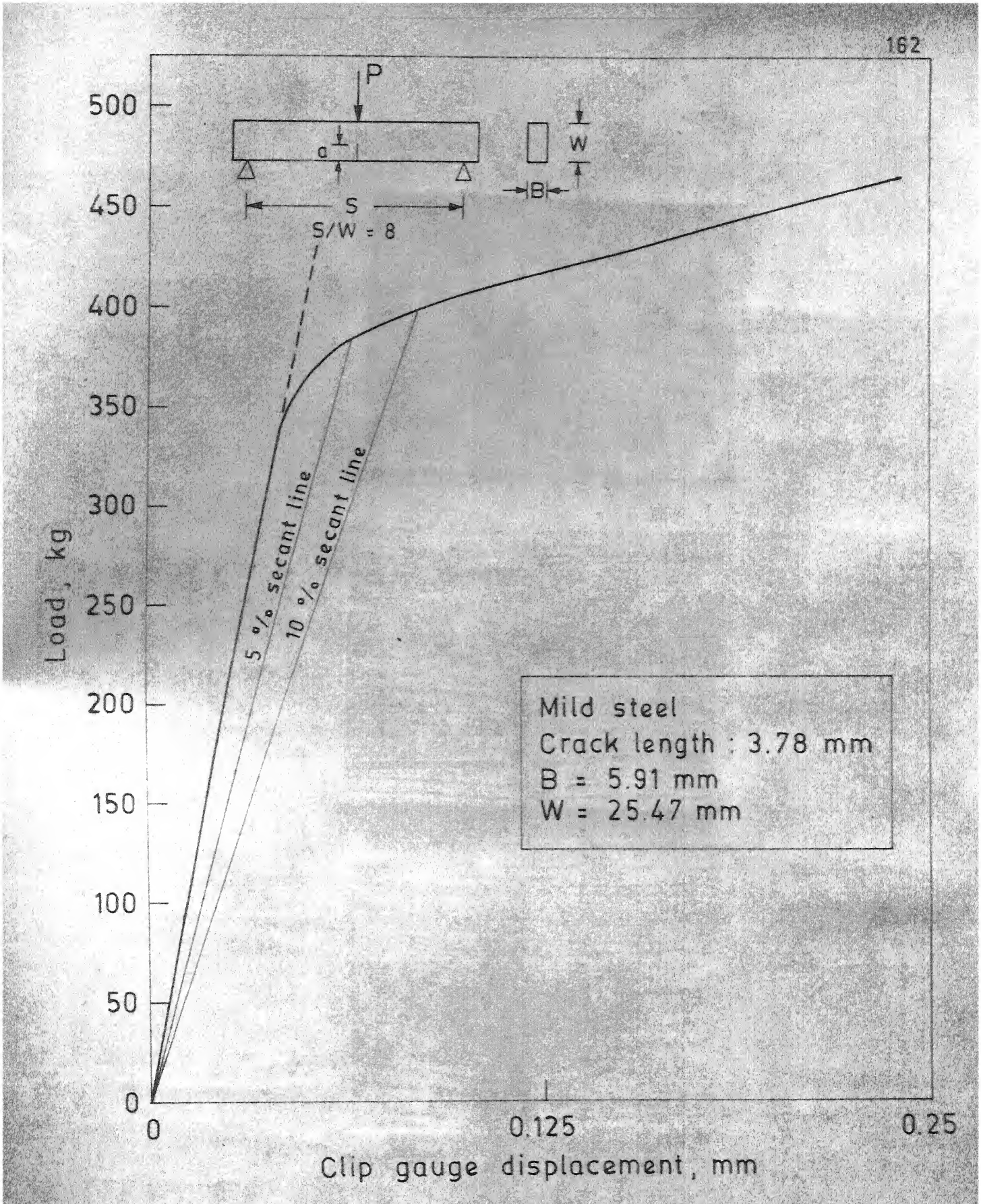

Fig. 4.50 Load versus clip gauge crack opening displacement for a crack length of 3.78 mm and thickness 5.91 mm in mild steel specimen.

(a)

250X

(b)

250X

(c)

250X

Fig. 4.51: Photographs showing the crack-tip deformations in mild steel at
(a) 330 Kg (σ/σ_y = 1.02), Magnification: 250X
(b) 394 Kg (σ/σ_y = 1.22), Magnification: 250X
(c) 410 Kg (σ/σ_y = 1.27). Magnification: 250X
(crack length = 3.78 mm, Thickness = 5.91 mm).

Fig. 4.52: Photograph showing isochromatic fringe pattern at crack-tip in mild steel at 410 Kg (σ/σ_y = 1.27) (crack length = 3.78 mm, Thickness = 5.91 mm).

	P, kg	σ/σ_y
d	410	1.27
c	330	1.02
b	270	0.83
a	200	0.62

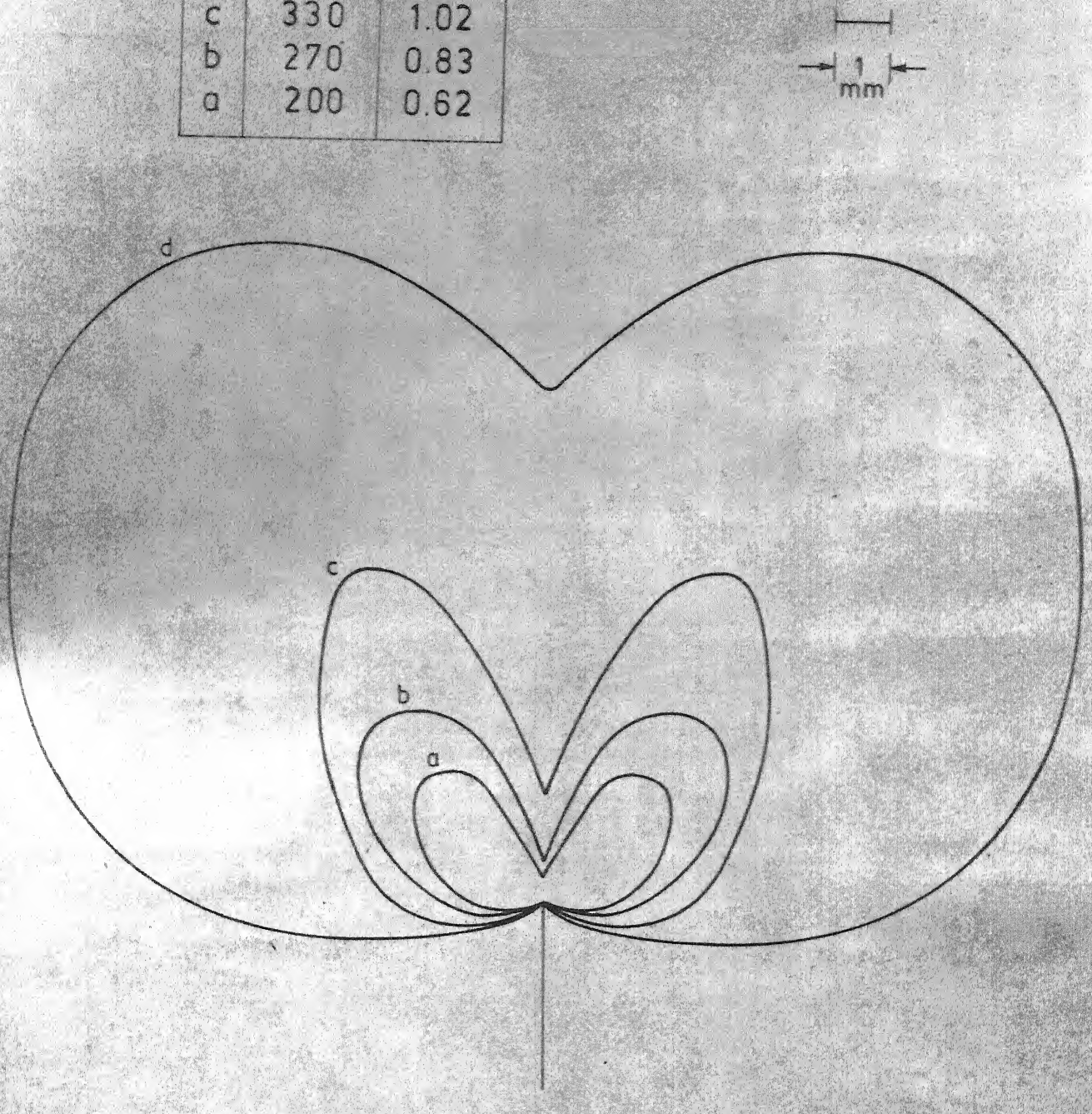

Fig. 4.53 Experimentally observed plastic zone sizes at the crack tip for different loads measured by photoelastic coating technique in mild steel specimen with crack length 3.78 mm and thickness 5.91 mm.

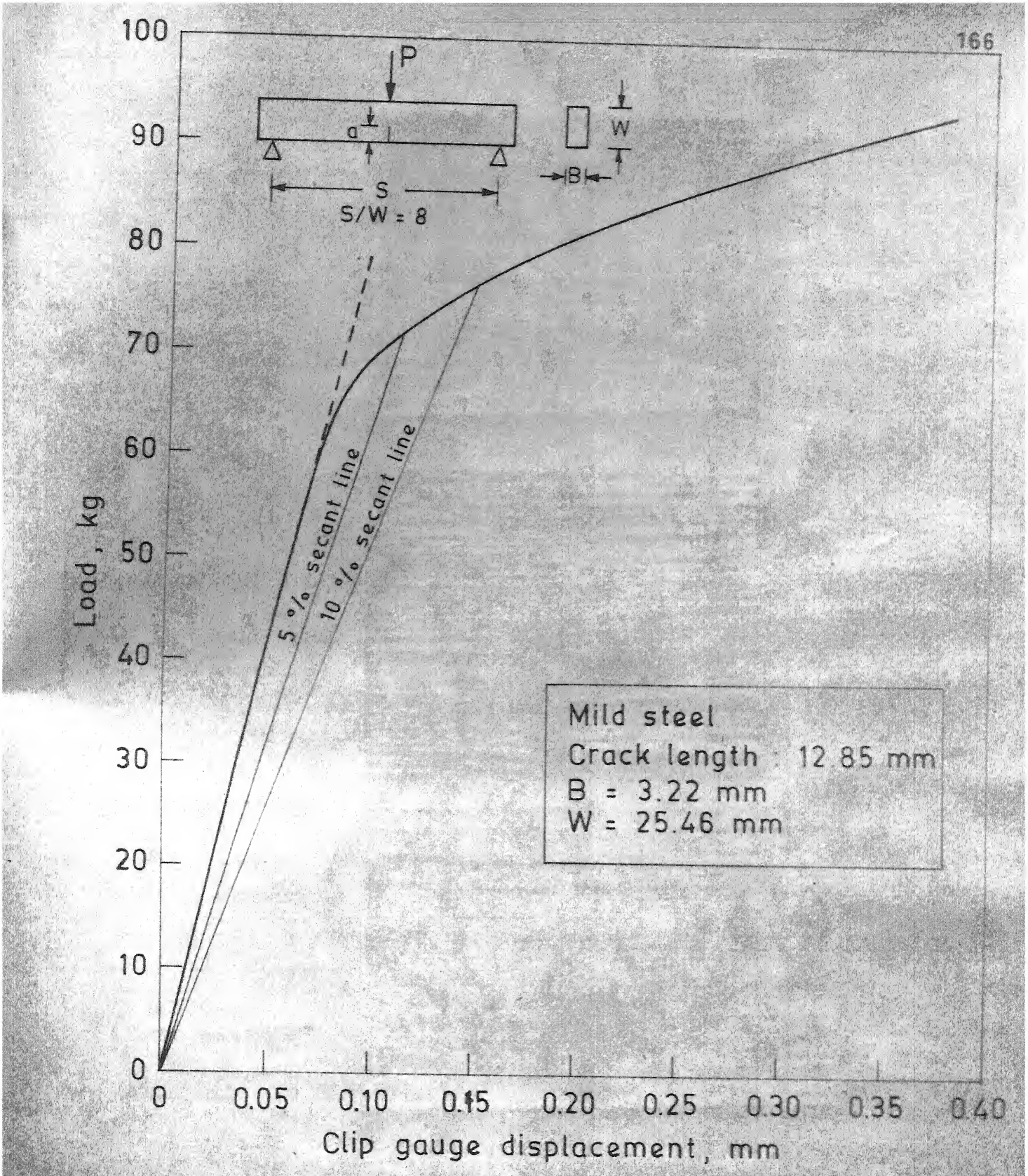

Fig. 4.54 Load versus clip gauge crack opening displacement for a crack length of 12.85 mm and thickness 3.22 mm in mild steel specimen.

(a)

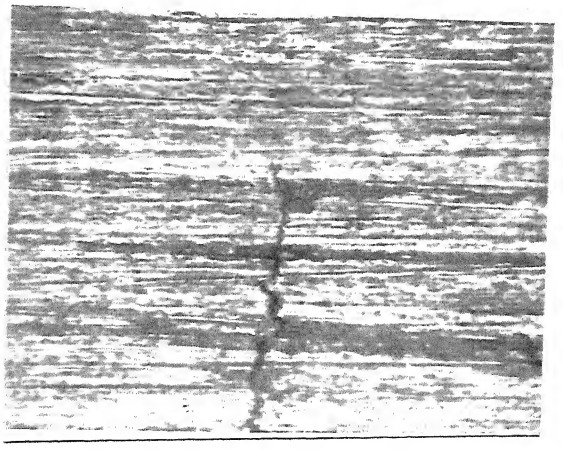

250X

(b)

250X

(c)

120X

Fig. 4.55: Photographs showing the crack-tip deformations in mild steel at

(a) 70 Kg (σ/σ_y = 0.40), Magnification: 250X

(b) 85 Kg (σ/σ_y = 0.48), Magnification: 250X

(c) 93 Kg (σ/σ_y = 0.53), Magnification: 120X

(crack length = 12.85 mm, Thickness = 3.22 mm).

(a)

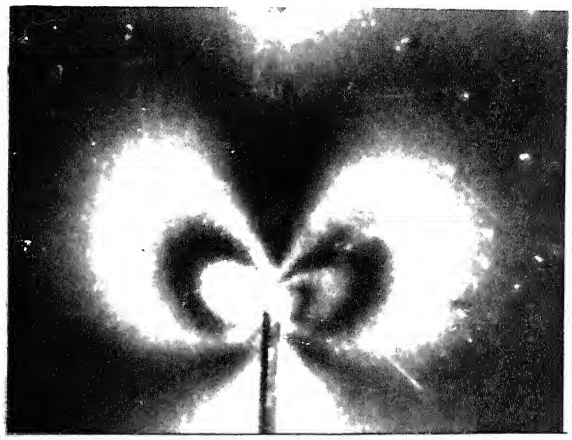

(b)

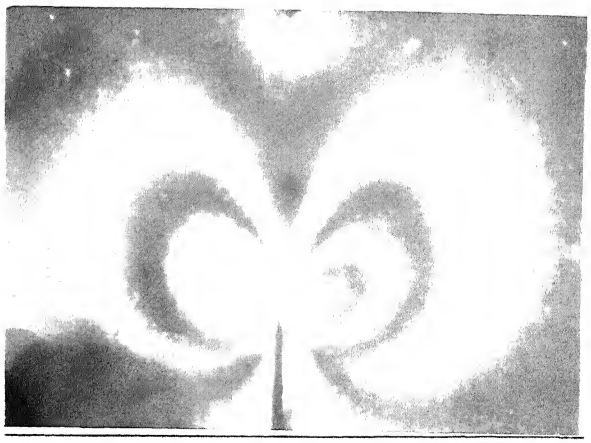

Fig. 4.56: Photographs showing isochromatic fringe patterns at crack-tip in mild steel at
(a) 85 Kg (σ/σ_y = 0.48)
(b) 93 Kg (σ/σ_y = 0.53)
(crack length = 12.85 mm, Thickness = 3.22 mm).

	P, kg	σ / σy
e	93	0.53
d	85	0.48
c	70	0.40
b	50	0.28
a	30	0.17

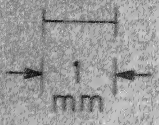

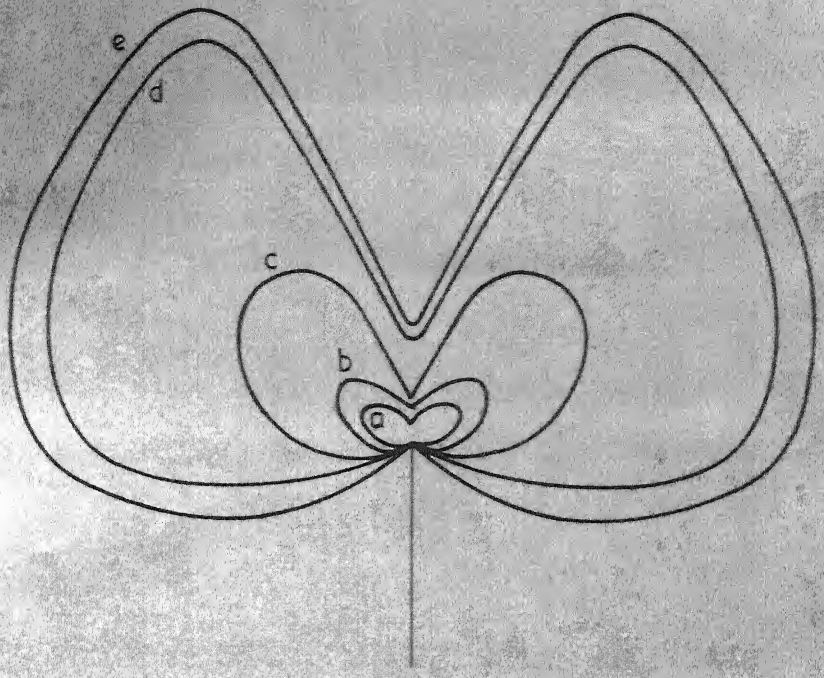

Fig. 4.57 Experimentally observed plastic zone sizes at the crack tip for different loads measured by photoelastic technique in mild steel specimen with crack length 12.85 mm and thickness 3.22 mm.

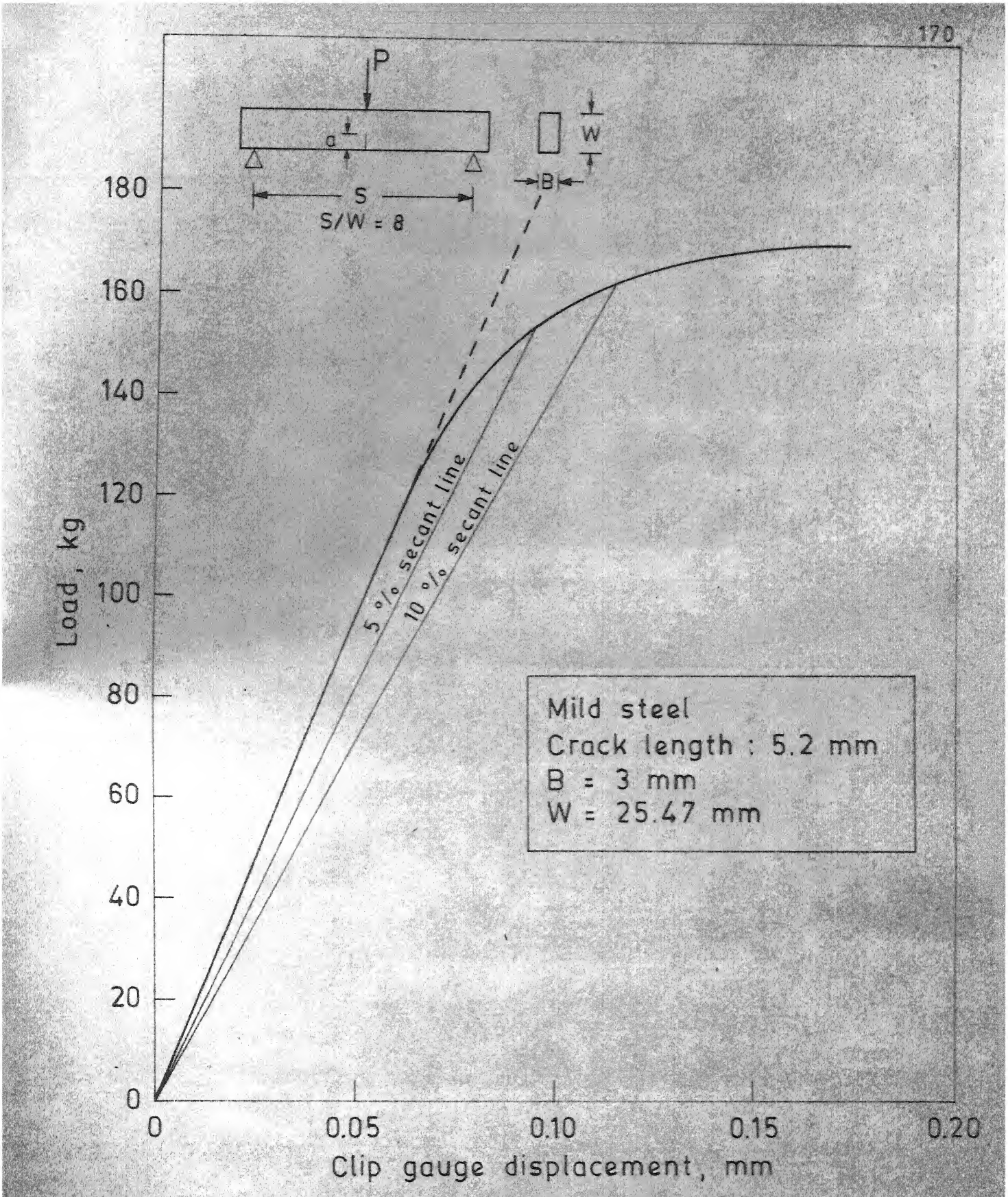

Fig. 4.58 Load versus clip gauge crack opening displacement for a crack length of 5.2 mm and thickness 3 mm in mild steel specimen.

(a) 250X

(b) 250X

(c) 120X

Fig. 4.59: Photographs showing the crack-tip deformations in mild steel at
(a) 130 Kg (σ/σ_y = 0.79), Magnification: 250X
(b) 160 Kg (σ/σ_y = 0.98), Magnification: 250X
(c) 170 Kg (σ/σ_y = 1.04), Magnification: 120X
(crack length = 5.2 mm, Thickness = 3 mm).

	P, kg	σ/σy
e	170	1.04
d	160	0.98
c	130	0.79
b	100	0.61
a	30	0.18

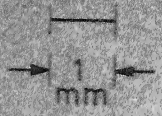

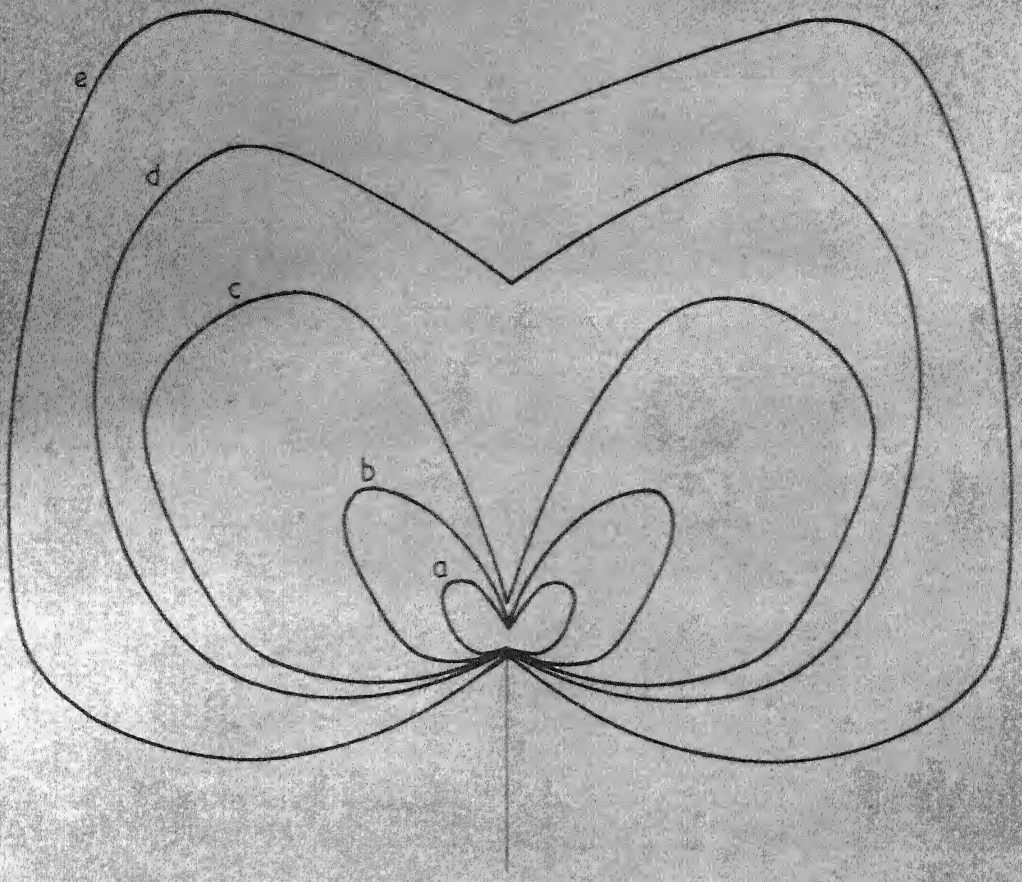

Fig. 4.60 Experimentally observed plastic zone sizes at the crack tip for different loads measured by photoelastic coating technique in mild steel specimen with crack length 5.2 mm and thickness 3.0 mm.

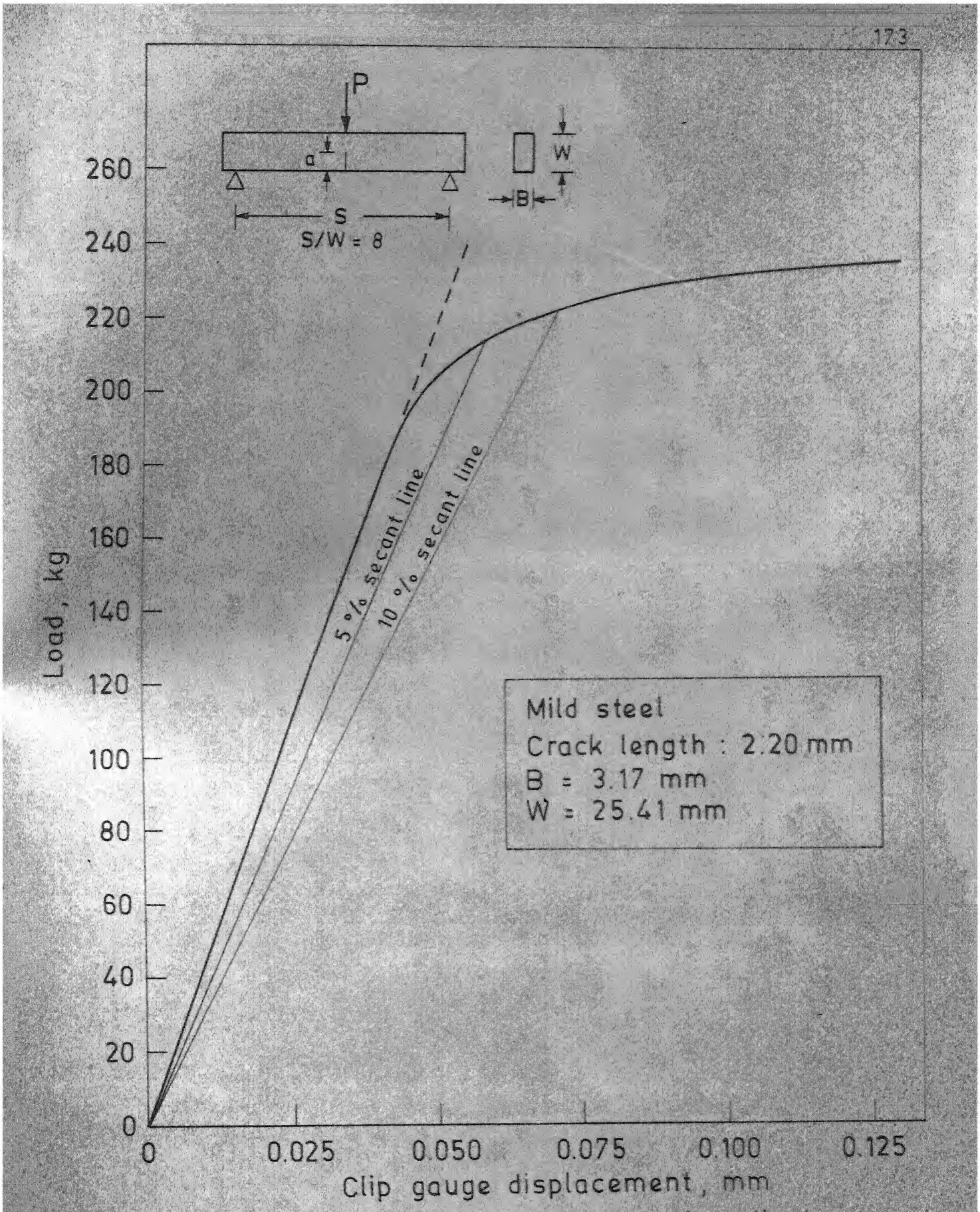

Fig. 4.61 Load versus clip gauge crack opening displacement for a crack length of 2.20 mm and thickness 3.17 mm in mild steel specimen.

	P, kg	σ/σy
d	200	1.28
c	190	1.10
b	170	0.99
a	130	0.76

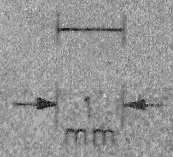

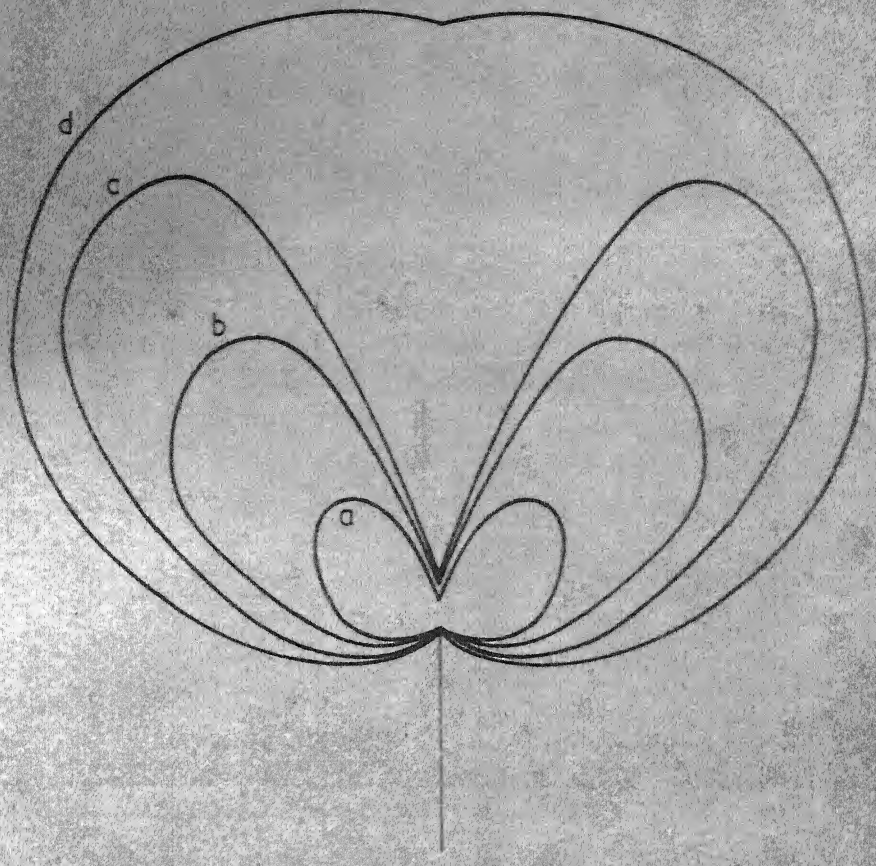

Fig. 4.62 Experimentally observed plastic zone sizes at the crack tip for different loads measured by photoelastic coating technique in mild steel specimen with crack length 2.20 mm and thickness 3.17 mm.

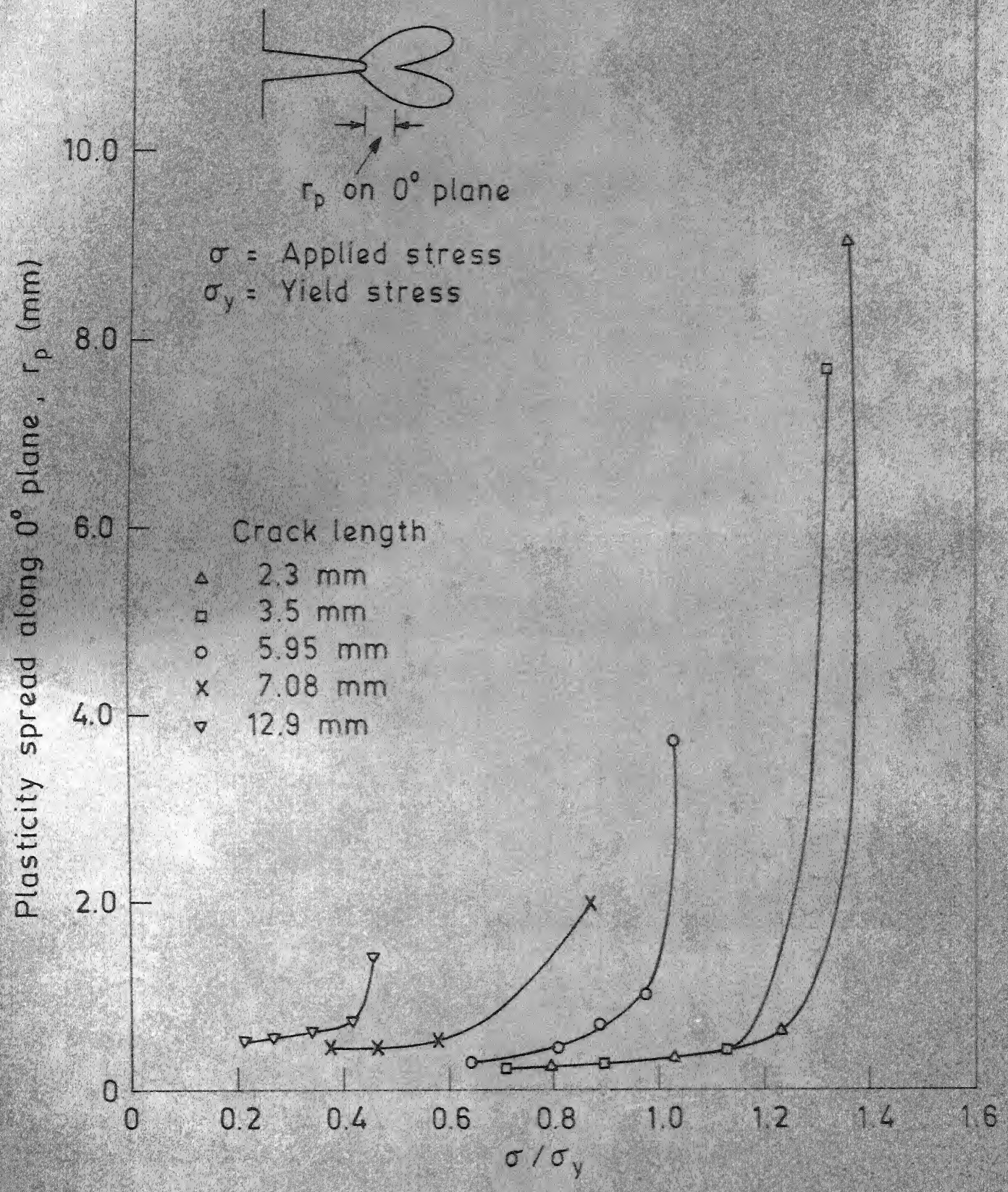

Fig. 4.63 Plastic zone size measured on the plane of the crack at different loads for various crack sizes in 10 mm thick mild steel specimens.

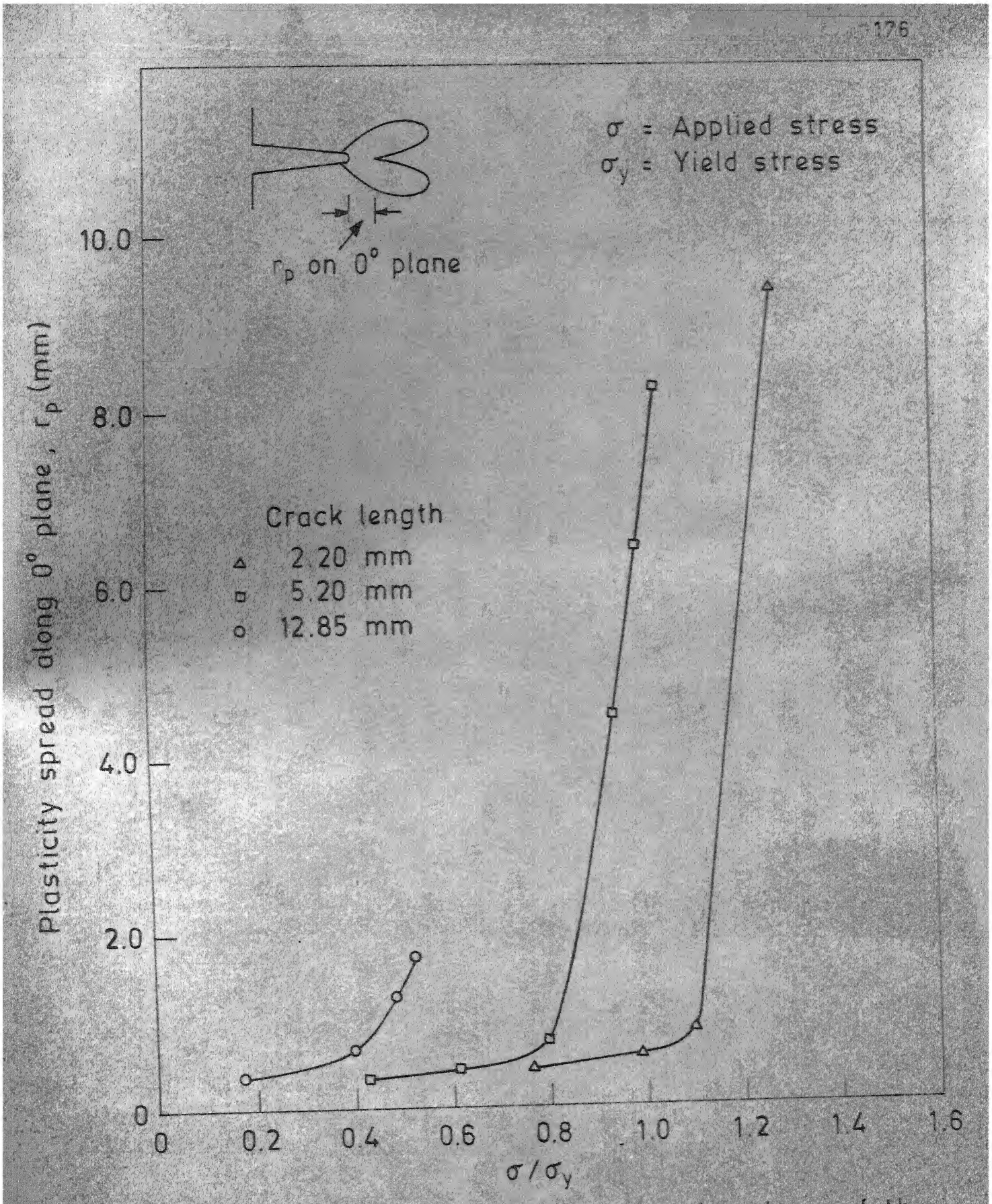

Fig. 4.64 Plastic zone size measured on the plane of the crack at different loads for various crack sizes in 3 mm thick mild steel specimens.

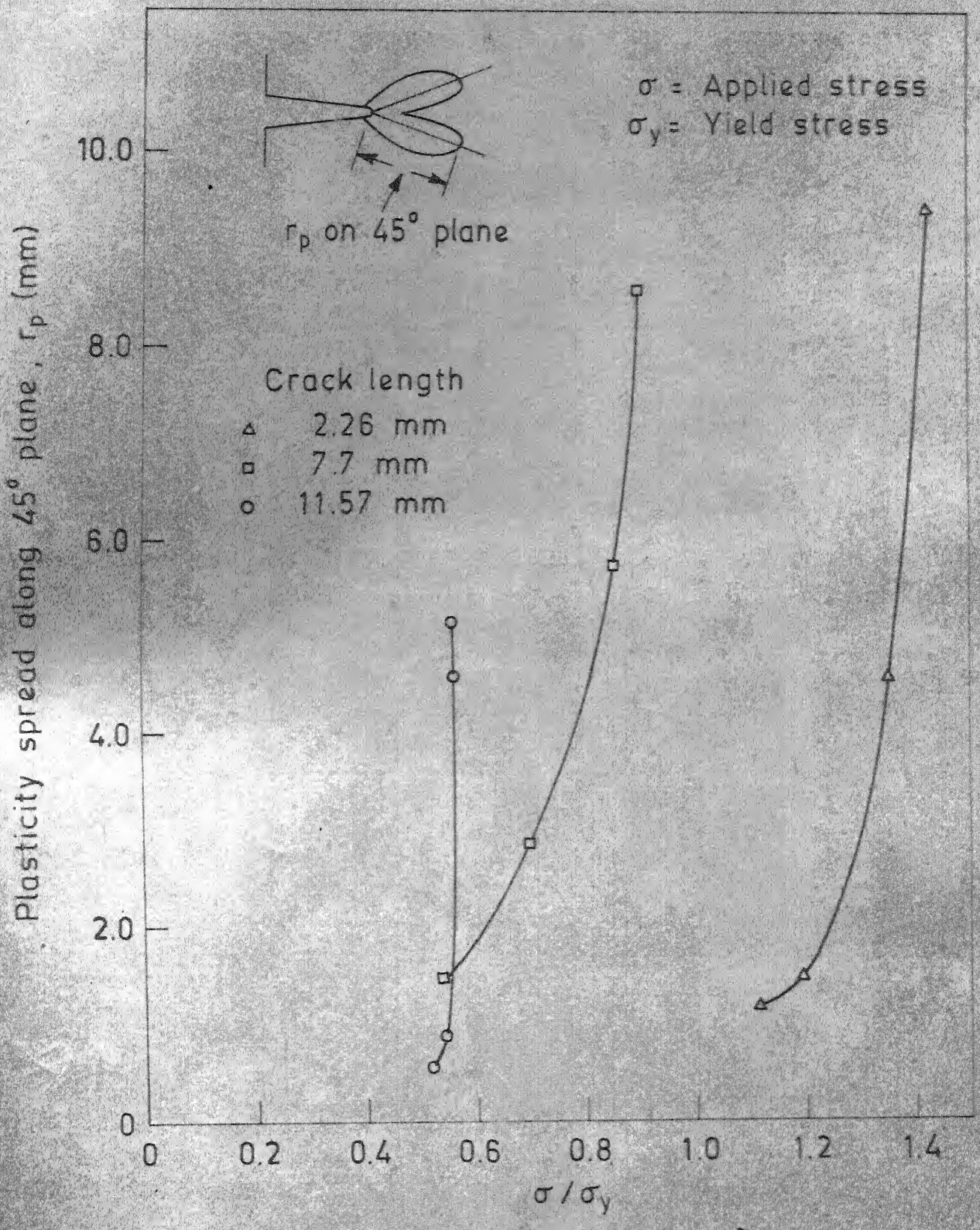

Fig. 4.65 Plastic zone size measured on 45° plane of the crack at different loads for 25 mm thick mild steel specimens.

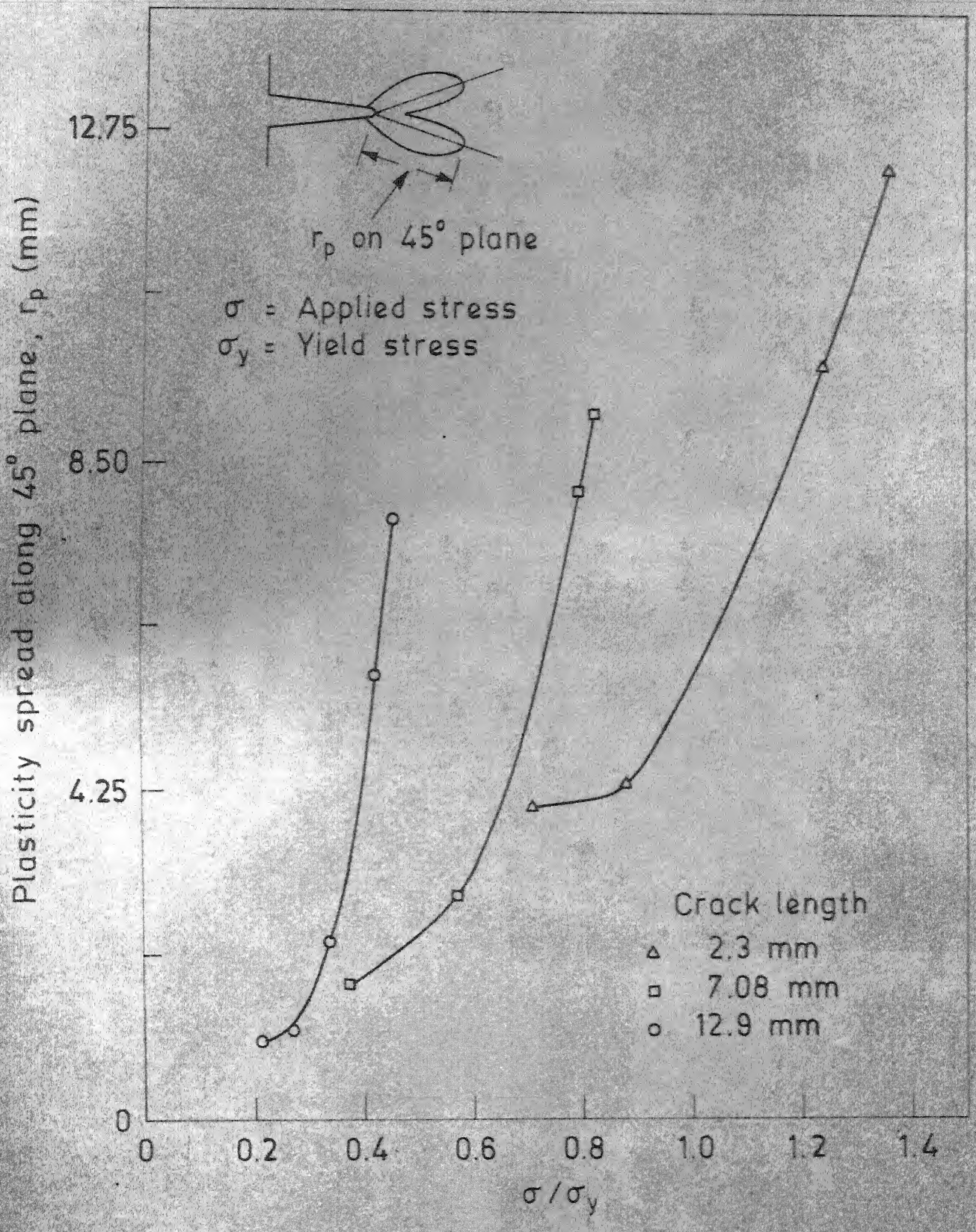

Fig. 4.66 Plastic zone size measured on 45° plane of the crack at different loads for 10 mm thick mild steel specimens.

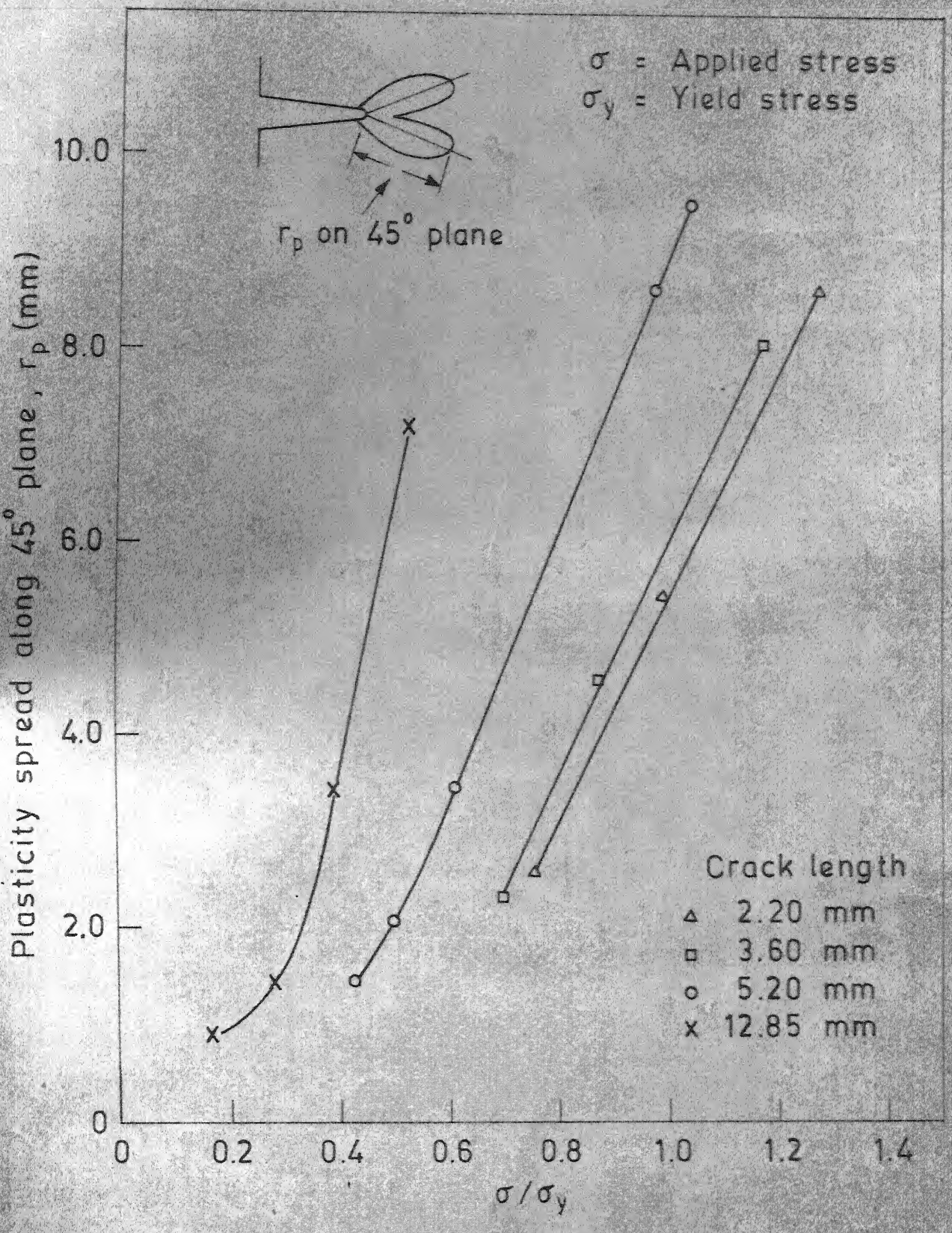

Fig. 4.67 Plastic zone size measured on 45° plane of the crack at different loads for 3 mm thick mild steel specimens.

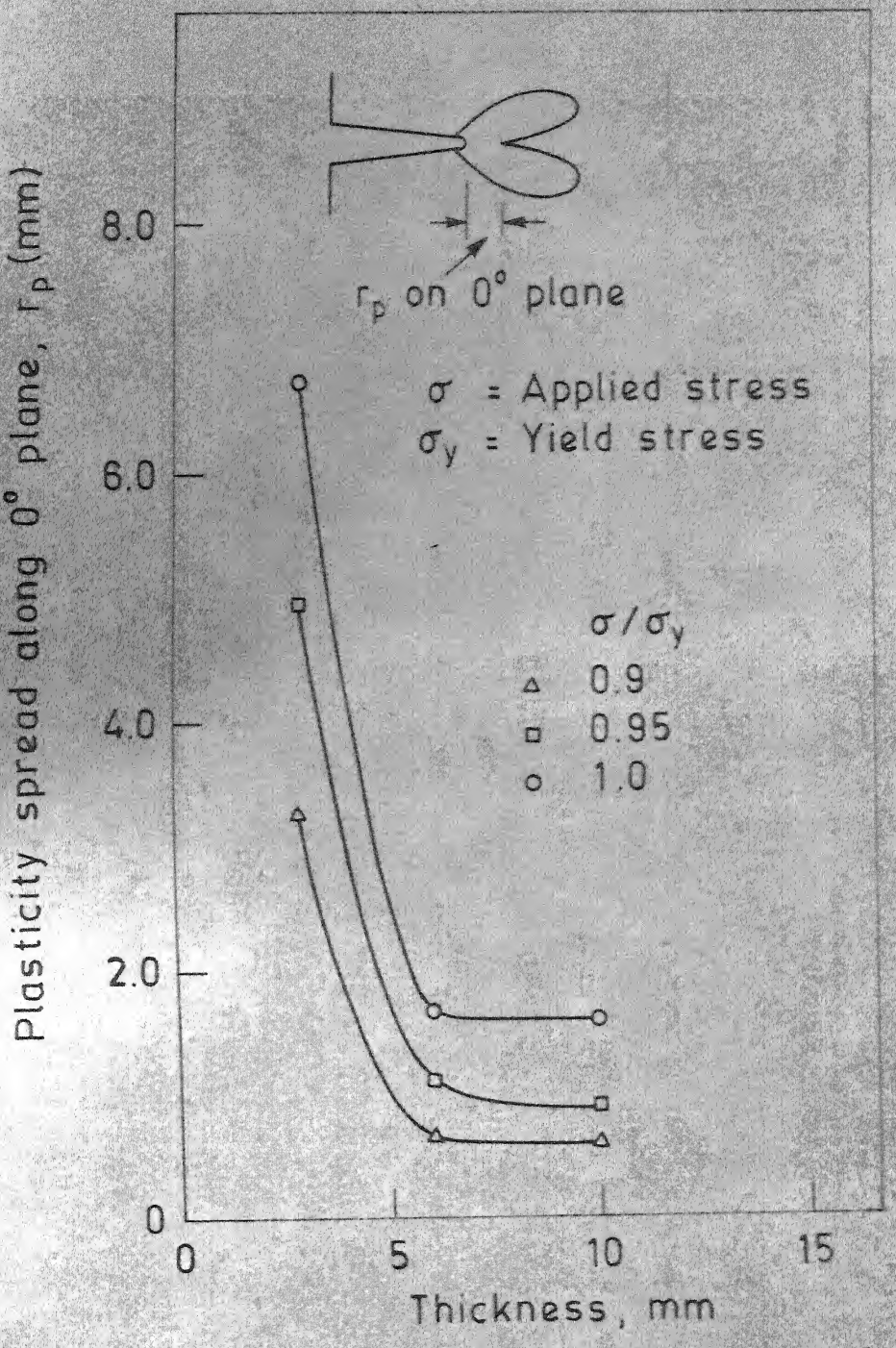

Fig. 4.68 Plot of plastic zone size measured along the plane of the crack against thickness of mild steel specimen with crack length 5.20 mm.

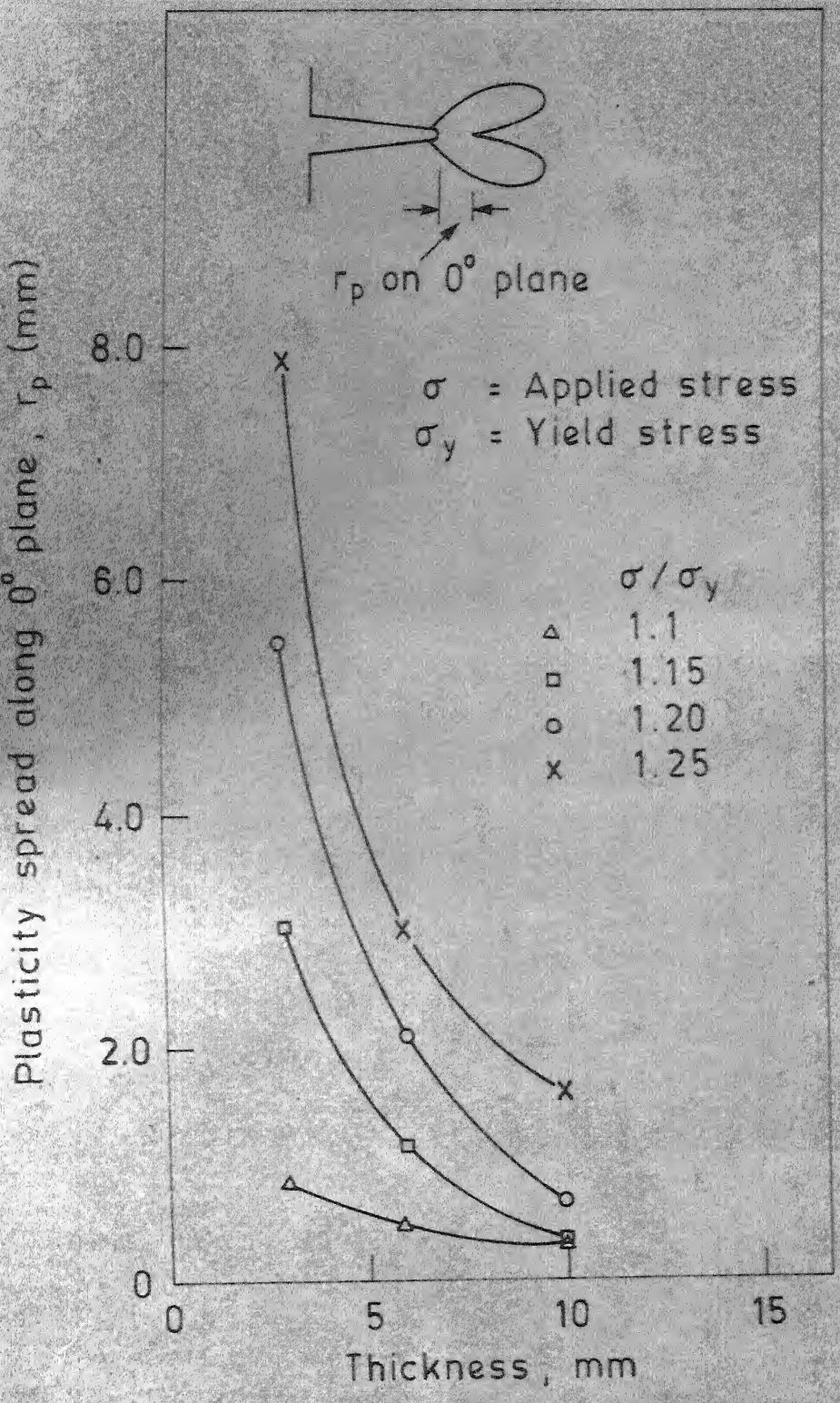

Fig. 4.69 Plot of plastic zone size measured along the plane of the crack against thickness of mild steel specimen with crack length 2.20 mm.

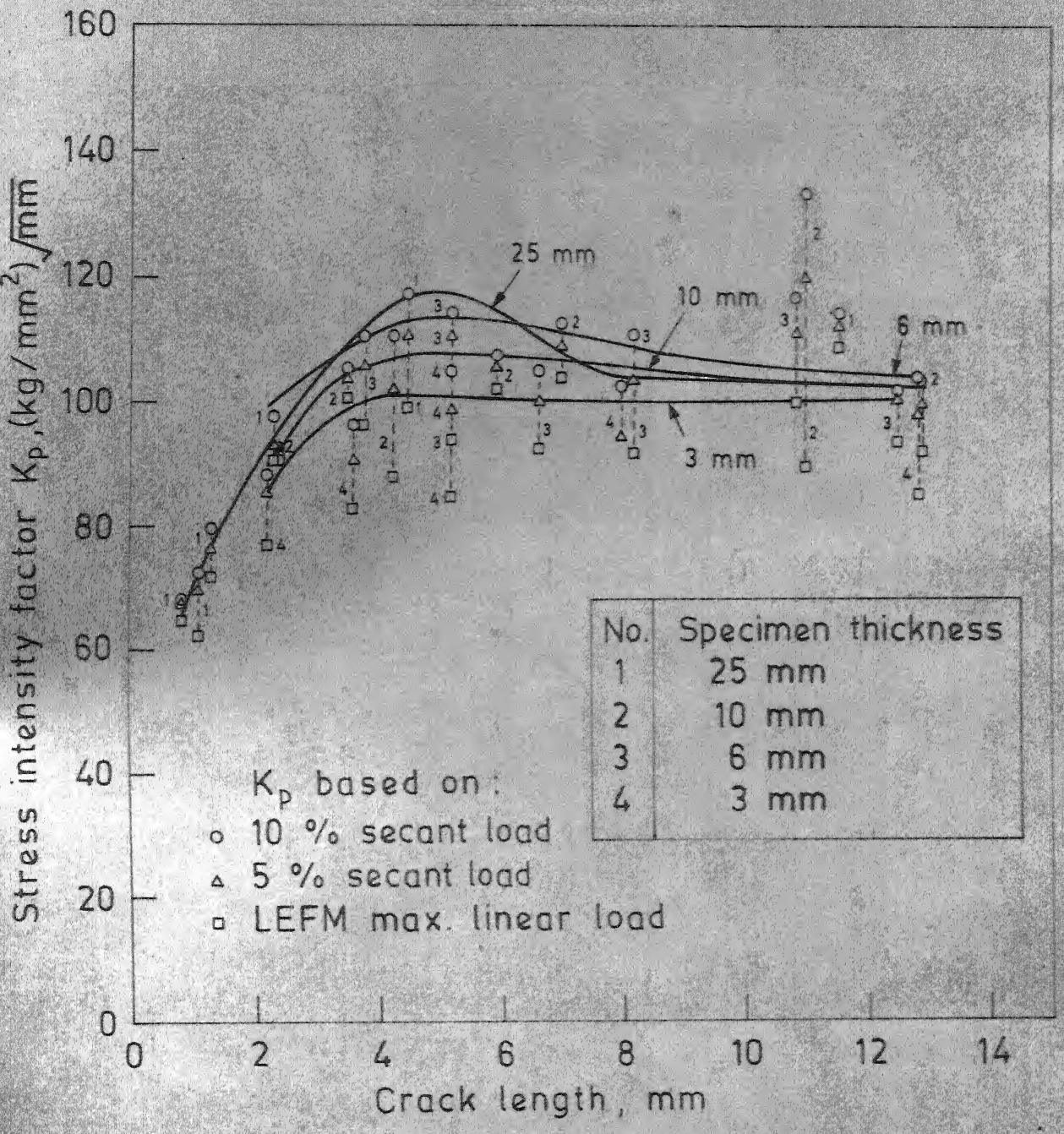

Fig. 4.70 Calculated stress intensity factor based on maximum linear load (5 % and 10 % secant-shift loads) for mild steel specimens.

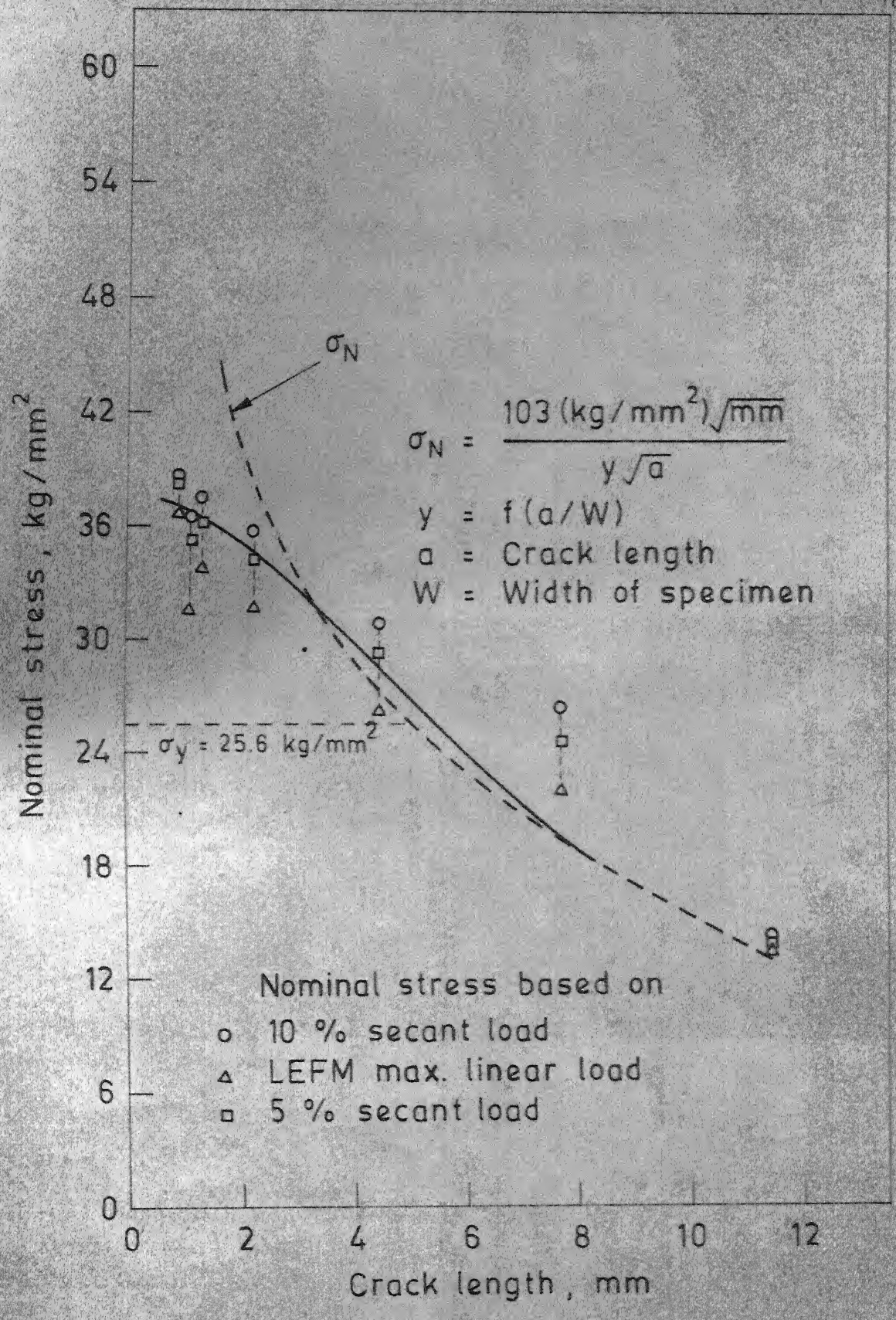

Fig. 4.71 Plot of nominal stress versus crack length in 25 mm thick mild steel specimen

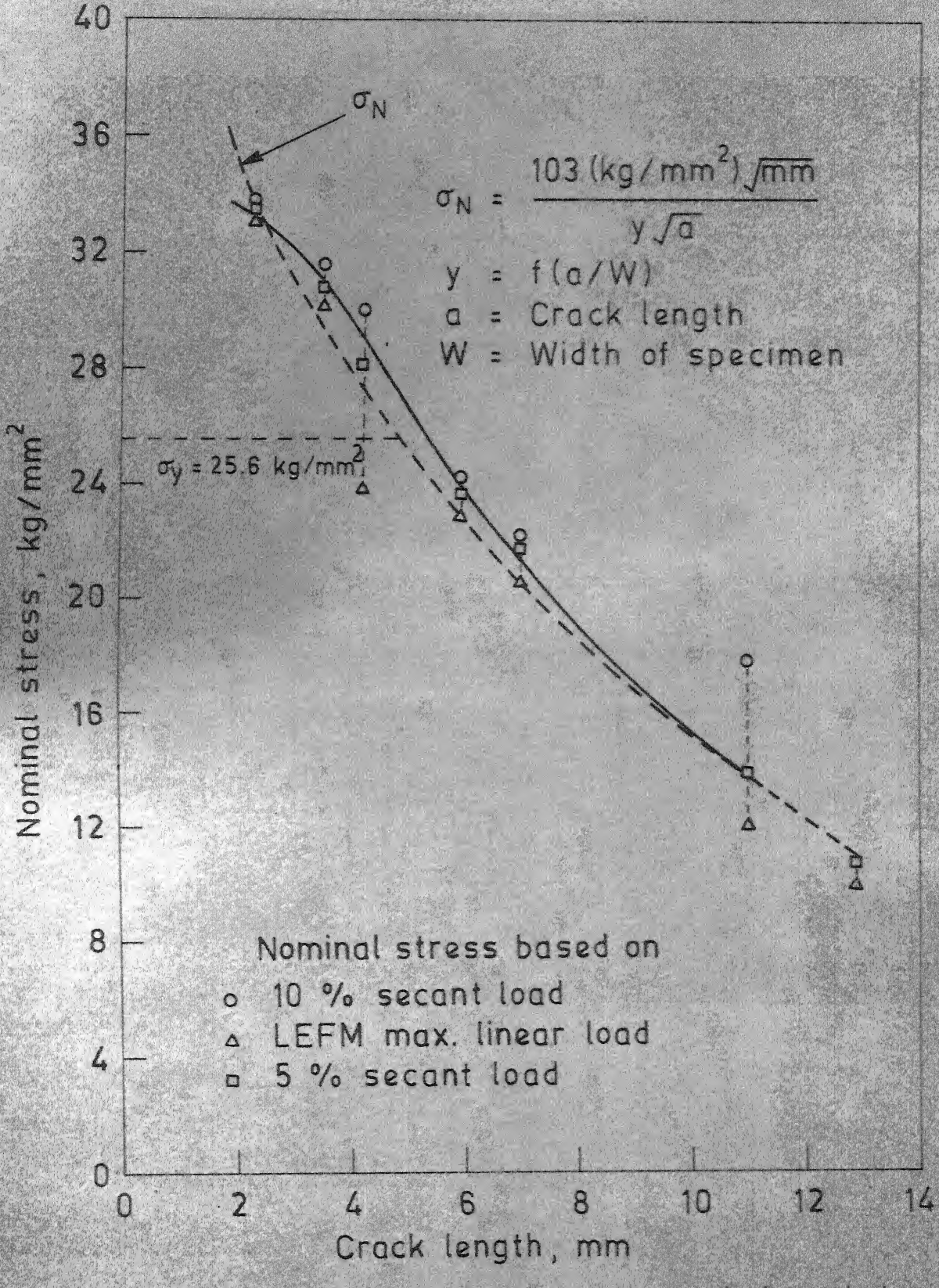

Fig. 4.72 Plot of nominal stress versus crack length in 10 mm thick mild steel specimens

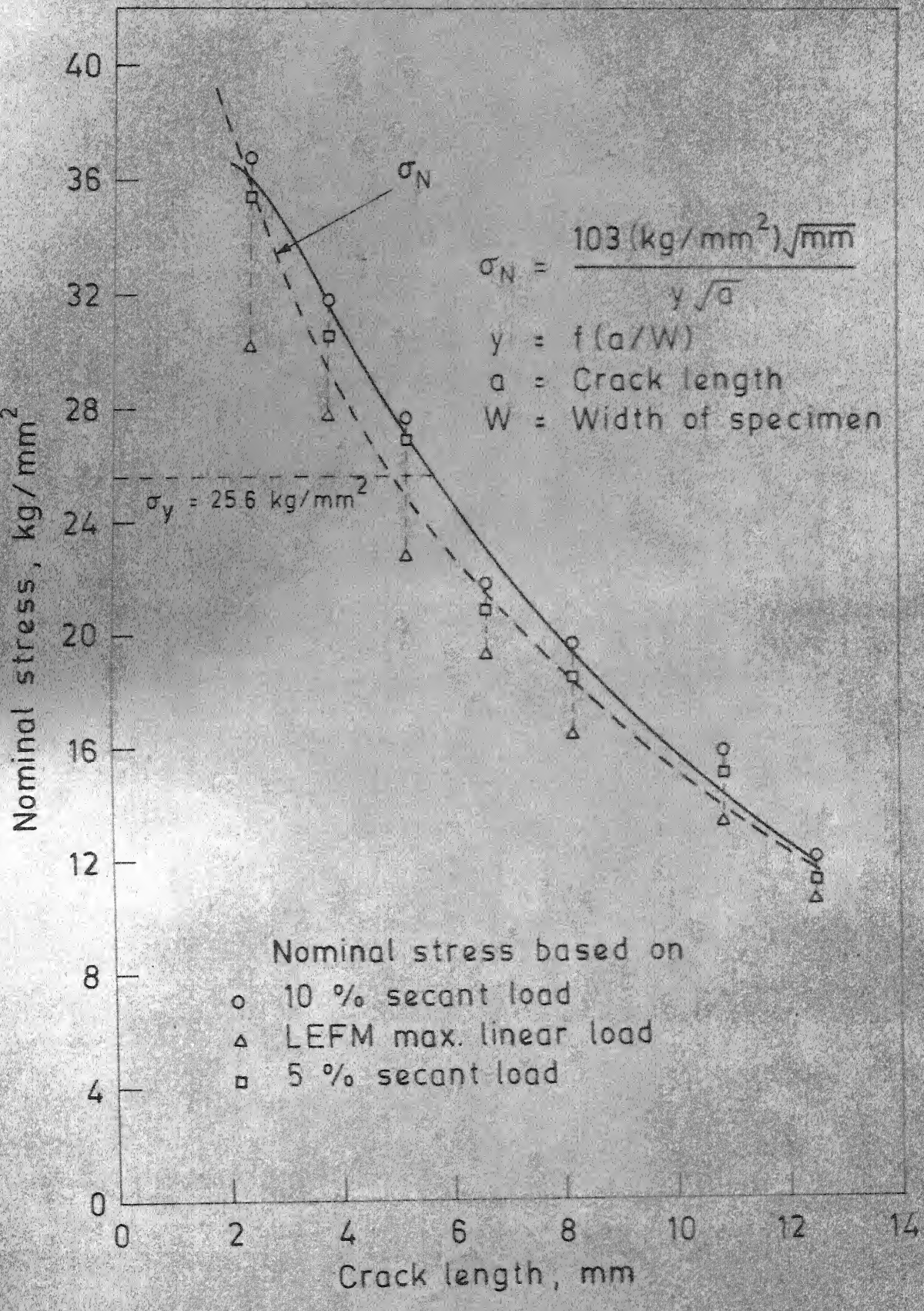

Fig. 4.73 Plot of nominal stress versus crack length in 6 mm thick mild steel specimen.

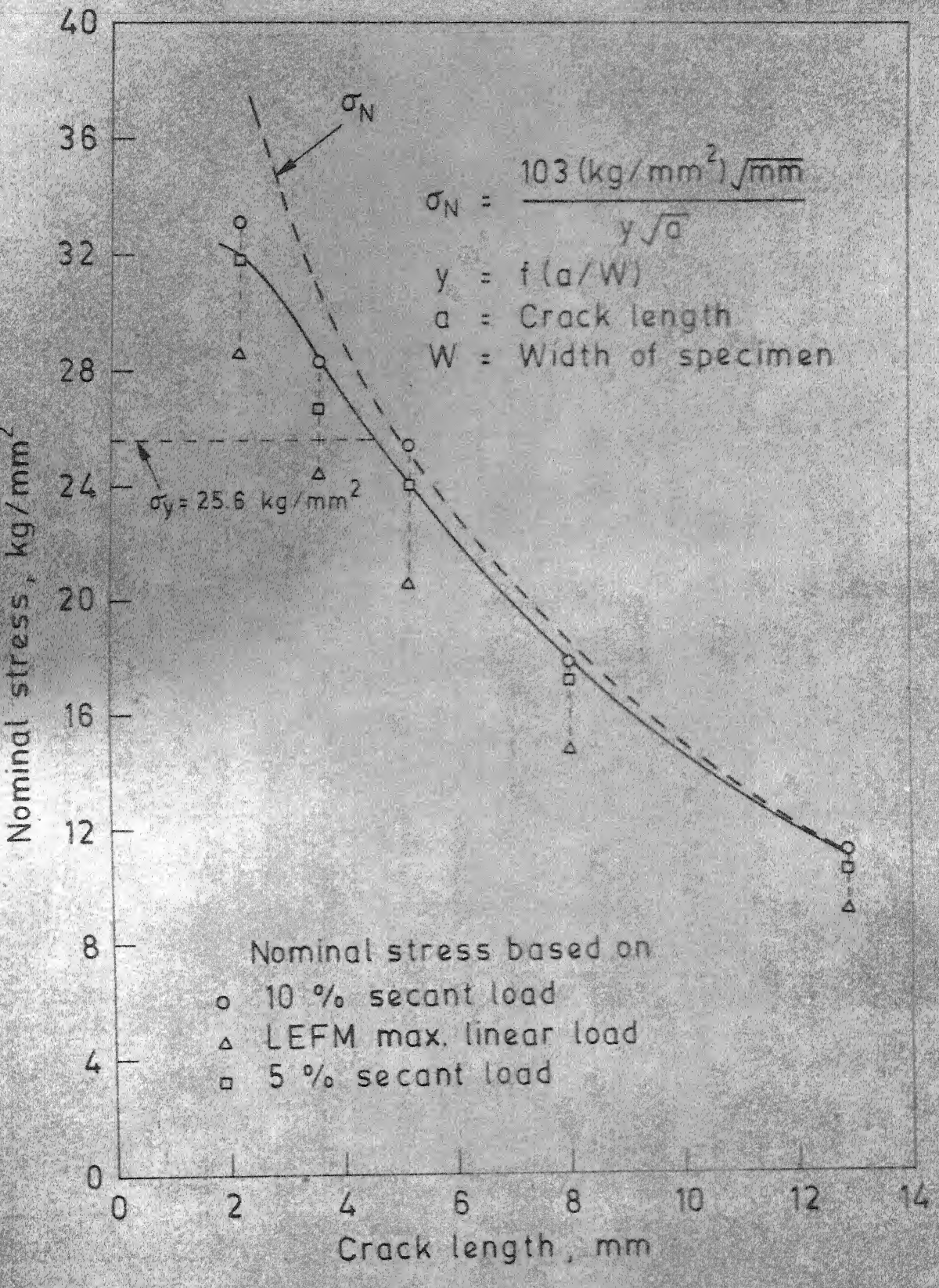

Fig. 4.74 Plot of nominal stress versus crack length in 3 mm thick mild steel specimens

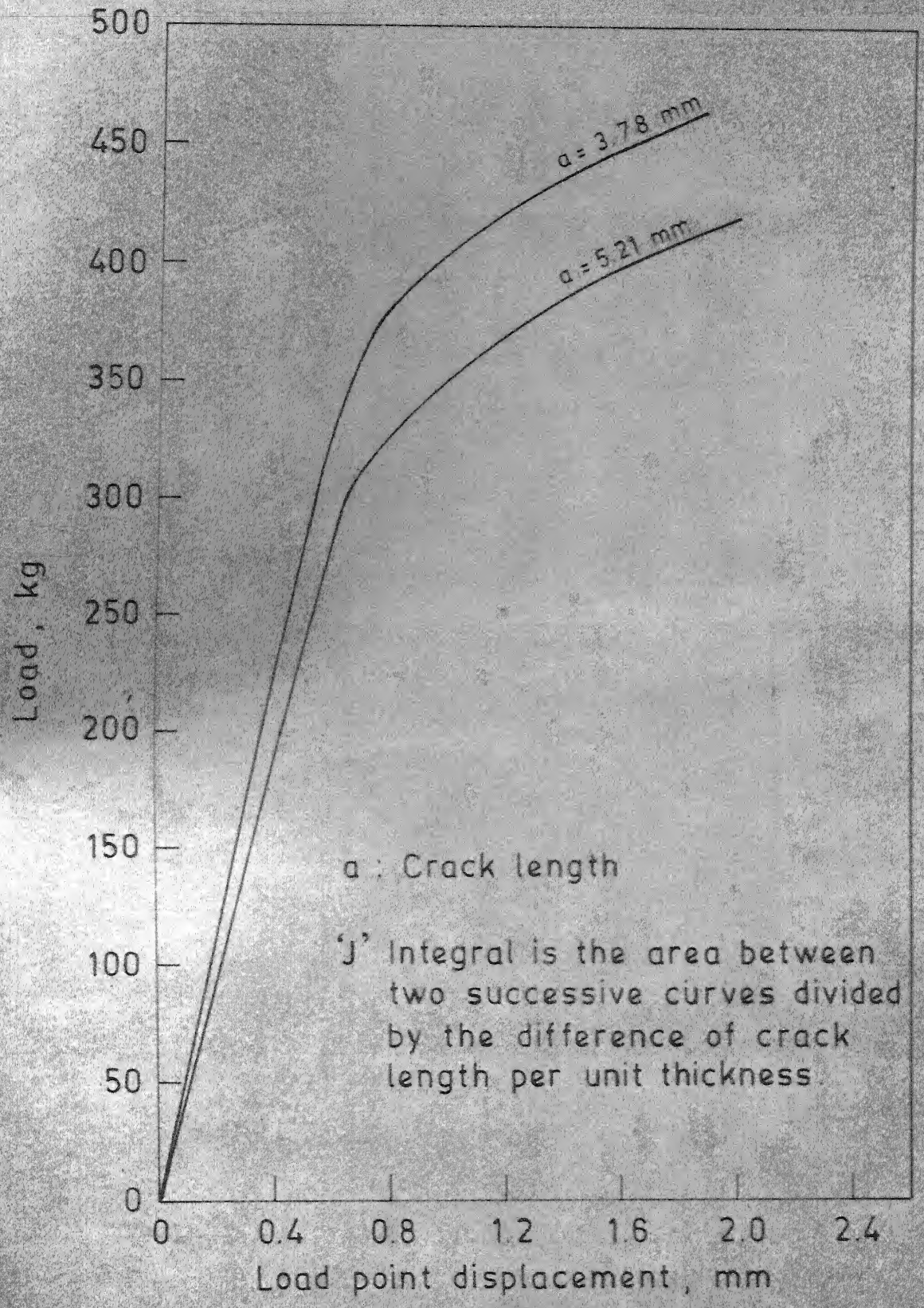

Fig. 4.75 Load vs load-point displacement diagram recorded during fracture tests of 6 mm thick mild steel specimens under three point bending.

Fig. 4.76 Shear load on a single prolate spheroidal cavity.

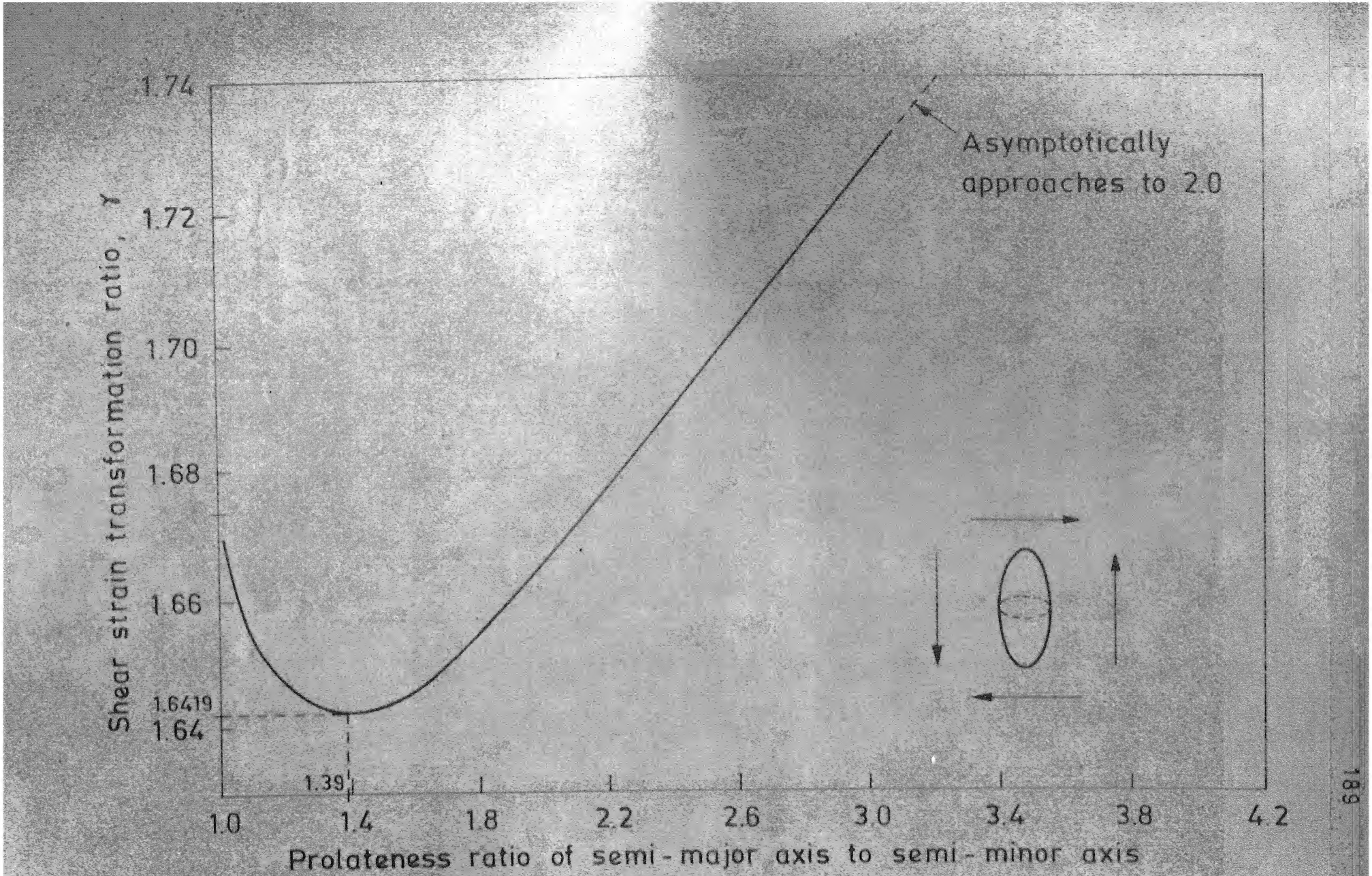

Fig. 4.77 Shear strain transformation ratio γ vs ratio of semi-major to semi-minor axis for prolate spheroidal cavity in an incompressible solid (Poisson's ratio = 1/2)

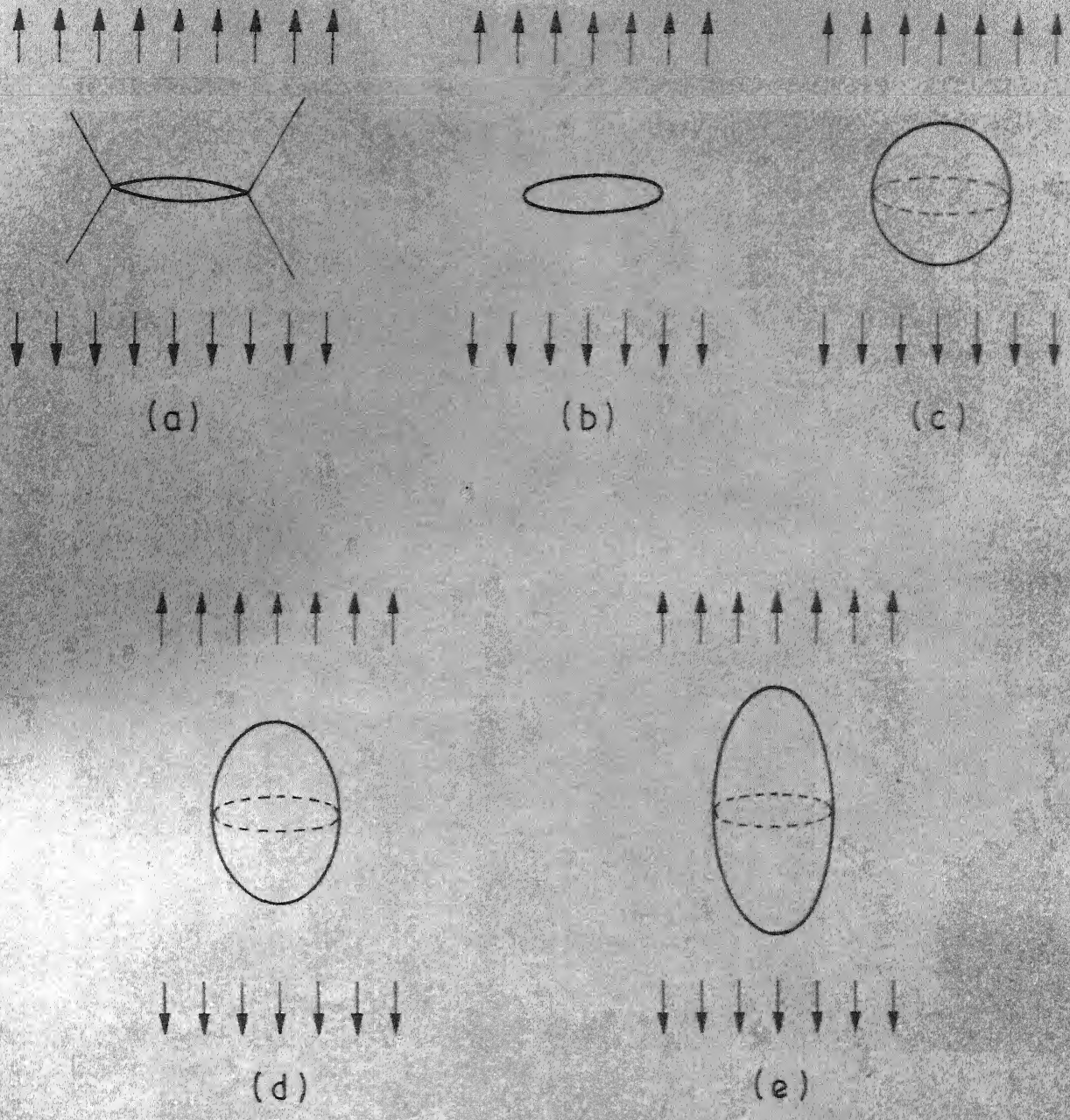

Fig. 4.78 Schematic diagram showing cavity growth in uniaxial tension loading (a) single-facet grain-boundary void, (b) oblate-spheroidal shape void, (c) void in the shape of a sphere, (d) prolate spheroidal void with major axis parallel to tension direction, (e) critical shape of void at the onset of shear instability.

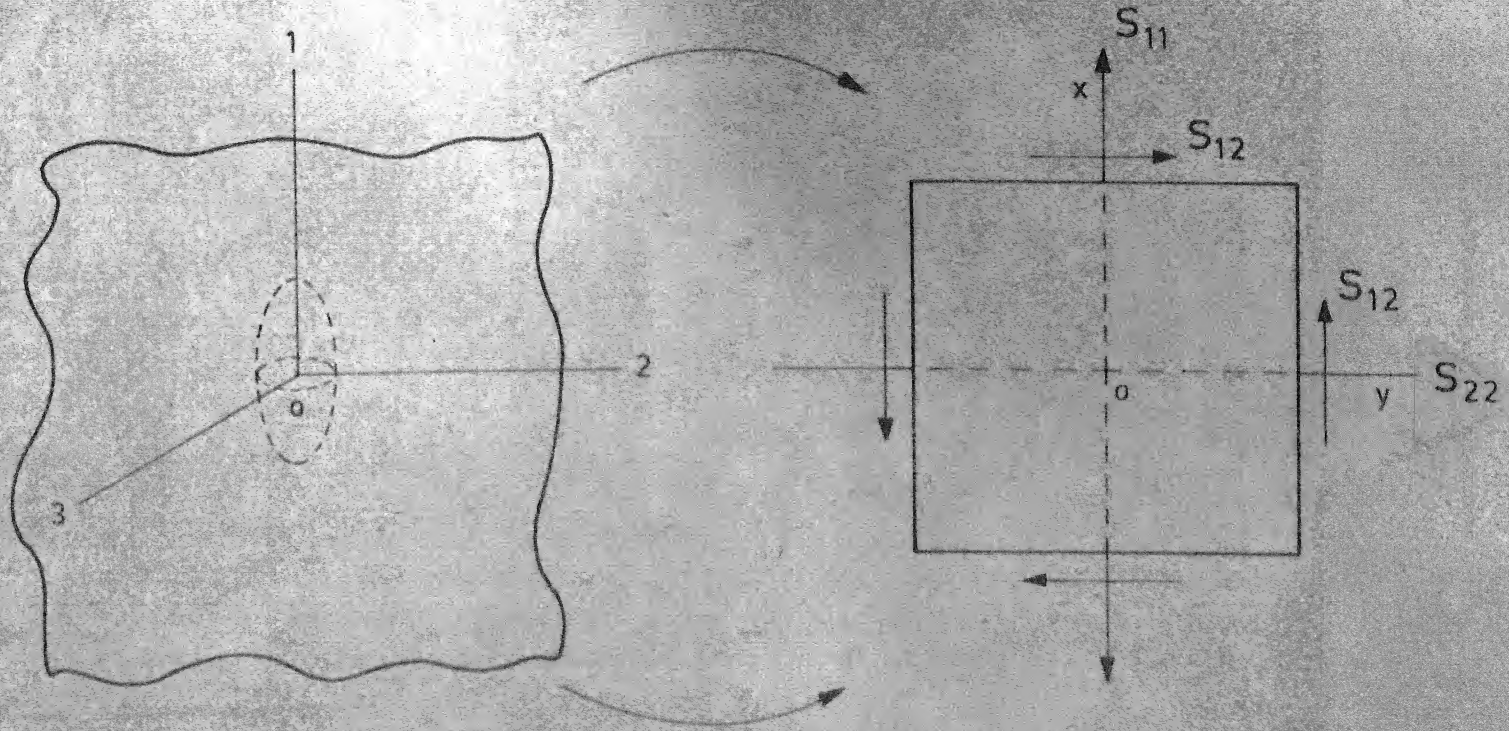

Fig 4.79 Two dimensional plane strain eqivalent incremental orthotropic elastic model for a material with a spheroidal cavity

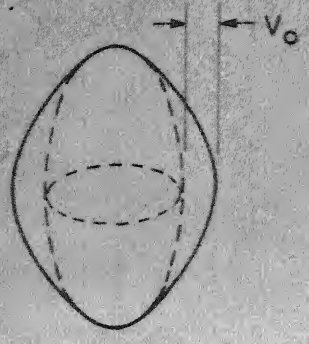

Fig. 4.80 Metastable void shape showing a large shear deformation.

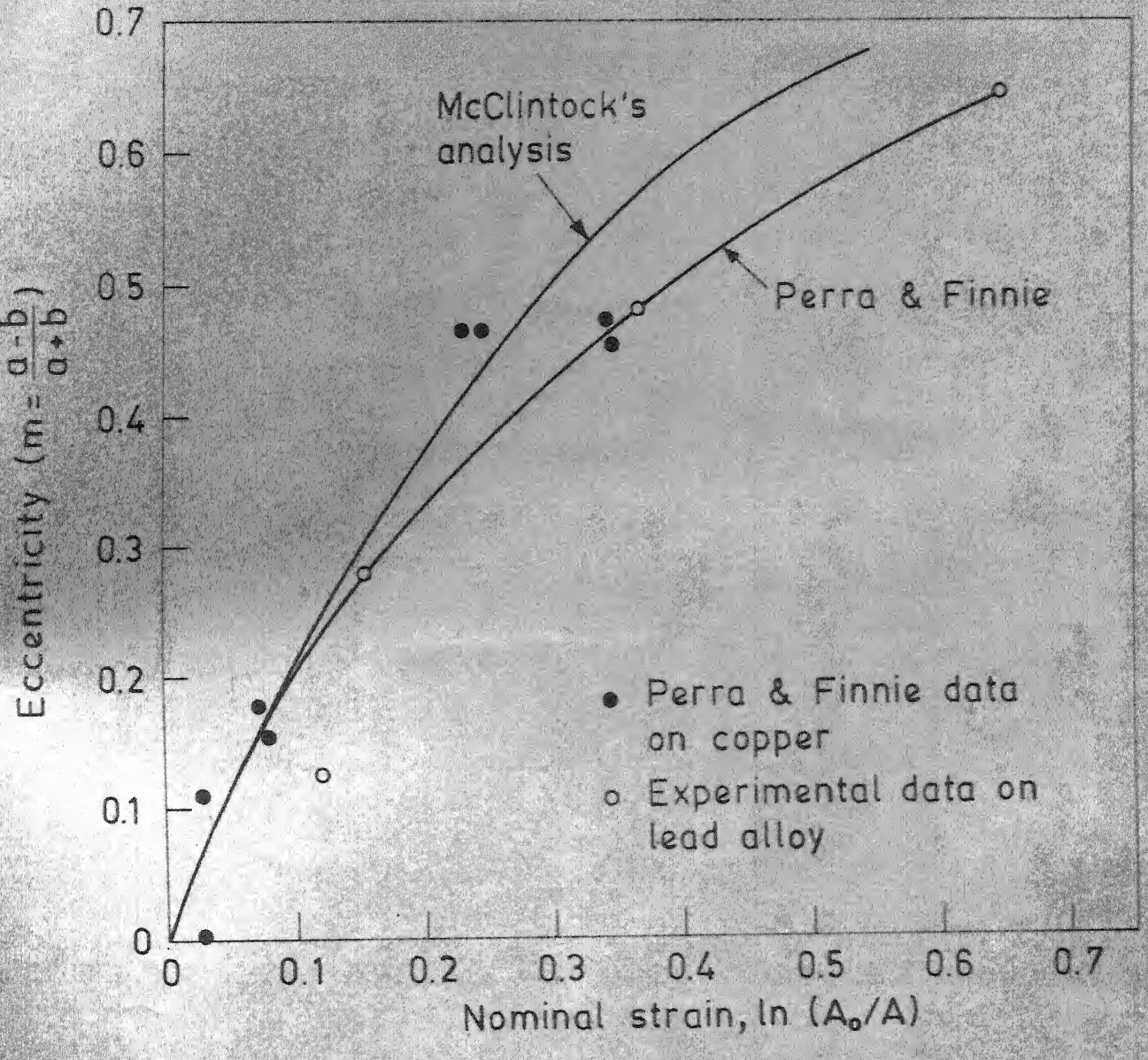

Fig. 4.82 Shape change of spheroidal hole in lead alloy due to uniaxial tensile deformation.
Eccentricity shown against nominal strain.

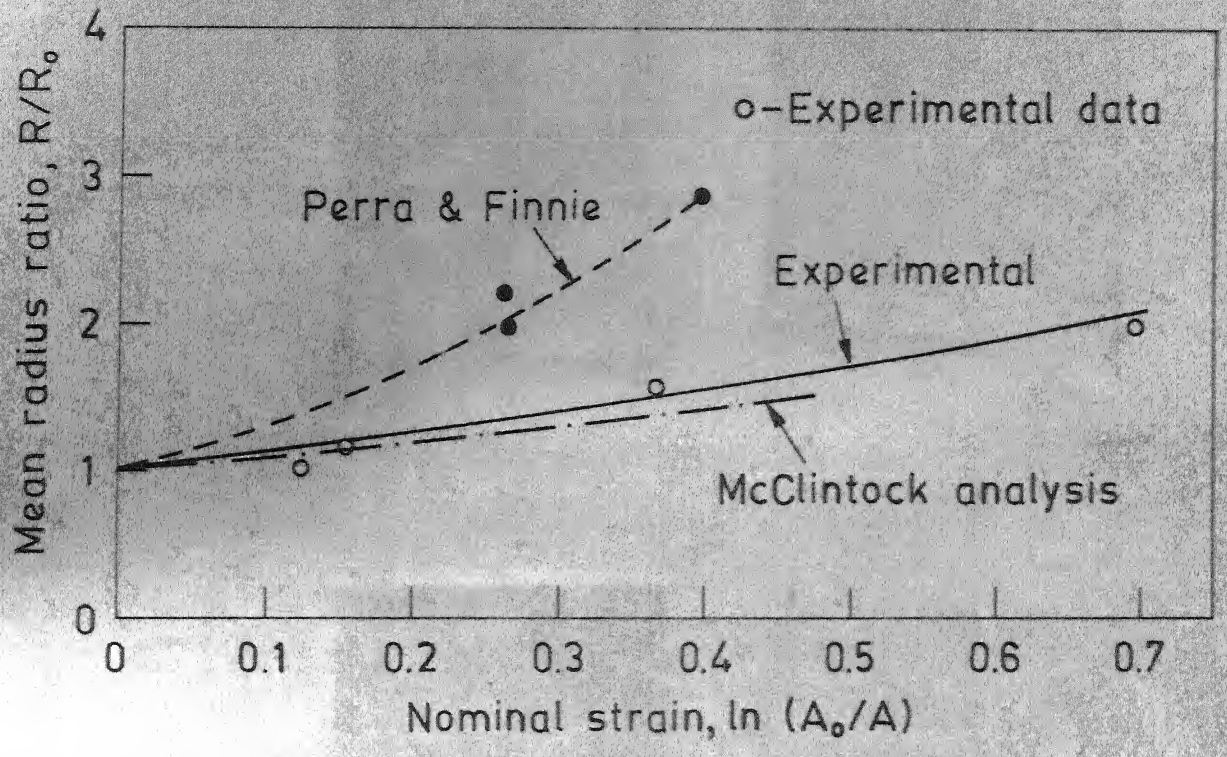

Fig. 4.8[2] Shape change of spheroidal hole in lead alloy due to uniaxial tensile deformation.
Mean radius ratio shown against nominal strain.

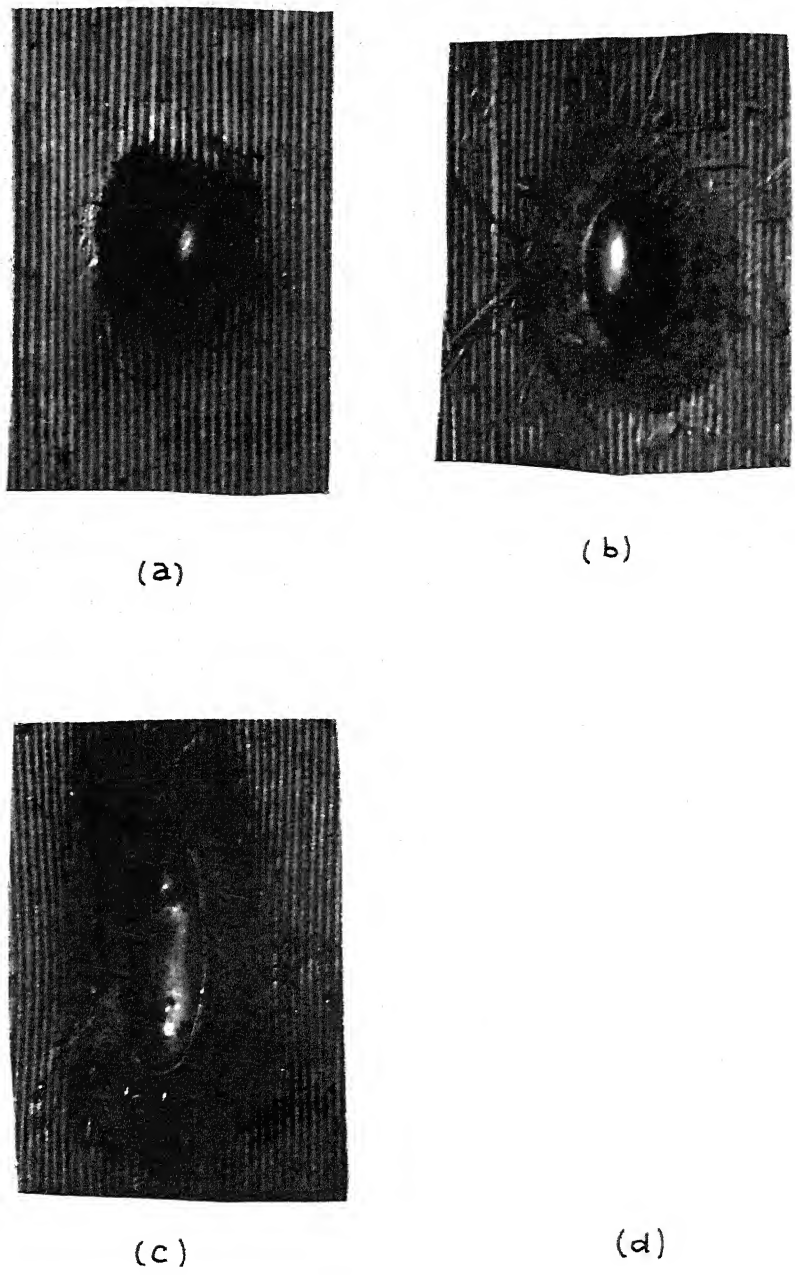

Fig. 4.83: Photograph showing the changes in void shape at different nominal strains (a) 10% (b) 20% (c) 40% (d) 50%.

CHAPTER - V

DISCUSSION

From the results of this investigation it may be seen that, 0.6% carbon steel and mild steel represent two different kinds of fracture behaviour. On one hand, 0.6% C steel fractured in a brittle manner with a slight amount of crack-tip yielding particularly in thin sections with short cracks. On the other hand, mild steel exhibited considerable crack-tip plastic flow without any fast fracture even in the heavy sections with longer cracks. In this work, firstly, the effects of specimen geometry on crack-tip yielding and fracture toughness are studied for 0.6% carbon steel, and secondly, the crack-tip plastic flow has been investigated in relation to the specimen thickness and crack-size in mild steel. These aspects on plastic flow and fracture of steels as well as the shape dependent instability of a single spheroidal void on an incompressible medium are discussed in the following sections.

5.1: Fracture of 0.6% Carbon Steel Specimens:

From the literature review it is clear that the validity of a toughness test depends on the specimen thickness and crack-size. The effects of these two parameters on the crack-toughness and associated plastic flow are studied in 0.6% C steel laboratory specimens. All the specimens

tested in this material fractured catastrophically with practically no slow stable crack growth. However, when the fracture stress is of the order of the yield strength of the material, the plastic deformation at the crack-tip is found to be appreciable. For this material, the increase in compliance is mainly due to the plastic deformation at the crack-tip. The plastic zone size increased as the crack length is decreased or the thickness is reduced. The fracture stress for more than 2 mm crack-size agrees favourably with Griffith's value giving a constant K_{Ic} = 150 $(Kg/mm^2)\sqrt{mm}$ for 10 and 25 mm thickness beams. For these thicknesses, when the crack length is in the order of 1 mm, the observed fracture stress is seen to be slightly lower than the Griffith's predicted value. However, for 3 mm thickness beams with crack-size less than 4 mm, the fracture stress is seen to be higher than the ideal Griffith's fracture stress value. When the crack length is very small, i.e. in the order of 1 mm or so, the fracture stress approaches to 1.5 times the yield strength of the material especially for 3 mm thickness beams. Thus, in Figure 4.25, the apparent toughness of the material initially increases with the decrease in crack length upto some value and then if the crack length is further reduced the apparent toughness decreases considerably even below the K_{Ic} value of the material. Thus, for short cracks, the effects of crack-tip blunting and plasticity spreads have changed the crack-tip geometry to a notch, which has effectively produced

a notch-strengthening. When the crack length is in the range of 1.5 to 4.0 mm in a 3 mm thickness beam the notch effect is quite evident. For 3 mm thickness, the plastically yielded zones are considerable, and they are of the order of the crack size near the fracture load. This indicates that there is a considerable deviation from an ideal plane strain situation. The increase in measured plastic zone is an indication as to why the toughness increases in thinner samples. The crack-tip observations also indicate appreciable crack-tip blunting and plastic flow in thinner samples leading to an increase in toughness over the thicker specimens with longer cracks. However, these crack-tip observations did not indicate any slow stable crack growth in this material.

ASTM recommends that $a \geq 25$ mm and $B \geq 25$ mm for a valid K_{Ic} test for this material. Figures 4.25 to 4.28 show, for 25 mm thickness beams a crack size of 3.5 mm would be sufficient for a valid test. If one reduces the thickness to 3 mm, a crack length of 5.0 mm would still give a valid K_{Ic} for this material. Hence, for 0.6% C steel in 25 mm thickness beams, a $\geq 0.35\ (K_{Ic}/\sigma_y)^2$ would be adequate, whereas for 3 mm thickness beams a $\geq 0.50\ (K_{Ic}/\sigma_y)^2$ would be sufficient for a valid test. Thus, it is seen from the above results that ASTM recommendations are somewhat overestimates by a factor of 5 to 7 for this material.

The plastic zone size on the crack extension plane measured on the surface of the specimen near the onset of fracture was found to be around 30% of the crack length for a specimen with a = 5 mm and B = 3 mm, whereas, the plastic zone size was of the order of the crack length for shorter cracks. This means, the plane strain approximation holds good even for specimens of 3 mm thickness with crack size longer than 5 mm. In this thickness range, as the crack size decreased, the deviation from plane strain towards plane stress was more evident. In order to obtain a fully plane stress situation, it is necessary to reduce the thickness further.

It was not possible to measure the maximum local stress elevation below the crack-tip which would have given better insight into this problem.

Finally, COD method was applied to short cracked thin beams to estimate the apparent toughness, wherever the deviation from linearity was considerable. Figure 4.19 shows a large non-linear behaviour in load-COD record before fracture, with a sizeable amount of plastic flow near the tip. K_Q based on COD gave a value of 199 $(Kg/mm^2)\sqrt{mm}$ for a crack size of 1.30 mm in 3 mm thickness beams. On the contrary, the SIF method underestimated the toughness value as 155 $(Kg/mm^2)\sqrt{mm}$ at the highest load. In such a situation, the toughness calculated based on SIF alone may not give an accurate value, whereas COD method gives a closer

approximation to the actual toughness. Thus, the apparent toughness of short cracked beams based on SIF approach mentioned in Figure 4.25 would be inappropriate and the apparent toughness values calculated by COD method given in Table 4.2 would be more representative. In the case of short cracked thin beams, due to crack-tip yielding the ideal plane strain condition would be difficult to maintain and the fracture could take place with some crack-tip opening but not as high as the plane stress COD value. In such a situation, if a simple plane stress approximation is made in estimating the toughness by COD method, it may lead to a lower value of toughness. Thus, in the case of short cracked 6 mm thickness specimens, SIF or COD method may not give an accurate measure of the toughness. The plastic zones observed in Figures 4.21 and 4.23 indicate that in 3 mm thickness beams the plastic flow and crack tip opening were considerably larger than 6 mm thick specimens. Table 4.2 shows that the toughness calculated by plane stress COD method gave larger values for such cases.

From the above discussion it is clear that, the ASTM recommendations are too conservative, which is also emphasized by Cottrell and Langstone[13], Jones and Brown[14] and many others[17,18]. The measured plastic zones on the plane of the crack were found to be less than the theoretical plane strain plastic zone size of 0.53 mm $= \frac{1}{6\pi}\left(\frac{K_{Ic}}{\sigma_y}\right)^2$ for specimens of less than 6 mm thickness. Hence, for

25 mm, 10 mm and 6 mm thick specimens, fracture occurred in plane strain condition with a high local plastic constraint. If one uses $G_{Ic} = \alpha \sigma_y \delta_c$ in calculating the plane strain fracture toughness based on COD criterion, α was found to be around 1.4 in the case of 6 mm thick beams with crack size upto 1.53 mm length.

Applying Irwin-McClintock's plasticity correction on crack length, the toughness calculated for a crack size of 4.3 mm in 6 mm thickness beams, was seen to be in agreement with the K_{Ic} value of the material. On the contrary, SIF approach, without plasticity correction, gave a slightly lower value.

LEFM approach was thus found to be adequate in most of the cases studied, except for very thin or short cracked beams, where some crack-tip yielding was visible. Unless the specimens are thin enough to get a complete plane stress yielding situation, a simple COD method may not give a measure of the toughness. Specimens less than 3 mm thickness might be required to get such a situation in this material.

5.2: Crack-tip Plastic-flow in Mild Steel Specimens:

Brittle fracture of mild steel can take place if the triaxial plastic constraint is sufficiently large, which means, a high local normal stress elevation below the notch root in mild steel would be required to have a fast propagation of crack. However, in most of the structural components,

it is not always possible to maintain such a high degree of local plastic constraint near the crack-tip, mainly due to the inadequacy in thickness requirement in low strength materials, such as mild steel. The other extreme is seen to be the ductile behaviour in mild steel thin sheets, where a plane stress condition prevails with significant plastic flow ahead of the crack-tip. There exists an intermediate range of thickness in which crack-tip plastic flow will be associated with a slow stable crack growth before fracture. Thus, fracture behaviour in materials like mild steel would be highly sensitive to the specimen thickness. For a fast brittle fracture in mild steel, not only a high plastic constraint is required but also the plastic zone should be small compared to the crack size, thickness and other characteristic dimensions. Hence, the nature of crack-tip flow and fracture would be very much dependent on the crack size as well. The present experimental results on the effects of thickness and crack size on crack-tip plastic flow for mild steel are examined in this context. The thickness range investigated in this work was from 3 mm to 25 mm, and even in the maximum thickness, it was found to be inadequate to produce a fast fracture.

The load-COD records of pre-cracked mild steel beams show initially a linear behaviour, and then suddenly an increase in compliance was seen to occur in all samples. Further loading caused a large crack opening displacement

at almost a constant stress level with considerable plastic flow near the crack-tip. In all samples a rapid change in the compliance was observed either at the maximum linear load or near 5% secant shift load. Therefore, careful observation on plastic flow and the yielded zones were made in this region upto around 10% secant shift load through photoelastic coating technique.

The photoelastic measurements of the plastic zone formation reveal that for 25 mm thickness beams, an abrupt plastic flow occurs along 45° plane (with respect to the plane of the crack) irrespective of the crack size. This means, a high localised plastic flow along 45° plane in preference to 0°-plane has caused a loss of resistance to crack-tip plastic flow. For 25 mm thickness beam with 11.57 mm crack size, this abrupt plastic flow along 45° is seen to occur around a nominal stress of 0.56 σ_y, whereas this happended around 1.35 σ_y on the same plane in the case of 2.26 mm crack length. In the case of long cracks in 10 mm thickness specimens, the abrupt plastic flow was seen along 45° plane, but for short cracks of the order of 2.3 mm, the abrupt flow was more on the 0°-plane. This behaviour is different from 25 mm thick specimens, 6 mm and 3 mm thickness specimen also behaved in a similar manner. When the crack size was in the order of 12 mm in 3 mm thickness beams, an abrupt plastic flow was seen to be along 45° plane, whereas, for crack size shorter than 5.2 mm the abrupt flow

was predominantly along the plane of the crack. This behaviour is also evident from Figures 4.63 to 4.67. As the loading increased further, crack opening as well as large crack-tip plastic flow was predominant. Figures 4.43 and 4.62 show the tendency towards a fully plane stress deformation for short cracks. On the contrary, Figures 4.68 and 4.69 show that the plastic zone sizes increase considerably by reducing the thickness of the beam at any given nominal stress and crack size.

It is apparent from the above results that the local normal stress build-up was not sufficient enough to cause any crack nucleation or extension, but an abrupt plastic flow either on 0° or 45° plane might result in micro-void formation ahead of the tip. Such abrupt plastic flow is commonly seen in ductile fracture of metals due to large shear strain localization around a thin non-deforming layer of material[94].

An approximate plane strain situation prevailed below the tip region in 25 mm thickness beams at less than 5% secant shift load and through thickness flow was negligibly small in this region. As no micro-cracks were visible or any crack extension was noticed along 0° plane, one might consider that the deviatoric part of the stress tensor was not sufficient enough to cause the yielding in the plane of the crack. In a recent work, Deysarkar and Bandyopadhyay[39] proved that local strain can build-up ahead of a crack like

notch either on 0° or on 45° plane for a plane strain deformation. The local jump in shear strain-derivative could be fairly large along 45° plane for a plane strain situation, whereas the radial strain derivative suffers a discontinuity on 0°-plane ahead of the notch-root for an elastic-plastic material. Thus, from the above analysis it is clear that in a material like mild steel which is weak in shear, an abrupt plastic flow should take place along 45° planes in long cracked thin beams or in thicker section beams. The present observations are in agreement with these theoretical predictions.

The present experimental observations on mild steel cracked beams have shown an abrupt flow localization ahead of the notch root well before the onset of crack extension. It is also known that a critical plastic strain (i.e. a critical COD) needs to be attained at the onset of crack extension on the notch surface. The present experiments show that an abrupt flow localization takes place within 5% secant shift load either on 0° or 45° plane depending on the constraint. This means, the local plastic constraint is abruptly released leading to a sudden increase in global compliance of the beam. In this region of load-COD diagram, the crack-tip remains relatively sharp as well. Unlike 0.6% carbon steel, the plastic zone extended abruptly instead of the crack extension. Hence a simple SIF approach should be applicable for analysing the loss in resistance to plastic

flow of the crack-tip in relation to specimen thickness and crack size.

As the size of the plastic zone usually reflects the condition for plane strain deformation at the crack-tip, the load at which an abrupt flow occurred can be assumed to be a sudden loss of local plane strain constraint. Thus, an ordinary Griffith's type of energy balance approach seems to be applicable based on plane strain deformation. This permits to make an assumption that the abrupt local loss of resistance to plastic flow will occur at a critical stress intensity factor. Accordingly, a critical stress intensity factor, K_{Pc}, based on the loss of resistance to local plastic flow is proposed. This new parameter which characterises the local plastic instability has been studied as a function of specimen thickness and crack size.

The values of stress intensity factor (K_p) were calculated for different thicknesses and crack sizes in mild steel, based on the maximum linear load, 5% and 10% secant shift loads. Figure 4.70 shows for very short cracks, K_p values are low for all thicknesses and then increase gradually as the crack size gets longer. In these observations, there is a tendency to approach a constant value, which is approximated as 103 Kg $mm^{-3/2}$ for the critical K_{Pc}. Analogous to Griffith's fracture stress theory, the apparent nominal stress at which abrupt local plastic flow takes place, agrees with the calculated values other than for very short

cracks. When the crack size is less than 2 mm in this material, the nominal stress is seen to be lower than the estimated values. This behaviour is similar to the apparent fracture toughness variation due to crack length in 0.6% carbon steel. 25 mm thick mild steel specimens with short cracks behaved like notched beams, and the effect of crack-tip blunting for short cracks was causing the deviation from ideal plane strain assumption.

The abrupt shear flow did not take place even upto 1.4 σ_y in short cracked beams maintaining a linear load-COD relation. This behaviour is indicative of notch strengthening effect in mild steel similar to that observed in 0.6% C steel specimens. Although, it was not possible to calculate the local plastic constraint factor, the gross constraint factor[99] is calculated to be of the order of 1.5 on the basis of net ligament section (W-a).

Table 4.4 describes the comparison between K_p values obtained by SIF approach and other equivalent standard methods. K_p based on more than 5% secant shift load, loses its meaning because of large crack-tip blunting. However, Irwin-McClintock's plasticity corrected crack length would yield a better result. An equivalent K_p value was also calculated based on crack opening displacement. For 3 mm, 6 mm and 10 mm thickness beams, K_p by COD approach with plane stress approximation gave a lower value than that of SIF method. This discrepancy is due to the assumption of plane stress

approximation used in calculating K_p by the COD method. The triaxial stress field effect in plane strain requires a higher local stress than σ_y. This can best be studied by considering the multiplying factor α of Eqn. (2.12). Figure 5.1 shows the plot of α against crack length for 6 mm thick beams. For short cracks, α is slightly more than unity as expected. As the crack length increases more and more, plastic constraint will be maintained and this will be seen from the increase in α.

For a plane strain situation, as α is always a function of the local maximum normal stress elevation, it could be fairly high. Argon[100] measured the local plastic constraint factor to be around 3.5 for a spheroidised steel. Deysarkar and Bandyopadhyay[39] also theoretically calculated a high value of plastic constraint factor in a crack like notch for a Von-Mises material in plane strain. Thus, in Figure 5.1 for 6 mm thick beams, a plane strain deformation would prevail upto 5% secant shift load beyond a crack length of 6 mm.

In order to obtain plane stress crack-toughness of mild steel, it is important to identify the COD value corresponding to the onset of crack growth. An accurate observation on the onset of crack extension in relation to the load-COD record requires a very sensitive COD measuring technique such as potential drop or scanning electron microscopy[31]. Due to the lack of adequate facility for

this purpose such techniques could not be used for detecting crack extension. However, a few specimens were loaded to various points in the local COD diagram at room temperature and then fractured in a brittle manner at a low temperature. From a careful examination of the fracture surface of these specimens (Figure 5.2) the onset of neck extension is found to be around $\delta_c = 0.024$ mm, which gave an equivalent K_Q value of 155 to 160 $(Kg/mm^2)\sqrt{mm}$ approximately.

To find the onset of crack extension, an alternative proposition could be by plotting the ratio of the measured plastic zone to the COD against the ratio of the CGD to crack length. Figure 5.3 shows a plot in the case of 6 mm thick specimen with a crack size of 6.65 mm, and it may be seen that there are two instabilities occurring at points B and D. Point B indicates the onset of abrupt plastic flow and point D is likely to be the onset of crack extension. The onset of crack extension point on the load versus CGD record thus obtained, is found to be approximately the same as that obtained by the low temperature tests.

Recent theoretical study on the misfit energy created ahead of a crack like notch in an elastic-plastic solid has revealed that there are two distinct instabilities at 0.2° and 0.6° notch opening angles[39]. During tensile test for a round specimen in a ductile material, two such instabilities are commonly observed. The first instability is recognised as the localized plastic flow, whereas the

second one is due to the surface instability. The present experimental work also shows similar observations giving firstly a local abrupt plastic flow ahead of the crack-tip and secondly by a new surface opening at the onset of crack extension.

From the view points of engineering design and practical applications, it is necessary firstly, to understand the nature of slow stable crack growth behaviour and secondly to evaluate the fracture toughness of such a yielding material like mild steel. R-curve method seems to be the most appropriate method in this case. As the major aim of the present investigation was not in this direction, no such detailed study on R-curve analysis has been made. However, some limited calculations were carried out on the basis of Rice's J-integral[36] and Witt-Mager's[51] modified equivalent energy methods. Table 4.4 gives such calculations based on these energy methods. K_Q based on the modified energy method from the load-COD diagram upto the point of crack extension would give an apparent toughness value.

The major point which is to be emphasized for such anyielding material is that there exists a critical stress intensity factor, K_{Pc}, at which there is an abrupt loss in the resistance to crack-tip plastic flow. Thus, in such a case, the fracture behaviour can be characterized by two stress intensity factors, one representing the condition for an abrupt loss of local plastic constraint and the

other representing the onset of crack extension. However, in the case of a high strength material, these two critical stress intensity factors may coincide causing a catastrophic failure.

5.3. On the Shape Dependent Instability of a Single Spheroidal Void Under Uniaxial Tension and Shear:

Nucleation, growth and coalescence of voids play an important role in ductile fracture of metals. The stability of deforming void shape and the local necking plastic instability of the matrix between two adjacent voids should be understood for ductile fracture in plane strain. The mechanism of ductile fracture involves firstly, a favourable situation for an abrupt strain jump causing flow-localization and secondly, a critical normal strain on the void surface. In shear loading, a single prolate spheroidal cavity can have a shape dependent instability at a particular prolateness, provided the void grows from spherical to prolate spheroidal shape keeping the void volume unchanged during shear deformation. Inside an incompressible solid, this is seen to occur at $a/b = 1.39$ prolateness ratio. Thus, a void has a shape dependent instability in shear loading. Furthermore, uniaxial tension would give rise to a similar instability at a particular prolateness ratio. On the basis of the shear strain amplification ratio at the void surface, it is seen that the rotational resistance offered by a prolate spheroidal void vanishes at $a/b = 1.39$ and reaches a maximum

around a/b = 2.3 prolateness ratio. Thus, an abrupt growth of void would be visible at a particular prolateness ratio under uniaxial tension. The present analysis on the tensile loading of a prolate spheroidal cavity inside an incompressible solid suggests that, a prolate hole in a symmetric loading can undergo a shearing instability, when the applied initial tensile stress exceeds the equivalent local slide modulus of the surrounding material in the presence of a void. Unlike symmetric loading on a spheroidal hole inside an isotropic material, a prolate spheroidal cavity can give a local abrupt shear growth inside an orthotropic material due to loading. As the tension is applied parallel to the direction of the major axis of the hole, which is energetically the most favourable orientation, the void will show an abrupt growth in the direction of the loading. At the onset of instability, the void will try to grow in an unstable manner with a large local strain concentration. Although, the loading as well as the void shape is symmetrical and also parallel to the direction of growth, this situation would be expected from the fluid mechanics analogy as well. A pure torque will be required to hold a rigid prolate spheroidal body in a laminar viscous fluid stream, when the flow is parallel to its major axis[101].

Deysarkar and Bandyopadhyay's[12] analysis further confirms the importance of rotational effect on void, which produces a localised shear strain causing the incipience

of flow localization in the matrix. In the present investigation no detailed study has been made to show the plastic instability in a real void growth situation inside metals. Some further work may consider this aspect. Nevertheless, these theoretical predictions agree favourably with the experimental observations of Orowan[10] and Perra and Finnie[86] on plane strain void growth situation.

In order to verify the theoretical analysis, a simple experiment was conducted on spherical hole growth in a highly ductile lead-tin alloy. No delamination from the glued araldite surface was observed even upto 50% elongation of the entire sample. The change in the void shape was recorded. Figure 4.82 shows a good agreement between McClintock's[8] theoretical predictions and the present experimental results on the mean radius ratio. The eccentricity measurements described in Figure 4.81 also agree favourably with Perra and Finnie's observation on hole growth in copper under plane strain. The increase in void volume was also measured and found to be constant upto 20% elongation of the specimen. On further increase in remote strain, there is a sudden growth of the void around 40% elongation producing approximately 40% increase in void volume. At 50% elongation, the increase in void volume is seen to be around 60%. This confirms that there is an abrupt growth of spheroidal hole at a particular prolateness ratio inside a

highly ductile material. These observations relating to the sudden growth of a single spheroidal void are in agreement with the theoretical predictions.

This investigation on the void shape instability is a step in the direction of understanding the mechanism of ductile fracture of metals.

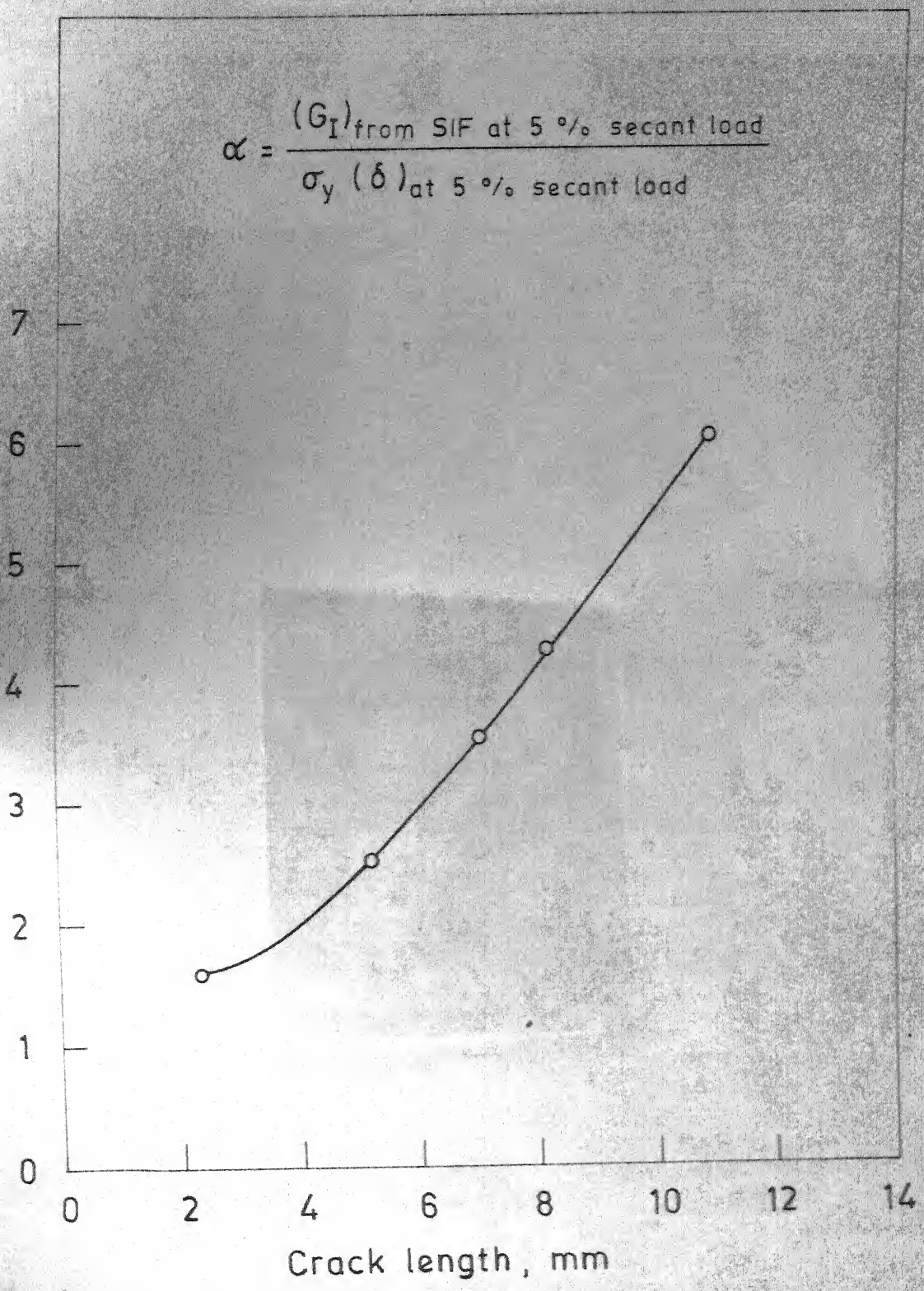

Fig. 5.1 Plot of α at 5 % secant load versus crack length in 6 mm thick mild steel specimens.

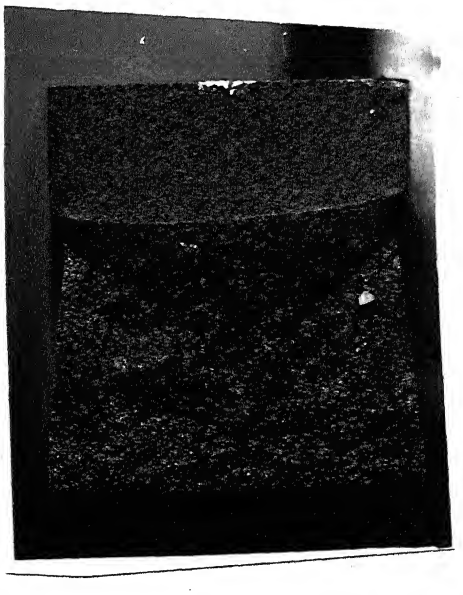

Figure 5.2: Photographs showing fractured surfaces of 0.6% carbon steel specimens.

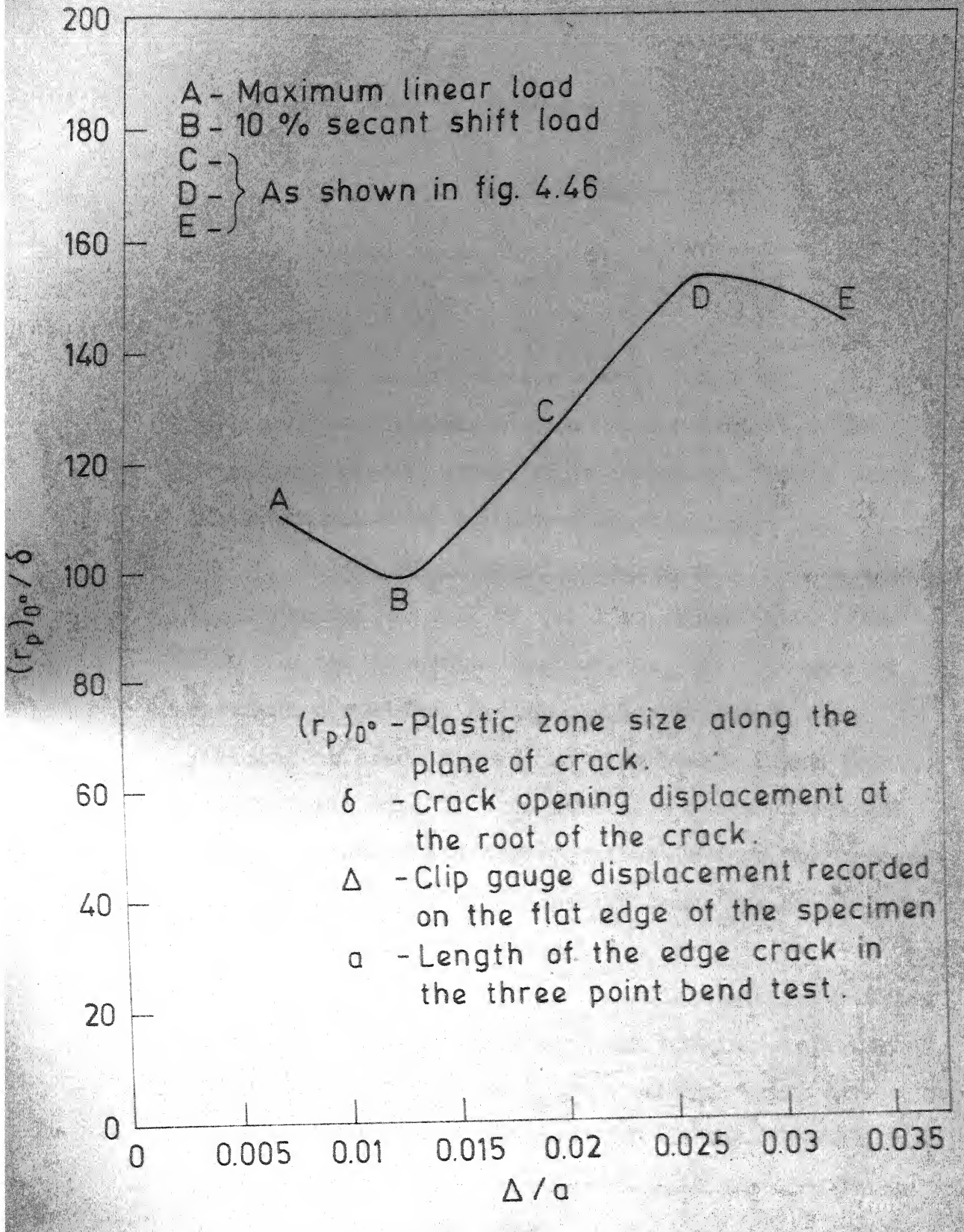

Fig. 5.3 Plot of $(r_p)_{0°}/\delta$ versus Δ/a for a 6 mm thick mild steel specimen with crack length of 6.65 mm.

CHAPTER - VI

CONCLUSIONS

The following conclusions can be drawn from the present investigation:

1. In the case of 0.6% carbon steel, for a valid K_{Ic} test, ASTM recommendations on size requirements are too conservative, and found to be oversafe. For a valid plane strain crack toughness test, $a \geq 0.5 (K_{Ic}/\sigma_y)^2$ and $B \geq 0.5(K_{Ic}/\sigma_y)^2$ would be adequate for this material. K_{Ic} measured for this material is around 150 $(Kg/mm^2)\sqrt{mm}$. In the non-valid test regime, the increase in specimen compliance was mainly due to the plastic yielding at crack-tip and no slow stable crack growth was observed even in 3 mm thickness beams with short cracks. A significant observation is that the apparent toughness for very short cracked beams was lower than the K_{Ic} value of the material.
2. No fast fracture was noticed in mild steel pre-cracked beams, even upto a sizeable crack opening displacement, for the thickness range 3 to 25 mm with crack size 1 to 12.5 mm, and a large plastic flow at the crack-tip was prevalent. A sudden increase in specimen compliance near about 5% secant shift load was noticed due to an abrupt plastic flow ahead of the crack-tip. This profuse

localized plastic flow ahead of the notch tip was considered to be a sudden loss of local plane strain plastic constraint. The abrupt increase in plastic zone was seen along 45° plane for thicker beams and/or longer cracks. On the other hand, the plastic zone extended more on the plane of the crack for thin beams with relatively short cracks. The SIF required for the loss of resistance to plastic flow was dependent on crack size and thickness analogous to the apparent toughness variation in high strength materials. The asymptotic value of the stress intensity factor (K_{Pc}) was measured to be of the order of 103 (Kg/mm^2) $\sqrt{mm}$ beyond a crack size of approximately 6 mm for all thicknesses. Due to notch strengthening effect, the load carrying capacity increased by about 50% of the yield load when calculated on the basis of net ligament section (W-a). Slow stable crack growth was noticed at a high COD value with an indication of plane stress deformation.

3. Theoretical investigation on the stability of deformed shape for a single prolate spheroidal void has revealed that, an isolated cavity will show an abrupt unstable shear growth beyond a certain prolateness ratio in tension or shear loading. These results agree favourably with the experimental observations in a lead-30% tin alloy.

BIBLIOGRAPHY

1. Brown, Jr., W.F. and Srawley, J.E., Plane Strain Crack Toughness Testing of High Strength Metallic Materials, American Society of Testing Materials, Special Technical Publications, No. 410 (1966).

2. McClintock, F.A. and Irwin, G.R., Plasticity Aspects of Fracture Mechanics, American Society of Testing Materials, Special Technical Publications, No. 381, p. 84 (1964).

3. Griffith, A.A., The Phenomena of Rupture and Flow in Solids, Philosophical Transactions, Royal Society of London, Ser. A, Vol. 221, p. 163 (1920).

4. Griffith, A.A., The Theory of Rupture, Proceedings of the Ist International Congress for Applied Mechanics, Delft, Holland, p. 55 (1924).

5. Orowan, E., Fracture and Notch Brittleness in Ductile Metals, A Discussion on Brittle Fracture in Mild Steel Plates, Engineering, Vol. 164, p. 581 (1947).

6. Irwin, G.R., Fracturing of Metals, Transactions of American Society of Metals, Vol. 40, p. 147 (1948).

7. Hill, R., The Mathematical Theory of Plasticity, University Press, Oxford (1950).

8. McClintock, F.A., On the Mechanics of Fracture from Inclusions, "Ductility", American Society for Metals, Metals Park, Ohio, p. 255 (1968).

9. McClintock, F.A., Effects of Root Radius, Stress, Crack Growth and Rate on Fracture Instability, Proceedings of the Royal Society of London, Ser. A, Vol. 285, p. 58 (1965).

10. Orowan, E., Fracture and Strength of Solids, Reports on Progress of Physics, Vol. 12, pp. 185 (1949).

11. Bandyopadhyay, S.N. and Singh, N., Stability of Void Growth in an Incompressible Solid Under Uniaxial Tension and Shear, Engineering Fracture Mechanics, p. 635, Vol. 11, No. 4 (1979).

12. Deysarker, H.K. and Bandyopadhyay, S.N., Shear Strain Localization and Ligament Instability Between Two Prolate Spheroidal Holes in an Incompressible Medium Under Uniaxial Tension, Paper submitted for publication in the International Journal of Fracture (1980).

13. Cottrell, C.L.M. and Langstone, P.F., ISI/BISRA Conference on Low Alloy Steels, p. 166, Scarborough (Iron Steel Institute, London), 1968.

14. Jones, M.H. and Brown, W.F. Jr., The Influence of Crack Length and Thickness in Plane Strain Fracture Toughness Tests, N.A.S.A. Lewis Research Centre, Report No. 731-25-03-09-22.

15. Cottrell, A.H., Mechanics of Fracture in Large Structures, A Discussion on Damage and Failure Mechanisms of Heavy Section Steels, Proceedings of the Royal Society of London, Ser. A, Vol. 285, p. 10 (1965).

16. Hult, J.A.H. and McClintock, F.A., Elastic-Plastic Stress and Strain Distributions Around Sharp Notched etc., 9th International Congress on Applied Mechanics, Brussels, Vol. 8, p. 51 (1957).

17. Bandyopadhyay, S.N. and Griffiths, J.R., Effects of Specimen Dimensions on the Fracture Strength of Guage Plate, Unpublished Research Report, Materials Divs., C.E.R.L., Leatherhead, Central Electricity Generating Board, England (1970).

18. Chell, G.G., Milne, I. and Kirby, J.H., Practical Fracture Mechanics in the Post-Yielded Regime, Metals Technology, Vol. 2, Pt. 12, p. 549, Dec. (1975).

19. Westergaard, H.M., Bearing Pressures and Cracks, Journal of Applied Mechanics, Vol. 6, No. 2, p. 49 (1939).

20. Williams, M.L., On the Stress Distribution at the Base of a Stationary Crack, Journal of Applied Mechanics, Vol. 24, No. 1, Trans. A.S.M.E., Ser. E, p. 109 (1957).

21. Muskhellisville, N.I., Some Basic Problems of the Mathematical Theory of Elasticity, (Translated from Russian), Noordhooff, Holland (1953).

22. Sih, G.C., The Mechanics Aspects of Ductile Fracture, ICF4, FRACTURE-1977, Vol. 4, p. 361, ed. by D.M.R. Taplin, University of Waterloo Press.

23. Sih, G.C. and Liebowitz, H., Mathematical Theories of Brittle Fracture, Chapter 2, Vol. 2, FRACTURE - An Advanced Treatise, Ed. by H. Liebowitz, Academic Press (1968).

24. Inglis, C.E., Stress in a Plate due to the Presence of Cracks and Sharp Corners, Proceedings of the Institute of Naval Architecht, London, Vol. 60, p. 219 (1913).

25. Barenblatt, G.I., The Mathematical Theory of Equilibrium Cracks in Brittle Fracture, Advances in Applied Mechanics, Vol. 7, p. 55, Academic Press, New York (1962).

26. Green, A.P. and Hundy, B.B., Initial Plastic Yielding in a Notch Bend Test, Journal of Mechanics and Physics of Solids, Vol. 4, p. 128 (1956).

27. Dugdale, D.S., Yielding of Steel Sheets Containing Slits, Journal of Mechanics and Physics of Solids, Vol. 8, p . 100 (1960).

28. Bilby, B.A., Cottrell, A.H. and Swinden, K.H., The Spread of Plastic Yield from a Notch, Proceedings of the Royal Society of London, Ser. A, Vol. 272, p. 304 (1963).

29. Goodier, J.N. and Field, F.A., Plastic Energy Dissipation in Crack Propagation, Fracture of Solids, ed. by D.C. Drucker and J.J. Gilman, p. 103, Wiley, New York (1963).

30. Nichols, R.W., Practical Fracture Mechanics for Structural Steel, U.K. A.E.A., Chapman and Hall Ltd. (1969).

31. Tetelman, A.S. and Robinson, A.S., Comparison of Various Methods of Measuring K_{Ic} on Small Precracked Bend Specimens that Fracture After General Yield, Technical Report No. 13, U.S. Army Research Office, Durham, UCLA-ENG-7409, Jan. (1974).

32. Banerjee, S. and Pandey, R.K., Strain Induced Fracture in Low Strength Steels, Engineering Fracture Mechanics, Vol. 10, p. 817 (1978).

33. Wells, A.A., Notch Ductility, Design and Specification of Permissible Defect Sizes in Weld Metal Structures, Practical Fracture Mechanics for Steel, Ed. by Nichols, R.W. and Dobson, M.O., U.K. A.E.A., Chapman and Hall Ltd. (1969).

34. Turner, C.E., Yielding Fracture Mechanics, The Journal of Strain Analysis, Vol. 10, No. 4, p. 201 (1975).

35. Green, A.P. and Knott, J.F., The Initiation and Propagation of Ductile Fracture in Low Strength Steels, Journal of Engineering Materials and Technology, Trans. A.S.M.E., Vol. 98, Ser. H, p. 37 (1976).

36. Rice, J.R., Mathematical Analysis in the Mechanics of Fracture, FRACTURE - An Advanced Treatise, Ed. by H. Liebowitz, Chapter III, Vol. II, Academic Press (1968).

37. Burdekim, F.M. and Turner, C.E., Review of Current Status of Yielding Fracture Mechanics, Atomic Energy Review, Vol. 12, No. 3 (1974).

38. Paris, P.C. and Irwin, G.R., Elastic-Plastic Crack Tip Characterization etc., Fracture - 1977, Vol. I, p. 93, ed. by D.M.R. Taplin, University of Waterloo Press (1977).

39. Deysarker, H.K. and Bandyopadhyay, S.N., Criteria for Fracture of a Crack Like Notch in Brittle and Ductile Materials, Paper submitted for publication at ICF5, To be held in Cannes, France, March (1981).

40. Irwin, G.R., Plastic Zone Near a Crack and Fracture Toughness, Seventh Sagamore Ordinance Materials Conference, August (1960).

41. Cottrell, A.H., Mechanisms of Fracture, Tewksbury Symposium on Fracture, p. 1, University of Melbourne (1963).

42. Sumpter, J.D.J. and Turner, C.E., Proceedings of Second International Conference on Pressure Vessel Techniques, San Antonio, A.S.M.E., Vol. 2, p. 1095 (1973).

43. Rice, J.R. and Sorensen, E.P., Continuing Crack-tip Deformation and Fracture for Plane Strain Crack Growth in Elastic-Plastic Solids, Journal of Mechanics and Physics of Solids, Vol. 26, p. 163 (1978).

44. Knott, J.F., Fundamentals of Fracture Mechanics, Butterworths, London (1973).

45. Broberg, K.B., On Stable Crack Growth, Journal of Mechanics and Physics of Solids, Vol. 23, p. 215 (1975).

46. Begley, J.A. and Landes, J.D., A Comparison of the J-integral Fracture Criterion with the Equivalent Energy Concept, Progress in Flaw Growth and Fracture Toughness Testing, A.S.T.M., S.T.P. No. 536, p. 246 (1973).

47. Bilby, B.A., "Fracture", Vol. IV, FRACTURE - 1977, ed. by D.M.R. Taplin, University of Waterloo Press (1977).

48. Rice, J.R., Paris, P. and Merkle, J.G., Some Further Results on J-integral Analysis and Estimates, A.S.T.M., S.T.P. No. 536, p. 231 (1973).

49. Vitek, V. and Chell, G.G., An Assessment of Some Post Yield Fracture Criteria, Materials Science and Engineering, Vol. 27, p. 209 (1977).

50. Taira, S. and Tanaka, K., Thickness Effect of Notched Metal Sheets on Deformation and Fracture Under Tension, Engineering Fracture Mechanics, Vol. 11, No. 2, p. 231 (1979).

51. Witt, F.J. and Mager, T.R., A Procedure for Determining Bounding Values on Fracture Toughness, K_{Ic} at Any Temperature, presented at the 5th National Symposium on Fracture Mechanics, University of Illinois, Urbana, Illinois, Sept. (1971).

52. Krafft, J.M., Sullivan, A.M. and Boyle, R.W., Effect of Dimensions on Fast Fracture Instability on Notched Sheet, Proceedings, Crack Propagation Symposium, Cranfield, England (1961).

53. Eftis, J. and Liebowitz, H., On Fracture Toughness Evaluation for Semi-Brittle Fracture, Engineering Fracture Mechanics, Vol. 7, p. 101 (1975).

54. Pandey, R.K., Post Yield Fracture Mechanics, Workshop on Fracture, Fatigue and Failure Analysis, A short course organised by National Aeronautical Laboratory, Bangalore during 26th Feb. to 10th March (1979).

55. Knott, J.F. and Green, G., On Effects of Thickness on Ductile Crack Growth in Mild Steel, Journal of Mechanics and Physics of Solids, Vol. 23, p. 167 (1975).

56. Chell, G.G. and Spink, G.M., A Post Yield Fracture Mechanics Analysis of Three-Point Bend Specimens and its Implications to Fracture Toughness Testing, Engineering Fracture Mechanics, p. 101, Vol. 9 (1977).

57. Tetelman, A.S., Wilshaw, T.R. and Rau, C.A., International Journal of Fracture Mechanics, Vol. 4, p. 147 (1968).

58. Heald, P.T., Spink, G.M. and Worthington, P.J., Post Yield Fracture Mechanics, Materials Science and Engineering, Vol. 10, p. 129 (1972).

59. Bandyopadhyay, S.N. and Mubeen, A., Plasticity Spread in Mild Steel Pre-Cracked Charpy Bars, Engineering Fracture Mechanics, Vol. 12, No. 2 (1979).

60. Dixon, J.R., Effects of Crack-front Geometry and Plate Thickness on the stress Distribution in Cracked Plates, Inst. Phys., Phys. Soc. Conf. Ser. No. 1, p. 6, Dec. (1966).

61. Boyd, G.M., Engineering Fracture Mechanics, Vol. 4, No. 3, p. 459 (1972).

62. Ritter, J.C., A Modified Thickness Criterion for Fracture Toughness Testing, Engineering Fracture Mechanics, Vol. 9, p. 529 (1977).

63. Miller, K.J. and Kfouri, A.P., An Elastic-Plastic Finite Element Analysis of Crack Tip Fields under Biaxial Loading Conditions, International Journal of Fracture, Vol. 10, No. 3, p. 393 (1974).

64. Knott, J.F. and Cottrell, A.H., Notch Brittleness in Mild Steel, Journal of the Iron and Steel Institute, Vol. 201, p. 249 (1963).

65. Griffiths, J.R. and Cottrell, A.H., Elastic Failure at Notches in Silicon Steel, Journal of Mechanics and Physics of Solids, Vol. 13, p. 135 (1965).

66. Griffiths, J.R. and Owen, D.R.J., An Elastic-Plastic Stress Analysis for a Notched Bar in Plane Strain Bending, Journal of Mechanics and Physics of Solids, Vol. 19, p. 419 (1971).

67. Wessel, E.T., Linear Elastic Fracture Mechanics for Thick Walled Steel Pressure Vessels, Practical Fracture Mechanics for Structural Steel.

68. Irwin, G.R., Kies, J.A. and Smith, H.L., Proceedings of American Society for Testing Materials, Vol. 58, p. 640 (1958).

69. Tetelman, A.S. and McEvily, A.J., Fracture of Structural Materials, Wiley, New York (1967).

70. May, M.J., American Society for Testing Materials, S.T.P. No. 463 (1970).

71. Pellini, W.S. et al, Naval Research Laboratory, Report No. 6300, Washington D.C. (1965).

72. Chell, G.G. and Worthington, P.J., The Determination of Fracture Toughness of a Tough Steel from Invalid Compact Tension Specimens of Varying Width and Thickness, Materials Science and Engineering, Vol. 26, p. 95 (1976).

73. Bluhm, J.I., A Model for the Effect of Thickness on Fracture Toughness, Proceedings of American Society of Testing Materials, Vol. 61, p. 1324 (1961).

74. Vitvitskii, P.M., Panasynk, V.V. and Yarema, S. Ya, Plastic Deformation Around Crack and Fracture Criteria, A Review Article, Engineering Fracture Mechanics, Vol. 7, p . 305 (1975).

75. Hahn, G.T. and Rosenfield, A.R., Local Yields and Extension of Crack under Plane Stress, Acta Metallurgica, Vol. 13, p. 293 (1965).

76. Ewing, D.J.F. and Richards, C.E., The Yield Point Loads of Singly-Notched Pin Loaded Tensile Strips, Journal of Mechanics and Physics of Solids, Vol. 22, p. 27, Jan. (1974).

77. Pratt, P.L. and Stock, T.A., The Distribution of Stress about a Running Crack, Proceedings of the Royal Society of London, Ser. A., Vol. 285, p. 73 (1965).

78. Gerberich, W., Stress Distribution about a Slowly Growing Crack Determined from Photoelastic Coating Method, Experimental Mechanics, Vol. 2, No. 12, p. 359 (1962).

79. Sedlow, J.L. et al, A Case of Elastic-Plastic Flow using a New Special Element, FRACTURE - 1977, Vol. 1, p. 117, ed. by D.M.R. Taplin, University of Waterloo Press (1977).

80. Irwin, G.R., A Discussion on the paper by Wells and Post, Proceedings of the Society of Experimental Stress Analysis, Vol. 16, No. 1 (1958).

81. Wells, A.A. and Post, D., The Dynamic Stress Distribution Surrounding a Running Crack, Proceedings of the Society of Experimental Stress Analysis, Vol. 16, No. 1, p. 69 (1958).

82. Yokobori, T., Kioshi, S. and Yamaguchi, Y., X-ray Microbeam Studies on Plastic Zone at the Tip of the Fatigue Crack, Reports of Research Institute for Strength and Fracture of Materials, Vol. 6, No. 2, p. 49, Tohuku University (1970).

83. Dudderar, T.D. and O'Regan, R., Measurement of Strain Field Near a Crack in Polymethylmethacrylate by Holographic Interferometry, Experimental Mechanics, Vol. 11, p. 49 (1971).

84. Theocaris, P.S., New Methods Based on Geometric Optics for the Solution of Fracture Mechanics Problems, Techn. Khron., Vol. 41, p. 145 (1972).

85. Iino, Y., Accumulated Plastic Zone Around Fatigue Crack in Type 304 Stainless Steel, Metal Science, Vol. 10, p. 159, May (1976).

86. Perra, M. and Finnie, I., Void Growth and Localization of Shear in Plane Strain Tension, FRACTURE - 1977, Vol. 1, p. 415, ed. by D.M.R. Taplin, University of Waterloo Press.

87. Price, R.J. and Kelly, A., Deformation of Age Hardened Aluminium, Alloy Crystals-II Fracture, Acta Metallurgica, Vol. 12, No. 9, p. 979 (1964).

88. Cottrell, A.H. and Stokes, R.J., Effects of Temperature on Plastic Properties of Aluminium Crystals, Proc. of Royal Society of London, Ser. A, Vol. 233, p. 17 (1955).

89. Beevers, C.J. and Honeycombe, R.W.K., Ductile Fracture of Single Crystals, FRACTURE - ed. by B.L. Averbach et al, Wiley, New York, p. 474 (1959).

90. Rudnicki, J.W. and Rice, J.R., Conditions for the Localization of Deformation in Pressure Sensitive Dilatant Materials, Journal of Mechanics and Physics of Solids, Vol. 23, p. 371 (1975).

91. Argon, A.S., Formation of Cavities from Non-Deformable Second Phase Particles in Low Temperature Ductile Fracture, Journal of Materials and Technology, Trans. A.S.M.E., Ser. H, p. 60, January (1976).

92. Backofen, W.A., Deformation Processing, Addison-Wesley, Reading, Massachusetts (1972).

93. Thomason, P.F., A Theory of Ductile Fracture by Internal Necking of Cavities, Journal of the Institute of Metals, Vol. 96, p. 360 (1968).

94. Nagpal, V., McClintock, F.A., Berg, C.A., and Subudhi, M., Traction Displacement Boundary Conditions for Plastic Fracture by Hole Growth, Foundations of Plasticity, International Symposium held at Warsaw, ed. by A. Sawczuk, Noordhooff Leyden, p. 365 (1972).

95. El-Sudani and Knott, J.F., On Plane Strain Void Growth, (Private communication), Cambridge University (1979).

96. Tait, R.A. and Taplin, D.M.R., Interaction Effects During the Growth of holes in a Superplastically Deforming Medium, Scripta Metallurgica, Vol. 13, p. 77 (1979).

97. Raj, R. and Ashby, M.F., Intergranular Fracture at Elevated Temperature, Acta Metallurgica, Vol. 23 (1975).

98. Bilby, B.A., Eshelby, J.D., Kundu, A.K., and Kolbuszewsky, M.I., The Change of Shape of a Viscous Ellipsoidal Region Embedded in Slowly Deformed Liquid Matrix Having a Different Viscosity, Techtonophysics, Vol. 35, p. 408 (1976).

99. Hahn, G.T., Rosenfield, A.R. and Votava, E., American Society of Metals Seminar, Ductility, Metals Park, Ohio, p . 63 (1968).

100. Argon, A.S. and Inn, J., Separation of Second Phase Particles in Spheroidized 1045 Steel, Cm - 0.6% Cr-alloy and Maraging Steel in Plastic Straining, Metallurgical Transactions, Vol. 6, Ser. A, p. 839-851 (1975).

101. Jeffery, G.B., The Motion of Ellipsoidal Particle Immersed in a Viscous Fluid, Proceedings of the Royal Society London, Ser. A, Vol. 102, p. 162 (1922).

102. Eshelby, J.D., The Determination of the Elastic Field of an Ellipsoidal Inclusion, and Related Problems, Proceedings of the Royal Society of London, Ser. A, Vol. 241, p. 276 (1957).

103.* Taplin, D.M.R. and Smith, R.F., Fracture during Superplastic Flow of Industrial Al-Mg Alloys, FRACTURE - 1977, ed. by D.M.R. Taplin, University of Waterloo Press (1977).

104.* Brown, L.M. and Embury, J.D., The Initiation and Growth of Voids at Second Phase Particles, Proceedings of 3rd International Conference on Strength of Metals and Alloys, Vol. I, Cambridge, England, Aug. (1973).

105.* Rice, J.R. and Tracy, D.M., On the Ductile Enlargement of Voids in Triaxial Stress Field, Journal of Mechanics and Physics of Solids, Vol. 17, p. 201 (1969).

106.* Mubeen, A., Fracture of a Beam When a Small Fatigue Crack Exists Ahead of a Notch, Ph.D. thesis, Indian Institute of Technology Kanpur (1977).

107*. Deysarker, H.K., Stresses at the Roots of Cracks, Notches and Cavities, and Mechanisms of Brittle and Ductile Fracture of Metals, Ph.D. thesis (submitted) Indian Institute of Technology Kanpur, November (1979).

---

* General References.

APPENDIX - A

When a prolate spheroidal cavity ($a > b = c$) in an incompressible material is subjected to a simple tension stress parallel to its major axis, the maximum strain amplification on the void surface is given by

$$e^{T}_{11} = \varepsilon e^{A}_{11} \tag{A.1}$$

where

$$\varepsilon = \frac{1 - S_{3333} - S_{2233} - S_{1133}}{(1 - S_{3333} - S_{2233})(1 - S_{1111}) - 2S_{1133}S_{3311}} \tag{A.2}$$

on the other hand, if the simple tension stress is perpendicular to the major axis, the maximum strains on the void surface is given by

$$e^{T}_{33} = \xi e^{A}_{33} \tag{A.3}$$

where

$$\xi = \frac{3}{4}\cdot\frac{1}{1 + S_{2233} - S_{3333}} + \frac{1}{4}\cdot\frac{1-S_{1111} - 2S_{3311}}{(1-S_{3333}-S_{2233})(1-S_{1111})-2S_{1133}S_{3311}} \tag{A.4}$$

In the case of an incompressible solid the values of S_{ijki} for a prolate spheroid may be expressed as:

$$S_{1111} = 1 - 2Aa^2, \qquad S_{2222} = S_{3333} = (3/4)(1 - Ac^2)$$

$$S_{1122} = S_{1133} = Ac^2, \qquad S_{2211} = S_{3311} = Aa^2$$

$$S_{2233} = S_{3322} = (1/4)(1 - Ac^2)$$

where

$$A = (3I_c - 4\pi)/4\pi\ (a^2 - c^2)$$

$$I_c = I_b = 2\pi x(x^2 - 1)^{-3/2}\ [x(x^2 - 1)^{1/2} - \cosh^{-1}x]$$

$$x = a/c\ (= a/b) = \text{Prolateness ratio}$$

and x is always greater than unity for a prolate spheroid.